ANNUAL REVIEW

INSTITUTE FOR MOLECULAR SCIENCE

1981

Errata (Annual Review 1981)

1. **Spread, Editorial Committee,**

   Tsunetaka Fujiyama* should read Tsunetake Fujiyama*

2. **p. vi, line 20 from the bottom,**

   Valatile should read Volatile.

3. **p.2, line 13 from the bottom,**

   Chi-aki HYODO should read Shi-aki HYODO.

4. **p.5, Foreign Visiting Staff,**

   John T. Hougen should read Jon T. Hougen.

5. **p.91, left column, Ref. 2,**

   Spectrose. should read *Spectrosc.*

6. **p.146, in the right top scheme,**

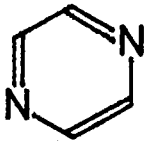

should read

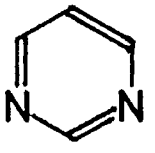

7. **p.172, The 11-th Okazaki Conference, one of the Organizers,**

   M. Tatsumi *(Tokyo Univ.)* should read **M. Tasumi** *(Univ. of Tokyo).*

ANNUAL REVIEW

INSTITUTE FOR MOLECULAR SCIENCE

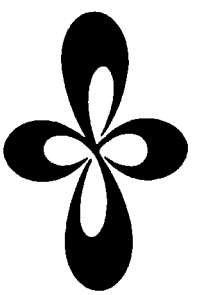

1981

Published by
Okazaki National Research Institutes
The Institute for Molecular Science
Myodaiji, Okazaki 444, Japan
Phone 0564—52—9770
Telex 4537-475 KOKKEN J
December 15, 1981

IMS 1981

On occasion of this fourth issue of IMS Annual Review, I am sorry to report that Dr. Akamatu retired at the end of March, 1981. Dr. Akamatu has been the director of IMS since it was founded six years ago and has contributed much to the success of IMS.

In the short time since its establishment, the Institute for Molecular Science has been highly recognized internationally and in Japan, both because of its research staff and because of its facilities, which have rapidly developed and expanded. We owe this recognition to Dr. Akamatu's enthusiasm and excellent leadership. Let me take this opportunity to express our deepest gratitude for the efforts and achievements he has made.

Following him puts a great deal of responsibility on me, and I will make every effort to fulfill this responsibility. It is my aim that IMS should function effectively as the inter-university national research institute and should contribute to the development of molecular science and related fields in Japan. The researchers in the Institute should be allowed to demonstrate their abilities and be encouraged to develop original areas of study. Finally, IMS should serve as a major center for molecular science research, both nationally and internationally.

With these goals in mind, I would like to continue to develop positive new approaches to further the work of the Institute. I would also like to direct my efforts toward the international exchange of scholars and in the promotion of joint studies.

In addition to IMS, there are in Okazaki two institutes in the field of biological science, the National Institute for Basic Biology and the National Institute for Physiological Sciences, both established in 1977. These institutes differ from IMS in their research fields and aims. However, in order to develop an effective administration, a new organization, the Okazaki National Research Institutes started in April 1981. From now on, IMS will be operated as one of the institutes which belong to this organization.

In August 1981, a new laboratory called Theoretical Studies II was started. Dr. Hiroki Nakamura from the Tokyo University of Agriculture and Technology is the professor of this laboratory.

The Ultraviolet Synchrotron Orbital Radiation (UVSOR) project has steadily progressed. The construction of an accelerator is now under way with a budget of ¥548,156,000 for the fiscal year starting in April 1981. In September 1981, Mr. Toshio Kasuga came from National Laboratory for High Energy Physics to become an associate professor for the UVSOR project.

From the viewpoint of promoting international exchanges of scientists and joint studies in the field of molecular science, I am pleased to see that the cooperative research programs in this field have started between the United Kingdom and Japan with Daresbury Laboratory and IMS as the key institutes. Also in September 1981, an implementing arrangement was made between the United States and Japan in the area of "Solar Energy Conversion by means of Photosynthesis," and IMS was designated as the official institute on the Japanese side.

Finally, we at IMS are delighted at the news that Professor Kenichi Fukui of Kyoto University is to be awarded the Nobel Prize in Chemistry for 1981. Professor Fukui is the vice-chairperson of the Council of IMS and has contributed much to the establishment of the Institute. I would like to extend my personal congratulations to him for this important award, recognizing his success in his field.

October 1981

S. Nagakura

Saburo Nagakura
Director-General

CONTENTS

ORGANIZATION AND STAFF

Organization

The Institute for Molecular Science, upon completion, will comprise 15 research laboratories —each staffed by a professor, an associate professor, two research associates and a few technical associates— and five research facilities. The laboratories are grouped into five departments as follows:

Department of Theoretical Studies	Theoretical Studies I
	Theoretical Studies II
	Theoretical Studies III[2)]
Department of Molecular Structure	Molecular Structure I
	Molecular Structure II[2)]
	Molecular Dynamics
Department of Electronic Sturcture	Excited State Chemistry
	Excited State Dynamics
	Electronic Structure[2)]
Department of Molecular Assemblies	Solid State Chemistry
	Photochemistry
	Molecular Assemblies Dynamics[1)]
	Molecular Assemblies[2)]
Department of Applied Molecular Science	Applied Molecular Science I
	Applied Molecular Science II[2)]
Research Facilities	Computer Center
	Instrument Center
	Low-Temperature Center
	Chemical Materials Center
	Development Workshop

1) To be established.

2) Professors and associate professors are adjunct professors from universities.

Scientific Staff

Saburo NAGAKURA	Professor, Director-General

Department of Theoretical Studies

Theoretical Studies I

Keiji MOROKUMA	Professor
Masaru TSUKADA	Associate Professor
Shigeki KATO	Research Associate
Chikatoshi SATOKO	Research Associate
Shigeru OBARA	Technical Associate
Nobuyuki SHIMA	Technical Associate

Toshiharu HOSHINO	Research Fellow (April '80—)
Yoshihiro OSAMURA	Research Fellow (April '81—)
Mitsuyasu HANAMURA	Graduate Student from Tohoku Univ.* (April '79—)
Yoshitaka WATANABE	Graduate Student from Osaka City Univ.* (April '81—)

Theoretical Studies II

Hiroki NAKAMURA	Professor

Theoretical Studies III

Teijiro YONEZAWA	Adjunct Professor from Kyoto Univ. (—March '81)
Takayuki FUENO	Adjunct Professor from Osaka Univ. (April '81—)
Suehiro IWATA	Adjunct Associate Professor from the Inst. for Phys. Chem. Res. (—March '81)
Kiyoyuki TERAKURA	Adjunct Associate Professor from the Univ. of Tokyo (April '81—)
Kazuo KITAURA	Research Associate (—September '81)**

Department of Molecular Structure

Molecular Structure I

Eizi HIROTA	Professor
Shuji SAITO	Associate Professor
Chikashi YAMADA	Research Associate
Yasuki ENDO	Research Associate
Kentarou KAWAGUCHI	Technical Associate
Tetsuo SUZUKI	Technical Associate
Keiichi NAGAI	Research Fellow (—February '81)

Molecular Structure II

Masamichi TSUBOI	Adjunct Professor from the Univ. of Tokyo (—March '81)
Ikuzo TANAKA	Adjunct Professor from Tokyo Inst. of Tech. (April '81—)
Tamotsu KONDO	Adjunct Associate Professor from the Univ. of Tokyo (April '80—)

Molecular Dynamics

Tsunetake FUJIYAMA	Professor
Yasuo UDAGAWA	Associate Professor
Tadashi KATO	Research Associate
Keiji KAMOGAWA	Research Associate
Kazuyuki TOHJI	Technical Associate
Ryosaku IGARASHI	Research Fellow (April '81—)
Nobuyuki ITO	Graduate Student from Tokyo Metropolitan Univ.* (October '79—)
Chi-aki HYODO	Graduate Student from Tokyo Metropolitan Univ.* (October '79—)

Department of Electronic Structure

Excited State Chemistry

Keitaro YOSHIHARA	Professor
Tadayoshi SAKATA	Associate Professor
Nobuaki NAKASHIMA	Research Associate
Tomoji KAWAI	Research Associate
Minoru SUMITANI	Technical Associate (Unit Chief)
Kazuhito HASHIMOTO	Technical Associate
Nobuo SHIMO	Visiting Research Fellow from Idemitsu Kosan Co., Ltd. (June '81—)
Shigemasa NAKAMURA	Graduate Student from Nagoya Univ.* (April '81—)

Excited State Dynamics

Ichiro HANAZAKI	Professor
Nobuyuki NISHI	Associate Professor
Iwao NISHIYAMA	Research Associate
Hisanori SHINOHARA	Research Associate
Masaaki BABA	Technical Associate
Ryoichi NAKAGAKI	IMS Fellow (May '80—)
Susumu KUWABARA	Graduate Student from Osaka Univ.* (April '79—)
Masayuki UMEMOTO	Graduate Student from Kyushu Univ.* (April '80—)

Electronic Structure

Hiroshi TSUBOMURA	Adjunct Professor from Osaka Univ. (April '80—)
Masahiro MATSUOKA	Adjunct Associate Professor from Kobe Univ. (—March '81)
Hajime KATO	Adjunct Associate Professor from Kobe Univ. (April '81—)

Department of Molecular Assemblies

Solid State Chemistry

Hiroo INOKUCHI	Professor
Inosuke KOYANO	Associate Professor
Kenichiro TANAKA	Research Associate
Kazuhiko SEKI	Research Associate
Naoki SATO	Technical Associate
Tatsuhisa KATO	Technical Associate
Kenji ICHIMURA	IMS Fellow
Masako YUDASAKA	Graduate Student from Tokyo Metropolitan Univ.* (—March '81)

Photochemistry

Katsumi KIMURA	Professor
Kosuke SHOBATAKE	Associate Professor
Yohji ACHIBA	Research Associate
Kiyohiko TABAYASHI	Research Associate
Kenji SATO	Technical Associate
Shinji TOMODA	Research Fellow

Molecular Assemblies

Yuji MORI	Adjunct Professor from Tokyo Inst. of Tech. (—March '81)
Motohiro KIHARA	Adjunct Professor from Nat. Lab. for High Energy Phys. (April '81—)
Katsuhide YOSHIDA	Adjunct Associate Professor from the Univ. of Tokyo (—March '81)
Yasuhiko SHIROTA	Adjunct Associate Professor from Osaka Univ. (April '81—)
Gunzi SAITO	Research Associate

Department of Applied Molecular Science

Applied Molecular Science I

Hiizu IWAMURA	Professor
Tasuku ITO	Associate Professor
Tadashi SUGAWARA	Research Associate
Koshiro TORIUMI	Research Associate
Yuzo KAWADA	Technical Associate
Masako SUGIMOTO	Technical Associate
Kazumasa KOBAYASHI	Graduatge Student from Yamaguchi Univ.* (—March '81)

Fumio UENO	Graduate Student from Tohoku Univ.* (April '80—)
Yukihiro YOKOYAMA	Graduate Student from Nagoya Inst. of Tech.* (April '81—)

Applied Molecular Science II

Junnosuke FUJITA	Adjunct Professor from Nagoya Univ. (—March '81)
Hideo YAMATERA	Adjunct Professor from Nagoya Univ. (April '81—)
Nobuyuki HARADA	Adjunct Associate Professor from Tohoku Univ. (April '80—)

Research Facilities

Computer Center

Hiroshi KASHIWAGI	Associate Professor
Shigeyoshi YAMAMOTO	Technical Associate
Unpei NAGASHIMA	Graduate Student from Hokkaido Univ.* (April '80—)

Instrument Center

Iwao YAMAZAKI	Associate Professor
Keisaku KIMURA	Research Associate
Toshiro MURAO	Technical Associate

Low-Temperature Center

Toshiaki ENOKI	Research Associate

Chemical Materials Center

Hidemasa TAKAYA	Associate Professor
Akira MIYASHITA	Research Associate
Masashi YAMAKAWA	Technical Associate

Development Workshop

Makoto WATANABE	Associate Professor
Tadaoki MITANI	Associate Professor
Toshio KASUGA	Associate Professor
Yoshihiro TAKAGI	Research Associate

* Conduct graduate studies at IMS on the Cooperative Education Programs of IMS with graduate schools.
** Present address: Faculty of Science, Osaka City University, Osaka, Japan

Technical Staff

Akira UCHIDA	Technical Division Head
Kusuo SAKAI	Technical Section Chief
Satoshi INA	Computer Center
Fumio NISHIMOTO	Computer Center
Takaya YAMANAKA	Instrument Center
Shunji BANDO	Instrument Center
Kenichi IMAEDA	Low-Temperature Center
Kazuo HAYAKAWA	Electronic Shop
Hisashi YOSHIDA	Electronic Shop
Masaaki NAGATA	Glassblowing Shop
Osamu MATSUDO	Machine Shop (Unit Chief)
Toshio HORIGOME	Machine Shop
Nobuo MIZUTANI	Machine Shop

Norio OKADA	Machine Shop
Mitsukazu SUZUI	Machine Shop
Masami HASUMOTO	Machine Shop
Shinji KATO	Machine Shop

Foreign Visiting Staff

Ronald D. McKelvey	Univ. of Wisconsin, La-Corosse, USA	May 19—Aug. 18, 1980
David S. Crumrine	Loyola Univ., Chicago, USA	Sept. 1—Dec. 31, 1980
Isaiah Shavitt	Battelle Memorial Inst., Columbus, USA	Oct. 1—Nov. 30, 1980
John T. Hougen	NBS, Washington, D.C. USA	Nov. 1, 1980—Apr. 30, 1981
Ilan S. Chabay	NBS, Washington, D.C. USA	Nov. 17, 1980—June 29, 1981
Karl H. Grellman	Max-Planck Inst. für Biophys. Chem., Göttingen, Germany	Jan. 5—Apr. 4, 1981
Sigrid D. Peyerimhoff	Univ. of Bonn., Bonn, Germany	Feb. 1—Mar. 31, 1981
Ewa Lipczynska-Kochany	Tech. Univ. of Warsaw, Warsaw, Poland	Apr. 1, 1981—
Bryan R. Henry	Univ. of Manitoba, Winnipeg, Canada	Apr.18—July 17, 1981
Imre G. Csizmadia	Univ. of Toronto, Canada	May 10—May 26, 1981

COUNCIL

Saburo NAGAKURA, Director-General

Councellors

Chairperson	Yasutada UEMURA	Professor, The University of Tokyo
Vice-Chairperson	Kenichi FUKUI	Professor, Kyoto University
	Hideo AKAMATU	Professor Emeritus, The University of Tokyo
	Hiroaki BABA	Director, The Research Institute of Applied Electricity, Hokkaido University
	Melvin CALVIN	Professor, University of California, U.S.A.
	Masao FUJIMAKI	Professor, Ochanomizu University
	Soichi IIJIMA	President, Nagoya University
	Tadao ISHIKAWA	President, Keio University
	Yoshiya KANDA	President, Kyushu University
	Noboru KOMATSU	President, Toyota Central Research & Development Laboratories, INC.
	Masao KOTANI	President, The Science University of Tokyo
	Daikichiro MORI	Director-General, The Institute of Space and Astronautical Science
	Takashi MUKAIBO	Professor Emeritus, The University of Tokyo
	Sir George PORTER	Director, The Royal Institution, U.K.
	Yoneichiro SAKAKI	President, Toyohashi University of Technology
	Osamu SHIMAMURA	Director, Sagami Chemical Research Center
	Yataro TAJIMA	Director-General, National Institute of Genetics

The Council is the advisory board for the Director-General. Two of the counsellors are selected among distinguished foreign scientists.

Administration Bureau

Hiroaki MIZUMURA	Director-General, Administration Bureau
Minoru SHIMIZU	Director, General Affairs Department
Hiroshi HIGURASHI	Director, Finance and Facilities Department

BUILDINGS AND CAMPUS

The IMS campus covering 62,561 m^2 is located on a low hill in the middle of Okazaki City. The inequality in the surface of the hill and growing trees are preserved as much as possible, and low-storied buildings are adopted for conservation of the environment. The buildings of IMS are separated according to their functions as shown in the map. The Research Office Building and all Research Facilities except for the Computer Center are linked organically to the Main Laboratory Building by corridors. Computer Center, Library, and Administration Buildings are situated between IMS and the neighboring National Institute for Basic Biology and National Institute for Physiological Sciences, because the latter two facilities are common to these three institutes.

The lodging facility of IMS called Yamate Lodge, located within 10 min. walk, has sleeping accommodations for 20 guests. Since June 1, 1981 a new lodging facility called Mishima Lodge has been opened. Mishima Lodge, located within four minutes' walk east of IMS can accommodate 30 guests and six families. Scientists who visit IMS as well as the two other institutes can make use of these facilities. Foreign visiting scientists can also live at these lodgings with their families during their stay.

The Institute for Molecular Science

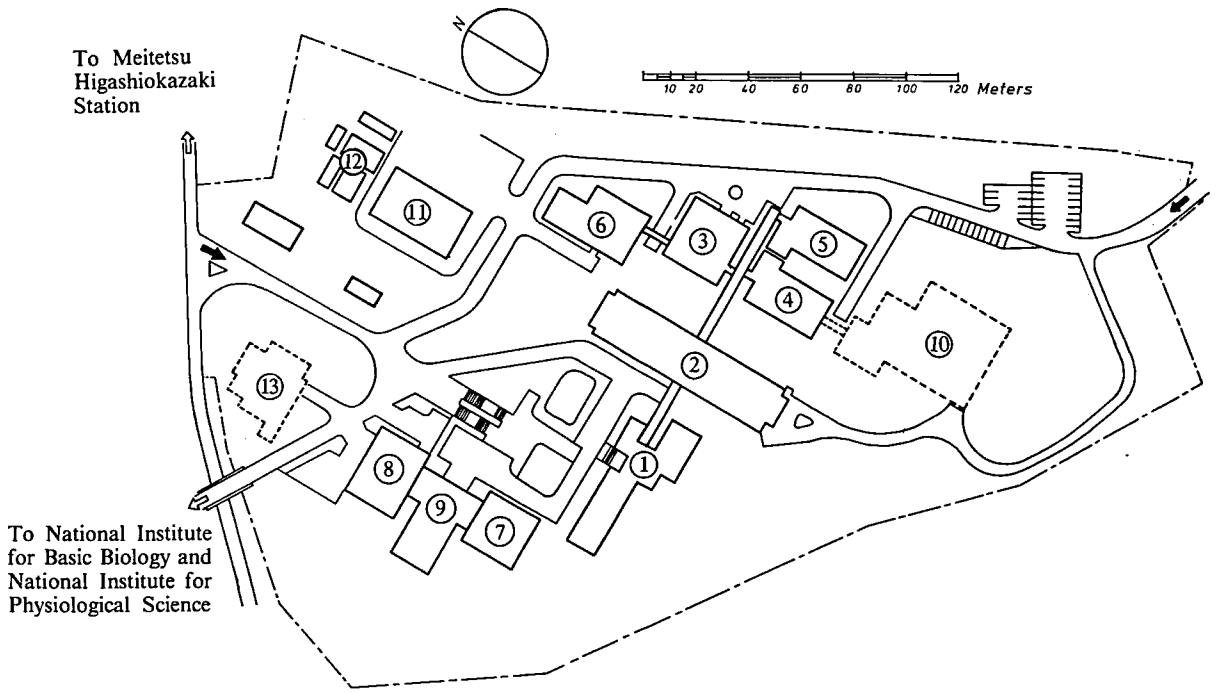

1. Research Office Building
2. Main Laboratory Building
3. Development Workshop
4. Instrument Center
5. Chemical Materials Center
6. Low-Temperature Center
7. Computer Center
8. Library
9. Central Administration
10. Special Experiment (UVSOR) Building†
11. Power Station
12. Waste-Water Disposition Facilities
13. Faculty Club

† Under construction

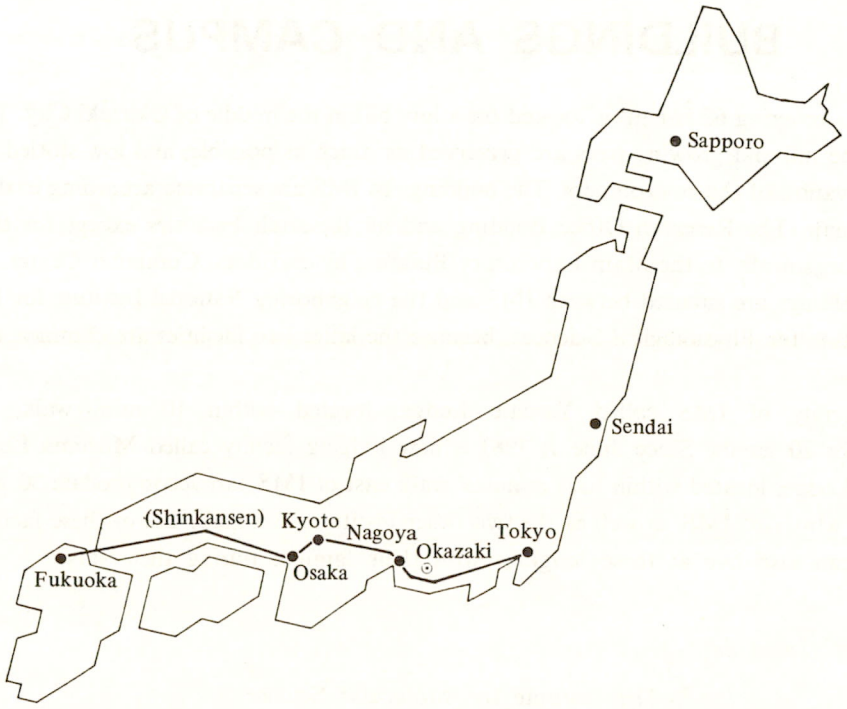

Okazaki (population 250,000) is 260 km southwest of Tokyo, and can be reached by train in about 3 hours from Tokyo via New Tokaido Line (Shinkansen) and Meitetsu Line.
The nearest large city is Nagoya, about 40 km west of Okazaki.

IMS, 1981

RESEARCH ACTIVITIES I
Department of Theoretical Studies

I—A Potential Energy Surfaces for Chemical Reactions

Molecular orbital studies of potential energy surfaces for chemical reactions remained to be one of the most important areas of study for our molecular quantum chemistry group. The energy gradient technique, both at the GVB and the SCF level, has been used to determine and characterize potential energy surfaces of simple organic reactions.

I-A-1 Photochemical Ring Opening Paths of Azirine — An Ab Initio GVB Energy Gradient Approach

Shigeki KATO and Keiji MOROKUMA

[*Chem. Lett.* 1021 (1981)]

The energy gradient method with the ab initio GVB wavefunction has been used to trace reaction paths of the photochemical ring opening of azirine. All the geometrical parameters have been optimized as functions of the CNC angle for the four low-lying electronic states. Based on the results, a new reaction mechanism has been suggested.

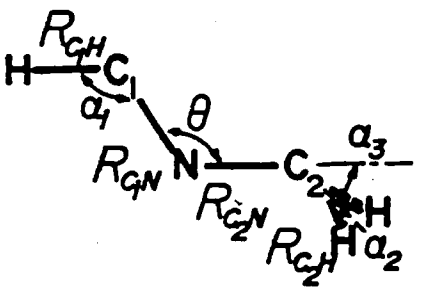

Figure 1. Geometrical parameters used. C_s assumed.

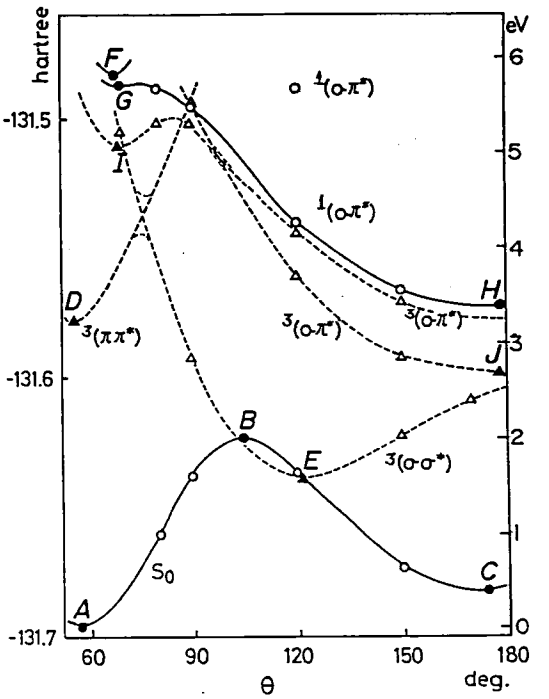

Figure 2. Energies of various states as functions of θ, with all other parameters optimized for each state. Solid and dashed lines are for singlet and triplet, respectively.

I-A-2 Potential Energy Surface of S_N2 Reaction in Gas Phase and Cluster

Keiji MOROKUMA

The S_N2 reaction is one of the most extensively studied chemical reactions in solution. The same reaction proceeds 20 orders of magnitude faster in the gas phase than in solution[1]. In the reaction (1),

$$OH^-(H_2O)_n + CH_3Br \rightarrow Br^-(H_2O)_n + CH_3OH \quad (1)$$

it has been found[2] that the reactivity of a hydroxide ion drops four orders of magnitude when the hydration number n changes from 0 to 3.

We have carried out a calculation of potential energy surfaces for a similar reaction (2).

$$Cl^-(H_2O)_n + CH_3Cl \rightarrow ClCH_3 + Cl^-(H_2O)_n \quad (2)$$

For n = 0, 1 and 2 many relevent equilibrium and saddle point geometries have been determined with the ab initio SCF energy gradient method with the 3-21G basis set. Figure 1 shows the calculated profile of potential energy surfaces.

In the reaction of an unhydrated chloride, Cl^- at first forms a complex (A) with CH_3Cl at the positively charged H_3 end and then climbs a barrier to reach the transition state (B). When Cl^- is hydrated by a water molecule, the barrier (E) is still below the energy of the reactants, $Cl^-(H_2O)$ and CH_3Cl. The structure (E) has a water molecule bridged between the two chlorine atoms forming two hydrogen bonds, transferring from one chlorine atom to the other concurrently with the CH_3 inversion. A sequential path has a slightly lower overall barrier. When $Cl^-(H_2O)_2$ is used as the reagent, we need the path connecting the strong complex (G) to the equivalent complex where the inversion took place and two water molecules transferred to the other end. A likely path is the initial transfer of one water molecule to form the complex (L) followed by the inversion through the transition state (H). The transition state (M) of the initial transfer step is yet to be determined.

Though this study is at a very preliminary stage, it is already providing a new insight into the mechanism of a chemical reaction in a cluster and, hopefully, in solution.

Reference

1) K. Tanaka, G. I. Mackay, J. D. Payzant and D.K. Bohme, *Can. J. Chem.*, **54**, 1643 (1976); W. N. Olmstead and J. I. Brauman, *J. Am. Chem. Soc.*, **99**, 4219 (1977).
2) D. K. Bohme and G. I. Mackay, *J. Am. Chem. Soc.*, **103**, 978 (1981).

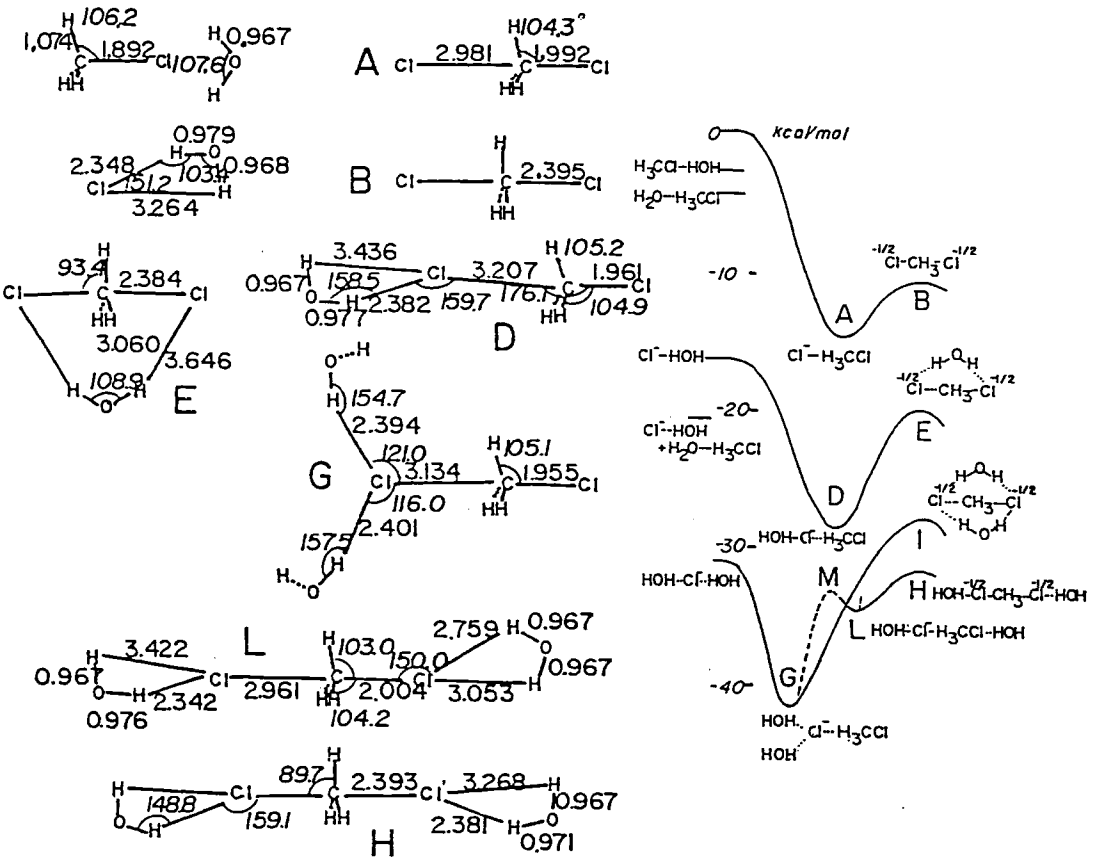

Figure 1. Some of optimized geometries and the plofile of potential energy surfaces.

I-A-3 Ab Initio MO Study on the Reactivity of the Si-C Double Bond

Mitsuyasu HANAMURA[1] **and Keiji MOROKUMA**

In an attempt to clarify the reactivity of Si-C double bond, we have carried out ab initio MO calculations for the reaction of $X_2Si = CH_2$ (X = H, F) with H_2O, a polar reagent. All calculations were carried out with split-valence 6-31G and plus polarization function 6-31G** basis set by means of the closed-shell Hartree-Fock (RHF). Geometries were full optimized by the use of the energy gradient.

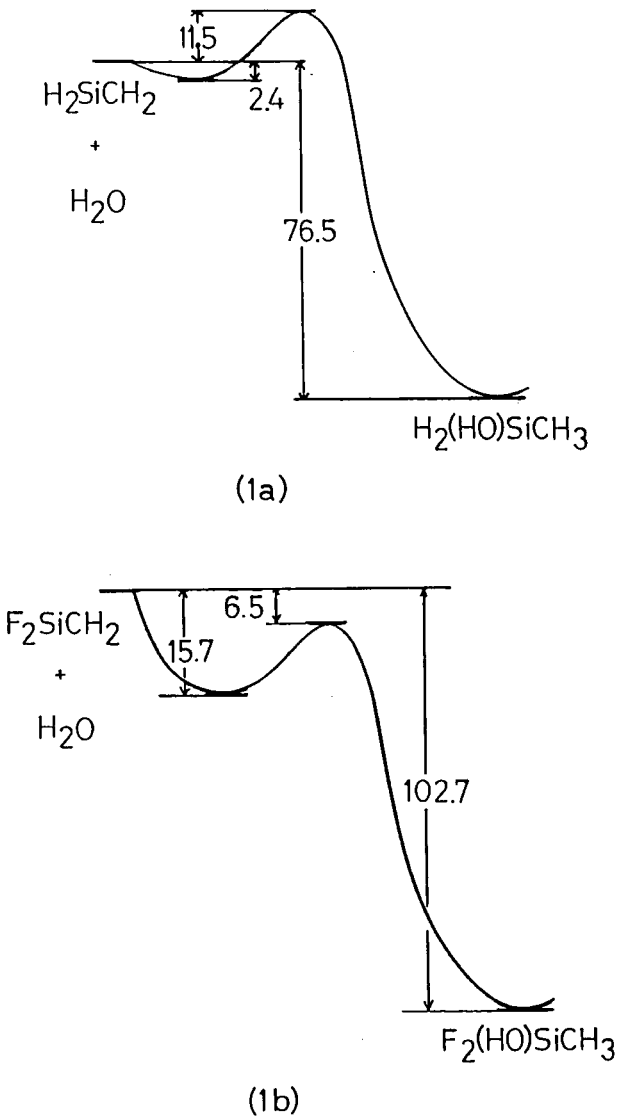

Figure 1. The energy profiles for the reaction of $X_2Si = CH_2$ (X = H; la, X = F; lb) with H_2O in the RHF method with the 6-31G** basis set at the 6-31G RHF optimized geometries.

Upon going from the reactant, $X_2Si = CH_2$ (X = H, F) + H_2O, to the final product, silanol, with a C_S symmetry constraint, we found two stationary points, an intermediate complex and a transition state (saddle point). The energy profile at the SCF level is given in Figure 1.

It is concluded that this reaction proceeds through a two-step process. First, a loose intermediate complex (due to electrostatic interaction between Si and O) is formed in the early stage without an energy barrier, and then it is transformed to the product via a four-center transition state. This process is the rate determing step for the reaction of $H_2Si = CH_2$. For $F_2Si = CH_2$, this process has the barrier lower in energy than the reactants and is not the rate-determing step.

Reference

1) IMS Graduate Student 1981—from Tohoku Univ.

I-A-4 Ab Initio MO Study on the Mechanism of Neopentyl-Type Solvolysis

Takashi ANDO,* Hiroshi Yamataka* *(*Osaka Univ.),* **Shigeru NAGASE** *(Yokohama National Univ.)* **and Keiji MOROKUMA**

Two mechanisms (concerted, k_Δ, and stepwise, k_c) have been proposed for the solvolysis of neopentyl esters. The purpose of this study is to calculate the isotope effects (IE) for both the k_Δ and the k_c process and clarify the mechanism by comparing the results with the experimental IE.[1]

The k_c and k_Δ processes were modeled by the ionization of 1-propyl alcohol to 1-propyl cation and to protonated cyclopropane, respectively. The isotope effects were calculated from the vibrational

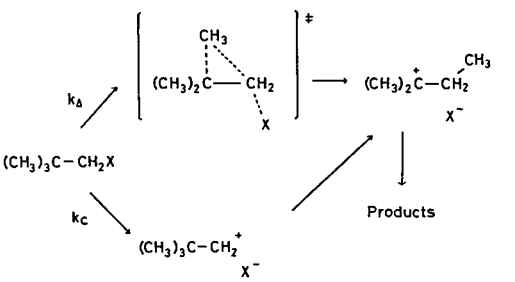

Scheme.

frequencies of these compounds which were determined by the ab initio SCF calculations with the 3-21G basis set. Table I lists the calculated IE together with the experimental values. The table shows a significant discrepancy in the γ-D_3 IE for the k_c process; a normal IE was observed while an inverse IE was calculated. On the other hand, the calculated IE for the k_Δ process are qualitatively in good agreement with the observed IE; the small differences can be reasonably explained by taking into account the contributions from the reaction-coordinate vibration which is not considered in these calculations. Thus, the present model study suggests that the titled reaction proceeds via the k_Δ process.

Table I. Calculated and Observed Isotope Effects for the Acetolysis of Neopentyl Ester at 100°C.

	IE (obsd)	IE (k_c)	IE (k_Δ)
α-^{14}C	1.073 ± 0.002	1.035	1.039
β-^{14}C	1.019 ± 0.002	1.029	1.026
γ-^{14}C	1.037 ± 0.003	1.039	1.047
α-D_2	1.187 ± 0.001	1.362	1.099
γ-D_3	1.123 ± 0.002	0.973	1.075

Reference

1) T. Ando, H. Yamataka, H. Morisaki, J. Yamawaki, J. Kuramochi and Y. Yukawa, *J. Am. Chem. Soc.*, **103**, 430 (1981).

I-A-5 Hydroboration of Substituted Olefins. The Reaction Mechanism and Directive Effects.

Shigeru NAGASE *(Yokohama National Univ.)* **and Keiji MOROKUMA**

Our previous study[1] clarified the overall reaction mechanism of the hydroboration reaction of BH_3 and C_2H_4. Our continuing interest is to see how substituents on olefins have an influence on the reaction mechanism and directive effects. For this purpose, the addition of BH_3 to CH_2=CHMe, CH_2=CHF, and CH_2=CF_2 was investigated using the ab initio SCF method with the 4-31G and 6-31G** basis sets. The stationary points on the potential energy surfaces were carefully characterized with the energy gradient technique.

As in the BH_3 + C_2H_4 reaction, the addition to CH_2=CHMe proceeds through a three-center π complex which subsequently transformed to the product via a four-center transition state. In the addition to CH_2=CHF and CH_2=CF_2, however, the formation of the π complex becomes obscure and the stabilization energy between BH_3 and CH_2=CF_2 is practically zero. Furthermore, the F substitution gives rise to an overall energy barrier two times as large as the one with the CH_3 substitution.

For all reactions examined, the anti-Markonikoff addition is found to be substatially more favarable, regardless of the electron donating or accepting characters of the substituents. Energy component analyses reveal that both electrostatic and exchange repulsion terms play an important role in the direction of addition to the F substituted olefin, while the contribution of a coupling term is significant in the addition to the CH_3 substituted olefin.

Reference

1) S. Nagase, N. K. Ray and K. Morokuma, *J. Am. Chem. Soc.*, **102**, 4536 (1980); *IMS Ann. Rev.*, 11 (1980).

I—B Problems of Molecular Structure and Molecular Interaction

The energy gradient technique in the ab initio method has found a wide range of application to problems of molecular structure and molecular interaction. For instance, the contour map of the force acting on interacting molecules can be plotted directly and used for the discussion of collision processes, as is done in B-2.

I-B-1 A Comparative Study of Ab-initio Effective Core Potential and All-Electron Calculation for Molecular Structures and Transition States

Shigeru OBARA, Kazuo KITAURA and Keiji MOROKUMA

[*Theo. Chim. Acta*, in press]

The reliability of the ab-initio effective core potential (ECP) method for calculating molecular geometries and energetics was tested for several polyatomic molecules by using the energy gradient technique.

The optimized geometries with and without the ECP were found to differ only within 0.04Å in bond lengths and 0.5 degrees in bond angles, regardless whether they are equilibrium, transition states, or 'super-saddle' points. The calculated relative energies agree within 2 kcal/mol. The ECP method reproduces the potential energy hypersurface of all-electron ab-initio method in a high degree of accuracy.

I-B-2 Ab Initio MO Approach to the Mode Selective Vibrational Excitation in Polyatomic Collision

Shigeki KATO and Keiji MOROKUMA

The energy transfer in molecular collision is of importance for the understanding of the primary process of chemical reaction. The mode selective vibrational excitation has been experimentally observed in some atom-polyatomic molecule collision systems.

In the present work, we have intended to interpret the mechanism of mode selective vibrational excitation in $CO_2 + Li^+$ collision with the use of ab initio potential energy surface. We have carried out ab initio SCF MO calculations for the collision system with the 6-31G* basis set. The forces acting on the normal coordinates were evaluated by the energy gradient method. In solving the scattering equation, the infinite order sudden (IOS) approximation has been applied for the rotational motion. The semiclassical method has been employed to treat the vibrational excitation. With the aid of physically simple representation due to the IOS approximation, we have discussed the origin of mode selectivity in polyatom − atom collisition in relation to the characteristic feature of potential energy surface.

I-B-3 Nonplanarity of π Systems. An Ab Initio Study of Norbornene and Norbornadiene

Georges WIPFF *(Univ. Strasbourg, France)* **and Keiji MOROKUMA**

[*Tetrahedron Lett.* **21**, 4445 (1980)]

The geometry of norbornene and norbornadiene fully optimized by ab initio calculations reveals the nonplanarity of the π systems. The exo addition of electrophiles on norbornene systems is analyzed in the context of nonplanarity in terms of the energy decomposition scheme.

I-B-4 Force Constants of Trans and Cis N-Methylformamide from Ab Initio SCF MO Calculations

Yoko SUGAWARA*, Akiko Y. HIRAKAWA*, Masamichi TSUBOI*, *(*Univ. of Tokyo)*, **Shigeki KATO and Keiji MOROKUMA**

[*Chem. Phys.* in press]

Ab initio SCF MO studies on the equilibrium geometries, force constants, vibrational frequencies, and dipole moment derivatives of trans and cis N-methylformamide have been carried out using the 4-31G and 4-31G* basis sets and an energy gradient method. Trans form was calculated to be 1.4 kcal/mole more stable than cis, in agreement with the experimental result. Discussions were made on the trans-cis differences in the geometry, force constants, and normal vibrations.

I—C Structure, Bonding and Reactivity of Transition Metal Complexes

The structure, bonding and reactivity of transition metal complexes became one of the most important areas of activity of our molecular quantum chemistry group. The development of the energy gradient technique with the effective core potential approximation, which was reported last year, provided an efficient means of probing potential energy surfaces of transition metal complexes. We report for the first time the fully optimized transition state for a chemical reaction involving a transition metal complex. The method has also been applied to several important systems of transition metal complexes.

I-C-1 Transition State of Oxidative Addition Reaction: $Pt(PH_3)_2 + H_2 \rightarrow Pt(H)_2(PH_3)_2$

Kazuo KITAURA, Shigeru OBARA and Keiji MOROKUMA

[*J. Am. Chem. Soc.* **103**, 2891 (1981)]

A transition state fully optimized in the ab initio method was obtained for the title reaction with the effective core potential approximation. The transition state has the C_{2v} symmetry, and its reaction coordinates consists mainly of the H_2 relative motion and the PPtP bending motion. It leads to the cis product. The calculated barrier height for the cis addition is 7 kcal/mol after the inclusion of the electron correlation. The zero-point energy correction changes the effective barrier to 8 kcal/mol. Most of the experimentally known diphosphine Pt(0) complexes have bulky phosphines as ligands. The mechanism of oxidative addition reaction is proposed that the reaction proceeds first via cis addition which is followed by the isomerization to the trans product because of the steric destabilization between bulky phosphine.

I-C-2 An Ab Initio MO Study of the CO Insertion Reaction

Shigeyoshi SAKAKI *(Kumamoto Univ.)*, **Kazuo KITAURA and Keiji MOROKUMA**

The CO insertion is one of the most important elemental processes of catalytic reactions. In this work, the CO insertion into the Pt-CH_3 bond was studied with ab initio MO method, where the effective core potential was used for core orbitals of Pt.[1] Various structures of reactants and products were optimized by using the energy gradient technique,[2] as is shown in Figure 1. The optimized bond lengths agree well with experimental values, except for the Pt-F bond length calculated to be too short. The Pt-CH_3 bond was calculated to be weaker in the isomer II than in I, due to the stronger trans-influence effect of the PH_3 ligand than the F ligand. From this result, it is suggested that the CO insertion occurs more easily from the isomer II than from I, in accord with the experimental result.[3] In the product, the structure V is most stable, and the structure III isomerizes to the structue V with little barrier. This result seems reasonable, because the actually obtained product, $[PtCl(COCH_3)(PPh_3)]_2$,[3] is considered to be easily formed from the acyl complex V.

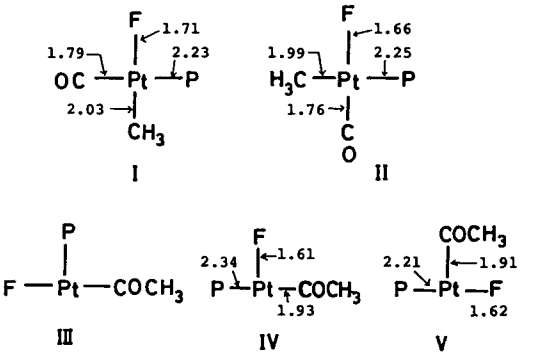

Figure 1. Examined structures of reactants and products. Numbers are optimized bond lengths. Structure III could not be optimized, for it isomerizes to V with little barrier.

References

1) H. Basch and S. Topiol, *J. Chem. Phys.*, **71**, 802 (1979).
2) K. Kitaura, S. Obara, and K. Morokuma, *Chem. Phys. Lett.*, **77**, 452 (1981).
3) G. K. Anderson and R. J. Cross, *J. Chem. Soc. Chem. Comm.*, 1978, 819.

I-C-3 Stabilities and Reactivities of Trans-$Pd(H)(C_2H_5)(PH_3)_2$. An Ab Initio MO Study.

Kazuo KITAURA and Keiji MOROKUMA

A theoretical study of the title model complex may be helpful for better understanding of stabilities and reactivities of transition-metal alkyls. We have calculated the structures of reactant, products and possible intermediates (**1-12**) involved in conceivable thermal decomposition pathways (Scheme I) of the title complex. Figure 1 shows the optimized geometries of three-coordinate hydrido-ethyl intermediates. The dissociation of PH_3 from **1** probably provides **2**. The ethyl ligand in **2** is nicely distorted for the succeeding β-hydrogen abstraction process. The complexes **3** and **4** probably undergo the reductive elimination.

Scheme I

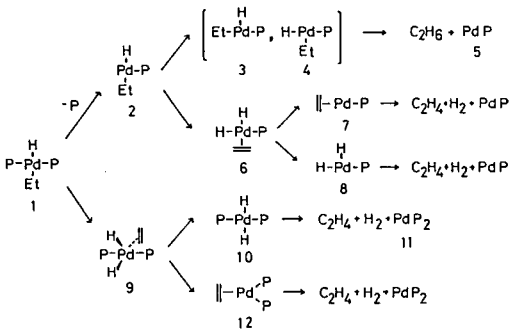

Figure 1. Optimized structures of three-coordinate hydrido-ethyl intermediates. Interatomic distances are in Å and angles in degrees. The relativistic effective core potential of Hay was used for Pd (P. J. Hay, *J. Am. Chem. Soc.*, **103**, 1390 (1981)).

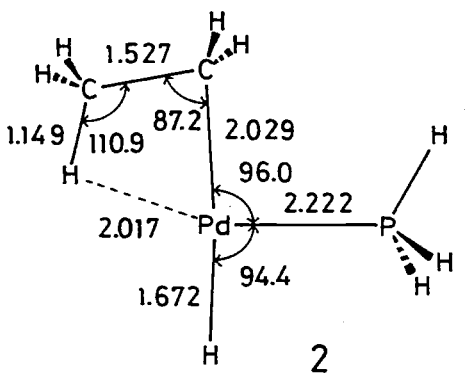

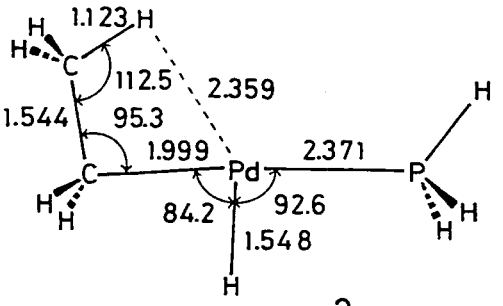

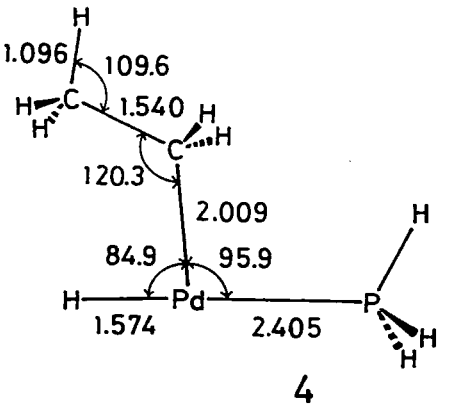

I-C-4 An Ab Initio MO Study on the Reaction Mechanism of $Co^+ + H_2$, CH_4, C_2H_4, and C_2H_6.

Shigeru OBARA, Kazuo KITAURA and Keiji MOROKUMA

We have been studying the mechanism of reactions of Co^+ ion with H_2, CH_4, C_2H_4, and C_2H_6 by the ab initio method with the effective core potential approximation. Molecular structures of reaction products $[CoH]^+$, $[CoCH_2]^+$, and $[CoCH_3]^+$ are fully optimized by the energy gradient technique in the GVB method. Calculations of relative energies are in progress. This study is intended to investigate theoretically the reaction observed in the Co^+ ion beam experiment by Beauchamp et al.[1]

References

1) P. B. Armentrout and J. L. Beauchamp, *J. Am. Chem. Soc.*, **102**, 1736 (1980).
P. B. Armentroug and J. L. Beauchamp, *ibid* **103**, 784 (1981).
P. B. Armentrout and J. L. Beauchamp, *J. Chem. Phys.*, **74**, 2819 (1981).

I-C-5 The Electronic Structure of Nickel Carbide

Kazuo KITAURA, Keiji MOROKUMA and Imre G. CSIZMADIA *(IMS and Univ. of Toronto)*

[*J. Mol. Str. THEOCHEM*, in press]

A sester (2.5) zeta basis set, which is double zeta in the inner shells and triple zeta in the valence shell, was used in the *ab initio* Generalized Valence Bond (GVB) calculations on NiC. The molecule had a closed electronic shell with a formal triple bond and two lone pairs (:Ni ≡ C:). The following structural properties were obtained by the computions: $r_e = 1.80_5$Å, $E_e = -1544.093$ hartree, $D_e = 23$ kcal/mole and $\omega_e = 1219$ cm^{-1}.

I—D Surface Electronic Strucuture of Metal Oxides and Chemisorption Mechanisms

Metal oxides provide us inexpensive and practical catalysts with a great variety of properties. They are also important as electrode materials on which many interesting electrode and photo-electrode processes take place. Though any of real reactions on surfaces proceeds through many intricate processes, their fundamental physical and chemical investigations are now becoming increasingly important.

Electronic structures of the polar surface of oxides are intensively studied this year. Our aim is to clarify the electronic origin of the structural stability and peculiar chemical reactivity of the polar surfaces. We have also studied the electronic structure of binary metal oxide catalyst ZrO_2/SiO_2, to elucidate the details of the Brönsted acid site and the mechanism of strong acidity.

I-D-1 Theory of Eelctronic Structure of the Polar ZnO Surface by the Cluster Models

Masaru TSUKADA, Eizo MIYAZAKI *(Tokyo Inst. Techn.)* **and Hirohiko ADACHI** *(Hyogo Univ. of Teacher Educ.)*

[*J. Phys. Soc. Jpn.* **50**, 3132 (1981)]

The electronic structures of the polar ZnO surfaces are investigated by the use of the DV-Xα cluster calculations. The compensating charge of about 18 ~ 28% of inner ionic charge is found to be induced on the polar surface of the cluster. The electronic origin of the charge compensation is discussed in detail. Drastic reduction of the ionic charge is revealed on the corner of the clusters, which is caused by the crossing of the surface level with the Fermi energy. Chemisorptions of oxygen and hydrogen on the ZnO polar surface are also studied by the cluster model.

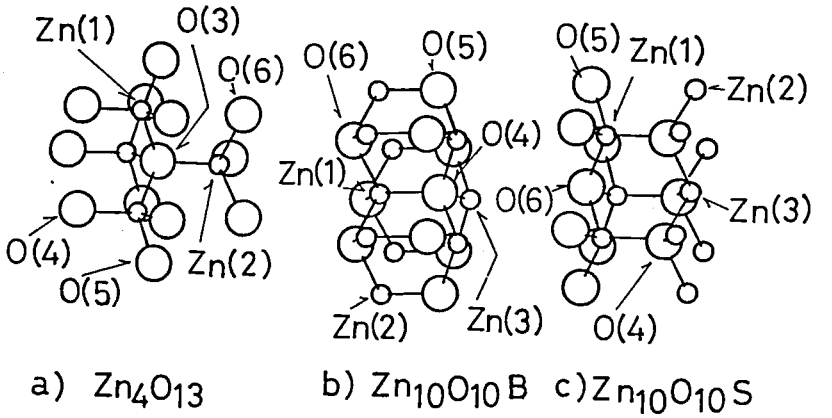

Figure 1. Structure of the clusters a) Zn_4O_{13}, b) $Zn_{10}O_{10}B$ and c) $Zn_{10}O_{10}S$ used in the present work.

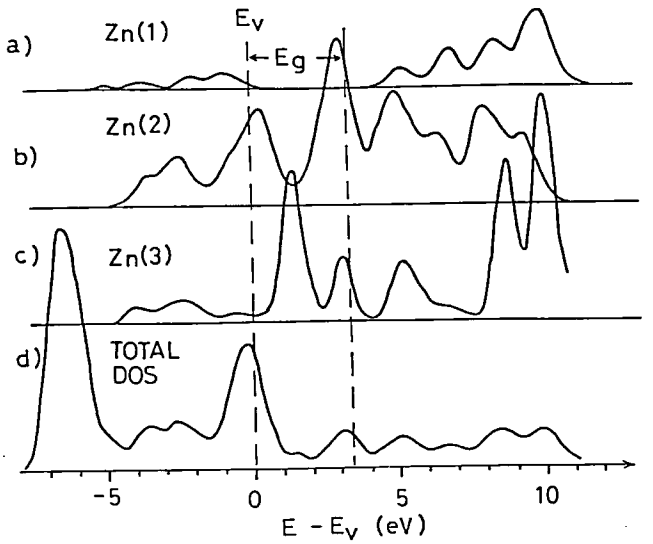

Figure 2. Partial state densities for the 4s, 4p orbital components of a) Zn(1), b) Zn(2) and c) Zn(3) ions in $Zn_{10}O_{10}S$ cluster. The total state density is shown in d).

I-D-2 Electronic Structure of Polar Surfaces: MgO(111) and TiC(111)

Masaru TSUKADA

The purpose of the present work is to study the drastic change of the electronic structure and the origin of the compensating charge on the polar surface of compound crystals. The electronic structure of MgO(111) and TiC(111) surfaces are calculated by the DV-Xα method for the model clusters $Mg_{13}O_{13}$ and $Ti_{13}C_{13}$ as shown in Figure 1.

The local electronic structure of the inner ions (O(3), Mg(5)) is almost the same as that of the bulk. On the other hand the local electronic structures of the ions on the polar surface or on the corner are quite different from those of the bulk. For example, MgO(111) surface shows metallic character (Figure 2). Mulliken charges of ions in the model clusters simulating several polar surfaces are shown in Table I. The amount of the mean compensating charge for the cluster models is close to the theoretically expected value for the infinite system.

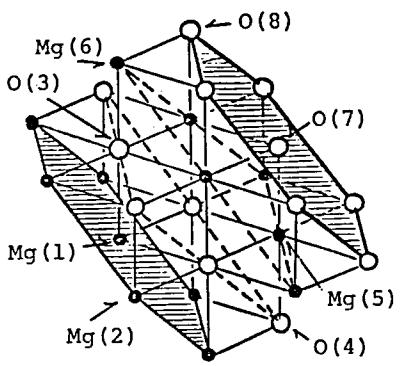

Figure 1. The structure of the model cluster $Mg_{13}O_{13}$ exposing MgO(111) polar surfaces. The same structure is assumed for $Ti_{13}O_{13}$ cluster.

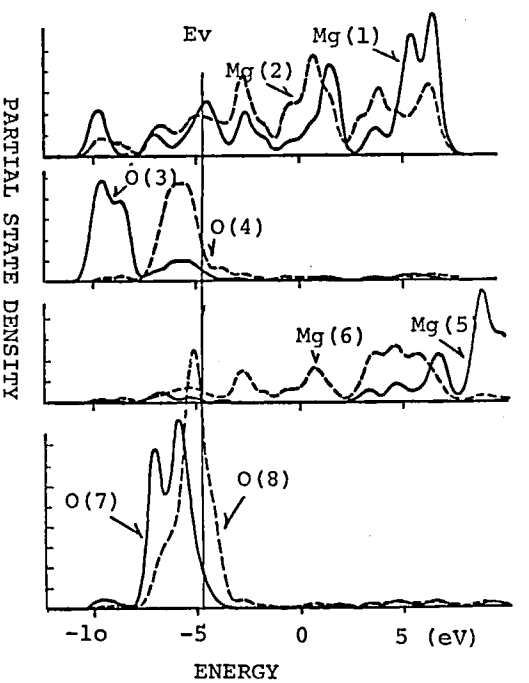

Figure 2. Partial state densities for various kind of ions in $Mg_{13}O_{13}$ cluster.

Table I. Mean net charges of bulk and surface ions for various clusters.

clusters		$Zn_{10}O_{10}B$	$Zn_{10}O_{10}S$	$Mg_{13}O_{13}$	$Ti_{13}C_{13}$
bulk	cation	1.33	1.18	1.46	1.55
	anion	−1.31	−1.16	−1.39	−1.48
surface	cation	1.07	0.97	0.63	0.73
	anion	−1.00	−0.83	−0.77	−0.76
$-\sigma_s/\sigma_b$		0.78	0.77	0.49	0.49
d/a		0.75	0.75	0.50	0.50

I-D-3 Surface Electronic Structure of Binary Metal Oxide Catalyst ZrO_2/SiO_2

Maki KAWAI *(Inst. Phys. Chem. Res.)* **and Masaru TSUKADA**

[*Surface Sci.* in press]

Surface electronic structure of binary metal oxide ZrO_2/SiO_2 was studied by means of XPS and the discrete variational (DV)-Xα cluster model calculation.

The calculated level structure for the cluster of Figure 1 and the valence band spectra obtained by XPS are shown in Figure 2. The overall level structure coincides with the experimental results.

The net charge on each atoms and the bond order between them of $ZrSi_2O_{10}H_8$ cluster and $Si_3O_{10}H_8$ cluster are shown in Table I. If we compare $Si_3O_{10}H_8$ cluster and $ZrSi_2O_{10}H_8$ cluster, the bond order between ^{6}Zr and ^{4}O became smaller from 0.26 to 0.10 when ^{6}Si was replaced by ^{6}Zr. At the same time, the bond order between ^{1}Si and the surrounding O became stronger from 0.2–0.3 to 0.4, while that of O-H remained unchanged (0.55). As for the ^{6}Zr-^{5}O-^{9}H unit, ^{6}Zr-^{5}O and ^{5}O-^{9}H are 0.21 and 0.54, respectively. It is seen that the covalent bond between Zr-O is much weaker than that between Si-O. The strength of surface Brönsted acid site is determined by the relative strength of the bond between metal-O to that between O-H. In the case of $ZrSi_2O_{10}H_8$ cluster, the bond order of ^{1}Si-^{2,3}O became 1.5 to 2 times larger than that of $Si_3O_{10}H_8$ cluster, whereas O-H bond remained unchanged. Above results provide an explanation for the appearence of strong acidic sites when SiO_2 and ZrO_2 are combined together to make binary metal oxide.

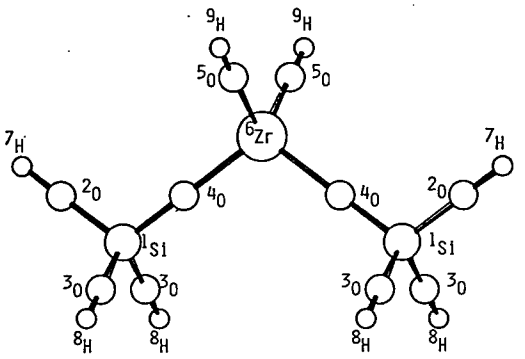

Figure 1. Structure of $ZrSi_2O_{10}H_8$ cluster. Kind of atoms are numbered on the left shoulders. The cluster $Si_3O_{10}H_8$ is obtained by the substitution of ^{6}Si for ^{6}Zr.

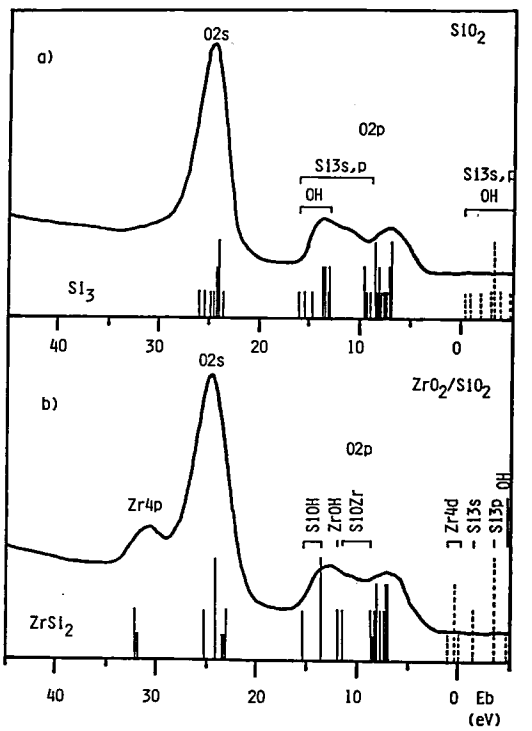

Figure 2. XPS spectra and the calculated energy levels of a) SiO_2 and b) ZrO_2/SiO_2. The energy levels which are closely located are arranged lengthwise. The assignment of each peak and the levels of the element hybridized to the main level are listed in the figure.

Table I. Calculated charge and bond order between each atoms for $Si_3O_{10}H_8$ and $ZrSi_2O_{10}H_8$ clusters.

	Mulliken charge	bond order		Mulliken charge	bond order
^{9}H	+0.56		^{9}H	+0.51	
		0.55			0.54
^{5}O	−1.28		^{5}O	−1.12	
		0.28			0.21
^{6}Si	+2.81		^{6}Zr	+2.67	
		0.26			0.10
^{4}O	−1.37		^{4}O	−1.31	
		0.20			0.44
^{1}Si	+2.61		^{1}Si	+2.59	
		0.27			0.41
^{2}O	−1.18		^{2}O	−1.21	
		0.55			0.55
^{7}H	+0.55		^{7}H	+0.55	
^{1}Si			^{1}Si		
		0.27			0.39
^{3}O	−1.20		^{3}O	−1.22	
		0.55			0.55
^{8}H	+0.56		^{8}H	+0.56	

I—E Electronic Structure of Low-Dimensional Materials

Recently a great deal of attention is concentrated on the development of new low-dimensional compounds of practical importance. Typical example may be the search of one-dimensional metals or superconductors. Intercalated compounds of graphite or other layer crystals have attracted much interest from the view point of superconductivity, catalyses, batteries and photovoltaic cells.

Reliable first principle calculations of the electronic structure is essential for the study of the properties of these materials. During the past year we performed the energy band calculation of the $NbSe_3$, which is the one-dimensional metal with a peculiar transport property.

I-E-1 Electronic Structure of $NbSe_3$

Nobuyuki SHIMA

Recently, linear chain materials, MX_3 (M is a transition metal and X is a charcogenide), have aroused much interest because of their unusual transport properties. $NbSe_3$, one of MX_3 materials, exhibits one-dimensional metallic condactance. Especially, its resistivity shows two giant peaks at T_1 = 142K and T_2 = 58K. These two peaks indicate two independent charge density wave (CDW) phase transitions.[1] A mechanism of CDW transition is strongly dependent on an electronic structure, especially on a shape of a Fermi surface. But there has been no self-consistent band calculation of $NbSe_3$ until now.

A band calculation is carried out by an LCAO-Xα method. The resulting band structure, and Fermi surfaces are shown in Figure 1-2. There are five conduction bands made of dz^2 orbitals of Nb atoms. And consequently there exist five pairs of Fermi surfaces. The fact that each Fermi surface except the most inside one is pretty flat suggests two independent nesting mechanisms that cause the two independent CDW transitions. Since the most inside Fermi surface is rather warped one, it is supposed that only this Fermi surface survives after the two CDW phase transitions. This conjecture can explain the experiments of heat capacity and magnetic resistivity qualitatively. We are now

calculating some physical properties of $NbSe_3$ and relativistic effects on the band structure.

Reference

1) N. P. Ong and P. Monceau, *Phys. Rev.*, **B16** 3443 (1977).

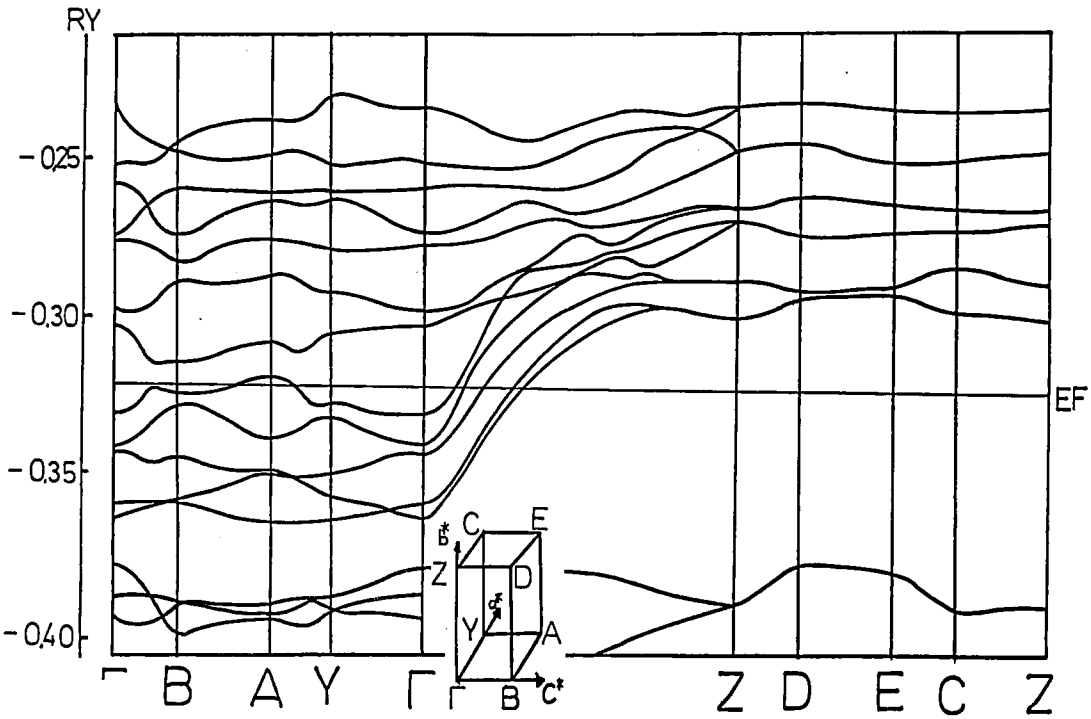

Figure 1. Energy band structure of $NbSe_3$.

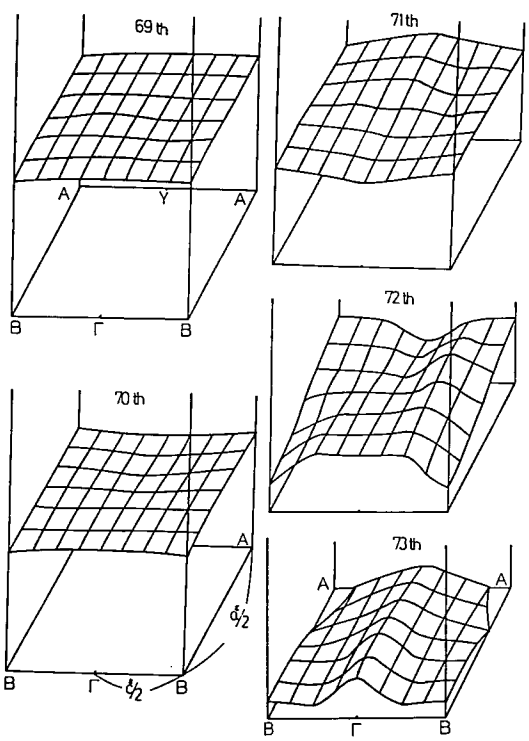

Figure 2. Fermi surfaces of $NbSe_3$.

I—F Theory of Semiconductor Surfaces

Physical and chemical properties of covalent semiconductor surfaces are quite different from those of metals or ionic crystals. Especially surface reconstruction is generally observed, which is closely related with the presence of the dangling bonds. Study of the surface atomic structure based on the electronic theory is indispensable for the elucidation of the various properties of the covalent semiconductor surfaces. Moreover the chemisorption mechanisms are closely related with the electronic and the atomic structure of the surfaces. The DV-Xα cluster method, the chemical pseudopotential method and the self-consistent empirical pseudopotential band calculation are applied for the Si(111) surfaces, to give a theoretical support for the proposed vacancy model of the 7 × 7 reconstruction.

I-F-1 Electronic Structure of Chlorine Covered Si(111) 7 × 7 Surface by the Cluster Method

Toshiharu HOSHINO and Masaru TSUKADA

[*Solid State Commun.* **38**, 231 (1981)]

Electronic Structure of Cl covered Si(111) 7 × 7 surface is calculated on the basis of the first principle DV-Xα cluster method. Two typical reconstruction models of the Si(111) 7 × 7 surface, i.e. the buckled and the vacancy models, are investigated in detail. The vacancy model, where two chemisorption sites of onefold and threefold coordinated geometries coexist, can explain the polarization dependence of the recent ultraviolet photoemission spectroscopy (UPS) results. The calculated results[1] of Si(111)/H, Ag will be also published in the near future.

Reference

1) T. Hoshino and M. Tsukada, *Surf. Sci.*, in press.

I-F-2 Electronic Structure of Vacancy and Chemisorptive Bond on Si(111) Surface by the DV-Xα Cluster Calculation

Masaru Tsukada and Toshiharu Hoshino

[*Intern. J. Quantum Chem., in press*]

The electronic structure of the Si(111) surface is investigated by the first principle DV (Discrete-Variational)-Xα method with the use of several model clusters such as $Si_{13,12}H_{15}$, $Si_{16}H_{21}$ and $Si_{19}H_{21}$. Chemisorptions of H, Cl and Ag on the Si(111) surface are also studied. The characteristics in the electronic structure are clarified in detail which are closely related with surface atomic arrangements and chemisorption geometries. The present calculation shows that the surface vacancy is essential to give the electronic structure which corresponds well with the observed UPS on the Si(111) 7 × 7 surface. Further, for Si(111)/Ag system it is elucidated that Ag atom is chemisorbed on top of Si atom at the low temperature phase.

I-F-3 Electronic Structure of Si(111) $\sqrt{3} \times \sqrt{3}$/Ag

Toshiharu HOSHINO and Masaru TSUKADA

On the atomic structure of Si (111) $\sqrt{3} \times \sqrt{3}$/Ag at high temperatures, the numerous distinct models[1] have been proposed so far. They have a common feature in that Ag atoms ride on the surface site. Recently, however, studying low energy ion scattering spectroscopy Saitoh et al[2] have derived a new model in which Ag atoms are embedded below the topmost Si layer. This model is also supported from analyses of low energy electron diffraction by the constant momentum transfer average method (LEED/CMTA)[3]. The purpose of the present paper is to investigate the electronic structures of the various models. We calculate the electronic structures for the specific atomic arrangements by the DV-Xα cluster method[4] and compare these results with the UPS data[5]. In the present work, $Si_{13}H_{15}Ag_{3,7}$ clusters (Figure 1) are used to simulate the semi-

infinite system Si(111) $\sqrt{3} \times \sqrt{3}$/Ag.

For example, the total and local densities for the embedded model cluster $Si_{13}H_{15}Ag_3$ are shown in Figure 2. There are double peaks (A) and a single peak (B), respectively, at −6 eV and −2 eV below the Fermi level. The direction of the back bond corresponding to the peak B is opposite to that of the back bond for the clean surface. These results agree with angle-resolved UPS data.[5] We have also found that any other model cannot explain the threefold azimuthal dependence of UPS. We now plan to investigate the electronic structure of metal-semiconductor interface.

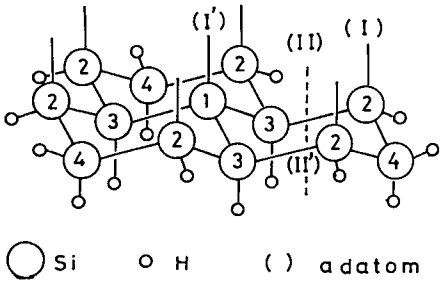

Figrue 1. Substrate cluster $Si_{13}H_{15}$ and the four chemisorption sites (I), (I'), (II) and (II') are shown.

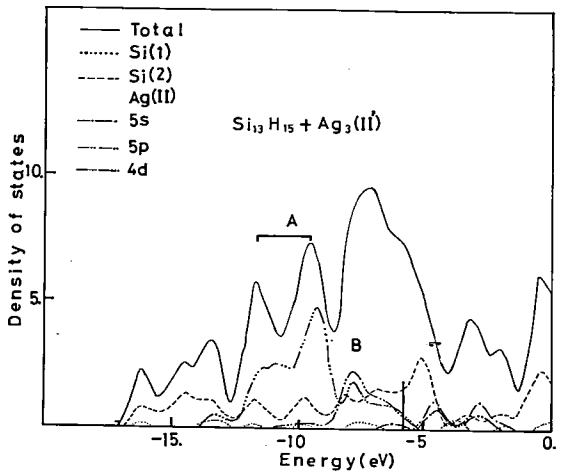

Figure 2. Total and local densities for the embedded surface cluster $Si_{13}H_{15}$ + Ag_3 (II') where Ag atoms are situated just at the middle of 1st and 2nd layers. The vertical line indicates the Fermi (highest occupied) level.

References

1) K. Spigel, *Surf. Sci.*, **7**, 125 (1967); G Lelay, G. Quentel, J. P. Faurie and A. Masson, *Thin Solid Films*, **35**, 273 (1976); F. Wehking, H. Beckermann and R. Niedermayer, *Surf. Sci.*, **71**, 364 (1978).
2) M. Saitoh, F. Shoji, K. Oura and T. Hanawa, *Jpn. J. Appl. Phys.*, **19**, L421 (1980).
3) Y. Terada, T. Yoshizuka, K. Oura and T. Hanawa, *Jpn. J. Appl. Phys.*, **20**, L333 (1981).
4) H. Adachi, M. Tsukada and C. Satoko, *J. Phys. Soc. Jpn.*, **45**, 875 (1978).
5) G. V. Hansson, R. Z. Bachrach and R. S. Bauer, *J. Phys. Soc. Jpn.*, **49** (1980) Suppl. A. p.1043.

I-F-4 Formation Energy of Vacancies on Si (111) Surface

Toshiharu HOSHINO and Masaru TSUKADA

The Si(111) surfaces show two different structures at room temperature: Si(111) 2 × 1 and Si(111) 7 × 7 reconstructed surfaces.[1] The 2 × 1 structure which is observed after cleavage is metastable and irreversibly converts to the stable 7 × 7 structure during anneals at elevated temperatures. For the Si(111) 2 × 1 surface, the Haneman model with alternate rows of raised and lowred atoms in the topmost layer is commonly accepted and its microscopic mechanism is elucidated theoretically.[2] For the Si(111) 7 × 7 surface, however, there is no decisive model although the vacancy model has been supported indirectly from the comparison between the theoretical calculation[3] of electronic structure and the observed UPS data. The purpose of the present paper is to propose a model for the formation of vacancies on Si(111) surface and to estimate the formation energy, based on chemical pseudopotential method.[2] The computation program in ref. 2 is revised on the following two points: (1) the analytic functions (Slater or Gaussian) are used to expand the atomic orbitals. (2) the integration over the Wigner-Seitz cell is performed by the Haselgrove method.[4]

It is known from many experiments that there are steps on Si(111) surface (Figure 1). We may consider the movement of Si atom from site A to site B of step edge which have the feature of Si(001) surface. The atomic movement forms a single vacancy on Si(111) surface. If we take into account the displacement of Si atoms around the vacancy, the formation energy becomes ~ −1.0eV per surface atom (energy gain). The interaction of vacancies on triangular sites[5] would further contribute to the stabilization energy.

References

1) W. Mönch, *Surf. Sci.*, **63**, 79 (1977).
2) K. Suzuki and T. Hoshino, *J. Phys. Soc. Jpn.*, **49** (1980) Suppl. A p.1055.
3) K. Nakamura, T. Hoshino, M. Tsukada, S. Ohnishi and S. Sugano, *J. Phys.*, **C14**, 2165 (1981); T. Hoshino and M. Tsukada, *Solid State Commun.*, **38**, 231 (1981); M. Tsukada and T. Hoshino, *Intern. J. Quantum. Chem.*, in press.
4) C. B. Haselgrove, *Math. Comp.*, **15**, 323 (1961).
5) S. Ino, *Jpn. J. Appl. Phys.*, **19**, 1277 (1980).

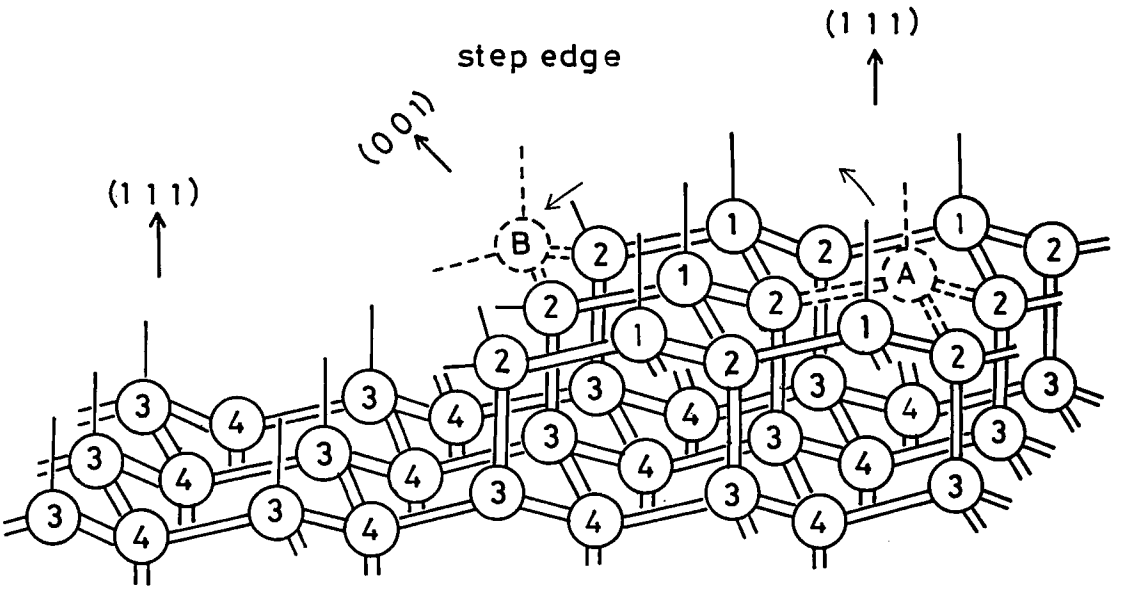

Figure 1. Step of Si(111) surface. The step edge has the feature of Si(001) surface.

I-F-5 Electronic Structure of the Si(111) Surface with Vacancies by the Pseudopotential Band Calculation

Hideo NAGAYOSHI *(Osaka Univ.)* **and Masaru TSUKADA**

No complete understanding of the atomic and electronic structure of the 7 × 7 reconstructed Si(111) surface has been obtained yet. The purpose of this work is to make clear theoretically what characteristics are introduced in the electronic structure by the vacancies in the top atomic layer of Si(111) surfaces and to check the validity of the vacancy model in explaining the experimental results reported on the 7 × 7 surface.

Self-consistent energy band calculations with a parametrized ion-core pseudopotential and the Slater's $X\alpha$ approximation are done[1] for the simplest vacancy model which has $\sqrt{3} \times \sqrt{3}$ periodicity and contains 33% vacancies in the top layer. Instead of the semi-infinite model we employ the super-lattice structure of 12 layer slabs and empty regions whose thickness is three times the Si-Si bond length.

Figure 1 shows the energy band structure in the fundamental gap region. There are 10 surface state bands in this region, which is consistent with the dangling bond picture. Four empty surface bands in the upper part of the gap are the characteristics of our results. They support the suggestion of the photovoltage experiment by Clabes and Henzler.[2] Calculated surface density of states is shown in Figure 2. As for the peak positions our results are consistent with the photoemission spectra experimentally obtained. Calculations for the system with relaxation of the top layer atoms are also done. The results show that the position of resonance like $d_{//}$ bands is sensitive to relaxation, which is consistent with the recent cluster calculations.[3]

References

1) M. Schlüter, J. R. Chelikowski, S. G. Louie and M. L. Cohen, *Phys. Rev.*, **B12**, 4200 (1975).
2) J. Clabes and M. Henzler, *Phys. Rev.*, **B21**, 625 (1980).
3) K. Nakamura, T. Hoshino, M. Tsukada, S. Ohnishi and S. Sugano, *J. Phys.*, **C14**, 2165 (1981).

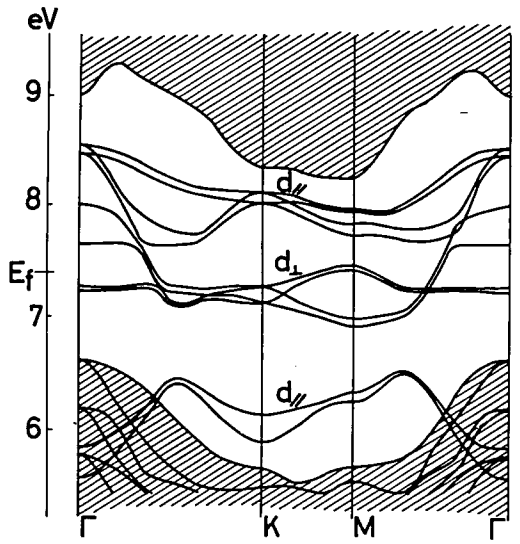

Figure 1. Eenrgy band structure of the Si(111) surface with vacancies in $\sqrt{3} \times \sqrt{3}$ period.

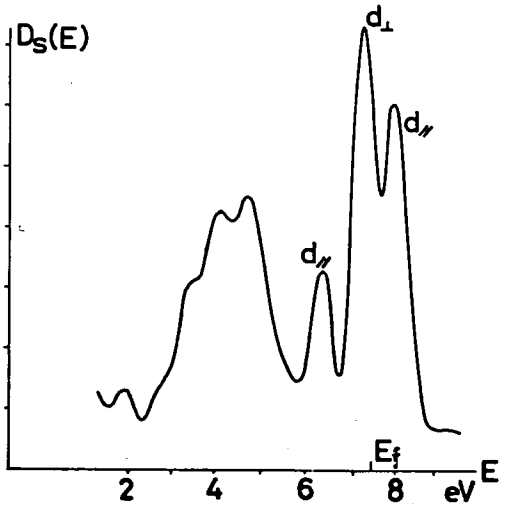

Figure 2. Surface density of states calculated from Figure 1.

I—G Development and Application of the LCAO-Xα Direct Fore Calculation Method

An energy gradient method is developed for the LCAO-Xα scheme, which is quite convenient for the numerical calculations of forces acting on each ions in the cluster. This method is applied for various problems including chemisorption systems.

I-G-1 Direct Force calculation in the LCAO-Xα Method

Chikatoshi SATOKO

[*Chem. Phys. Lett*, **83**, 111 (1981)]

A direct force calculation method provides a powerful tool for thoretical studies of molecules or surface geometries. Chemical insights into the interaction between the atoms are also gained by a study of the change in the force along the reaction path.

The direc force acting on the μ-th atom is given by the minus derivative of the total energy with respect to the μ-th nuclear coordinate. The force can be decomposed into the effective pair forces between the atoms:

$$F_\mu = \sum_\tau f_\mu^\tau. \qquad (1)$$

The force due to the τ-th atom, f_μ^τ , is parted into three terms. The first term is the electrostatic force between the electronic charge and the nuclear charge of the μ-th and τ-th atoms. The second term is the force due to the derivative of their wave functions with respect to the nuclear coordinate. The third term is due to the Xα exchange correlation potential.

We have written a program to calculate the force in the LCAO-Xα theory. The decomposed forces are calculated using the self-consistent wave functions. The HFS and force matrix elements are numerically evaluated by the quadrature method.[1)]

We are applying this force analysis to the study of the equilibrium geometry of the surface atom, the adsorbed atom and the atoms around the defect in the bulk or on the surface.

Reference

1) A. H. Strout, Approximate Calculations of Multiple Integrals (prentice-Hull, Englewood Cliffs, New Jersey, 1971).

I-G-2 Oxygen Chemisorption on the Al(111) and Mg(0001) Surfaces

Chikatoshi SATOKO

Oxidation process on metal surfaces has been studied by many experimetnal methods. The oxygen molecules are chemisorbed dissociatively on most metal surfaces. The dissociated atoms form a superlattice structure on the surface or are incorporated into the surface. The chemisorption of O_2 on Al and Mg surface causes the emission of photons or electrons at much lower pressure.[1] The dissociated oxygen atoms on Al(111) surface are chemisorbed in the threefold centered hollow site,[2] while the oxygen atoms on Mg(0001) are absorbed in the surface lattice plane.[3] To understand these chemisorption process, we have calculated the forces as a function of the position of the oxygen atom above or below the surface plane.

The calculated results of the force acting on the atoms and the potential curve for the Al(111) surface have been published in Chem. Phys. Letters.[4] In this report we present in Figure 1 the pair force between the atoms defined by equation 1 of the preceding section. The equilibrium position (R_h = 1.0 a.u.) of the oxygen atom above the Al surface is at the balance point between the attractive force, $f_o^{Al(1)}$, and the repulsive force, $f_o^{Al(2)}$ The activation energy of the oxygen penetration of the surface is due to the more repulsive force with the second layer Al(2) than the attractive force with the first layer Al(1). On the other hand there is no activation energy of the oxygen for Mg(0001) surface, for the interaction between the oxygen and the second layer Mg(2) is attractive.

References

1) B. Kasemo, E. Törnqvist, J. K. Nørskov and B. I. Lundqvist, *Surface Sci.*, **89**, 554 (1979).
2) C. W. B. Martinson and S. A. Flodström, *Solid State Commun.*, **30**, 671 (1979).
3) H. Namba, J. Darville and J. M. Gilles, *Surface Sci.*, **108**, 446 (1979).
4) C. Satoko, *Chem. Phys. Lett.*, **83**, 111 (1981).

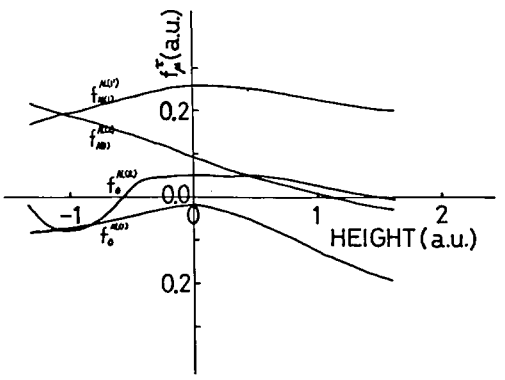

Figure 1. The calculated forces, f_μ^τ , acting on the μ-th atom due to the τ-th atom as a function of the height of the chemisorbed oxygen atom. The Al(1) and Al(2) are the first layer and second layer aliminums, respectively. The $f_{Al(1)}^{Al(1)}$ is the force between the first layer Al atoms.

I-G-3 Dissociative Chemisorption of Hydrogen on Metals

Chikatoshi SATOKO and Masaru TSUKADA

Theoretical studies of the hydrogen chemisorption on matals have been done by many theoretical methods such as EH, VB, SCF, MCSCF and jellium methods. It has been shown in the jellium model that the dissociation of hydrogen molecule on simple metal occurs more favourable for the high density than for the low density.[1] The jellium model is not a good approximation in the case of the strong coupling chemisorption. On the other hand the ab-initio calculations have been done for the chemisorption on transition metal such as Ni and Cu.[2] They conclude that the 4s electrons contribute to the formation of the chemisorption bond with the H atom and the 3d electrons don't contribute. The 3d electrons remain localized on the each transition metal because of the strong intra-atomic Coulomb interaction. However, it is questionable whether 3d electrons of the solid surface have such a strong Coulomb interaction as the electrons of the free atom.

We are studying the chemisorption process of the hydrogen molecule using the force calculation in the LCAO-Xα method. We calculate the Ni_2H_2 and Cu_2H_2 molecules of the same trapezoidal geometry with earlier calculations.[2] The calculated results of orbital energy levels for the Ni_2H_2 are shown in Figure 1. Some of the electrons are exchanged

between the Ni and H atoms along the reaction path of the elongatin of the hydrogen bond parallel to the surface. The electrons belonging to the a_1 symmetry are transferred from the hydrogen atom to the nickel atoms. The electrons belonging to the b_2 symmetry are transferred in the opposite direction. However, there is no orbital conversion between the occupied and unoccupied levels. The activation barrier is obtained as about a few eV so that the dissociation of the hydrogen along this path doesn't occur. For the Cu_2H_2 molecule the orbitals between the occupied a_1 and unoccupied b_2 orbital reverse at 2.0 bohr of the hydrogen bond length.

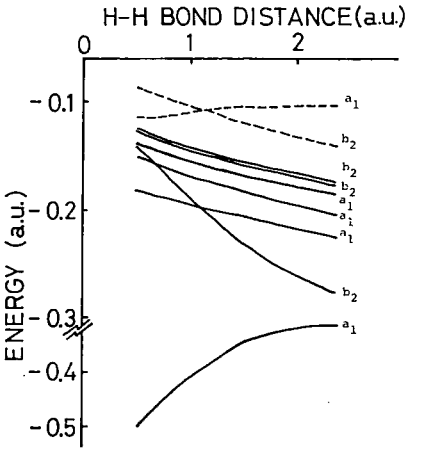

Figure 1. Orbital energy curves of the Ni_2H_2 molecular complex as a function of the H-H bond length. The orbitals belonging to the a_2 and b_1 symmetry are omitted in this figure. The unoccupied orbitals are indicated by dashed lines. The Ni-Ni bond length is 2.49 A while the height is 1.48 A.

References

1) P. K. Johansson, *Surface Sci.*, **104**, 510 (1981).
2) C. F. Melius, J. W. Moskowitz, A. P. Mortola, M. B. Baillie, and M. A. Ratner, *Surface Sci.*, **59**, 279 (1976).

I—H Dynamial Theory of Gas-Surface Interaction

We started from this year theoretical study of dynamical interactions of atoms and molecules on solid surface. Even their fundamental aspects, especially for chemisorption systems with or without non-adiabatic processes remain unsolved in spite of great interests from various research fields.

Our present target should be the elucidation of the basic mechanisms of the dynamical behaviour, rather than detailed calculation of the individual potential energy surface.

I-H-1 Dynamical Theory of Chemisorption with Non-Adiabatic Processes

Masaru TSUKADA

Theory based on a single adiabatic potential energy surface cannot describe dynamical processes of dissociative chemisorption or chemisorption with a large change in the adsorbate charge. Such processes should be studied by means of the motion over the many potential energy surfaces corresponding to different electronic states. The transition probability between the potential energy surfaces and energy dissipation during the transition are very important for the gas/surface dynamical interactions.

We study the time evolution of the adsorbate electronic state near the crossing region of the potential energy surfaces. A simple model Hamiltonian is assumed which includes stochastic interactions due to the many electron-hole pair excitation or phonon excitation on the surface. The equation of motion corresponding to the Hamiltonian is numerically integrated by the stochastic trajectory method and the transition probability and the energy dissipation are statistically determined.

I—I Theoretical Study of Molecular Ionic and Excited States

The ab initio CI programs, called EFCI, were improved and applied to studying the ionic and excited states of molecules. In particular, the calculations were carried out in close collaborations with the spectroscopists.

I-I-1 Configuration Interaction Assignments of He(I) Photoelectron Spectra

Suehiro IWATA[1] *(Inst. Phys. Chem. Res. and IMS)*

[partly in "Handbook of HeI Photoelectron Spectra of fundamental Organic Molecules". See also IV-I-1]

In order to compile He(I) photoelectron spectra of 200 fundamental organic molecules in a handbook together with theoretical assignments, we have recently carried out ab initio configuration interaction (CI) calculations of ionic states for more than 50 basic molecules.

The results obtained from the CI calculations are generally sensitive both to the molecular orbitals used and to the way of generating the electron configurations in the expansion. The molecular orbitals are determined by a new method which is described in the following subsection.

In the present work, five levels of CI calculations, CI-I to CI-V, have been examined for small molecules. The CI-I and CI-II levels have been used for most of the molecules studied. Several trends are found by comparing the CI ionization energies with the experimental ones. The overall agreement is less than 0.5 eV, and the assignments of the photoelectron spectra can be helped by the CI calculations. It is found that the calculation often underestimates the ionization energy for the lone pair type orbital by about 1 eV.

Reference

1) IMS Adjunct Associate Professor for 1979—1981. Present address: Keio Univ., Yokohama.

I-I-2 Double Breakdown of Koopmans' Theorem and Strong Correlation Satellites in the He II Photoelectron Spectrum of O_3

Nobuhiro KOSUGI,* Haruo KURODA* *(Univ. of Tokyo)* **and Suehiro IWATA**[1] *(Inst. Phys. Chem. Res. and IMS)*

[*Chem. Phys.* **58**, 267 (1981)]

Because of the biradical nature of the ground state of O_3 and the presence of some lone-pair orbitals, it is necessary to take into account both the initial-state and final-ionic-state configuration interaction (ISCI and FISCI) effects in analyzing the photoelectron spectrum (PES) of O_3. The disagreement concerning both experimental and theoretical assignments of the second and third states of O_3^+ is resolved by performing nearly full-valence CI calculations with the minimal basis set. The third ionized state is identified with the $^2A_2$ state which is described mainly by the ionization from the highest occupied molecular orbital la_2; Koopman's theorem is doubly broken. In addition, the complicated structures observed below 22 eV in the He II PE are discussed in terms of ISCI and FISCI.

Reference

1) IMS Adjunct Associate Professor for 1979—1981. Present address: Keio Univ., Yokohama.

I-I-3 Valence Type Vacant Orbitals for Configuration Interaction Calculations

Suehiro IWATA[1] *(Inst. Phys. Chem. Res. and IMS)*

[*Chem. Phys. Lett.* **83**, 134 (1981)]

A method is proposed to determine the valence

type vacant orbitals, which are suitable for CI calculations and for the initial guess orbitals in MCSCF calculations. The method was applied to calculate the ionization energies of series of molecules and to draw the potential energy curves of various states on N_2 and N_2^+.

Reference

1) IMS Adjunct Associate Professor for 1979—1981. Present address: Keio Univ., Yohohama.

I-I-4 Photoionization Mass Spectrometric Study of Acetylene in the VUV Region

Tatsuji HAYAISHI*, Suehiro IWATA[1)] *(Inst. Phys. Chem. Res. and IMS)*, **Michio SASANUMA**, Eiji ISHIGURO**** *(Osaka City Univ.)*, **Yumio MORIOKA**, Yoshiro IIDA*, and Masatoshi NAKAMURA*** *(Univ. of Tsukuba)*

[*J. Phys. B.* in press]

Photoionization mass spectroscopic measurements on acetylene have been made between 1100 Å and 400 Å by using synchrotron radiation as a light source. Photoionization efficiency curves are obtained for molecular ion $C_2H_2^+$, and also for fragment ions C_2H^+, C_2^+, CH_2^+ and CH^+. To assign the structures of $C_2H_2^+$, ab initio calculations have been performed for excitation from the second ($3\sigma_g$) and third ($2\sigma_u$) occupied molecular orbitals. Two broad maxima at 930 Å and 810 Å between the first and second ionization thresholds are assigned to the autoionisation from valence type excited states, which can be called shape resonance. And also new Rydberg series ($np\pi_u$) converging to the second ionisation threshold is found. The appearance potentials of fragment ions by photoexcitation are given and discussed in terms of the heats of formation of molecular ions. For each of C_2^+ and CH^+, two values of the appearance potential are obtained from a double step structure. The maximum heat of formation of C_2^+ is estimated to 1980 kJ/mole from the appearance potential.

Reference

1) IMS Adjunct Associate Professor for 1979—1981. Present address: Keio Unov., Yokohama.

I—J The Analysis of the Electron Distribution in Molecules

The ab initio method is a quantitative technique in nature. Besides, it can provide the qualitative picture of the chemical bonds and of the electron distribution in molecules. In addition to the traditional ways such as the Mulliken population anaylsis and the electron density map, a new method to see the electron distribution in molecules is developed. The change of the electron distribution around an atom in molecules with various oxidation numbers and with the excited states is examined.

I-J-1 Electron Distribution of Sulfur and Chlorine Compounds with Various Oxidation Numbers

Keiko YAMADA,* Haruo HOSOYA* *(Ochanomizu Univ.)* **and Suehiro IWATA[1)]** *(Inst. Phys. Chem. Res. and IMS)*

[*J. Am. Chem. Soc.* in press]

The electron distribution around sulfur and chlorine atoms in molecules was analyzed in detail with the ab initio molecular orbital calculations. The number of electrons N(R) and averaged electron density $\rho_0(R)$ in a sphere with radius R at a sulfur or chlorine atom were calculated, and the changes $\Delta N(R)$ and $\Delta\rho_0(R)$ from the sum of the component atoms were also examined. N(R), $\rho_0(R)$, $\Delta N(R)$, and $\Delta\rho_0(R)$ were plotted against R. Their dependencies on the oxidation number of atoms were studied. It was found that the change $\Delta\rho_0(R)$ is linear to the oxidation number. This result was confirmed by checking the basis set dependency, i.e., by use of STO-3G, STO-6G, 4-31G, and 4-31G** functions.

Reference

1) IMS Adjunct Associate Professor 1979—1981. Present address: Keio Univ., Yokohama.

RESEARCH ACTIVITIES II
Department of Molecular Structure

II—A High Resolution Spectroscopy of Transient Molecules

During the course of chemical reactions many transient molecules appear as intermediates. However, because of their high reactivities (i.e. short lifetimes), the knowledge on these transients is still very much limited. Many of them have open-shell electronic structures, which characterize such species as free radicals and cause splittings in their high-resolution spectra because of fine structure and/or hyperfine structure interactions of unpaired electrons. Analyses of these structures provide us with information on the electronic properties of molecules which is not obtainable for molecules without unpaired electrons. High resolution spectroscopy not only provides molecular constants of transient molecules at very high precision, but also allows us to unambiguously identify such species in chemical reaction systems and to unravel the details of reaction mechanisms. The present project will also be of some significance in related fields such as astrophysics and environmental researches.

II-A-1 Diode Laser Spectroscopy of the BO_2 ν_2 Fundamental Band

Kentarou KAWAGUCHI and Eizi HIROTA

The BO_2 radical has been well known as a classical example showing the Renner-Teller effect in its spectrum. It has been investigated in detail by electronic absorption and emission spectroscopy.[1] However, because of selection rules, the two fundamental states, (0,1,0) and (0,0,1), could not have been located in the ground electronic state by direct spectroscopic observations. We have recently observed the ν_3 band by diode laser spectroscopy.[2] Although our observation included a hot band from the (0,1,0) state as well, the transitions we observed were limited to F_1 - F_1 and F_2 - F_2 types, and the spin uncoupling constants which were derived were subjected to rather large uncertainties. We thus extended our measurements to the ν_2 fundamental band.

Because diodes are available in the region above 580 cm^{-1}, only the $(0,1,0)\kappa^2\Sigma \leftarrow (0,0,0)^2\Pi_{3/2}$ transition has so far been observed. By combining the data on the $(0,1,1)\kappa^2\Sigma \leftarrow (0,1,0)\kappa^2\Sigma$ transition obtained in Ref. 2), we redetermined molecular constants for the $(0,1,0)\kappa^2\Sigma$ and $(0,1,1)\kappa^2\Sigma$ states, as shown in Table I. The spin uncoupling constants for the $\kappa^2\Sigma$ states have thus been improved in precision by a factor of 15 to 17, establishing an increase in the constant with the ν_3 excitation. The observed values of γ^κ and $\gamma_D{}^\kappa$ listed in Table I were explained by rovibronic interactions.

Table I. Molecular Constants of $^{11}BO_2$ in the $(0,1,0)\kappa^2\Sigma$ and $(0,1,1)\kappa^2\Sigma$ States (cm^{-1})[a]

Constant	$(0,1,0)\kappa^2\Sigma$	$(0,1,1)\kappa^2\Sigma$
B	0.330 376 96(69)	0.326 778 2(87)
$D \times 10^7$	1.326(80)	1.312(94)
γ^κ	0.153 48(17)	0.167 38(19)
$\gamma_D{}^\kappa \times 10^7$	−5.92(77)	−7.57(80)
ν_0 $[(0,1,0)\kappa^2\Sigma \leftarrow (0,0,0)^2\Pi_{3/2}]$		633.804 9(9)
ν_0 $[(0,1,1)\kappa^2\Sigma \leftarrow (0,1,0)\kappa^2\Sigma]$		1268.818 5(8)

a. Values in parentheses denote three standard deviations and apply to the last digits of the constants. The ground-state parameters were fixed to the values of Ref. 2).

References

1) J. W. C. Johns, *Canad. J. Phys.*, **39**, 1738 (1961).
2) K. Kawaguchi, E. Hirota, and C. Yamada, *Mol. Phys.*, **44**, 509 (1981).

II-A-2 Dye Laser Excitation Spectroscopy of the Deuterated Fluorocarbene DCF

Tetsuo SUZUKI, Shuji SAITO, and Eizi HIROTA

[*J. Mol. Spectrosc.*, in press]

Fluorocarbene is one of the simplest carbenes. Because of important role the carbene is playing in the field of chemical reaction, we are carrying out a systematic study on simple carbenes using high resolution spectroscopy. The $\tilde{A}^1A''(0,0,0) \leftarrow \tilde{X}^1A'(0,0,0)$ vibronic transition of HCF has been investigated in detail in a previous paper.[1] In the present work the same band of DCF was observed in a similar way to determine the molecular structure of the molecule and also to detect possible perturbations in the upper vibronic state.

The DCF molecule was generated by a reaction of CD_3F with CF_4 discharge products; typical partial pressures were about 3 mTorr for CD_3F and about 80 mTorr for CF_4. The region from 16000 to 17500 cm^{-1} was scanned using a dye laser, and the observed spectra were assigned to 858 transitions with $K_a' - K_a'' = 4-5, 3-4, 2-3, 1-2, 0-1, 1-0, 2-1, 3-2, 3-3, 2-2, 1-1, 0-0, 2-0$, and $0-2$. The spectra were found to be nearly free of perturbations, and were readily analyzed to give molecular constants as listed in Table I. By combining with the rotational constants of HCF reported in Ref. 1), the molecular structure parameters were calculated as shown in Table II.

Table I. Molecular Constants of DCF (MHz)[a]

Constant	$\tilde{A}^1A''(0,0,0)$	$\tilde{X}^1A'(0,0,0)$
A	452 680(19)	264 659.4(83)
B	30 413.7(14)	33 583.6(12)
C	28 316.8(14)	29 674.0(13)
Δ_J	0.084 7(27)	0.100 4(20)
Δ_{JK}	-0.780(87)	1.478(21)
Δ_K	458.2(28)	25.58(46)
δ_J	0.008 53(64)	0.012 45(63)
δ_K	2.09(35)	1.20(13)
Φ_J	$3(20) \times 10^{-7}$	
Φ_{JK}	$-1.3(14) \times 10^{-4}$	
Φ_{KJ}	$1.13(45) \times 10^{-2}$	
Φ_K	$1.43(13) \times 10$	
T_{00} (cm^{-1})	17 293.425 7(28)	

a. Values in parentheses denote 2.5 times standard deviations and apply to the last digits of the constants.

Table II. Molecular Structure of Fluorocarbene[a]

Parameter	$\tilde{A}^1A''(0,0,0)$	$\tilde{X}^1A'(0,0,0)$
r(C − H) (Å)	1.063(13)	1.138(10)
r(C − F) (Å)	1.308(6)	1.305(6)
∠H − C − F (°)	123.8(8)	104.1(13)

a. r_0 structure. Values in parentheses denote 2.5 times the standard deviation and apply to the last digits of the parameters.

Reference

1) M. Kakimoto, S. Saito, and E. Hirota, *J. Mol. Spectrosc.*, **88**, 300 (1981).

II-A-3 Microwave Optical Double Resonance of HNO: Rotational Spectrum in $\tilde{A}^1A''$ (0,2,0)

Kojiro TAKAGI *(Toyama Univ.)*, **Shuji SAITO, Tetsuo SUZUKI, and Eizi HIROTA**

Microwave optical double resonance (MODR) is one of the methods which allow us to determine rotational levels in excited electronic states to a precision of a few MHz. We have applied this technique to the $\tilde{A}^1A''(1,0,0)$ state of HNO.[1] In order to clarify the origin of perturbations observed for this vibronic state, we have also investigated the $\tilde{A}^1A''(0,2,0)$ state by MODR spectroscopy.

The rotational transitions observed include a-type R-branch transitions, $1_{01} - 0_{00}$ and $2_{02} - 1_{01}$, K-type doubling transitions of $K = 1, J = 2 \sim 8$, $K = 2, J = 2 \sim 9$, and $K = 3, J = 3 \sim 5$ and $10 \sim 12$, and finally four b-type transitions, $5_{15} - 6_{06}$, $6_{16} - 7_{07}$, $8_{08} - 7_{17}$, and $9_{09} - 8_{18}$. Many of these transitions were found to be perturbed, as in the case of the (1,0,0) state. A particularly interesting case is $10_{37} - 10_{38}$, which appeared as a doublet because either the upper or lower level of the transition is mixed with a perturbing level to a considerable extent. Six perturbed transitions (K-doublet transitions of $J_K = 8_2, 4_3, 5_3, 10_3, 11_3$, and 12_3) were found to show Zeeman effects when observed with a magnetic field of about 2 kG. Similar Zeeman effects were observed also for some of K-type doubling transitions ($K = 2$ or 3) in the $\tilde{A}^1A''(1,0,0)$ state.[2] A more quantitative measurement of Zeeman effects is under way.

References

1) K. Takagi, S. Saito, M. Kakimoto, and E. Hirota, *J. Chem. Phys.*, **73**, 2570 (1980).
2) A similar study on the Zeeman effects has recently been reported by R. N. Dixon, M. Noble, and C. A. Taylor, *Faraday Discussion* No. 71, to be published.

II-A-4 Infrared-Optical Double Resonance Spectroscopy of the NH_2 Radical

Kentarou KAWAGUCHI, Tetsuo SUZUKI, Shuji SAITO, Takayoshi AMANO *(Univ. of Tokyo)*, **and Eizi HIROTA**

It is well-known that the ground electronic state ($\tilde{X}^2B_1$) of the NH_2 radical interacts strongly with the excited state ($\tilde{A}^2A_1$), because the two states are derived from the linear $^2\Pi$ conformation by a strong Renner-Teller interaction. Therefore, many rovibrational levels in the $\tilde{A}$ state are expected to be perturbed by higher excited levels associated with the $\tilde{X}$ state. We have, in fact, detected an example of such perturbing levels near the $\tilde{A}$ $v_2 = 10$, 2_{11} level by infrared-optical double resonance.

In the present work we searched for similar cases by pumping the $\tilde{A}^2A_1(0,11,0)N_{0,N} - \tilde{X}^2B_1(0,0,0)N_{1,N}$ and the $\tilde{A}^2A_1(0,12,0)N_{1,N-1} - \tilde{A}^2A_1(0,11,0)N_{0,N}$ transitions ($N \leqq 7$), respectively, by a dye and a CO_2/N_2O laser. For $N = 3$ and 5, signals corresponding to decreases in the total fluorescence intensity were observed, suggesting the presence of perturbing levels. Figure 1 shows infrared spectra with the $\tilde{A}(0,11,0)3_{03}$ as the lower level. Besides the "normal" transition $(0,12,0)3_{12} - (0,11,0)3_{03}$ designated by broken lines, many signals were observed; those observed using the N_2O R(J = 16–19) and CO_2 P(J = 8, 10) laser lines were mainly assigned to a transition to an N = 5 level and the majority of the remaining signals to another transitions to an N = 4 level, as shown in Figure 2. The lower level $\tilde{A}(0,11,0)3_{03}$ is also thought to be perturbed by an N = 4 level, making the former transition allowed.

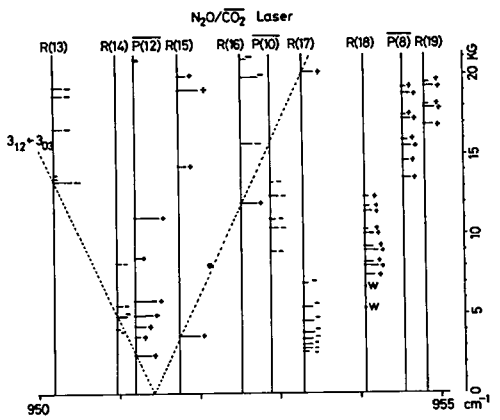

Figure 1. Infrared transitions ($\Delta M = \pm 1$) of NH_2 with $\tilde{A}(0,11,0)3_{03}$ as the lower level. The +, − signs denote those of the Zeeman coefficient ($\partial\nu/\partial B$). The "normal" transition $\tilde{A}(0,12,0)3_{12} - \tilde{A}(0,11,0)3_{03}$ is designated by broken lines.

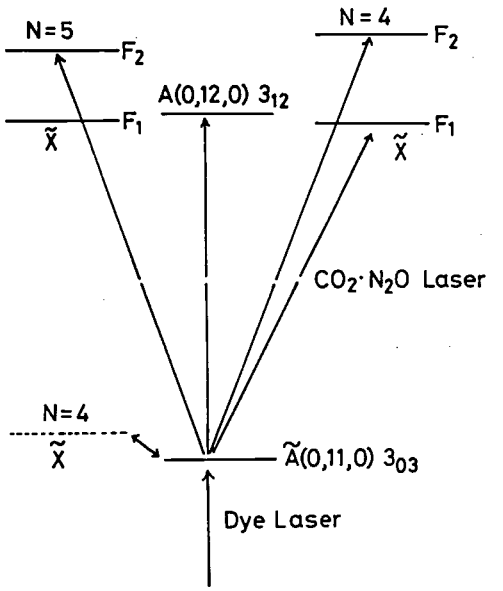

Figure 2. Infrared transitions of NH_2 starting from the $\tilde{A}(0,11,0)3_{03}$ level. Perturbing levels near $\tilde{A}(0,12,0)3_{12}$ give most of the signals shown in Figure 1.

II-A-5 Diode Laser Spectroscopy of the FSO ν_1 and ν_2 Bands

Yasuki ENDO, Keiichi NAGAI, and Eizi HIROTA

The FSO radical may be considered as a derivative of HO_2, which has played important roles in many reaction systems. We have recently investigated FSO by microwave spectroscopy[1] and have evaluated precise molecular constants for $F^{32}SO$ in the ground and $v_3 = 1$ states and also for $F^{34}SO$ in the ground state. However, it is well known that vibrational effects often make obscure the physical meaning of the molecular constants obtained from ground-state rotational spectra. To assess contributions of such effects the ν_1 and ν_2 bands of FSO were observed by diode laser

spectroscopy.

The FSO radical was generated as in Ref. 1). The ν_1 band could be recorded only with Zeeman modulation, whereas both Zeeman and source-frequency modulation could be applied to the ν_2 band. The molecular constants in the upper states thus evaluated are summarized in Table I [the ground-state parameters were fixed to the microwave values of Ref. 1)]. The harmonic force field evaluated in Ref. 1) was improved by adding the two fundamental frequencies obtained here to the input data. As shown in Table II, however, we still needed F_{13} to be assumed. Table II summarizes r_z structure parameters along with the r_0 values of Ref. 1) for comparison. The r_e structure is discussed in II-A-16.

Table I. Molecular Constants of $^{19}F^{32}S^{16}O$ in the ν_1 and ν_2 States (MHz)[a]

Constant	ν_1	ν_2
A	38 467.93(75)	38 625.29(50)
B	9 316.9(31)	9 286.48(21)
C	7 484.2(34)	7 463.33(23)
Δ_N	0.010 6(7)	0.009 90(61)
Δ_{NK}	−0.082 5(57)	−0.083 6(25)
Δ_K	0.858 1(79)	0.896 4(46)
δ_N	[0.002 899][b]	[0.002 899][b]
δ_K	[0.027 11][b]	[0.027 11][b]
ε_{aa}	−344.7(53)	−331.9(29)
ε_{bb}	28.3(61)	40.7(25)
ν_0 (cm^{-1})	1 217.188 2(18)	757.506 60(44)

a. Values in parentheses denote 2.5 times standard deviations and apply to the last digits of the constants.
b. Fixed (ground-state values).

Table II. Harmonic Force Field of FSO[a]

F_{11} (md/Å)	9.2101	F_{12} (md/Å)	−0.1453
F_{22} (md/Å)	4.0678	F_{13} (md)	[0.2][b]
F_{33} (mdÅ)	1.2557	F_{23} (md)	0.0880

a. The internal coordinates used are 1: ν(S−O), 2: ν(S−F), 3: δ(F−S−O).
b. Assumed.

Table III. Molecular Structure of FSO

Parameter	r_z	r_o[a]
r(S−F) (Å)	1.607 9	1.602
r(S−O) (Å)	1.451 0	1.452
θ(F−S−O) (°)	108.19	108.32

a. Taken from Ref. 1).

Reference

1) Y. Endo, S. Saito, and E. Hirota, *J. Chem. Phys.*, **74**, 1568 (1981).

II-A-6 Microwave Spectroscopy of the CCl Radical

Yasuki ENDO, Shuji SAITO, and Eizi HIROTA

The CCl radical has been investigated by ultraviolet emission spectroscopy.[1,2] Recently Yamada et al.[3] succeeded in observing the $v = 1 \leftarrow 0$ and $2 \leftarrow 1$ bands in the ground electronic state by diode laser spectroscopy. The present work was started mainly to clarify the hyperfine structure in the molecule.

Because of the short lifetime of CCl, a 3.7 m long discharge cell was replaced by a 1 m long cell with a 50 ϕ side arm, which was connected to a 67 l/sec booster pump to increase the pumping speed. The CCl radical was generated directly in the cell by a glow discharge in CCl_4; the pressure of CCl_4 was 20 mTorr and the discharge current was 10 mA. The rotational transitions were observed for J up to 4.5 $\leftarrow$ 3.5 both for the $^2\Pi_{1/2}$ and $^2\Pi_{3/2}$ states. Table I summarizes molecular constants obtained from an analysis of the observed spectra. By using the α^B value of Ref. 2), B_e and r_e were calculated to be 0.697121 (17) cm^{-1} and 1.645197 (27) Å, respectively, where the values in parentheses denote 3σ. It is interesting to note that $(c + 3d)/3$ is 69.1 MHz, in

Table I. Molecular Constants of CCl (MHz)[a]

Λ-doulbing parameter:	p_v	401.696(25)
	q_v	1.176(48)
Rotational dependence of A:	A_J	−4.6464(13)
Rotational constant:	B_0	20 797.1725(38)
Centrifugal distortion constant:	D_0	0.05271(12)
Hyperfine interaction constant:		
	a + (b + c)/2	66.46(11)
	a − (b + c)/2	93.936(37)
	b	12.0(15)
	d	82.212(37)
	$(eQq)_1$	−34.26(13)
	$(eQq)_2$	−84.6(95)

a. $A = 134.96\ cm^{-1}$ and $\gamma = 0$ MHz were assumed. Values in parentheses denote 2.5 times standard errors and apply to the last digits of the constants.

close agreement with a (80.199 MHz), i.e. the unpaired-electron orbital and spin densities are close. The Fermi term a_F was calculated from b + c/3 to be −1.2 (15) MHz, nearly equal to zero, and $\langle\sin^2\theta\rangle_{av}$ calculated from d is 0.792; therefore, the unpaired electron orbital seems to be very close to a pure p orbital. The spin density at the Cl nucleus was calculated to be 20%, as compared with 18% at the F nucleus in CF.

References

1) R. D. Gordon and G. W. King, *Canad. J. Phys.*, **39**, 252 (1961).
2) R. D. Verma and R. S. Mulliken, *J. Mol. Spectrosc.*, **6**, 419 (1961).
3) C. Yamada, K. Nagai, and E. Hirota, *J. Mol. Spectrosc.*, **85**, 416 (1981).

II-A-7 Fine Structure Transitions of the Helium Atom by Infrared Diode Laser Spectroscopy

Keiichi NAGAI, Keiichi TANAKA *(Kyushu Univ.)*, **and Eizi HIROTA**

The energy levels of the neutral helium atom ^{4}He have been investigated in detail, and a comprehensive list is now available for n (the principal quantum number) up to 22.[1] In the past two decades new spectroscopic techniques of high resolution and high precision were applied to He to improve the accuracy of both electrostatic and relativistic fine structure intervals in the atom; e.g. microwave-optical double resonance (MODR), anticrossing, quantum beat, and laser magnetic resonance (LMR). In the present work we applied diode laser spectroscopy to observe transitions between electrostatic fine structure separations in the infrared region, where the observation of atomic spectra has been rather rare.

The helium gas was excited by a DC discharge in a cell made of an 8 mm inner diameter Pyrex glass tube; the distance between two electrodes for discharge was about 600 mm. The helium pressure was about 100 mTorr. The observed transitions and wavenumbers are listed in Table I, where the values calculated from Martin's table are given for comparison. Le et al.[2] have recently measured the $4^3P_1 - 4^3S_1$ transition wavenumber by LMR, and their result agrees with ours, as shown in Table I. However, our $4^3P_2 - 4^3P_1$ interval shows a small deviation from a more accurate MODR result,[3] because the $4^3P_1 - 4^3S_1$ transition is partially overlapped by the stronger $4^3P_2 - 4^3S_1$ transition.

Table I. Observed Fine Structure Transitions of ^{4}He (cm^{-1})

Transition	Present	Ref. 1)	Ref. 2)
$4^3P_0 \leftarrow 4^3S_1$	919.0463(3)	919.033	
$4^3P_1 \leftarrow 4^3S_1$	918.9368(3)	918.923	918.9371(4)
$4^3P_2 \leftarrow 4^3S_1$	918.9270(3)	918.914	
$3^1P_1 \leftarrow 3^1S_0$	1344.5350(4)	1344.535	
$6^1F \leftarrow 5^1D$	1344.1404(10)	1344.11	
$6^3F \leftarrow 5^3D$	1345.2712(10)	1345.24	
6G ← 5F	1341.6009[a]	1341.66	
6H ← 5G	1341.1785[a]	1341.16	

Triplet separation	Present	Ref. 3)
$4^3P_2 - 4^3P_0$	0.11931(18)	0.119309(33)
$4^3P_2 - 4^3P_1$	0.0098(10)	0.009020(23)

a. Tentative assignment.

References

1) W. C. Martin, *J. Phys. Chem. Ref. Data*, **2**, 257 (1973).
2) H. Le, M. Rosenbluh, B. Lax, and T. A. Miller, *Phys. Rev.*, to be published.
3) T. A. Miller and R. S. Freund, *Phys. Rev.*, **A5**, 588 (1972).

II-A-8 Diode Laser Study of the ν_2 Band of the Methyl Radical

Chikashi YAMADA, Eizi HIROTA, and Kentarou KAWAGUCHI

[*J. Chem. Phys.*, in press]

Because of its importance in a wide range of fields, the CH_3 radical has been a subject of many spectroscopic investigations. Although most of these works suggest the molecule to be planar in the ground electronic state, knowledge on the potential function to the out-of-plane bending vibration has been very limited, making the conclusion of the planar structure of the molecule rather uncertain. In the present work we applied diode laser spectroscopy to the ν_2 band to eliminate the uncertainty about the planarity.

Source laser diodes in the 16 μm region were supplied to us by the Fujitsu Laboratories. We generated the CH_3 radical directly in a multiple

reflection cell by a 60 Hz discharge in di-tert-butyl peroxide. We roughly estimated the CH_3 radical concentration in the cell to be about 10^{13} molecules/cm^3. Figure 1 shows a Q branch series of lines, N = K = 1 to 5, recorded with Zeeman (the upper trace) and soure (the lower trace) modulation, which gave us the first clue to the assignment. We have thus observed the $v_2 = 1 \leftarrow 0$, $2 \leftarrow 1$, and $3 \leftarrow 2$ bands, and molecular constants derived therefrom are listed in Table I. The three vibrational term values were explained in terms of either a series-expansion potential function (I) or a vibronic-interaction potential function (II). Table II summarizes potential constants derived, and (I) and (II) are shown, respectively, by curves A and B in Figure 2. Curve C corresponds to the harmonic term of (II). The planarity of the methyl radical is thus definitely established.

Table I. Molecular Constants of the CH_3 Radical in the Ground, ν_2, $2\nu_2$, and $3\nu_2$ States (cm^{-1})[a]

	G.S.	ν_2	$2\nu_2$	$3\nu_2$
E	0.0	606.4531(6)	1288.0900(10)	2019.1657(11)
B	9.577 89(16)	9.258 14(16)	8.933 20(22)	8.609 74(28)
C	4.742 02[67][b]	4.811 643(71)[b]	4.871 213(87)[b]	4.926 55(21)[b]
D_N	0.000 769 9(88)	0.000 494(10)	0.000 231(15)	−0.000 039(24)
D_{NK}	−0.001 358(18)	−0.000 706(26)	−0.000 033(36)	0.000 636(73)
D_K	0.000 634[14][c]	0.000 257(19)[d]	−0.000 150(25)[d]	−0.000 556(59)[d]
		0.000 282[20][c]	−0.000 090[28][c]	−0.000 457[56][c]
H_N	−0.000 000 32(37)	−0.000 000 45(25)	−0.000 000 55(36)	−0.000 000 86(48)
H_{NK}	0.000 001 0(14)	0.000 001 4(11)	0.000 002 3(14)	0.000 003 8(19)
H_{KN}	−0.000 000 4(19)	−0.000 001 3(17)	−0.000 002 9(20)	−0.000 004 9(21)
H_K	−0.000 000 2[19][e]	0.000 000 54(16)[f]	0.000 001 35(58)[f]	{0.000 001 76}[g]
		0.000 000 4[16][e]	0.000 001 2[19][e]	0.000 001 9[21][e]
ε_{bb}	0.011 68(61)	0.011 36(52)	0.010 77(8)	
ε_{cc}	0.000 1(21)	0.000 1(23)	0.001 5(24)	

a. Values in parentheses denote one standard diviation and apply to the last digits of the constants.
b. C_0 was calculated assuming the inertia defect to be 0.0348[5] uÅ^2. The value in square brackets is mainly due to the uncertainty of 0.0005 uÅ^2 in the calculated inertia defect. Uncertainties for excited states are due to fitting errors.
c. Calculated from the planarity condition, $2D_N + 3D_{NK} + 4D_K = 0$.
d. Calculated assuming the ground-state D_K to be 0.000634 cm^{-1}. Uncertainties are due to fitting errors.
e. Calculated from the planarity condition, $3H_N + 4H_{NK} + 5H_{KN} + 6H_K = 0$.
f. Calculated assuming the ground-state H_K to be −0.000 000 17[185] cm^{-1}. Uncertainties are due to fitting errors.
g. Fixed.

Table II. Potential Function for the Out-of-Plane Bending Vibration of the CH_3 Radical[a]

(I)	$V_2(z) = (1/2)k_{22}z^2 + (1/4!)k_{2222}z^4 + (1/6!)k_{222222}z^6$	
	k_{22}	0.3475 md/Å
	k_{2222}	35.61 md/Å^3
	k_{222222}	−1496. md/Å^5
(II)	$V_2(z) = (1/2)k_{22}^{(0)}z^2 + (1/2)\Delta E - (1/2)(\Delta E^2 + 4a^2z^2)^{1/2}$	
	$k_{22}^{(0)}$	2.7888(29) md/Å[b]
	a	1.0599(77) md[b]
	$\Delta E = E(^2A_1') - E(\tilde{X}^2A_2'')$	[46205 cm^{-1}][c]

a. The coordinate z is defined as the distance of the C atom from the plane made by the three hydrogen atoms.
b. Values in parentheses denote standard deviations and apply to the last digits of the constants.
c. Assumed. This value is equal to the separation between the $\tilde{B}$ and $\tilde{X}$ states.

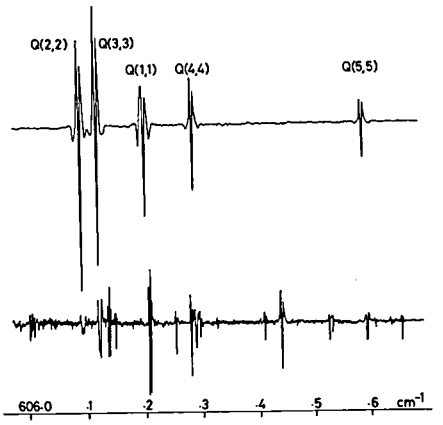

Figure 1. Q branch transitions of N = K = 1 to 5 of the CH_3 ν_2 fundamental band. The upper trace was recorded with Zeeman modulation and thus shows only the CH_3 spectra, in contrast with the lower trace, which was obtained by source frequency modulation and thus shows lines of diamagnetic species in addition to the CH_3 lines.

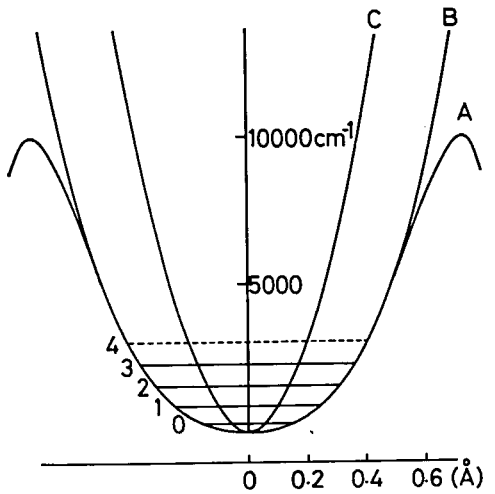

Figure 2. Potential functions for the out-of-plane bending vibration, ν_2. Curves A and B correspond, respectively, to (I) and (II) of Table II, whereas curve C designates only the harmonic term of (II).

II-A-9 Intramolecular Motions and Potential Constants of the CH_3 Radical

Eizi HIROTA and Chikashi YAMADA

In order to assess the physical significance of molecular constants of the CH_3 radical obtained in II-A-8, a normal coordinate analysis was carried out. The input data were four fundamental frequencies and an information provided by the vibration-rotation constants, α_2^B and α_2^C. A fair agreement was obtained between the calculated and observed values for the ground-state centrifugal distortion constants and for the change of the inertia defect upon ν_2 excitation, as shown in Table I. The observed values of α_2^B and α_2^C and of a vibrational anharmonicity constant ωx_{22} have also been analyzed using formulas for these constants which have been derived from well-established vibration-rotation theory.[1] The anharmonic potential constants thus derived are summarized in Table II.

The present analysis based upon a small-amplitude vibration approximation may not be adequate, because, as shown in II-A-8, the ν_2 mode deviates considerably from the harmonic vibration. Therefore, the conventional vibration-rotation theory was extended so as to include the effects of the large, negative anharmonicity of the ν_2 mode. This extension has shown that the small-amplitude vibration approach as applied above is essentially correct, provided that potential constants are taken into account to the fourth power in the internal coordinates.

Table I. Centrifugal Distortion Constants and Inertia Defect of the CH_3 Radical

Constant	Obs.	Calc.[a]
D_N (cm^{-1})	0.000 769 9(81)[b]	0.000 683 3
D_{NK} (cm^{-1})	−0.001 358(17)[b]	−0.001 192 4
D_K (cm^{-1})	0.000 634(16)[b,c]	0.000 552 7
Δ_2 (u$Å^2$)	−0.173 0[d]	−0.179 36
	−0.175 3	
	−0.180 7	

a. The force field used is F_{11} = 5.9930 md/Å, F_{22} = 0.0892 mdÅ, F_{33} = 5.7128 md/Å, F_{44} = 0.4142 mdÅ, and F_{34} = −0.3601 md.
b. The ground-state values.
c. Obtained from the planarity condition $2D_N + 3D_{NK} + 4D_K = 0$.
d. The three values are differences between the inertia defects of two successive states among the ground, ν_2, $2\nu_2$, and $3\nu_2$ states.

Table II. Anharmonic Potential Constants of the CH_3 Radical

α_2^C = −0.085 24(57) cm^{-1} ωx_{22} = 56.900 7(35) cm^{-1}	input data	
cubic constant	ϕ_{122}	1050.4(7.0) cm^{-1a}
third-order constant	F_{122}	−0.049(10) md[a]
quartic constant	ϕ_{2222}	2011(15) cm^{-1}
fourth-order constant	F_{2222}	0.761(23) mdÅ

a. The sign of Q_i or S_i is taken to be positive when the C − H bonds are elongated.

Reference

1) See, for example, I. M. Mills in "Molecular Spectroscopy: Modern Research" (K. N. Rao and C. W. Mathews, Eds.), pp.115—140, Academic Press, New York, 1972.

II-A-10 Microwave Spectroscopy of the DO_2 Radical

Shuji SAITO, Yasuki ENDO, and Eizi HIROTA

The hydroperoxyl radical has long been known as an important intermediate in many oxydation or combustion reactions, but the high-resolution spectroscopic study started recently with a far-infrared laser-magnetic-resonance (LMR) observation of HO_2 by Radford et al. in 1974.[1] Since then the HO_2 molecule has been investigated by microwave spectroscopy, electron paramagnetic resonance, infrared LMR, and near-infrared emission spectroscopy. The deuterated species has also been studied nearly as extensively as HO_2, but its microwave observation has so far been limited only to the $N = 1 \leftarrow 0$ transition by Beers and Howard in 1976.[2] Because microwave spectroscopy provides most accurate data, we have extended Beers and Howard's measurement.

We generated DO_2 by a DC discharge in a mixture of CH_3OD (10 mTorr) and O_2 (10 mTorr) contained in a 3.5 m long absorption cell. In the region of 50 to 200 GHz nine a-type R-branch and five b-type P- or R-branch ($K = 1 - 0$) transitions were observed, which consisted of 56 fine structure and hyperfine structure transitions in total. Among them 38 well-resolved lines were subjected to the least-squares analysis, and led to molecular constants shown in Table I, which are one or two orders of magnitude more precise than those previously reported. The deuterium hyperfine structure was resolved for the first time. By combining the data on HO_2, the principal values of the dipole-dipole interaction tensor were evaluated, as shown in Table II.

References

1) H. E. Radford, K. M. Evenson, and C. J. Howard, *J. Chem. Phys.*, **60**, 3178 (1974); J. T. Hougen, H. E. Radford, K. M. Evenson, and C. J. Howard, *J. Mol. Spectrosc.*, **56**, 210 (1975).

2) Y. Beers and C. J. Howard, *J. Chem. Phys.*, **64**, 1541 (1976).

Table I. Molecular Constants of the DO_2 Radical (MHz)[a]

Constant	Value	Constant	Value
A	335 598.175(73)	ε_{aa}	−27 145.02(30)
B	31 656.209(16)	ε_{bb}	−391.96(11)
C	28 811.104(20)	ε_{cc}	6.96(13)
		$\lvert(\varepsilon_{ab} + \varepsilon_{ba})\rvert/2$	45.(10)
Δ_N	0.094 30(46)		
Δ_{NK}	2.262 5(32)	Δ_{NK}^s	0.29(48)
Δ_K	[38.21][b]	Δ_K^s	6.70(21)
δ_N	0.008 20(43)		
δ_K	[1.55][b]		

a. Values in parentheses denote 2.5 times standard deviations and apply to the last digits of the constants.
b. Assumed.

Table II. Hyperfine Structure Constants of the Hydroperoxyl Radical (MHz)[a]

Constant	HO_2[b]	DO_2
a_F	−27.48(38)	−4.187(64)
T_{aa}	−8.34(55)	−0.93(11)
T_{bb}	19.68(78)	2.8(11)
Principal values of the T tensor for HO_2[c]		
T_{xx} −17.4(90),	T_{yy} 28.8(90),	T_{zz} −11.34(95)

a. See Footnote a of Table I.
b. C. E. Barnes, J. M. Brown, A. Carrington, J. Pinkstone, T. J. Sears, and P. J. Thistlethwaite, *J. Mol. Spectrosc.*, **72**, 86 (1978).
c. The x and y axes are in the molecular plane, and the y axis is nearly parallel to the O-H bond.

II-A-11 Diode Laser Spectroscopy of the SF Radical

Yasuki ENDO, Keiichi NAGAI, Chikashi YAMADA, and Eizi HIROTA

The first detection of the SF radical in the gas phase was made by Carrington et al. using electron paramagnetic resonance spectroscopy,[1] and its ground vibronic state ($^2\Pi_{1/2}$, $^2\Pi_{3/2}$) has now been very well characterized by microwave spectroscopy.[2] However, nothing has been known about the vibrational spectrum. Becasue most molecular constants are known to be very susceptible to vibrational effects, we observed vibration-rotation spectra of SF using a diode laser spectrometer, to assess the effects in the molecule.

The SF radical was generated directly in a multiple reflection cell by a 60 Hz discharge in an OCS/CF_4 mixture. First, Zeeman modulation was

employed, which gave us 10 lines of the $^2\Pi_{3/2}$, v = 1 ← 0 band in 823 to 838 cm^{-1}, but did not allow us to observe $^2\Pi_{1/2}$ lines, because the Zeeman effects of these lines were too small. Then a discharge-current modulation technique described in the II-B-1 was developed, and we could observe the v = 1 ← 0 and 2 ← 1 bands both in the $^2\Pi_{3/2}$ and $^2\Pi_{1/2}$ states by this method. The Λ-doubling in $^2\Pi_{1/2}$ was too small to be resolved. By fixing the ground-state parameters to the microwave values,[2] molecular constants of the v = 1 and 2 states were evaluated by the least-squares analysis of the observed spectra, as shown in Table I. The rotational constants of the three vibrational states were fitted to the equation, $B_v = B_e - \alpha_e(v + 1/2) + \gamma_e(v + 1/2)^2$, (cf. Table I), and the equilibrium distance was calculated from B_e to be 1.596 244 (22) Å, where the error includes the uncertainty of the Planck constant.

Table I. Molecular Constants of the SF Radical (cm^{-1})[a]

Constant	v = 1	v = 2
A_v	−386.9162(11)	−386.8309(21)
A_{Dv}	0.58(25) × 10^{-4}	0.67(24) × 10^{-4}
B_v	0.548 501(12)	0.544 069(12)
D_v	[0.97534 × 10^{-6}][b]	[0.97534 × 10^{-6}][b]
ν_0(v=1←0)	828.702 73(57)	
ν_0(v=2←1)	819.763 67(80)	
B_e 0.555 173(11), α_e 0.004 459(25), γ_e 0.000 007(6)		
r_e 1.596 244(22) Å		

a. Values in parentheses denote 2.5 times standard deviations and apply to the last digits of the constants.
b. Assumed.

References

1) A. Carrington, G. N. Currie, T. A. Miller, and D. H. Levy, *J. Chem. Phys.*, **50**, 2726 (1969).
2) T. Amano and E. Hirota, *J. Mol. Spectrosc.*, **45**, 417 (1973); Y. Endo, S. Saito, and E. Hirota, *IMS Ann. Rev.*, 46 (1980).

II-A-12 Diode Laser and Microwave Spectroscopy of a New Linear Triatomic Molecule: ClBO

Kentarou KAWAGUCHI, Yasuki ENDO, and Eizi HIROTA

Although XBS and XBSe (X = H, CH_3, or halogen) have been confirmed by spectroscopic techniques to exist in the gas phase, little has been known about the XBO molecule. In the course of searching for the ν_2 band of BO_2 by diode laser spectroscopy (see II-A-1), we observed a series of diamagnetic lines which were probably ascribed to a linear molecule with a lifetime somewhat longer than that of BO_2. The rotational spacing suggested those lines to be due to the ClBO molecule, probably to its B-Cl stretching band.

We subsequently confirmed this tentative assignment by observing microwave spectra of the molecule. A DC discharge in an O_2/BCl_3 mixture (both with a partial pressure of 26 mTorr) gave very

Table I. Molecular Constants of the ClBO Molecule (MHz)[a]

Constant	$^{35}Cl^{11}B^{16}O$	$^{35}Cl^{10}B^{16}O$	$^{37}Cl^{11}B^{16}O$	$^{37}Cl^{10}B^{16}O$
B_0	5 202.396 6(24)	5 224.578 5(36)	5 091.740 6(20)	5 115.241 5(50)
D_0	0.001 297 1(75)	0.001 302 8(96)	0.001 204(56)	0.001 251(13)
H_0	−0.65(45) × 10^{-8}			
B_1	5 189.457 8(31)	5 211.28(18)	5 078.88(14)	
D_1	0.001 343 8(93)	0.001 390(81)	0.001 291(48)	
H_1	−0.86(48) × 10^{-8}			
B_{2c}	5 214.485 2(76)		5 103.622 1(72)	
D_{2c}	0.001 314(20)		0.001 265(20)	
B_{2d}	5 220.061 9(78)		5 108.974 7(74)	
D_{2d}	0.001 349(14)		0.001 280(20)	
$(eQq)_0$	−47.8(15)			
$\nu_0(\nu_1)$ (cm^{-1})	676.036 85(36)	680.761 6(27)	668.591 2(28)	

a. Values in parentheses denote three standard deviations and apply to the last digits of the constants.

strong signals, and absorption lines were easily assigned to Cl and B isotopic species, not only in the ground state, but also in the v_1(B-Cl stretching) = 1 and v_2(Cl-B-O bending) = 1 states. Table I summarizes molecular constants obtained from the least-squares analysis of the observed spectra; both infrared and microwave data were used for the ground and $v_1 = 1$ states (except for $^{37}Cl^{10}BO$), and only microwave spectra for the $v_2 = 1$ state. Table II lists the r_s structure parameters.

Table II. The r_s Structure of the ClBO Molecule (Å)

Parent species	Cl-B	B-O	Cl·····O
$^{35}Cl^{11}B^{16}O$	1.682 817	1.206 265	2.889 082
$^{35}Cl^{10}B^{16}O$	1.682 813	1.206 255	2.889 068
$^{37}Cl^{11}B^{16}O$	1.682 826	1.206 233	2.889 059
$^{37}Cl^{10}B^{16}O$	1.682 831	1.206 242	2.889 073
Av.	1.682 825	1.206 249	2.889 070
range	0.000 018	0.000 032	0.000 024

II-A-13 Dye Laser Excitation Spectroscopy of the HCF Molecule: Perturbations in the $\tilde{A}^1A''(0,1,0)$ State

Tetsuo SUZUKI, Shuji SAITO, and Eizi HIROTA

Merer and Travis[1] have reported the observation of the HCF $\tilde{A} - \tilde{X}$ transition in absorption and have noticed large perturbations on the $\tilde{A}(0,1,0) - \tilde{X}(0,0,0)$ band. In view of the importance of HCF in various fields, we reinvestigated this band with an order of magnitude better resolution (Doppler limited), i.e., by using a cw dye laser as a means of excitation.

Among the observed spectra, we assigned the subbands of $K_a' - K_a'' = 3 - 4, 2 - 3, 1 - 2, 0 - 1, 1 - 0, 2 - 1, 0 - 0, 1 - 1, 2 - 2, 2 - 0$, and $0 - 2$, using ground-state combination differences. However, there remain many lines unassigned. Figure 1 shows two $^rQ_0$ series of transitions; because the $\tilde{A}(0,1,0)$ $J_{1,J}$ levels mix with nearby levels through interactions, transitions terminating in these perturbing levels also acquire transition probabilities large enough to produce an additional Q branch series. These perturbations for the $K_a' = 1$ levels were accounted for by an electronic Coriolis interaction. According to this model the separation between two interacting levels is given by $\Delta E = \{ [\delta E + \delta\overline{B}_{eff}J(J+1)]^2 + 4\varepsilon^2 \}^{1/2}$. The meaning of the three terms in the right-hand side of this equation and their values determined by the least-squares fitting are given in Table I. We also observed Zeeman effects of perturbed lines, but we have so far found it difficult to explain the observed Zeeman effects quantitatively.

Table I. Molecular Constants of HCF in the $\tilde{A}^1A''(0,1,0)$ State $(cm^{-1})^a$

Unperturbed energy separation between two fictitious levels of J = 0:	
δE	−4.46(11)
Difference in the effective rotational constants:	
$\delta\overline{B}_{eff}(J_{1,J-1})$	0.1851(90)
$\delta\overline{B}_{eff}(J_{1,J})$	0.0858(58)
Interaction parameter:	
$\lvert \varepsilon \rvert = \lvert\langle\tilde{A}^1A'' \rvert AL_a \rvert \tilde{X}^1A'\rangle\rvert$	2.888(28)

a. Values in parentheses denote standard deviations and apply to the last digits of the constants.

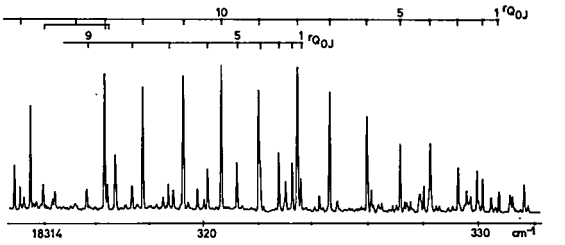

Figure 1. A part of the dye laser excitation spectrum of the HCF $\tilde{A}^1A''(0,1,0) - \tilde{X}^1A'(0,0,0)$ band; two $^rQ_0$ series are shown, as explained in the text.

Reference

1) A. J. Merer and D. N. Travis, *Canad. J. Phys.*, **44**, 1541 (1966).

II-A-14 Microwave Spectroscopy of the CF_3 Radical

Yasuki ENDO, Chikashi YAMADA, Shuji SAITO, and Eizi HIROTA

In contrast with the CH_3 radical, which is just established to be planar in the ground electronic state as shown in II-A-8, the CF_3 radical has been known to be non-planar in the ground state from matrix electron-spin-resonance spectra, especially their ^{13}C hyperfine structures, and also from infrared spectra both in the gas phase and in

matrices. Yamada and Hirota[1] have recently obseved the ν_3 band of CF_3 by diode laser spectroscopy, and have succeeded in assigning Q branch transitions. In the present work we observed pure rotational spectra by microwave spectroscopy to obtain an accurate B_0 rotational constant and to resolve fine and hyperfine structures.

We have tested a few CF_3-group containing compounds to generate CF_3, and $(CF_3CO)_2O$ has so far been found to be most suitable for microwave experiment; about 20 mTorr of this compound was decomposed in a 1 m long free-space cell by a DC discharge of the current of 7 to 10 mA. Three groups of paramagnetic lines were thus observed at 87, 109, and 131 GHz, and were assigned to the N = 4 ← 3, 5 ← 4, and 6 ← 5 transitions. Figure 1 shows the observed N = 6 ← 5 transition which consists of many fine and hyperfine components. The analysis of fine and hyperfine structures was carried out; the discussion of Hougen[2] on the hyperfine structure in CH_3O was found to be useful. The hyperfine structures can be understood in most cases by introducing the total nuclear spin of 1/2 and 3/2 for K ≠ 3n and K = 0 or 3n, respectively. An exception is the K = 1 levels, which are split in the first order by the dipole-dipole interaction term (a term in $T_{aa} - T_{bb}$). Table I summarizes molecular constants obtained from the least-squares analysis of the observed spectra. Although a unique determination of the molecular structure is not possible, C-F = 1.32 Å and ∠F-C-F = 110.3° may be a reasonable set of the structure parameters.

Table I. Molecular Constants of the CF_3 Radical in the Ground State (MHz)[a]

B_0	10 900.911 8(52)	a_F	408.5(16)
D_N	0.013 882(87)		
D_{NK}	−0.023 43(17)	T_{cc}	320.01(20)
		$\lvert T_{aa} - T_{bb} \rvert$	40.1(49)[b]
ε_{bb}	−36.500(42)		
ε_{cc}	3.35(15)		

a. Values in parentheses denote 2.5 times standard deviations and apply to the last digits of the constants.
b. Determined from K = 1 splittings. However, T_{ac} could not be obtained. T_{aa}(or T_{bb}) and T_{bb}(or T_{aa}) are −140.0 and −180.1 MHz, respectively.

References

1) C. Yamada and E. Hirota, *IMS Ann. Rev.*, 42 (1980).
2) J. T. Hougen, *J. Mol. Spectrosc.*, **81**, 73 (1980).

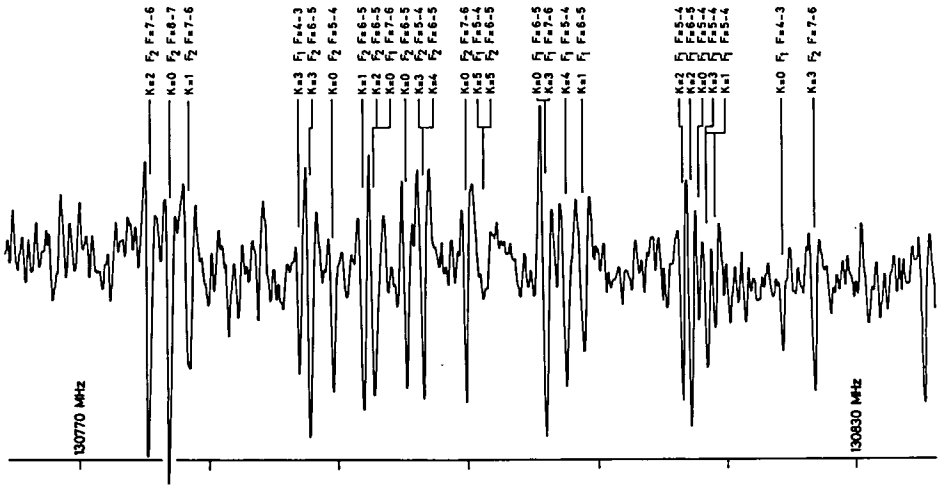

Figure 1. Observed fine and hyperfine structures of the N = 6 ← 5 transition of CF_3.

II-A-15 Microwave Spectroscopy of the PH_2 Radical: Hyperfine Interactions

Yasuki ENDO, Shuji SAITO, and Eizi HIROTA

The PH_2 radical has been extensively investigated in the visible region by observing the $\tilde{A}^2A_1 - \tilde{X}^2B_1$ transition in both absorption and emission under high resolution.[1] The ground-state parameters have later been made more precise by far-infrared (FIR) and infrared (IR) laser magnetic resonance (LMR) spectroscopy.[2] The present work was started

primarily to make the hyperfine structures in the ground vibronic state much more accurate than those previously reported.

The PH_2 radical was generated by a DC discharge in a PH_3 (25 mTorr) and O_2 (25 mTorr) mixture. A 1 m long free-space cell was used. Because the molecule is light, only two rotational transitions, $1_{10} - 1_{01}$ and $2_{20} - 2_{11}$, appear in the region covered by our spectrometer. They were observed to consist of 28 fine and hyperfine components in total. The rotational, the centrifugal distortion, and the spin-rotation interaction constants were determined by adding the present data to the FIR and IR LMR results,[2] as listed in Table I, whereas the hyperfine interaction constants shown in Table II were obtained from the present data, with other parameters fixed to the values of Table I. Table II lists also the hyperfine interaction constants derived from the FIR LMR[2] and intermodulated fluorescence (IMF)[3] experiments for comparison.

Table I. Molecular Constants of the PH_2 Radical in the $\tilde{X}^2B_1$ State (MHz)[a]

A	273 784.5(27)	ε_{aa}	−8 433.6(38)
B	242 354.6(30)	ε_{bb}	−2 450.9(35)
C	126 344.6(27)	ε_{cc}	−17.2(33)
Δ_N	16.40(12)	Δ_N^s	1.01(37)
Δ_{NK}	−52.86(34)	Δ_{NK}^s	−6.8(18)
Δ_K	84.90(31)	Δ_K^s	13.2(21)
δ_N	7.460(30)		
δ_K	−3.14(11)	$T_0^0(g_r)$	−0.000 93(78)

a. Values in parentheses denote 2.5 times standard deviations and apply to the last digits of the constants.

References

1) R. N. Dixon, G. Duxbury, and D. A. Ramsay, *Proc. Roy. Soc., London*, **A296**, 137 (1967); J. M. Berthou, B. Pascat, H. Guenebaut, and D. A. Ramsay, *Canad. J. Phys.*, **50**, 2265 (1972).
2) FIR LMR: P. B. Davies, D. K. Russell, B. A. Thrush, and H. E. Radford, *Chem. Phys.*, **44**, 421 (1979); IR LMR: G. W. Hills and A. R. W. McKellar, *J. Chem. Phys.*, **71**, 1141 (1979); A. R. W. McKellar, *Faraday Discussion* No. **71**, to be published.
3) M. Kakimoto and E. Hirota, *IMS Ann. Rev.*, 43 (1980).

Table II. Hyperfine Interaction Constants of the PH_2 Radical in the $\tilde{X}^2B_1$ State (MHz)[a]

Nucleus	Constant	MW (present)	FIR LMR (Ref. 2)	IMF (Ref. 3)
Magnetic hyperfine interaction constants				
P	a_F	207.25(15)	217(10)	208.2(43)
	T_{aa}	−300.25(15)	−303(16)	−312(12)
	T_{bb}	−321.85(35)	−318(12)	−315.0(93)
H	a_F	−48.85(14)	−49(2)	−48.9(38)
	T_{aa}	−0.99(10)	−3(7)	−6.0(88)
	T_{bb}	−4.47(26)	−3(7)	−3.2(70)
Nuclear spin-rotation interaction constant				
P	C_{aa}	0.969(76)		
	C_{bb}	0.51(11)		
	C_{cc}	0.16(20)		

a. See Footnote a of Table I.

II-A-16 Microwave Spectroscopy of the NCO Radical in the Ground, ν_2, and $2\nu_2$ States: the Renner-Teller Effect

Kentarou KAWAGUCHI, Shuji SAITO, and Eizi HIROTA

A linear molecule with an electronic angular momentum shows the Renner-Teller effect, when excited to the bending states. Dixon[1] has reported the observation of the $\tilde{A}^2\Sigma^+ - \tilde{X}^2\Pi$ and $\tilde{B}^2\Pi - \tilde{X}^2\Pi$ electronic transitions of NCO in absorption. His data on the $\tilde{A} - \tilde{X}$ transition were later refined in part by Bolman et al.[2] The NCO radical in the $\tilde{X}$ X state has also been investigated in detail by gas-phase electron paramagnetic resonance[3] and by microwave spectroscopy.[4] Although these previous studies have made it possible for us to understand fine details of the Renner-Teller effect in the

molecule, we initiated the present work to improve precisions of molecular constants in the ground state and also to examine how rotational levels in the $v_2 = 1$ and $v_2 = 2$ states are affected by the Renner-Teller effect; we have recently found such interactions to be important for another Renner-Teller molecule, BO_2.[5]

As in previous studies,[4] we generated NCO by the reaction of HNCO (4 mTorr) with CF_4 (6 ~ 7 mTorr) discharge products. A free space cell of 1 m length was employed. The observed transitions are listed in Table I. Among them transitions in the $v_2 = 1$ $\mu^2\Sigma$ and $\kappa^2\Sigma$ states are expected to be much influenced by the Renner-Teller effect through rovibronic interactions.

References

1) R. N. Dixon, *Phil. Trans. Roy. Soc. London*, **A252**, 165 (1960); *Canad. J. Phys.*, **38**, 10 (1960).
2) P. S. H. Bolman, J. M. Brown, A. Carrington, I. Kopp, and D. A. Ramsay, *Proc. Roy. Soc. London*, **A343**, 17 (1975).
3) A. Carrington, A. R. Fabris, B. J. Howard, and N. J. D. Lucas, *Mol. Phys.*, **20**, 961 (1971).
4) S. Saito and T. Amano, *J. Mol. Spectrosc.*, **34**, 383 (1970); T. Amano and E. Hirota, *J. Chem. Phys.*, **57**, 5608 (1972).
5) K. Kawaguchi, E. Hirota, and C. Yamada, *Mol. Phys.*, **44**, 509 (1981).

Table I. Observed Rotational Transitions of the NCO Radical

Ground state:		
$^2\Pi_{1/2}$	$J = 9/2 \leftarrow 7/2, \cdots, 13/2 \leftarrow 11/2$	} (81 ~ 153 GHz)
$^2\Pi_{3/2}$	$J = 7/2 \leftarrow 5/2, \cdots, 13/2 \leftarrow 11/2$	
$v_2 = 1$ state:		
$^2\Delta_{3/2}$	$J = 9/2 \leftarrow 7/2, \cdots, 13/2 \leftarrow 11/2$	} (81 ~ 153 GHz)
$^2\Delta_{5/2}$	$J = 9/2 \leftarrow 7/2, \cdots, 13/2 \leftarrow 11/2$	
$\mu^2\Sigma$	$N = 2 \leftarrow 1, \cdots, 7 \leftarrow 6$	} (46 ~ 167 GHz)
$\kappa^2\Sigma$	$N = 2 \leftarrow 1, \cdots, 7 \leftarrow 6$	
$v_2 = 2$ state;		
$^2\Phi_{7/2}$	$J = 13/2 \leftarrow 11/2$	(152 GHz)

II-A-17 Molecular Structures and Anharmonic Force Fields of Bent Triatomic Molecules: HO_2 and FSO

Eizi HIROTA and Yasuki ENDO

It is now well known that the zero-point vibration often makes obscure the physcal significance of molecular constants obtained from ground-state spectra. The molecular structure is a good example; structure parameters evaluated from rotational spectra are often subject to large uncertainties because of vibrational contributions. If we know all the cubic (or third-order) anharmonic potential constants, we can calculate vibration-rotation constants α_s and correct the observed rotational constants for zero-point vibration contributions. The rotational constants thus corrected can then be interpreted geometrically, because they correspond to the equilibrium structure. For polyatomic molecules such corrections are, however, extremely difficult to make, and, in fact, examples so far proved to be successful are limited only to the linear and bent symmetric XY_2 type molecules. In the present work we attempted to extend a similar approach to bent XYZ type molecules, because a few transient molecules we have recently investigated are of such type.

There are ten third-order potential constants for a bent XYZ molecule. Some of the α_s constants available from experiments obviously constitute the main source of information on the anharmonicity, and are augmented by similar data on isotopic species, if available. To proceed further, we must appeal to our past experience with the anharmonicity, althogh very limited; e.g. we have found that the "diagonal" anharmonic term F_{iii} is by far the most important. Tables I-V summarize our preliminary results on HO_2 and FSO. We have judged the validity of our anharmonic potential, based on a consistency among calculated equilibrium structures.

Table I. Two Typical Sets of Third-Order Anharmonic Potential Constants of the Hydroperoxyl Radical[a]

Constant	Set I	Set II
F_{111} (md/Å^2)	−45.2(32)	−45.2(27)
F_{222} (md/Å^2)	−35.9(10)	−39.4(11)
F_{333} (md Å)	−0.547 0(78)	−0.572 6(74)
F_{112} (md/Å^2)	+3.7(11)	+3.55(93)
F_{122} (md/Å^2)	+3.59(30)	[0]
F_{113} (md/Å)	[0]	[0]
F_{133} (md)	[0]	[0]
F_{223} (md/Å)	[0]	−2.06(15)
F_{233} (md)	−1.766(33)	−2.020(39)
F_{123} (md/Å)	[0]	[0]

a. The internal coordinates are chosen as 1: ν(H-O), 2: ν(O-O), and 3: δ(H-O-O). Values in parentheses denote standard errors in the fitting and apply to the last digits of the constants. Square brackets mean the values were fixed in the fitting.

Table II. Observed and Calculated Vibration-Rotation Constants of the Hydroperoxyl Radical (MHz)[a]

Isotopic species	Constant	Obs. (σ)	Calc. Set I	Calc. Set II
HO_2	α_1^A	23 640.(150)	23 107.	23 103.
	α_1^B	−40.9(30)	−113.2	−112.8
	α_1^C	−131.4(30)	−52.8	−52.4
	α_2^A	−18 014.6(20)	−18 011.2	−18 012.2
	α_2^B	49.1(52)	47.1	93.8
	α_2^C	187.1(53)	179.0	221.0
	α_3^A	1 423.4(17)	1 423.8	1 423.9
	α_3^B	374.9(11)	379.0	380.1
	α_3^C	409.8(11)	402.1	403.1
DO_2	α_2^A	−7 121.2(13)	−7 123.8	−7 122.6
	α_2^B	−25.3(20)	29.0	6.5
	α_2^C	290.8(21)	333.6	314.8

a. The α constants were taken from references listed below. HO_2 ν_1: C. Yamada and Y. Endo, *IMS Ann. Rev.*, 48 (1980), ν_2: K. Nagai, Y. Endo, and E. Hirota, *J. Mol. Spectrosc.*, **89**, 520 (1981), ν_3: A. R. W. McKellar, Faraday Discussion No. 71, to be published, DO_2 ν_2: A. R. W. McKellar, loc. cit.

Table III. Molecular Structure of the Hydroperoxyl Radical

Parameter	Present (r_e)	Tuckett et al.[a] (r_0)	Barnes et al.[b] (r_0)
H-O (Å)	0.989 ± 0.003	0.97_5	0.9774
O-O (Å)	1.323 ± 0.002	1.32_9	1.3339
H-O-O (°)	106.5 ± 0.3	104.0	104.15

a. R. P. Tuckett, P. A. Freedman, and W. J. Jones, *Mol. Phys.*, **37**, 403 (1979).
b. C. E. Barnes, J. M. Brown, and H. E. Radford, *J. Mol. Spectrosc.*, **84**, 179 (1980).

Table IV. Two Typical Sets of Third-Order Anharmonic Potential Constants of the FSO Radical[a]

Constant	Set I	Set II
F_{111} (md/Å^2)	−17.063	−18.035
F_{222} (md/Å^2)	−49.441	−53.787
F_{333} (md Å)	−2.823	−3.140
F_{112} (md/Å^2)	−12.974	−10.692
F_{113} (md/Å)	[0]	[0]
F_{122} (md/Å^2)	−1.851	[0]
F_{223} (md/Å)	[0]	[0]
F_{133} (md)	−2.753	[0]
F_{233} (md)	[0]	−6.040
F_{123} (md/Å)	[0]	1.171

a. The internal coordinates are chosen as 1: ν(S−F), 2: ν(S = O), and 3: δ(F−S−O). See Footnote a of Table I.

Table V. Equilibrium Structure of the FSO Radical

r(S−F)	1.6068 ± 0.0014	Å
r(S = O)	1.4426 ± 0.0014	Å
θ(F−S−O)	107.921 ± 0.025°	

II—B Development of New Instruments and New Experimental Methods for High Resolution Spectroscopy

The scope of researches is limited by capabilites of instruments available. This is particularly true for spectroscopic investigations of simple molecules, one of the fundamental problems the Department is interested in. When we repeat experiments using spectrometers of similar performance, we will obtain almost identical results. It is therefore very urgent for us to always maintain our research facilities at levels of performance as high as possible. High precision with which we determine molecular parameters often unravels new aspects of molecular properties that have escaped experimental observations. Needless to say, high sensitivity will supply us with fundamentally new information on molecular systems we are investigating. Along with these efforts to improve our facilities and with their applications to more interesting problems, we should also try to develop methods that are based upon something new. This project obviously premises not only detailed knowledge on molecules under investigations, but also that connecting with related fields. Various kinds of technical problems are to be solved. In this sense jont researches including collaboration with the Development Workshop are indispensable. Developments of new instruments that are thus brought about will open new research areas in the field of molecular science.

II-B-1 A Discharge-Current Modulation Technique in Diode Laser Spectroscopy: Lifetime Measurements for a Few Free Radicals

Yasuki ENDO, Keiichi NAGAI, Chikashi YAMADA, and Eizi HIROTA

Zeeman modulation in diode laser spectroscopy has been proved to be extremely efficient in picking up paramagnetic lines from among many other diamagnetic lines. However, it cannot be applied to transitions with too small Zeeman effects to be modulated. Furthermore, there are many unstable species of fundamental importance that are diamagnetic. Good examples are molecular ions of the form MH^+, where M denotes a stable molecule. We have recently shown that a discharge-current modulation technique can be useful for such cases.

We inserted a triode between a discharge electrode and the earth to switch on and off the discharge current, and detected the absorption signal by using a phase-sensitive detector (PSD). To eliminate 1/f noise, however, this modulation is preferably combined with conventional source-frequency modulation, i.e., the first PSD is employed to demodulate source-modulation signals, and its output is then fed into the second PSD for discharge current modulation. Because of a finite time constant of the first PSD, the discharge current modulation frequency was limited in our case to lower than 500 Hz. An example of SF spectra recorded with this double modulation is shown in Figure 1.

If we assume the absorption signal I to decrease as exp $(-t/\tau_0)$ after the discharge is switched off, we may estimate the lifetime τ_0 by plotting log I versus log ω, where ω denotes the discharge current modulation frequency. The lifetime of SF was thus

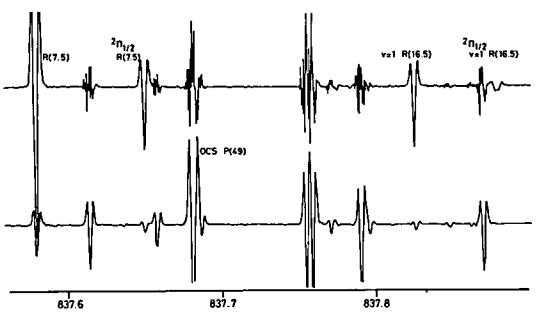

Figure 1. A part of the SF vibration-rotation spectrum around 838 cm^{-1}. The lower trace was recorded with conventional source-frequency modulation with 2f detection, i.e. the second derivative of the original absorption signal is displayed. The upper trace was obtained by feeding the signal (the lower trace) into a second PSD operated at the discharge-current modulation frequency. Carbonyl sulfide, which is abundant in the cell as a reactant, gives very strong signals, which thus appear also in the upper trace because of incomplete filtering. But their overall phases look opposite to those of SF lines.

estimated to be 0.5 msec or longer under the condition of II-A-11. Similarly the CH_3 radical generated as described in II-A-8 was found to live for about 1.4 msec on average after the discharge was switched off.

II-B-2 A mm-Wave Spectrometer in the 180-221 GHz Region

Shuji SAITO, Yasuki ENDO, and Eizi HIROTA

As a part of a Large Scale Research Equipment, "High Resolution Spectroscopic System in the Far-Infrared Region", a mm-wave spectrometer was constructed.

As mm-wave sources six klystrons were installed, which cover the region from 180 to 203 GHz and also from 218 to 221 GHz. A backward-wave oscillator, Carcinotron CO 10, was added as a source in the 285 to 305 GHz region. The typical output of these sources ranges from 0.5 to 8 mW, which is large enough for straight absorption spectroscopy. An InSb detector, QMC QFI/2, which operates at the liquid He temperature, was found to be very efficient in observing absorptions of mm-wave by molecules.

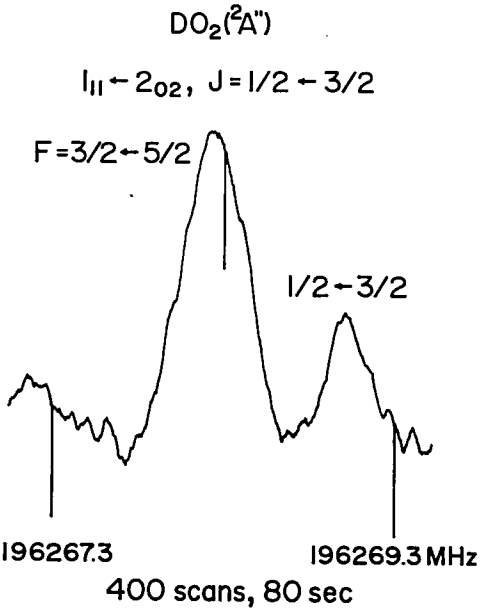

Figure 1. The hyperfine components of the $1_{11} \leftarrow 2_{02}$, J = 1/2 ← 3/2 transition of DO_2. An InSb photo-conductive detector cooled to 4.2°K was used for the observation.

The spectrometer has already been employed to observe rotational transitions of a few radicals: PH_2 (II-A-15), CCl (II-A-6), DO_2 (II-A-10), and SF [IMS Ann. Rev. 46 (1980)], and also those of NO_2 in excited vibrational states (II-C-1). Figure 1 shows the $1_{11} \leftarrow 2_{02}$, J = 1/2 ← 3/2 transition of DO_2 as an example of mm-wave spectra recorded with the present spectrometer.

II-B-3 A Far-Infrared Laser Magnetic Resonance Spectrometer

Kentarou KAWAGUCHI, Chikashi YAMADA, and Eizi HIROTA

As a part of a Large Scale Research Equipment, "High Resolution Spectroscopic System in the Far-Infrared Region", a far-infrared (FIR) laser magnetic resonance (LMR) spectrometer was constructed. The light source is a CO_2-laser pumped FIR laser. The CO_2 laser used for pumping is an Appolo Model 560 laser, which has been improved in stability by supporting the cavity with invar rods; the maximum output was found to be 50 W. The FIR cavity consists of two concave mirrors, one with R = 2 m and the other with R = 1.5 m; the latter can be displaced by a differential micrometer. The cavity length is about 1.1 m. A 10 μm thick polyethylene film fixed at the Brewster angle to the FIR laser beam separates the FIR laser gain tube from a sample cell. The pumping CO_2 laser beam is introduced into the gain tube through a side window, and is reflected back and forth by a 56 ϕ Cu pipe of an effective length of 24 cm placed in the gain tube,[1] the inside of which has been polished for efficient pumping. The FIR laser output is coupled out in a direction perpendicular to the laser axis by a Cu block 45° cut.

We have observed many laser lines oscillating in the region from 70 μm down to 500 μm. The typical output of the CH_3OH 118.8 μm line was 0.3 mW. The absorption cell is made of a 50 ϕ quartz tube, which is placed between pole caps of a Varian V 7301 12 inch magnet. The maximum magnetic field available is 16 kG. The magnetic field is modulated by a 100 kHz AC field of a few Gauss. Figure 1 gives an overall view of the spectrometer. The sensitivity was tested by observing oxygen

transitions at 163 μm. The FIR laser used was a CH_3OH laser, and the FIR output was detected by an InSb detector, QMC QFI/2, cooled to 4.2 K.

Reference

1) K. M. Evenson, private communication.

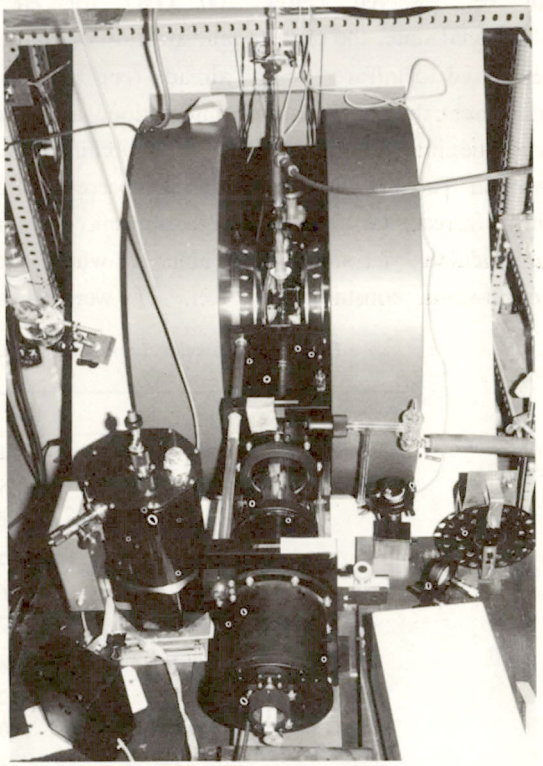

Figure 1. A far-infrared LMR spectrometer. The FIR source is a CO_2-laser pumped laser.

II—C High Resolution Spectroscopy of Molecules of Fundamental Importance

Needs for high quality spectroscopic data have recently been increasing, especially for fundamental molecules. Such spectroscopic data have been accumulated in the past perhaps because of interest in precise molecular structure determination. However, research activities in other related fields such as reaction kinetics, environmental researches, and astronomy have recently been so advanced that precise spectroscopic data are indispensable as means of monitoring molecules. Spectroscopic data available are not necessarily good enough and must be replaced by new spectra that meet necessary requirements. Such spectroscopic data on stable molecules will be presented in this section.

II-C-1 The Microwave Spectra of NO_2 in the Excited Vibrational States: Fine and Hyperfine Structures

Mitsutoshi TANIMOTO *(Sagami Chem. Res. Center)*, **Shuji SAITO, Eizi HIROTA, and Takehiko TANAKA** *(Kyushu Univ.)*

Because of its importance in photochemistry, the NO_2 molecule has been investigated many times by high-resolution infrared spectroscopy.[1] High vibrational states associated with the ground electronic state are now recognized to perturb excited electronic states, causing very complicated NO_2 spectra in the visible region. We started the present microwave observation of NO_2 to make energy levels, not only of the rotation, but also of the fine and hyperfine structures, much more precise than those previously reported.

A source-modulation microwave spectrometer with a 3.5 m long free-space cell at IMS was employed. The cell was heated to about 100°C to increase intensities of vibrational satellites. Because the molecule is so light that only 7 or 8 transitions

can be observed below 200 GHz for each vibrational state, the centrifugal distortion constants were fixed to infrared results already reported. The rotational, the spin-rotation interaction, and the hyperfine interaction constants thus obtained are given in Table I. By combining the present data with infrared data,[1] the vibration-rotation constant are calculated as shown in Table II, where the ground-state constants of Ref. 2) were also employed.

References

1) M. Laurin and A. Cabana, *J. Mol. Spectrosc.*, **69**, 421 (1978); J.-M. Flaud, C. Camy-Peyret, V. M. Devi, P. P. Das, and K. N. Rao, *J. Mol. Spectrosc.*, **84**, 234 (1980); A. Cabana, M. Laurin, C. Pépin, and W. J. Lafferty, *J. Mol. Spectrosc.*, **59**, 13 (1976); W. J. Lafferty and R. L. Sams, *J. Mol. Spectrosc.*, **66**, 478 (1977).
2) J. M. Brown, T. C. Steimle, M. E. Coles, and R. F. Curl, Jr., *J. Chem. Phys.*, **74**, 3668 (1981).

Table I. Molecular Constants of NO_2 in the Excited Vibrational States (MHz)[a]

Constant	ν_1	ν_2	$2\nu_2$	ν_3
A	242 636.701(76)	251 048.865(48)	263 171.241(64)	233 064.918(56)
B	12 932.202(6)	12 999.939(5)	12 997.236(5)	12 919.951(13)
C	12 226.425(11)	12 278.237(8)	12 250.956(9)	12 226.755(21)
$\varepsilon_{aa} + \Delta_K^S$	5 498.78(12)	5 947.18(5)	6 575.58(32)	5 158.42(48)
ε_{bb}	7.82(1)	6.98(1)	6.19(1)	7.77(3)
ε_{cc}	−99.79(2)	−97.63(1)	−100.22(2)	−94.75(5)
a_F	146.10(4)	146.71(3)	146.26(7)	146.29(15)
T_{aa}	−22.04(9)	−22.28(7)	−22.40(35)	−21.25(71)
T_{bb}	39.62(4)	40.05(4)	40.24(16)	38.92(32)
$(aa)_Q$	0.72(15)	0.57(5)	0.79(21)	0.31(37)
$(bb)_Q$	−1.74(8)	−1.66(4)	−1.82(11)	−1.65(18)

a. Values in parentheses denote standard deviations and apply to the last digits of the constants.

Table II. Vibration-Rotation Constants of NO_2 (MHz)[a]

Constant	A	B	C
α_1	−2 536.0(48)	71.30(13)	76.58(13)
α_2	−10 088.0(45)	2.22(12)	25.46(11)
α_3	6 619.5(28)	83.12(20)	75.11(20)
γ_{11}	−2.5(12)	0.211(53)	0.797(57)
γ_{22}	489.15(26)	−0.229(37)	−0.385(38)
γ_{33}	129.4(17)	0.36(14)	0.86(14)
γ_{12}	757.7(87)	1.19(20)	1.05(18)
γ_{13}	−355.7(19)	0.622(72)	−7.852(75)
γ_{23}	−602.0(24)	−0.310(36)	−1.669(32)

a. See Footnote a of Table I.

II—D Local Structure Formations in Solutions

The space-time correlation between the positions and between the orientations of different molecules are useful information for understanding the mixing state of solutions from a molecular view point. Coherent visible light scattering experiments afford information about these correlations in the form of fluctuations in the semimacro-regions. Mean square amplitudes and time correlations of concentration fluctuations can be obtained by observing the Rayleigh line intensity and the Rayleigh line shape, respectively. Based upon these observations, the local structure formations can be discussed from the view points of the spacial correlations between the positions of different molecules and the velocity correlations between different molecules. In our laboratory, a light scattering method has been established to study local structures formed in solutions and has been extensively applied for variety of systems with fruitful success. At the same time, it has been recognized that a complementary usage of a varitey of experimental methods are necessary for the complete understanding of local structures formed in solutions. From this respect, a few experimental and theoretical methods have been developed.

II-D-1 Observation of Mutual Diffusion Coefficients and Cooperative Motions in Binary Solutions of t-Butyl Alcohol-Water and 2-Butoxyethanol-Water.

Nobuyuki ITO[1] *(Tokyo Metropolitan Univ.)*, **Koichi SAITO**[2] *(Tokyo Metropolitan Univ.)*, **Tadashi KATO, and Tsunetake FUJIYAMA**

[*Bull. Chem. Soc. Jpn.*, **54**, 991 (1981)]

Rayleigh scattering spectra were observed for the binary solutions of t-butylalcohol (TBA)-water and 2-butoxy-ethanol (BE)-water. The observed line-widths were reduced to mutual diffusion coefficients. The observed concentration dependencies of the mutual diffusion coefficients were well explained by postulating the existence of "moving units", namely, a group of molecules which move together for a time much longer than the velocity autocorrelation time.

The structure of the moving units which are formed in the TBA-water solution was,

$(H_2O)_{20}TBA \qquad (x_{TBA} \leq 0.05)$

$4(H_2O)_{20}TBA \qquad (x_{TBA} > 0.05)$

where x_{TBA} is the mole fraction of TBA. For the BE-water soultion, the structure was found to be,

$(H_2O)_{50}BE \qquad (x_{BE} \leq 0.02)$

$3(H_2O)_{50}BE \qquad (x_{BE} > 0.02)$

where x_{BE} is the mole fraction of BE. These results were compared with the results which had been obtained from the concentration dependencies of the mean-square concentration fluctuation values.[3-5]

Note and References

1) IMS Graduate Student from Tokyo Metropolitan University for 1981.
2) An undergraduate student of Tokyo Metropolitan University.
3) K. Iwasaki and T. Fujiyama, *J. Phys. Chem.*, **81**, 1908 (1977).
4) K. Iwasaki and T. Fujiyama, *J. Phys. Chem.*, **83**, 463 (1979).
5) T. Kato, N. Ito, and T. Fujiyama, *Bull. Chem. Soc. Jpn.*, **53**, 2167 (1980).

II-D-2 Determination of Local Structure and Moving Unit Formed in Binary Solution of t-Butyl Alcohol and Water

Nobuyuki ITO[1] *(Tokyo Metropolitan Univ.)*, **Tadashi KATO, and Tsunetake FUJIYAMA**

[*Bull. Chem. Soc. Jpn.*, **54**, 2573 (1981)]

The concentration dependences of the mutual diffusion coefficients at 24, 37, and 63°C were observed for a binary solution of t-butyl alcohol (TBA) and water by the use of the light scattering method. The observed concentration dependences of the mutual diffusion coefficients were explained

well by postulating the existence of a "moving unit", namely, a group of molecules which move together for a time much longer than the velocity correlation time. The structure of the moving units which are formed in the solution are $(H_2O)_{11}$TBA at 24°C and $(H_2O)_{20}$TBA at 63°C in the concentration range of $0 < x_{TBA} < 0.1$, where x_{TBA} is the mole fraction of TBA. Taking into account of the local structures, which had been determined from the concentration dependences of the mean-square concentration fluctuation values, we could conclude that water molecules form a polyhedron which encages a TBA molecule and that these cages then gather together to form an aggregate. It is essential that these polyhedra do not share their faces with each other in the aggregate. It was also concluded that the number of cages which form an aggregate increases with an increase in the temperature. This suggests the existence of a pseudo-critical temperature for this system. That is to say, the TBA-water solution can separate into two phases under high pressure, a TBA-rich phase and a water-rich phase, in the latter of which almost all the molecules form polyhedra.

In Figure 1, the schematic representation of the mixing state of the TBA-water solution is given only for 24°C.

Figure 1 (a)

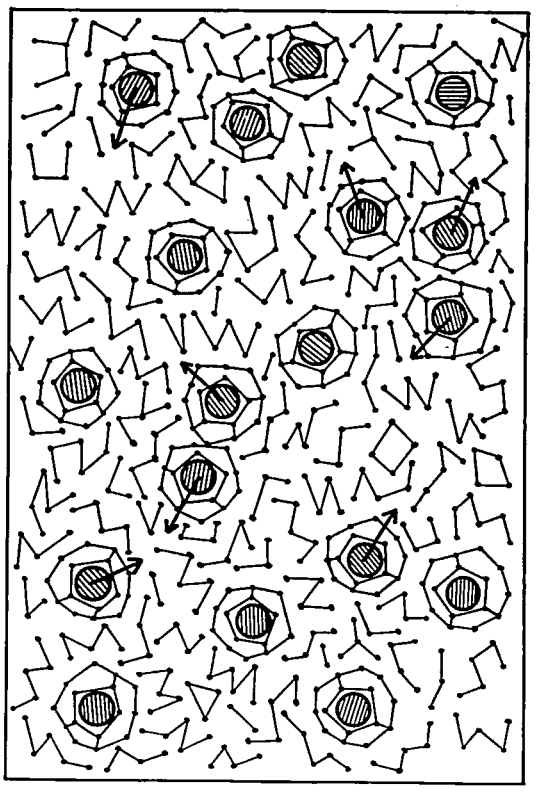

Figure 1 (b)

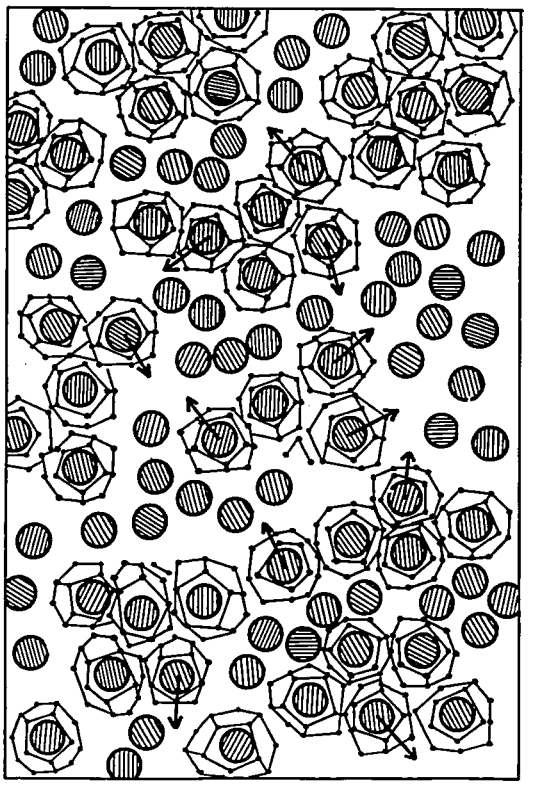

Figure 1. Mixing State of TBA-water solution for: (a) $X_{TBA} \simeq 0.01$, (b) $x_{TBA} \simeq 0.09$ (schematic) at 24°C. (●) and (◍) represent a water and a TBA molecule, respectively.

Note and References

1) IMS Graduate Student from Tokyo Metropolitan University for 1981.
2) K. Iwasaki and T. Fujiyama, *J. Phys. Chem.*, **81**, 1908 (1977).
3) K. Iwasaki and T. Fujiyama, *J. Phys. Chem.*, **83**, 463 (1979).

II-D-3 Light Scattering Study of the 12-Hydroxyoctadecanoic Acid and Benzene Mixture in the Gel State

Nobuyuki ITO[1] *(Tokyo Metropolitan Univ.)*, **Masako YUDASAKA**[1] *(Tokyo Metropolitan Univ.)*, **and Tsunetake FUJIYAMA**

[*Bull. Chem. Soc. Jpn.*, **54**, 1939 (1981)]

The structure of the 12-Hydroxyoctadecanoic acid-benzene gel was studied by the use of the light scattering spectrometer. The angular dependence of the scattering intensity and the time correlation function of the electric field were measured. In Figure 1 show the observed correlation functions

for the 33 mmol·dm^{-3} 12-hydroxyoctadecanoic acid-benzene gel at 24°C.[2,3]

It was found that the coarse mesh network and the fine mesh network coexisting in this gel. The former was detected by the intensity measurement, while the latter was detected by the intensity fluctuation spectroscopy. The structure of the network constructed in this gel system is schematically illustrated in Figure 2. The usefulness of the light scattering technique was incidentally emphasized.

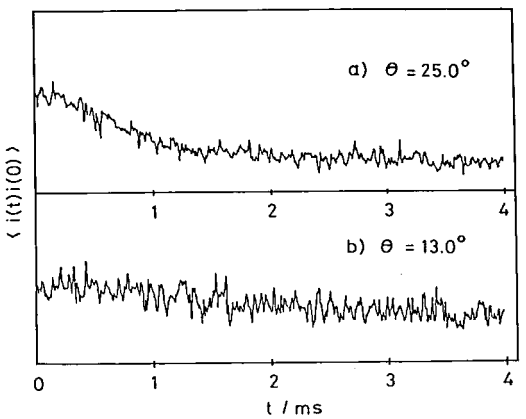

Figure 1. The observed correlation function for the 33 mmol dm^3 12-hydroxyoctadecanoic acid-benzene gel at 24°C. The scattering angles are: a) 25.0° and b) 13.0°.

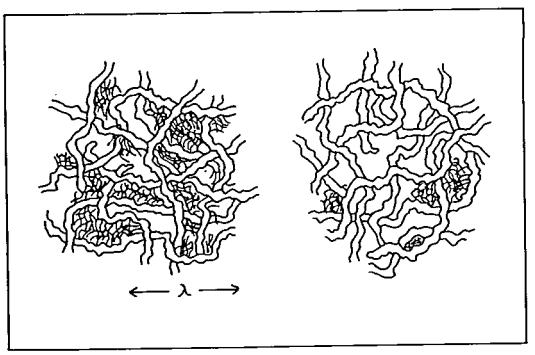

Figure 2. The structure of the network constructed in the 12-hydroxyoctadecanoic acid-benzene gel (schematic). λ is several thousand Angstroms which corresponds to the wave-length of the incident light.

Note and References

1) IMS Graduate Student from Tokyo Metropolitan University for 1981.
2) T. Tachibana, T. Mori, and K. Hori, *Bull. Chem. Soc., Jpn.*, **53**, 1714 (1980).
3) T. Tachibana and H. Kambara, *Bull. Chem. Soc. Jpn.*, **42**, 3422 (1969).

II-D-4 Brillouin Scattering Study of Clathrate Hydrate Formation in Acetone-Water Solution

Tadashi KATO, Masako YUDASAKA[1] *(Tokyo Metropolitan Univ.)*, and Tsunetake FUJIYAMA

[*Bull. Chem. Soc. Jpn.*, **53**, 1632 (1981)]

Light Scattering spectra have been observed for binary solutions of acetone and water at 24, 34, and 44°C in the concentration range of $0 < x_{AC} < 0.25$, where x_{AC} is the mole fraction of acetone. The hypersonic velocities and the adiabatic compressibilities at 4.5 GHz were obtained from the observed values of Brillouin shifts. In Figure 1 shows the concentration dependence of the adiabatic compressibility for the acetone-water system at 24, 34, and 44°C. The observed concentration and temperature dependencies of the adiabatic compressibility were interpreted by assuming the existence of clathrate hydrate-like local structures in the solutions.

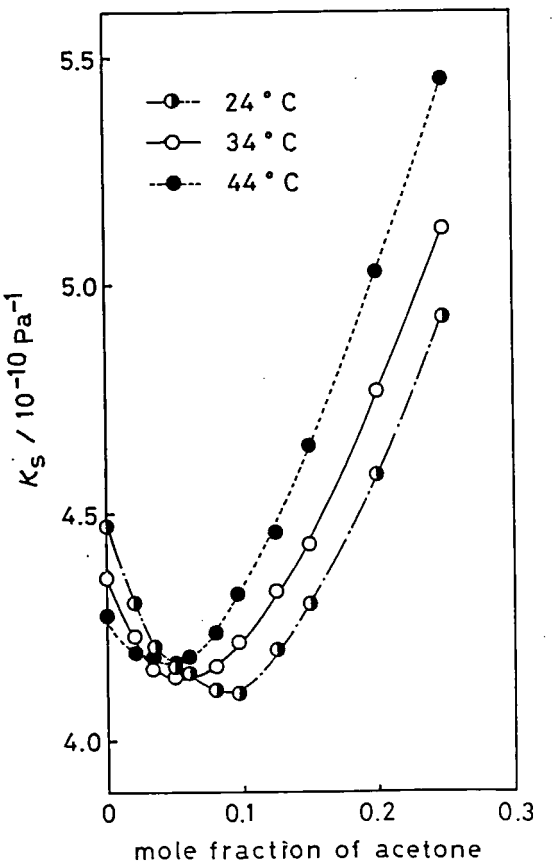

Figure 1. Concentration dependence of adiabatic compressibility for acetone-water system at 24, 34, and 44°C.

The adiabatic compressibilities for binary solutions of t-butyl alcohol (TBA) and water were used as reference data.[2] A comparison is made between the local structure formed in the acetone-water solution and that in the TBA-water solution.[3,4]

Note and References

1) IMS Graduate Student from Tokyo Metropolitan University for 1981.
2) J. Stone and R. E. Pontinen, *J. Chem. Phys.*, **47**, 2407 (1967).
3) K. Iwasaki and T. Fujiyama, *J. Phys. Chem.*, **81**, 1098 (1977); **83**, 463 (1979).
4) N. Ito, K. Saito, T. Kato, and T. Fujiyama, *Bull. Chem. Soc. Jpn.*, **54**, 991 (1981).

II-D-5 X-Ray Diffraction Study of Liquid Methanol

Masami TANAKA[1] *(Tokyo Metropolitan Univ.)*, **Keiko NISHIKAWA**[2] *(Gakushuin Univ.)*, **and Tsunetake FUJIYAMA**

[*Chemistry Lett.*, 327 (1981)]

The X-ray diffraction intensity measurements of liquid methanol were carried out by the use of an energy-dispersive X-ray diffractometer. No apparent maximum due to hydrogen bonded oxygen-oxygen interference was detected in the electronic distribution function. The diffraction intensity curve and distribution function observed in the preset study are consistent with Harvey's results[3], but in contradiction to those of Wertz and Kruh.[4] In Figure 1 shows the electronic radial distribution function from which the bulk density is subtracted.

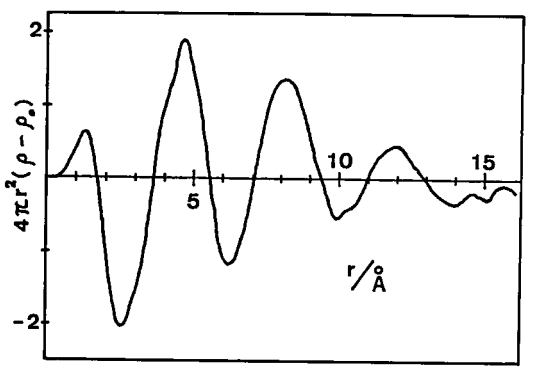

Figure 1. Electronic Radial distribution function from which the bulk density was subtracted (liquid methanol at room temperature).

Note and References

1) IMS Graduate Student from Tokyo Metropolitan University for 1981.
2) IMS Joint Researcher from Gakushuin University for 1981.
3) G. G. Harvey, *J. Chem. Phys.*, **6**, 111 (1938).
4) D. L. Wertz and R. K. Kruh, *J. Chem. Phys.*, **47**, 388 (1967).

II-D-6 Spectroscopic Studies of Surfactant Solubility, 3. Side-Chain Effects of Phosphatidyl Compounds in Chloroform Solutions

Mitsuyo OKAZAKI *(Tokyo Medical and Dental Univ.)*, **Ichiro HARA** *(Tokyo Medical and Dental Univ.)*, **Yumiko K. TSUTSUI** *(Tokyo Metropolitan Univ.)*, **and Tsunetake FUJIYAMA**

[*Bull. Chem. Soc. Jpn.*, **54**, 2399 (1981)]

The infrared spectra of phosphatidyl and related compounds were studied with respect to their side-chain effects on solubility. Our special interest lies in the solubility of the phosphatidyl compounds, which have this structure:

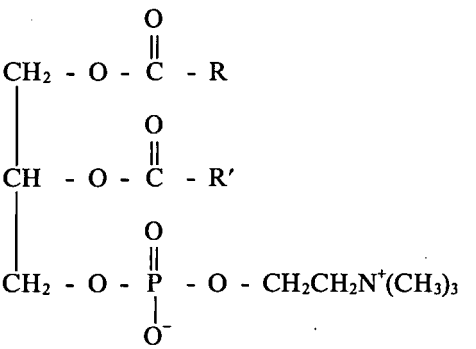

with respect to:

1) the role of a phosphate group (a polar group),
2) the role of a choline moiety (an end group),
3) the role of an acyloxyl group, and
4) the role of double bond chains,

to the solubilities in chloroform. We focused our attention on the infrared absorption band of chloroform, which is related to the hydrogen bonding between chloroform and a phosphate group. As we could get quantitative knowledge about the hydrogen bonding between chloroform and a phophate group, we could relieve the effects of the other moieties on the solubilities.

It was clarified that the existence of a hydrogen-bonding between chloroform and a phosphate

group is essential for these phosphatidyl compounds to form stable solutions in chloroform. The existence of double bond alkyl-chains and acyloxyl groups was clarified to be very useful for those compounds to have a strong solvent-phobic character without losing their solubility in solvents. The role of a choline moiety was also clarified. The details of the analysis of the infrared intensity were also described. It was emphasized that the intensity enhancement due to hydrogen-bond formation can be quantitatively related to the enthalpy change due to hydrogen-bond formation. The anomalous phase separation were observed for a few chloroform solutions of alkylphosphorylcholines.

References

1) M. Okazaki, I. Hara, and T. Fujiyama, *J. Phys. Chem.*, **80**, 64 (1976).
2) M. Okazaki, I. Hara, and T. Fujiyama, *J. Phys. Chem.*, **80**, 1586 (1976).
3) M. Okazaki, I. Hara, and T. Fujiyama, *Chem. and Phys. of Lipids*, **17**, 28 (1976).

II-D-7 Chloride-35 NMR Studies of the Ion Pairing of the Chloride Ion in Water and Aqueous Acetone

Masako YUDASAKA[1] *(Tokyo Metropolitan Univ.)*, **Tadashi SUGAWARA, Hiizu IWAMURA, and Tsunetake FUJIYAMA**

[*Bull. Chem. Soc. Jpn.*, **54**, 1933 (1981)]

The chloride-water mixture and the chloride-water-acetone mixtures were studied by measuring the ^{35}Cl NMR spectra. From the line-width analyses, it has been concluded that the line-widths of the chloride solutions are affected only by the nearest neighbours of the chloride ions, which makes it possible to study the interaction between the chloride ion and the solvent molecules microscopically. In Figure 1 shows the concentration dependence of the half-line-width of the aqueous potassium chloride system at 30°C, where no remarkable concentration dependence could be observed. Figure 2 shows the concentration dependence of the half-line-width in the aqueous tetraethylammonium chloride, while that in the aqueous acetone-tetraethylammonium chloride is shown in Figure 3. The line-broadening observed in the latter two systems are due to the breaking down of the local symmetry around the chloride ions, which is brought about by the asymmetric solvation of the chloride ion.

The problem concerning the ion pair formation in solutions was discussed. It has been emphasized that the observation of the concentration dependence of line-widths can be very powerful method for the detection of contact ion pairs formed in the solutions.

Note

1) IMS Graduate Student from Tokyo Metropolitan University for 1981.

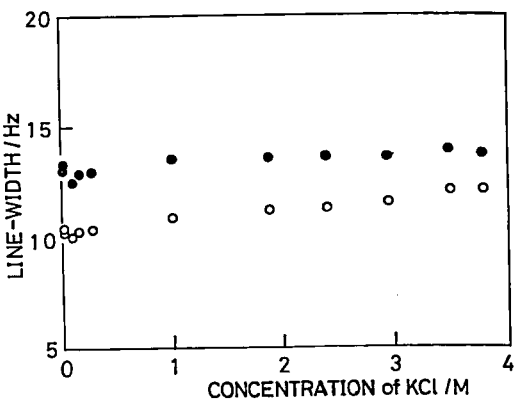

Figure 1. Concentration dependence of the half-line-width of the auqeous potassium chloride system at 30°C.
(○): The observed value, (●): the viscosity corrected value.

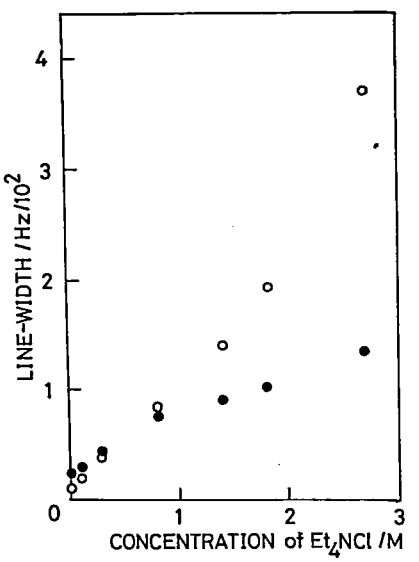

Figure 2. Concentration dependence of the half-line-width in the aqueous tetraethylammonium chloride system at 30°C.
(○): The observed value, (●): the viscosity corrected value.

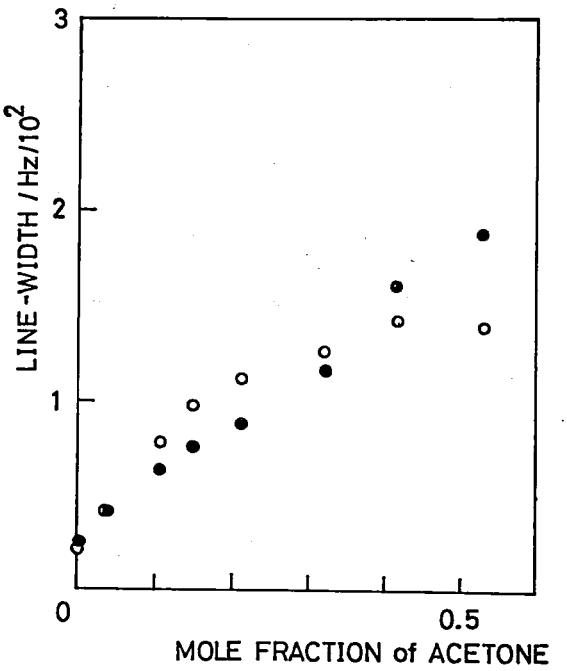

Figure 3. Dependence of the half-line-width of the tetraethylammonium chloride-aqueous acetone system on the mole fraction of acetone at 30°C (the concentration of tetraethylammonium chloride is 0.1 mol dm^{-3}).
(○): The observed value, (●): the viscosity corrected value.

II-D-8 Light Scattering Spectrometer for Intensity Measurement, 2.

Nobuyuki ITO[1] *(Tokyo Metropolitan Univ.)* **and Tsunetake FUJIYAMA**

A light scattering spectrometer was constructed for the purpose of observing an angular dependence of light intensity scattered from a binary solution in its critical region.

A schematic diagram of the spectrometer is shown in Figure 1. The light source is an argon ion laser (Spectra-Physics, 165–09). The power of incident light is adequately attenuated by a ND filter. The incident light is focused into a sample cell (20 mm outer diameter). The temperature drift of sample is controlled within ±0.01 K for the temperature range of 80–373 K. The scattering angle θ is defined by two slits (s = 1.0 mm) which are 25 cm apart from each other. The angular acceptance is less than 0.5° and, therefore, the fractional error in $\sin^2(\theta/2)$ is less than 3%. A photomultiplier tube (HTV 1P28) is operated at about 800 V. The output power is integrated at a

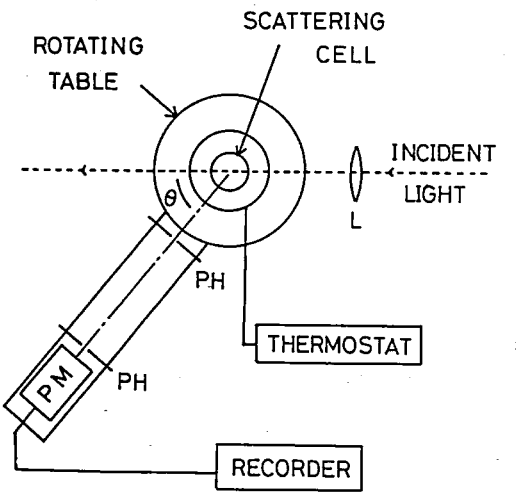

Figure 1. Schematic diagram of the light scattering spectrometer for intensity measurement.

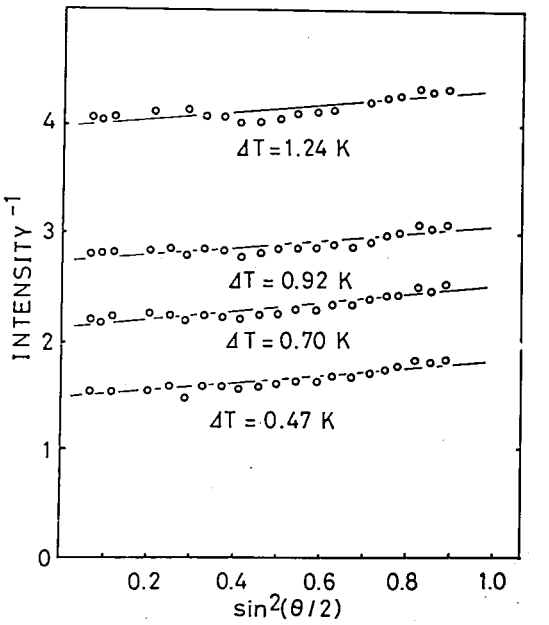

Figure 2. Reciprocal scattering intensity plotted against $\sin^2(\theta/2)$ observed for nitrobenzene-n-hexane system.

time constant of 1s and is recorded on an recorder.

The reliability of the optical set-up was confirmed by ascertaining the fluorescence from a rhodamine-6G solution had no angular dependence over an angle range of 35–140°.

Figure 2 shows a plot of reciprocal intensity against $\sin^2(\theta/2)$ observed for the nitrobenzene-n-hexane system at the critical mixing composition in the temperature range of ΔT = 1.24–0.47 K, where $\Delta T \equiv T_c - T$ and T_c is a critical temperature. The critical index ν for this system was obtained from

the temperature dependence of the density correlation length of fluctuation as 0.6.

Note

1) IMS Graduate Student from Tokyo Metropolitan University for 1981.

II-D-9 Coherent Anti-Stokes Raman Scattering Spectrometer

Ryosaku IGARASHI and Tsunetake FUJIYAMA

The coheren anti-Stokes Raman scattering (CARS) spectrometer set up in this laboratory is shown schematically in Figure 1.

A Nd:YAG laser system (Quanta-Ray, DCR-1A) provides a 532 nm beam. The 532 nm beam is split into two beams. One is used as ω_1 beam and the other is used for pumping a dye laser (Qanta-Ray, PDL-1) that produced a beam at ω_2. The direction of the polarization of ω_1 and ω_2 are adjusted by the use of Glan-Laser prism polarizers, GP1 and GP2. The two light beams ω_1 and ω_2 are adjusted to be parallel with each other before the lens L_1, and then focused into a sample cell. The coherent scattering light at frequency ω_3, where $\omega_3 = 2\omega_1 - \omega_2$, is selected out by the use of an iris. The polarization direction of CARS light at ω_3 is selected out by a Glan prism, GP3, and focused into a monochromator. The monochromated CARS light is detected by a photomultiplier (RCA 1P-28A) connected to a dual-channel boxcar averager (NF, BX-531). The calculated output, which has been corrected for the intensity fluctuation of the ω_2 beam, is recorded on an X-Y recorder.

An example of CARS spectra which was observed by this spectrometer is shown in Figure 2.

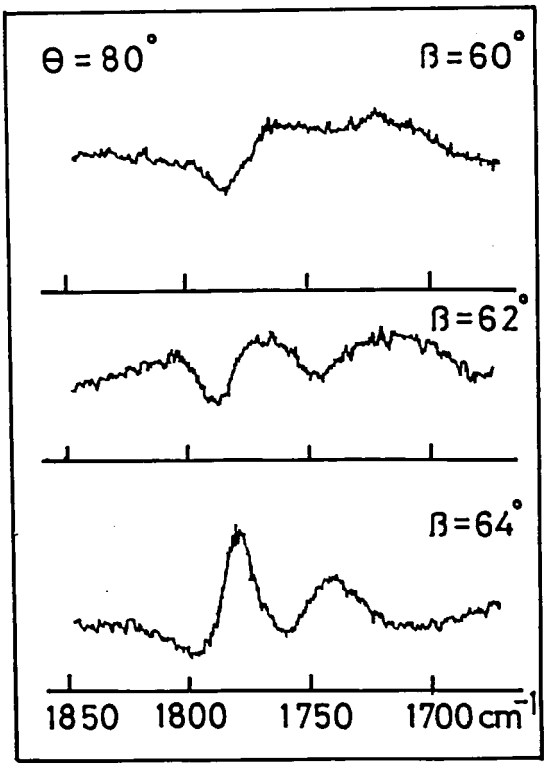

Figure 2. Polarization CARS spectra of hexachloroacetone in $(\omega_1 - \omega_2) = 1650 - 1850$ cm^{-1} region.

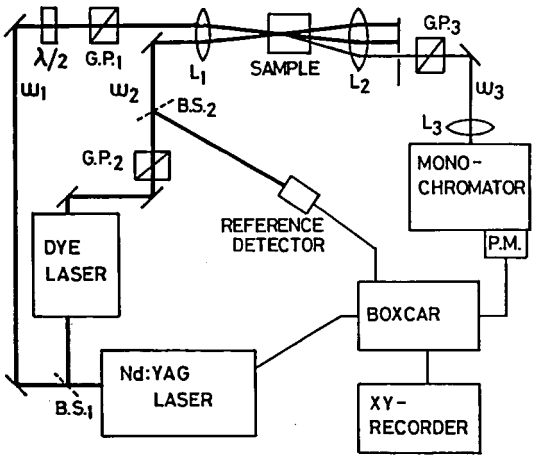

Figure 1. Schematic Diagram of the CARS spectrometer.

II-D-10 Conduction Correlator Analyzer

Tadashi KATO, Kohji OHBAYASHI[1], and Tsunetake FUJIYAMA

The time-correlation function for the concentration fluctuation of an ion affords information about dynamical structures of electrolyte solutions. For example, the relaxation time of the association-dissociation reaction of ions is strongly correlated with the life-time of the local structures for the measurement of the electrical conductivity fluctuation. The experimental arrangement is schematically illustrated in Figure 1.

The sampel cell is made of pyrex glass. The two reservours which contain the sample solution are jointed by a capillary. The length and the radius of the capillary are 0.5–1.0 mm and 0.02–0.05 mm, respectively. The two pairs of electrodes are made of platinum.

A constant current source is provided by a battery (300–500V) connected to the outer electrodes through a resistance (20–30 MΩ) which is much larger than that of the cell. The voltage across the inner electrodes is made up of dc component and the fluctuating component which carries the information in question. The latter is amplified by a low-noise preamplifier (PAR 113). After further amplification, the fluctuating voltage is autocorrelated by a 400 channel correlation and probability analyzer (KANOMAX SAI-43A). The computed time correlation function of the voltage is, then, displayed on an oscilloscope and recorded on an X-Y recorder. The cell, battery, and first preamplifier are mounted in an aluminum box for the purpose of shielding them from other electrical noises.

By the use of this apparatus, we can observe the electrical conductivity fluctuations whose relaxation time is about 1–100 ms. The time correlation function of the electrical conductivity observed in the aqueous solution of $BeSO_4$ is illustrated in Figure 2.

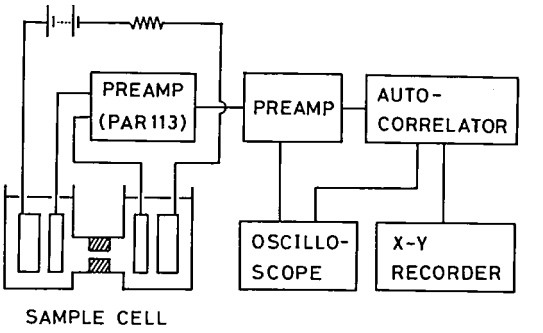

Figure 1. The experimental arrangement of the conduction correlator analyzer.

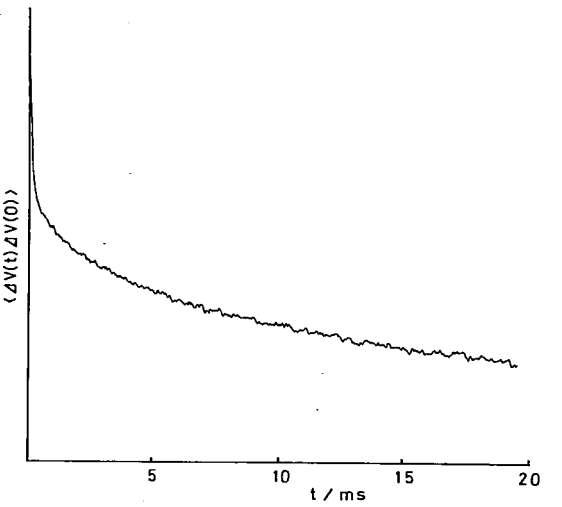

Figure 2. The time correlation function observed for the aqueous solution of $BeSO_4$.

Note and Reference

1) A joint researcher from Hiroshima University.
2) K. Ohbayashi and Tatsuya Yasunaga, *J. Chem. Phys.* (submitted, 1981).

II—E Optical Spectroscopy of Molecular Ions

Molecular ions have unique properties of spectroscopic interest such as Jahn-Teller effect, which stable closed shell molecules usually do not have. Although abundant knowledge has been accumulated so far on stable molecules, much is to be revealed on molecular ions. Making use of the resolving power, optical spectroscopy can supply basic information on the geometrical structure of both ground and electronically excited states. Not only that the spectroscopic properties of molecular ions are of basic value, ions are important in various fields of chemistry. For example, they play crucial role as reaction intermediates, as fragments in mass spectroscopy and as interstellar medium. To know the geometrical structure, electronic configuration and internal dynamics of ions are necessary in the understanding of many aspects of chemistry.

II-E-1 Fluorescence Spectra from Fluorobenzene Cations in the Gaseous State

Yasuo UDAGAWA, Ryosaku IGARASHI, Tsunetake FUJIYAMA, and Nobuyuki ITO
(Tokyo Metropolitan Univ.)

Cations of benzene and its symmetric derivatives have degenerate ground state and Jahn-Teller effect is expected. Since fluorobenzene cations fluoresce with quantum yield of nearly unity, many studies have been published. Of the most detailed is the study by laser induced fluorescence of cations in rare gas matrices at low temperature.[1] For the study of the structure and potential, however, it is

desirable to observe ions in gaseous state.

In this study, molecular ions are formed by electron impact on a pulsed supersonic beam of parent molecule seeded in rare gas. Because of the extensive rotational and vibrational cooling accompanying adiabatic expansion from high pressure source, fluorescence spectra observed are extremely simple and allow detailed analysis.

The apparatus is shown schematically in Figure 1. Pulsed beam of parent molecules seeded in rare gas expands through a nozzle whose diameter is 1 mm. Duration of the pulse is about 0.5 msec and the repetition rate of 10 Hz was obtained with 1500 l/sec oil diffusion pump. Electrons intersect it at right angles and the fluorescence is collected on the third axis and focused on the entrance slit of a 0.8 m double monochromator (Spex 1403). Signal is detected by a PMT (R464) and processed by a boxcar intergrater. The electron gun is made of a filament, a grid and three stage electrostatic lenses. With 100 ev electron energy, electron current of 200 μA was obtained.

The fluorescence spectra of $C_6F_6^+$ in Ar and in He are shown in Figure 2. As is seen from the assignment indicated in the Figure, vibrational structure of the fluorescence consists of irregular progression of two degenerate vibrational modes (ν_{17} and ν_{18}), besides the totally symmetric one (ν_2). This is in sharp contrast with the fluorescence spectra from benzene derivatives of low symmetry (ex. $C_6H_2F_4$), which shows regular vibrational structure of totally symmetric vibration, and is a manifestation of the existence of Jahn-Teller effect.

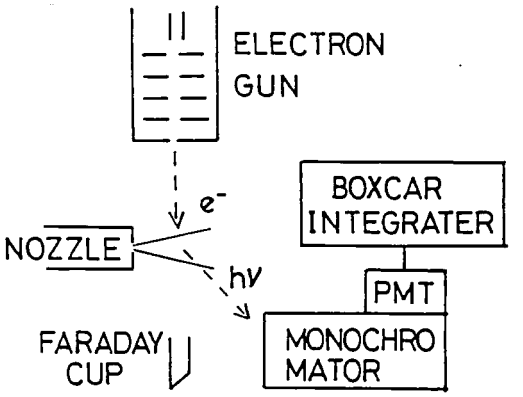

Figure 1. The apparatus for the fluorescence spectra of gas phase molecular ions.

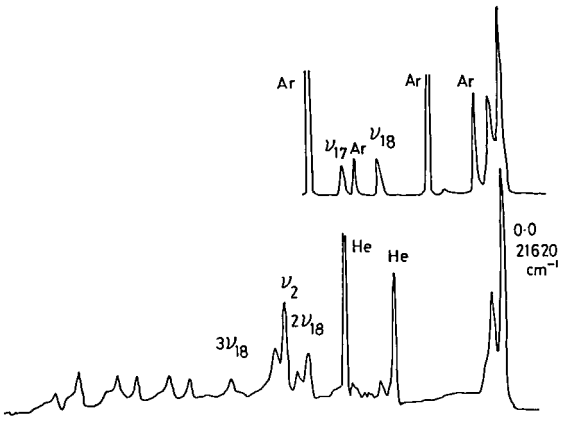

Figure 2. Fluorescence spectra of $C_6F_6^+$ in Ar (upper trace) and in He (lower trace). Bands without assignment in the figure are attributed to the combination bands of ν_2 and ν_{17} and ν_{18}.

Reference

1) V. E. bondibey et al. *J. Chem. Phys.*, **73**, 3053 (1980).

II—F Intensity Measurement of Vibration Spectra

It has been a long lasting dream of a vibration spectroscopist to measure intensities of individual lines precisely for a series of vibration-rotation spectra. Although the resolving power of conventional spectrometers was not sufficient enough to observe individual vibration-rotation lines separately, the development of a diode laser source has enabled us to observe absorption spectra with extremely high resolution. It is right time to examine to what extent does the improvement of a laser source in infrared region make progress the intensity measurement of vibration spectra. It is also important to establish a reliable method for measuring an intensity of a single vibration-rotation line by the use of a diode laser source.

II-F-1 Measurement and Analysis of the ν_4 Band of Fluoroform and Its Molecular Constants

Susumu SOFUE[1] *(Tokyo Metropolitan Univ.)*, **Kentarou KAWAGUCHI, Eizi HIROTA, and Tsunetake FUJIYAMA**

[*Bull. Chem. Soc. Jpn.*, **54**, 897 (1981)]

The ν_4 fundamental of fluoroform has been measured with a tunable diode-laser source spectrometer. The following molecular constants were determined from the spectral analysis.

Table I. Molecular constants of the ν_4 band of CHF_3 (cm^{-1})

ν_0	1377.84567(33)	η_4^J	$1.436(35) \times 10^{-6}$
B_4	0.3447884(12)	η_4^K	$-8.20(28) \times 10^{-7}$
C_4	0.18913390(54)		Ground State
$(C\zeta)_4$	0.186195(10)	B_0	0.34520105(7)
D_4^J	$3.7774(85) \times 10^{-7}$	C_0	0.18925(10)
D_4^{JK}	$-5.735(18) \times 10^{-7}$	D_0^J	3.779×10^{-7}
D_4^K	$2.941(12) \times 10^{-7}$	D_0^{JK}	$-6.0375(134) \times 10^{-7}$
q_4	$-1.115(12) \times 10^{-4}$	D_0^K	3.72×10^{-7}

Numbers in parentheses denote the standard deviation^.

Using the molecular constants of the $2\nu_3$, the Coriolis x-y interaction constant between the ν_4 fundamental and $2\nu_3$, $|\ \zeta_{334}\ |$, was estimated to be 0.065.

A part of the high resolution spectra observed by the diode laser-source spectrometer is illustrated in Figure 1.

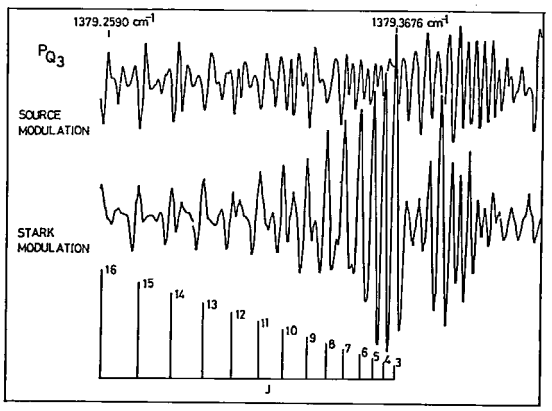

Figure 1. The high resolution spectra observed by the diode laser-source spectrometer (upper: source modulation, lower: Stark modulation).

Note

1) IMS Graduate Student from Tokyo Metropolitan University for 1980.

II-F-2 Absolute Intensity Measurement of ν_4 Band of Fluoroform by the Use of a Tunable Diode Laser Source

Susumu SOFUE[1] *(Tokyo Metropolitan Univ.)*, **Kentarou KAWAGUCHI, Eizi HIROTA, and Tsunetake FUJIYAMA**

[*Bull. Chem. Soc. Jpn.*, **54**, 2089 (1981)]

The absolute infrared absorption intensities have been measured for the $^PP_{35}(35)$ and $^PP_{36}(36)$ lines which belong to the ν_4 fundamental of fluoroform by the use of a tunable diode laser source. Based upon the assignment of the rotation-vibration lines[2], the line intensities were converted to the integrated intensity, Γ. The observed Γ value of 5360 ± 220 cm^2mol^{-1} was compared with that observed by the conventional method.[3] The final results are summarized in Table I.

Table I Absolute Intensities Γ/ cm^2mol^{-1}

5360 ± 220	present result
6360 ± 312	S. Saeki, et al.[a]
4960 ± 240	b)

a) S. Saeki, M. Mizuno, and S. Kondo, *Spectrochim. Acta, Part A*, **32**, 403 (1976).
b) The intensity for the ν_4 fundamental calculated from the value of a), assuming T = 293 K.

The raliability of the intensity measurement by the use of a tunable diode laser source has been thoroughly discussed.

As the method was established, we observed the line-intensities for the $^PP_{J-6}(J)$ series lines, because it has been established in our previous work[2] that the x-y type Coriolis interaction affects the energy levels of this line series considerably. A part of the results is shown in Table II. The systematic decrease in the effective transition dipole moment with the increase of J and K values for $v_4 = 1$ was analyzed in view of the x-y type Coriolis interaction. It was concluded that the interaction is "positive".

Table II Line Intensities of $^{P}P_{J-6}(J)$

Line	$S/cm^{-2}atm^{-1}$	μ_{ij}/D
$^{P}P_{24}(30)$	0.277	0.121
$^{P}P_{27}(33)$	0.237	0.117
$^{P}P_{30}(36)$	0.191	0.111

D(Debye) = $10^{-18}g^{1/2}cm^{5/2}s^{-1}$

Note and References

1) IMS Graduate Student from Tokyo Metropolitan University for 1980.
2) S. Sofue, K. Kawaguchi, E. Hirota, and T. Fujiyama, *Bull. Chem. Soc. Jpn.*, **54**, 897 (1981).
3) S. Saeki, M. Mizuno, and S. Kondo, *Spectrochim. Acta, Part A*, **32**, 403 (1976).

II—G Study of NO_3 by Laser Induced Fluorescence

Takashi ISHIWATA,* Ichiro FUJIWARA,* Yukio NARUGE,* Kinichi OBI,* and Ikuzo TANAKA *(*Tokyo Institute of Technology and IMS)*

The nitrate radical, NO_3, has been directly detected by laser induced fluorescence method. The band structure of fluorescence excitation spectrum was fairly consistent with that of absorption. The excitation at 662 nm corresponding to the 0-0 transition exhibited the fluorescence spectrum showing progressions at 1050 and 1480 cm^{-1} intervals, presumably corresponding to the symmetrical stretching (ν_1) and degenerate stretching (ν_3) modes of NO_3 with D_{3h} symmetry, respectively. The collision-free fluorescence lifetime was 2.8 μsec being compatible to the radiative lifetime assuming $^2E' \leftarrow {}^2A_2'$ transition. No predissociation occurs at the lowest vibratioal state of electronically excited NO_3.

II—H Large Amplitude Intra-Molecular-Motions

II-H-1 Degenerate Inversion in Hydrazine

Masamichi TSUBOI and Yoshiaki HAMADA

Hydrazine NH_2NH_2 has two amino groups with internal rotation angle of 90° from each other around the N-N bond as axis. There is, therefore, almost no interaction between the inversion motions of the two amino groups. Hence, one of the inversion levels in every vibrational state is nearly degenerate. The dengeneracy, however, is removed if there is an appreciable amount of interaction between the inversion motions, because this causes an amount ($\pm\zeta\hbar$) of angular momentum around the molecular axis, so that the angular momentum of the pure rotation becomes $(K \mp \zeta)\hbar$ and the rotational energy levels

$$E_{rot} = \overline{B}[J(J+1) - K^2] + A(K \mp \zeta)^2$$

$$= \overline{B}J(J+1) + (A - B)K^2 \mp 2\zeta KA + A\zeta^2.$$

From an analysis of a microwave specgrum (S. Tsunekawa and T. Kojima, *J. Phys. Soc. Japan* **49** 1957 (1980)), we have estimated ζ'' (for the ground vibrational state) to be 0.000098. From our diode laser spectroscopic measurements (with Laser Analytics Model LR-3, through the courtesy of Professor E. Hirota, Dr. C. Yamada, and Dr. K. Kawaguchi), in combination with the inversion splittings estimated for the ground vibrational state, ζ' (for the first excited state of the antisymmetric amino-wagging vibration) has been estimated to be 0.000736.

II-H-2 Infrared Absorption Spectrum of $^{15}NO_2$ — Analyses of the ν_2 and ν_3 Bands

Naoki TANAKA, Yoshiaki HAMADA, and Masamichi TSUBOI

The ν_2 (bending) band of $^{15}NO_2$ (isotopic purity > 99.1%) was examined by a Laser Analytics

Model LR-3 diode laser system. In the 670 ~ 790 cm^{-1} range, 20 lasing modes were obtained each of which had a 0.3 ~ 0.8 cm^{-1} tuning range. The sample pressure was 1 torr, cell length 80 cm, and the temperature 60 ~ 70°C. The calibration was made by the use of the known lines of CO_2 (650–700 cm^{-1}), those of C_2H_2 (740–790 cm^{-1}), and a wavemeter constructed by K. Nagai et al. (*J. Mol. Spectrosc.*, **84** 197 (1980)). A part of the spectrum is illustrated in Figure 1, where both components (F_1 and F_2) of the spin splitting are clearly identified.

The ν_3 (antisymmetric stretching) band was examined with a Nicolet 7199 FTIR spectrophotometer. Resolution was 0.06 cm^{-1}, the number of accumulation 128, the sample pressure 10 torr, cell length 10 cm, and the temperature 60–70°C. The spectral range examined was 1500–1650 cm^{-1}, where lines of K = 0 ~ 11 and N = 0 ~ 50 are involved. This is an A-type band, and many lines are overlapping one another. The analysis was made stepwise by a simultation method by the use of a program BC3 written by Dr. T. Nakagawa. The coriolis interaction between the ν_3 and $2\nu_2$ (1480 cm^{-1}) has been ignored because its effect reaches only 0.02 cm^{-1} at D = 5 and N = 30. The values of the molecular parameters so far obtained are given in Table I.

Table I Molecular constants of $^{15}NO_2$ (cm^{-1})

Vibrational state	(000)	(001)
T_0	0.0	1582.109(6)
A	7.63077	7.4193(5)
B	0.433762	0.43095(6)
C	0.409446	0.40705(6)
$10^7\Delta_N$	3.26150	3.41(32)
$10^5\Delta_{NK}$	−1.67549	−2.085(96)
$10^3\Delta_K$	2.39841	2.288(21)
$10^8\delta_N$	3.36095	−2.95(345)
$10^6\delta_K$	3.88132	3.938(11)

Standard errors are given in the parentheses.

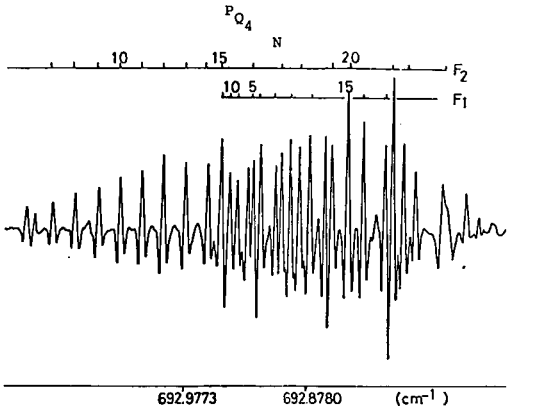

Figure 1. A diode laser spectrum of $^{15}NO_2$.

II—I Production of Highly Excited Atoms from Molecules

II-I-1 Dissociative Excitation of Nitrogen Molecule by Electron Impact for the Production of Nitrogen Atom in Highly Excited Rydberg States

Tamotsu KONDOW *(University of Tokyo and IMS)*, **Shigeru OHSHIMA** *(University of Tokyo)*, **Tsutomu FUKUYAMA** *(National Institute for Environmental Studies)*, **and Kozo KUCHITSU** *(University of Tokyo)*

The dynamics of the production of atomic nitrogen in highly excited Rydberg states (N**) by electron impact on nitrogen molecules was studied by measuring the distributions of the kineitc energy and the principal quantum number (n) of N**, as a function of the scattering angle. The experiments were performed on a crossed molecular- and electron-beam geometry. The detailed description of the apparatus is reported elsewhere.[1] Figure 1 shows the excitation function for the production of N** and N_2^{**} ($16 < n < 50$). In the threshold region at about 25 eV, most of the excited species were N_2^{**}, and N** became prominent at impact energies higher than 45 eV, as evidenced in the TOF spectra shown in Figure 2. The TOF spectra for N** shown in Figure 3 give single peak (7.5 eV) at the impact energy of 60 eV while the other peak (13 eV) appears at impact energies higher than 70 eV. The excitation function for each peak indicates that the 7.5 and the 13 eV peaks seem to correspond to the processes, $N_2 + e \rightarrow N(^4P) + N^+(^3P)HR$ and $N^+(^3P) + N^+(^3P)HR$, respectively, where HR represents

high Rydberg states. The angular distributions, $I(\theta)/I(90°)$, were measured and are shown in Figure 4 in the scattering angles between 70 and 115°. Here, $I(\theta)$ refers to the signal intensity at a given angle θ. The distributions suggest that a $\Sigma_g^+ \rightarrow \Sigma_g^+$ transition of N_2 is responsible to the N** production. In addition, the n-distribution at the impact energy of 100 eV was measured by use of the field ionization technique (see Figure 5). In the n-region lower than 18, the short radiation lifetime deactivates N** before arriving at the detector, while in the region higher than 18, the excitation cross section limits the population of N**. The photoionization of N** by a far infrared laser was examined in order to determine the n-distribution more precisely and to study its feasibility as a detector of far infrared light. The laser was designed by Kawaguchi of IMS.

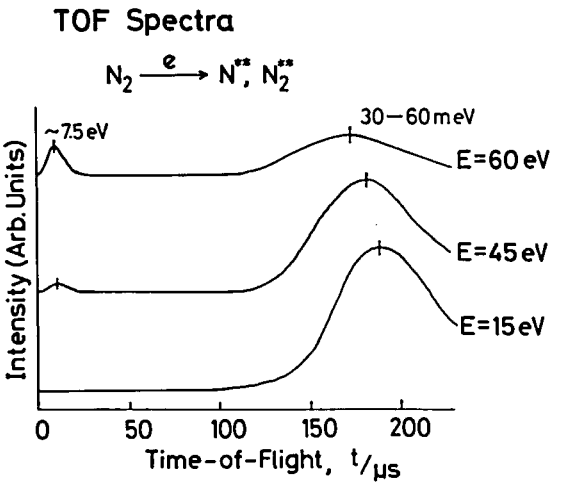

Figure 2. The time-of-flight spectra of N** and N_2^{**}.

Reference

1) T. Kondow, T. Fukuyama, S. Ohshima and K. Kuchitsu, *Ann. Rev. IMS* (1980).

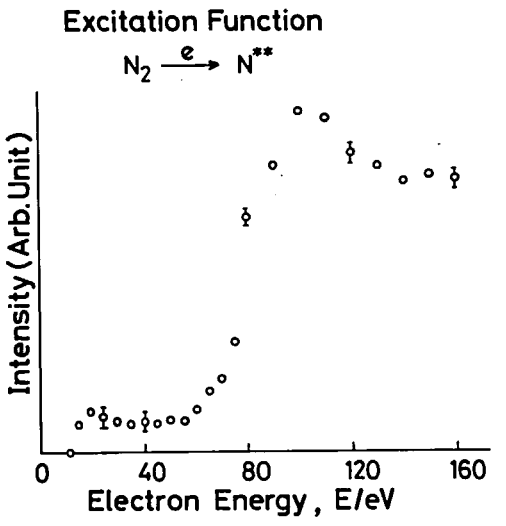

Figure 1. The excitation function for the production of N** and N_2^{**} from N_2 by electron impact.

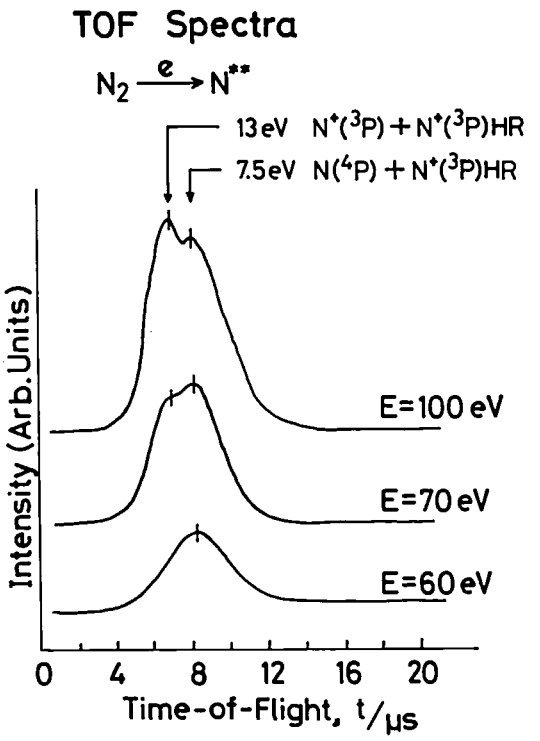

Figure 3. The time-of-flight spectra of N**.

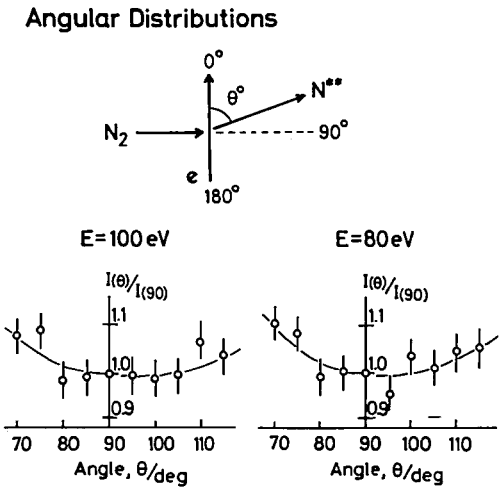

Figure 4. Angular distributions of N**.

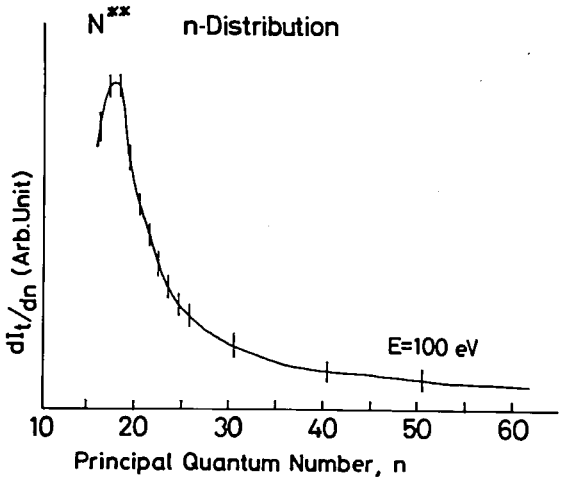

Figure 5. The n-distribution of N** at the impact energy of 100 eV.

RESEARCH ACTIVITIES III
Department of Electronic Structure

III—A Primary Photochemical Reactions of Organic Compounds

III-A-1 Direct Observation of the Rate for Cis → trans and Trans → cis Photoisomerization of Stilbene with Picosecond Laser Photolysis

Minoru SUMITANI and Keitaro YOSHIHARA

[*Bull. Chem. Soc. Jpn.*, in press]

The rates for the direct cis → trans and trans → cis photoisomerizations of stilbene in solution were measured with a newly developed monitor light source for picosecond laser photolysis in the UV region. The analytic light was generated by focussing the fundamental laser beam onto the electrode of a high pressure Xe lamp (Figure 1). Figure 2(a) shows the time course of the analytic light (~245 nm) when *trans*-stilbene is excited by fourth harmonic (266 nm) of a mode-locked Nd:YAG laser. The time course shows the rate of trans → cis isomerization is 1.2×10^{10} s^{-1} in hexane at 295 K. The fluorescence decay rate constant of the S_1 state of *trans*-stilbene has the same value. Thus, the decay of the S_1 state is the rate limiting step and the lifetime of an intermediate perpendicular state has to be very short. The cis → trans isomerization is very fast as shown in Figure 2(b) and the half life of the excited *cis*-isomer is less than a few picosecond. This is in good agreement with our laser-induced fluorescence experiment by a picosecond double pulse.[1] These observations strongly indicate that the isomerization reaction proceeds through the potential surface of the singlet excited states.

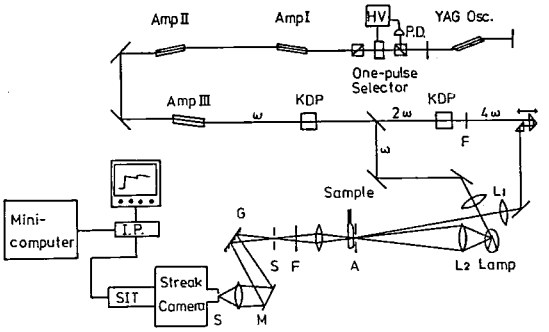

Figure 1. Schematic diagram of apparatus employed for picosecond photolysis in the UV region.

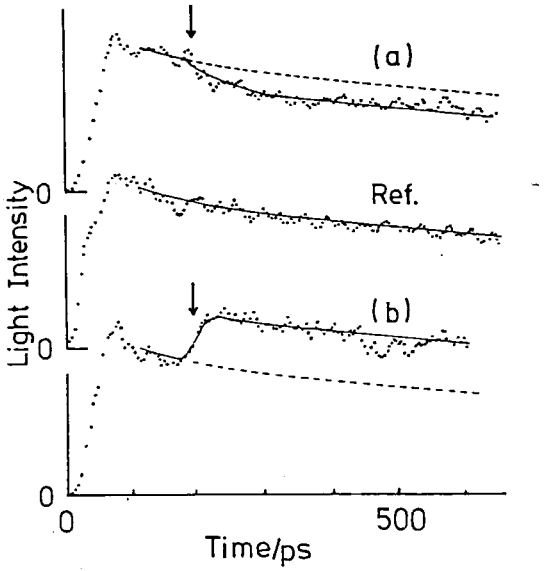

Figure 2. Time dependent transmission change; (a) and (b) were observed at 240—250 nm upon excitation of solutions of *trans*-stilbene (a) and *cis*-stilbene (b), respectively. Broken curves represent the reference light profile (ref.). The data represent the average of 5 shots. The arrows indicate the time of excitations by the fourth harmonic light (266 nm).

Reference

1) M. Sumitani, N. Nakashima, and K. Yoshihara, *Chem. Phys. Lett.*, **68**, 255 (1979).

III—B Electronic Structures of Excited States

III-B-1 Laser Flash Photolysis of Benzene IV. Physicochemical Properties of Mist Produced by Laser Excitation.

Nobuaki NAKASHIMA and Keitaro YOSHIHARA

Since 1975 laser induced particle(mist) formation has been observed in several systems. Formation of solid alkalihalides from alkali metal vapor and H_2[1], of polymers from NO_2 and SO_2, and of sulfer or polymer from $SF_6 + H_2$, CS_2, and Cl_2CS are induced by irradiation with either a CW or a pulsed laser. During the course of the laser-flash photolytic study of gaseous benzene, we observed mist formation for the first time in an organic system.[2]

Mist formation is observed when gaseous benzene(8–75 torr) with oxygen($\lesssim 10^{-5}$ – 860 torr) is irradiated by a KrF excimer laser as shown in Figure 1. The lower photograph shows light (He-Ne laser) scattering by mist. Time courses of the scattered light after irradiation are shown in Figure 2. It requires a few tens of second for mist to grow. The falling speed of mist shows that the their size varies from 2 to 6 μm depending on the gas pressure. The number of droplets produced by irradiation with a 100 mJ/cm^2 pulse is estimated to be 1×10^5/cm^3 by measuring the benzene pressure change and also by a light extinction measurement. The nuclei seem to be produced by two-photon excitation of benzene and to grow into mist through a susequent oxidation and/or polymerization reaction. The photochemical disapperance yield of benzene was 0.1 and phenol was identified with a quantum yield of 0.01. We suggest that the components of the mist are non-volatile photoproducts and not pure benzene as discribed in our preliminary report.[2]

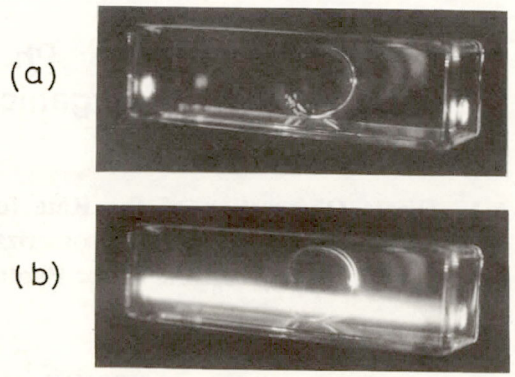

Figure 1. Mie scattering by mist produced from gaseous benzene when excited by a KrF laser. a) Sample cell before irradiation, b) after irradiation of 40 torr of benzene and 2 torr of oxygen. The size of the sample cell is $4 \times 1 \times 1$ cm^3. The area of the laser beam is 2.5×0.5 cm^2. The sample is irradiated without focussing the beam.

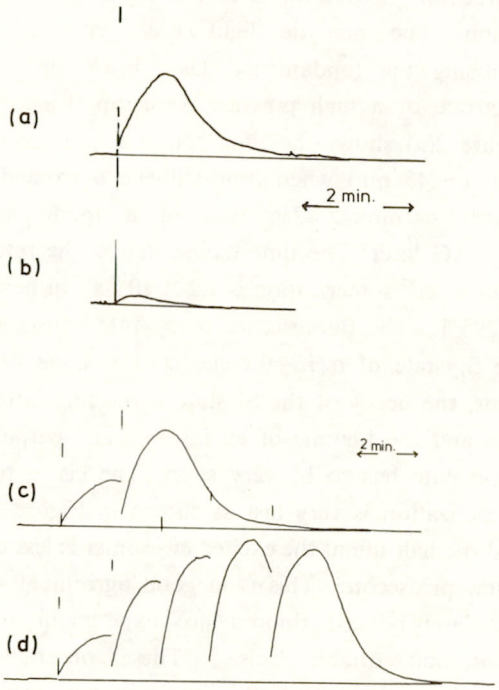

Figure 2. Time courses of the light scattered at 90°. a) 20 torr of benzene with 0.08 torr of oxygen, b) the same sample as a), but without oxygen. c) and d) repeated excitation of laser pulses quenched the scattered light. The spikes indicate noise due to the laser pulses.

References

1) A. Tam, G. Moe, W. Happer, *Phys. Rev. Lett.*, **35**, 1630 (1975).
2) N. Nakashima, H. Inoue, M. Sumitani, and K. Yoshihara, *J. Chem. Phys.*, **73**, 4693 (1980).

III—C Studies on Transient Phenomena in Biology

III-C-1 Picosecond Laser Fluorometry of FAD in D-Amino Acid Oxidase-Benzoate Complex

Kunio YAGI *(Nagoya Univ.)*, **Fumio TANAKA** *(Mie Nursing College)*, **Nobuaki NAKASHIMA, and Keitaro YOSHIHARA**

[in "Flavins and Flavoproteins", V. Massay and H. Williams, Jr., ed. Elsevier, Amsterdam (1981), in press]

Effect of the binding of benzoate, a typical competitive inhibiter with substrate, to D-amino acid oxidase [D-amino acid: O_2 oxidoreductase (deaminating), EC 1.4.3.3] on the dissociation constant of the coenzyme, FAD, and its microenvironments were investigated through the measurements of the coenzyme fluorescence. The difference in the properties between monomer and dimer of the enzyme-benzoate complex were compared with fluorescence characteristics. Fluorescence lifetime of FAD in the complex was measured by using mode-locked Nd:YAG laser and a streak camera as shown in Figure 1 and Table I. The value of the lifetime was 60 ± 10 ps in the monomer of the complex. Fluorescence of the dimer was extremely short (M 5 ps). Upon complex formation with benzoate, a marked decrease in lifetime was observed with the dimer (reduced to less than 1/10) and a slight decrease with the monomer (reduced to one half).[1] By analyzing the fluorescence decay curve, dissosiation constant of the monomer-dimer equilibrium in D-amino acid oxidase-benzoate complex was evaluated to be 0.4 ± 0.3 μM, which is much smaller than that of the holoenzyme.[1] The relative quantum yield of the fluorescence of FAD in the ternary complex to that of free FAD obtained by fluorescence intensity and anisotropy exhibited applicable dependence on the complex formation: larger at lower concentration. These results suggest that a molecular interaction between FAD and amino acid residue(s) is strengthened by

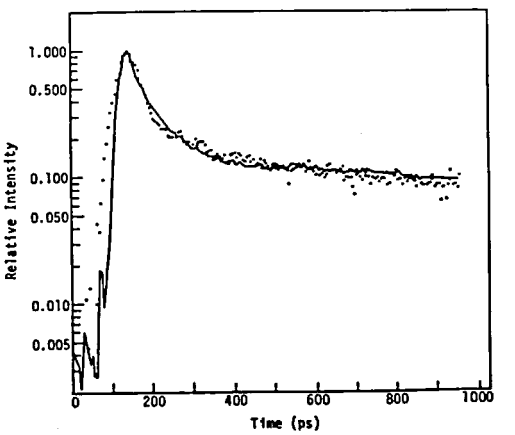

Figure 1. Fluorescence decay curve of FAD in D-amino acid oxidase-benzoate complex solution. Observed data are indicated by dots. Calculated decay curve is shown by a solid curve. Concentration of the benzoate complex was 50 μM in 0.017 M pyrophosphate buffer (pH 8.3) containing 0.1% benzoate.

Table I. Fluorescence Decay Parameters of Fan in D-Amino Acid Oxidase-Benzoate Complex Solution

	Concentration (μM)	τ_1 (ps)	α_1	τ_2 (ps)	α_2	τ_3 (ps)	α_3	RMS
I	5	13	0.86	530	0.14			0.0672
	10	15	0.90	620	0.10			0.0533
	50	14	0.90	460	0.10			0.0635
	100	12	0.90	350	0.10			0.0544
II	5	1.2	0.915	70	0.067	2300	0.018	0.0568
	10	0.4	0.910	50	0.076	2300	0.014	0.0442
	50	0.8	0.920	60	0.069	2300	0.011	0.0472
	100	0.6	0.925	660	0.066	2300	0.009	0.0414

Buffer system: 0.017 M pyrophosphate-HCl containing 0.1% benzoate (pH 8.3).
I: 2-component analysis; II: 3-component analysis. Fluorescent species with lifetime τ_1, τ_2 and τ_3 were assigned to the dimer, monomer and FAD dissociated from the complex, respectively. α_1, α_2 and α_3 are component fractions corresponded to τ_1, τ_2 and τ_3, respectively. RMS: root of mean square between the observed and calculated fluorescence intensities.

the complex formation, which contributes to the stability of the complex.

Reference

1) N. Nakashima, K. Yoshihara, F. Tanaka, and K. Yagi, *J. Biol. Chem.*, **255**, 5261 (1980).

III-C-2 Picosecond Fluorescence Studies of P700-Enriched Particles of Spinach Chloroplasts

Keiji KAMOGAWA, John M. MORRIS, Yoshihiro TAKAGI, Nobuaki NAKASHIMA, Keitaro YOSHIHARA, and Isamu IKEGAMI
(Teikyo Univ.)

Dynamic properties were investigated on the picosecond fluorescence of highly enriched reaction-center particles of photosystem I (8 – 10 chlorophylls/P700) prepared from spinach. The number (N) of photons to excite chlorophyll molecules per reaction center was controlled from 0.06 to 80. The 1/e lifetime was ca. 25 ps for $N \lesssim 1$ as shown in Figure 1, which is much shorter than the ones already known for photosystem I particles. The initial fluorescence intensity tends to saturate at higher intensities ($N \gtrsim 1$), as in the case of the transient absorption study.[1] This was interpreted in terms of interaction and annihilation among excited chlorophyll molecules which occured dominantly within a duration time of a laser flash. The spectrum-resolved fluorescence decay was faster at 690 nm than at 680 nm as shown in Figure 2. This implies that two kinds antenna chlorophylls, apart from and in close proximity to P700, have differenct lifetimes. Heat treatment gave rise to a much slower fluorescence decay component. Its growth upon temperature increase gave a good correlation to the efficiency of photo-induced oxidation.

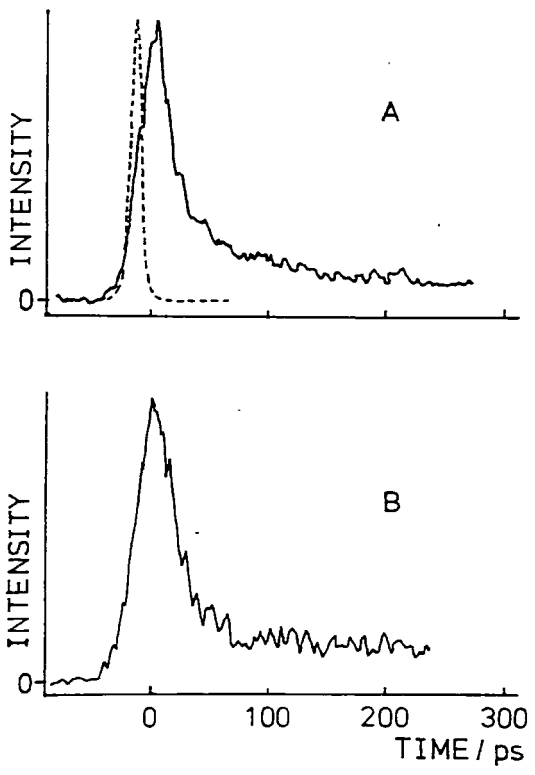

Figure 1. Fluorescence decay of P700-enriched particles prepared from spinach chloroplasts. (A) The exciting light intensity was controlled to excite only one chlorophyll molecule in the reaction center. In the present experiment 0.92 photons are absorbed per reaction center. (B) gives a decay curve under multiple photon excitation (6.4 photons/P700). The broken line shows a profile of the exciting laser pulse.

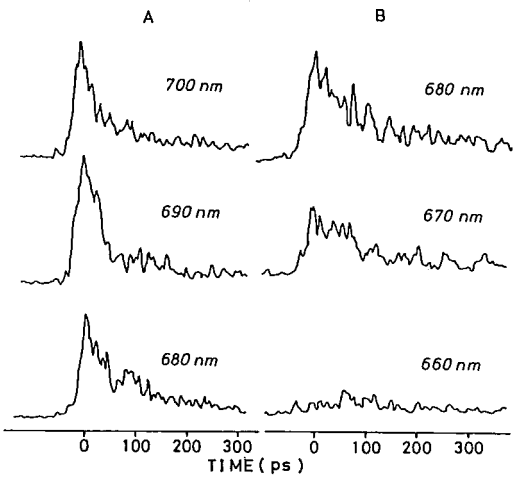

Figure 2. Spectral dependence of Fluorescence decay observed by a fast image processor equipped with a streak camera. Fluorescence was dispersed by a grating monochromator. (A) Observed between 680 nm and 700 nm, exciting intensity was 2.1 photons/P700, (B) between 660 nm and 680 nm, 1.5 photons/P700. Three decay curves in (A) or (B) are taken by a single laser excitation.

Reference

1) K. Kamogawa, A. Namiki, N. Nakashima, K. Yoshihara, and I. Ikegami, *Photochem. Photobiol.*, **33**, 511 (1981).

III—D Solar Energy Conversion by Using Photocatalytic Effects of Semiconductors — Decomposition of Water and Hydrogen Evolution

III-D-1 Photochemical Diode Model of Pt/TiO_2 Particle and its Photocatalytic Activity

Tadayoshi SAKATA, Tomoji KAWAI and Kazuhito HASHIMOTO

Photocatalytic effects of semiconductors have been interested for the potentiality in the direct conversion of solar energy into chemical energy. These several years the surface modification by adding Pt, Pd or RuO_2 to powdered semiconductors such as TiO_2, $SrTiO_3$ and CdS has been found to increase their photocatalytic activity by $10-10^3$ times compared with semiconductor alone. We have demonstrated that the photocatalytic activity of TiO_2 is increased enormously by supporting metal or metal oxide such as Pt and RuO_2. By using these surface modified photocatalyst water can be splitted into oxygen and hydrogen. Futhermore, hydrogen evolution was achieved with high efficiencies by reducing water with various organic compounds such as carbon, alcohols, carbohydrates, amino acids, fatty oil, fossil fuels, various biomasses and artificial polymers which act as electron donors. Similar effects are commonly observed among other semiconductors such as CdS, GaP, MoS_2, WS_2 etc. Therefore, it is important to elucidate the mechanism of photocatalytic reactions on these metal loaded particle semiconductors. The fundamental properties of powdered semiconductor photocatalysts can be explained by the photochemical diode model. Figure 1 shows the electronic structure of a TiO_2/Pt particle, both in the dark (solid line) and under illumination (dotted line), in a neutral aqueous solution (pH 7). Hydrogen evolution becomes possible due to the upper shift of the fermi level of Pt under illumination. The hydrogen evolution rate depends strongly on the kind of metal which is supported on the semiconductor surface. For instance, Pt, Pd or Rh increase the hydrogen evolution rate by 20—100 times in the water-ethanol mixture (1:1), whereas Fe on TiO_2 gives a bad influence. This remarkable dependence is considered to come mainly from the catalytic effect of metals on hydrogen evolution. Table I shows the hydrogen evolution rate using TiO_2/Pt particle photocatalysts for various electron donors. As shown in this table, the hydrogen evolution rate is quite small for H_2O, $S_2O_3^{2-}$, I^- and Fe^{2+}, even though they are easy to oxideze except for H_2O. On the other hand, it is very high for metanol, ethanol, ethylene-glycol and glycerol, even though they are not so easy to oxidize. This result indicates that there is a intimate correlation between the efficiency of hydrogen evolution and the irreversibility of the reactions on the powdered semiconductor photocatalyst. Hydrogen evolution rate was also found to depend on particle seize of TiO_2.

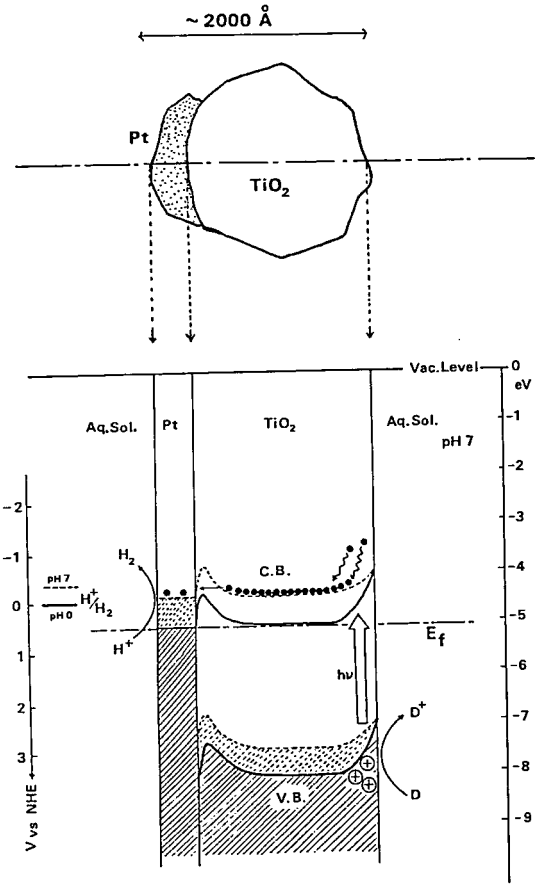

Figure 1. The energy structure of the photocatalyst, TiO_2/Pt, in the electrolyte (pH 7). The following data are used to estimate the energy levels: The work function of Pt: 5.6 eV, the flat band potential of TiO_2 in the electrolyte at pH 7: −0.6 V vs NHE, the rest potential of the electrolyte: +0.5 V vs NHE at pH 7 (observed value).

Table I. Correlation between hydrogen evolution rate and the reversibility of the reaction.

	Reactant (electron donor)	H_2 evolution rate (μmol/10h)[a]
Reversible system	H_2O	1 >
	Fe^{2+}	1
	$S_2O_3^{2-}$	6
	I^-	1 >
Irreversible system	CH_3OH	9000
	C_2H_5OH	8000
	glycerol	7500
	ethylene-glycol	5800

a) 500W Xe lamp; irradiation for 10h. photocatalyst: TiO_2/Pt.

III-D-2 Hydrogen Evolution with Visible Light by Using Various Semiconductors

Tomoji KAWAI, Kazuhito HASHIMOTO, and Tadayoshi SAKATA

Although TiO_2 semiconductor is a very active photocatalyst, only 9% of the solar energy can be utilized to excite it, since its band gap wavelength is short, 410 nm. To exploit a new photocatalyst which works efficiently with visible light, we have examined the photocatalytic activity of various kinds of semiconductors which can absorb visible light. Table I shows the hydrogen evolution from water-ethanol mixture (1:1) by using various platinized semiconductor photocatalysts. Among a number of photocatalysts CdS/Pt was found to be the most active one, which works stably for a long time. Table II shows the result of hydrogen evolution from various organic compounds as electron donors and water for CdS/Pt photocatalyst. Although CdS photocatalyst is very active for hydrogen evolution from ehtanol as shown in these tables, it is not able to decompose acetic acid, which is quite different from TiO_2 photocatalyst. It indicates that the oxidation by CdS photocatalyst is milder than by TiO_2 photocatalyst, since the energy level of valence band is located higher in CdS than in TiO_2. Interestingly, the dependence of hydrogen evolution rate on the exciting wavelength is different, depending on the kind of organic molecules. It suggests that the hot holes generated in the valence band contributes to the oxidation.

Table I. Hydrogen production from water-ethanol mixture by using various platinized semiconductors.

semiconductor	H_2 production rate (μmol/10h)	
	neutral	alkaline
SiC	120	420
SiC (λ > 430 nm)	66	290
GaP	42	28
Si	69	—
CdSe	170	1300
CdS	8300	32500
TiO_2	5800	600
$MoSe_2$	380	170
MoS_2	360	1100
$MoTe_2$	110	96
Fe_3O_4	92	180
Fe_2O_3	30	150
WO_3	10	—
CdTe	102	24
WS_2	92	530
WSe_2	480	25
GaAs	48	740
InP	26	25

500 W Xe lamp, platinized photocatalyst: 300 mg ethanol: water ≃ 1:1.

Table II. Hydrogen evolution from various organic materials and water using platinized CdS photocatalyst.[a]

organic material	Hydrogen production rate (μmol/10h)	
	Xe lamp full	λ > 430 nm
methanol	2500	980
ethanol	6800	4300
sugar	310	68
glycine	790	200
polyethyleneglycol	1200	310
urea resin	550	170
acetic acid	0	0
polyvinylchloride	0	0
polyethylene	0	0
(water)[b]	0	0

a) water: 30 ml, organic material: 500 mg, 500 W Xe lamp (Ushio Co.), CdS/Pt: 300 mg.
b) without organic material.

III-D-3 Application of Semiconductor Photo catalysts to Organic Reactions

Tadayoshi SAKATA, Tomoji KAWAI, and Kazuhito HASHIMOTO

Since the photocatalytic reactions by using semiconductor photocatalyst are essentially redox

reactions, its application to various organic reactions besides hydrogen production would be one of the interesting possibilities. For that purpose, it is possible to control the oxidation and reduction power by selecting a semiconductor whose conduction and valence band are located appropriately. Table I shows one example: Hydrogen and CO_2 evolution from an aqueous solution of pyruvic acid. As shown in this table, both hydrogen and CO_2 evolve for TiO_2 photocatalyst, but only CO_2 evolves for the other semiconductors such as WO_3, Fe_2O_3, MoS_2 and Bi_2O_3 whose reduction power is considered to be low, since their conduction bands are located lower than redox potential of H^+/H_2. Even by using TiO_2/Pt, the amount of hydrogen evolved is 1/7 of CO_2. These facts indicate that the reactions other than hydrogen evolution take place. Actually, ethanol, acetaldehyde and acetic acid were found in the aqueous medium. The above result could be explained by assuming the following reactions.

$$CH_3COCOOH + p \longrightarrow CH_3CO\cdot + H^+ + CO_2 \quad \cdots\cdots (1)$$

$$CH_3CO\cdot + e + H^+ \longrightarrow CH_3CHO \quad \cdots\cdots (2)$$

$$CH_3CHO + H_2O + 2p \longrightarrow CH_3COOH + 2H^+ \quad \cdots\cdots (3)$$

$$CH_3CHO + 2H^+ + 2e \longrightarrow C_2H_5OH \quad \cdots\cdots (4)$$

When MoS_2 or WS_2 are used for the decomposition of allyl alcohol the following reaction was found to take place selectively.

$$CH_2 = CHCH_3 + H_2O \quad \cdots (5)$$

$$CH_3 = CHCH_2OH + 2H^+ + 2e \longrightarrow CH_3CH_2CH_2OH \quad \cdots\cdots (6)$$

The photocatalytic reaction of carbohydrates, organic acids, and alcohols are being investigated from the view point of organic synthesis by semiconductor photocatalysts.

Table I. Decomposition of pyruvic acid

$$CH_3\text{-}CO\text{-}COOH + H_2O \xrightarrow[\text{phot.cat.}]{h\nu} CO_2, (H_2)$$

phot.cat.	H_2 (μmol/10h)	CO_2 (μmol/10h)
TiO/Pt	330	2440
WO_3/Pt	0	620
Fe_2O_3/Pt	0	590
MoS_2/Pt	0	1150
Bi_2O_3/Pt	0	5290

III-D-4 Lifetime of Excited $Ru(bipy)_3Cl_2$ Adsorbed on Photocatalyst Semiconductors

Takashi KAJIWARA *(Toho Univ.)*, **Kazuhito HASHIMOTO, Tomoji KAWAI and Tadayoshi SAKATA**

In order to obtain detailed informations about the initial stage of dye sensitization of oxide semiconductor photocatalysts, the dynamic spectroscopic properties of the excited state of Ru $(bipy)_3Cl_2$ adsorbed on powdered semiconductors (TiO_2, SnO_2, $SrTiO_3$ and ZrO_2) have been studied by using pulsed dye laser (6 ns, 450 nm) as the exciting source. The behaviour of $Ru(bipy)_3Cl_2$ adsorbed on powdered SiO_2 and on microcrystalline powder of methylviologen has been also studied.

The observed luminescence decay is not a single exponential one and has been decomposed to a sum of several exponential decays (Table I). Furthermore the luminescence spectra have been found to be time dependent. They involve at least two kinds of spectra with different lifetimes (see Figure 1, one of which has a maximum at about 580 nm and has relatively short lifetimes (120 ~ 20 ns). This luminescence must originate from tightly adsorbed $Ru(bipy)_3Cl_2$ molecule and the electron transfer rate from these molecules to the substrate is sufficiently large for effective sensitization ($k_t \geqq 1/20$ ns $\gg k_n = 1/500$ ns; k_n is natural lifetime in solution at room temperature). The other spectrum has a maximum at about 630 nm and corresponds to long lifetimes and can be assigned to more or less loosely held molecules. In spite of the small mean adsorption density (less than 0.1 of monolayer density) of $Ru(bipy)_3Cl_2$, the relative weight of slow

components are substantial. This means that the oxide semiconductors are not good adsorbent of $Ru(bipy)_3Cl_2$ and this prevents effective sensitization (see Table II).

On SiO_2, decay components with long lifetimes were dominant. This agrees with the fact that electron transfer between SiO_2 and excited $Ru(bipy)_3Cl_2$ is energetically forbidden. The. component with shorter lifetime (50 ns) may be due to charge separation in the $Ru(bipy)_3Cl_2$ aggregate formed on SiO_2 surface by both or either of the following mechanisms; $2[Ru(bipy)_3^{+2}]^* \rightarrow Ru(bipy)_3^{+1} + Ru(bipy)_3^{+3}$, $[Ru(bipy)_3^{+2}]^* + Ru(bipy)_3^{+2} \rightarrow Ru(bipy)_3^{+1} + Ru(bipy)_3^{+3}$. Indeed, similar fast decay has been also observed for pure crystals of $Ru(bipy)_3Cl_2$. The conduction edge of ZrO_2 is slightly higher than the electron energy of the excited $Ru(bipy)_3Cl_2$, and the luminescence of $Ru(bipy)_3Cl_2/ZrO_2$ shows somewhat similar behaviour with $Ru(bipy)_3Cl_2/SiO_2$.

Table I. Lifetime of Decay Component and Relative Weight

Substrate	Concentration	Temperature	Lifetime and Relative Weight
MV	1/1000 w/w	room temp. liq. N_2 temp.	3.3ns (0.81), 13ns (0.19), 3.1ns (0.81), 14ns (0.17), 130ns (0.02)
TiO_2	1/1000 w/w	room temp. liq. N_2 temp.	18ns (0.52), 64ns (0.32), 280ns (0.16) 21ns (0.64), 100ns (0.28), 530ns (0.07)
SnO_2	1/1000 w/w	room temp. liq. N_2 temp.	14ns (0.63), 65ns (0.30), 260ns (0.07) 15ns (0.95), 140ns (0.31), 1000ns (0.10)
$SrTiO_3$	1/1000 w/w	room temp. liq. N_2 temp.	12ns (0.58), 40ns (0.22), 130ns (0.13) 500ns (0.06) 12ns (0.50), 60ns (0.26), 280ns (0.17) 1200ns (0.07)
ZrO_2	1/1000 w/w	room temp. liq. N_2 temp.	17ns (0.35), 130ns (0.38), 530ns (0.27) 20ns (0.25), 240ns (0.29), 810ns (0.45)
SiO_2	1/1000 w/w	room temp. liq. N_2 temp.	50ns (0.33), 420ns (0.36), 1200ns (0.31) 50ns (0.25), 1300ns (0.26), 3500ns (0.60)

*YAG laser (25ps, 530nm) was also used as an exciting light source.

Table II. Sensitization by $Ru(bipy)_3Cl_2$ of hydrogen production from saturated methanol-water mixed vapour at 25°C.

Photocatalyst	Production rate (μmol/10h)	
	a) UV + VIS	b) VIS
TiO_2	8.4	0.7
TiO_2-$Ru(bipy)_3Cl_2$ (2.5wt%)	9.7	1.3
Pt/TiO_2	—	10
Pt/TiO_2-$Ru(bipy)_3Cl_2$ (2.5wt%)	580	15

Light source; a) Total radiation of 500W Xe-lamp, b) 500W Xe-lamp with Filter VY-44 (Sharp cut-off at 440nm).

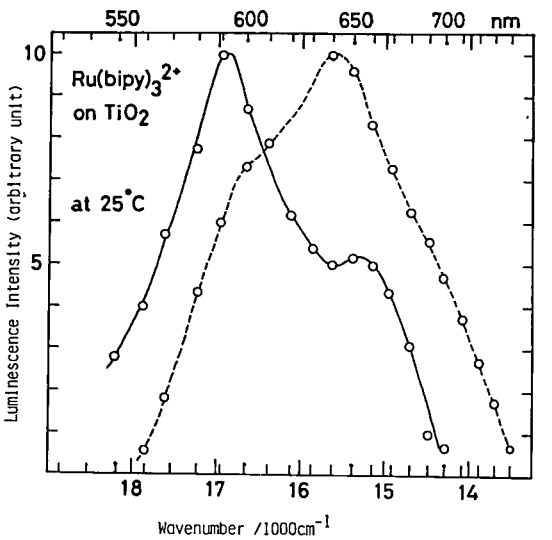

Figure 1. Normalized luminescence spectra of fast and slow decay components of $Ru(bipy)_3Cl_2$ on TiO_2 at 25°C.
——— component of 18 ns lifetime
- - - - - component of 64 ns and 280 ns lifetime

III-D-5 Hydrogen Production with Visible Light by Using Dye-Sensitized Semiconductor

Kazuhito HASHIMOTO, Tomoji KAWAI and Tadayoshi SAKATA

Photo-induced water splitting reaction by using TiO_2 or $SrTiO_3$ as a photocatalyst has been investigated by many researchers. However, most semiconductors which are stable under irradiation in electrolyte solution have wide band-gaps; they can absorb mostly UV light. To extend the effective wavelength region, we studied hydrogen production on making use of dye sensitization of semicondctor. The dyes used in this study were $Ru(pby)_3Cl_2$, various porphyrins and some other organic dyes. TiO_2 was used as a substrate semiconductor and then it was platinized to accelate hydrogen production. EDTA was used as a reducing agent. Hydrogen was surely produced under visible light illumination ($\lambda > 440$ nm) when the solution contained a dye. This reaction is considered to be consist of the following processes. (1) The dye adsorbed on the semiconductor is excited by the light and (2) the electron transfers from the excited dye to the conduction band of the semiconductor and (3) it moves to Pt and hydrogen is produced at a platinum site and (4) oxidized dye accepts an electron from a reducing agent. These processes are similar to those of a photochemical cell with a dye sensitized semiconductor electrode. At present the efficiency of hydrogen production is quite low. This result, however, may be the first example of hydrogen production based on dye sensitization.

Table I. Rate of hydrogen production; light source 500W Xe lamp ($\lambda > 440$ nm)

Dye	red. agent	rate (μmol/h)
$Ru(bpy)_3Cl_2$	methanol (gas)	0.5
ibid.	ibid. (liq.)	0.2
ibid.	EDTA	1
Zn-TPP	ibid.	0.1
TPPS	ibid.	0.1
TMPyP	ibid.	0.06
Safranin T	ibid.	1
Rhodamin B	ibid.	0.4
Rose Bengal	ibid.	5
none	methanol (liq.)	< 0.41
none	EDTA	< 0.04

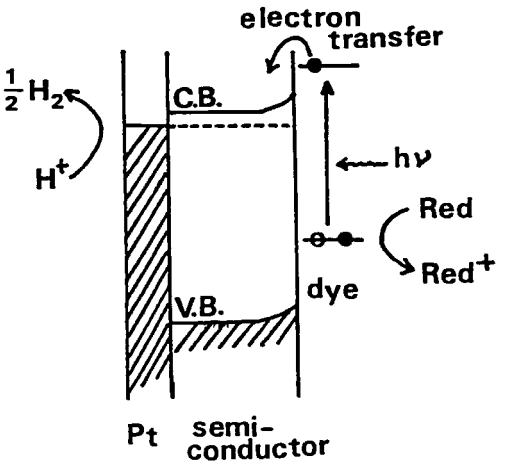

Figure 1. Schematic mechanism of dye sensitization of semiconductor.

III-D-6 Efficient Hydrogen Production with Visible Light by Fluorescein Derivatives

Kazuhito HASHIMOTO, Tomoji KAWAI and Tadayoshi SAKATA

For hydrogen production in homogeneous system, only a limited number of photocatalysts like $Ru(bpy)_3Cl_2$ and water soluble zinc porphyrins have been used. In this report, some fluorescein derivaties are also shown to be efficient dyes for hydrogen production. The solution of these dyes containing triethanolamine (TEOA) as a reducing agent and platnized semiconductor (or colloidal platinum) can produce hydrogen under visible light illumination with a high rate which is almost equal to that used $Ru(bpy)_3Cl_2$. This reaction is efficient in the high PH range. From the studies about the dynamic behaviors of photochemical cell composed of these dyes and a semiconductor as a electrode, this reaction was elucidated to be a photogalvanic one; (1) the dye in solution is excited by the light and (2) the excited dye is reduced to a stable anion radical by TEOA and (3) the anion radical arrived at the surface of semiconductor by diffusion transfers an electron to the semiconductor and (4) the hydrogen is produced at platinum. In the case of colloidal platinum, the *anion radical* may supply directly an electron to a proton on the platinum surface. Becasue of a long-living nature of the intermediate, a two-component redox system can be constructed for hydrogen production. This is

different from three component systems which are commonly used with an electron acceptor like methylviologen.

Table I. Hydrogen production rate compared to other systems.
(a) J. Kiwi et al. Nature **281** (1979), 657
(b) K. Kalyanasundaram et al. J. C. S. Chem. Comm., **1979**, 1137.

dibromo-fluorescein 5×10^{-3} M	$Ru(bipy)_3Cl_2$ 4×10^{-5} M	Proflavine 2×10^{-5} M
Pt/TiO_2	Pt-PVP	Pt-PVP
	MV^{2+} 2×10^{-3} M	
TEOA 3×10^{-1} M	EDTA 3×10^{-2} M	EDTA 1×10^{-2} M
PH = 12.1	PH = 5.0	PH = 6.0
H_2 : 320 μmol/h 0.17 *l*/day, 10 ml	560 μmol/h[a] 0.30 *l*/day, 25 ml	0.75 μmol/?[b]

Table II. Relative rate of hydrogen production; each rate is normalized aganist that in the case of dibromofluorescein

Dye	rate of H_2 production
(a) Fluorescein	15 (~40)
(b) Dibromofluorescein	100
(c) Dichlorofluorescein	16
(d) Dichlorofluorescein diacetate	51
(e) Mercurochrome	38 (~100)
(f) Gallein	0

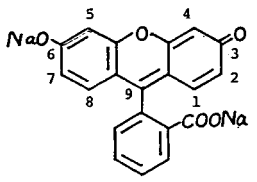

(a) fluorescein
(b) 4,5 – Br
(c) 2,7 – Cl
(d) 2,7 – Cl, 3,6 – $OCOCH_3$
9 – H
(e) 2,7 – Br, 5 – HgOH
(f) 4,5 – OH

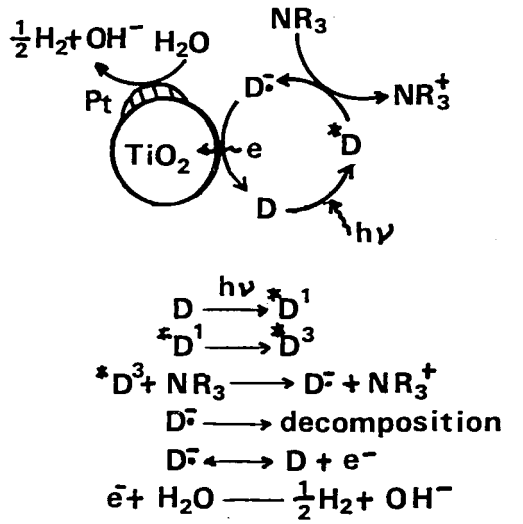

Figure 1. Mechanism of the hydrogen production NR_3 ; TEOA, D ; dye.

III-D-7 Laser-Induced Particle Emission from the Surface of Zinc Oxide

Takeyoshi NAKAYAMA, Hitoshi ICHIKAWA, Noriaki ITOH *(Nagoya Univ.)*, **Tomoji KAWAI, Kazuhito HASHIMOTO, and Tadayoshi SAKATA**

In this report, we present a new type of laser-induced particle emission, consisting of thermal and nonthermal components.

A ZnO crystal was irradiated with pulsed light beam from a nitrogen laser, and neutral particles emitted from the surface was analyzed with a mass spectrometer and the energy spectra were obtained with a time of flight method. Time-of-flight spectra of neutral zinc atoms obtained at room temperature and 250°C are shown by curves a and b in Figure 1, respectively. Two components peaked at 65 μs (fast) and 140 μs (delayed) are observed in both curves. The curbe b can be decomposed into a non-Maxwellian fast component peaked at 0.22 eV and a Maxwell-Boltzmann distribution ($T \fallingdotseq 530$K). Similar energy specra were obtained for oxygen atoms and molecules emitted from the surface. The signal intensity was found to be proportional to I^n (I: laser intensity), where $n = 6$ for the thermal component and $n > 6$ for the nonthermal component.

In previous studies of laser-induced particle emission from metal and insulaters, only a thermal component with a characteristic temperature near the melting point has been observed,[1),2)] while the present energy spectra consist of a non-Maxwellian and a Maxwellian with a characteristic temperature much lower than the melting point (1970°C). Similar energy spectra have been obtained for alkali halides[3)] but they are known to be proportional to the absorbed energy and to be due to the excitonic photochemical process. The present results suggest that a photochemical decomposition of zinc oxide surface is induced under high density excitation, probably due to the multiple excitation. Photo desorption induced by multiple excitation has been already invoked by Knotek.[4)]

References

1) A. T. Prengel, J. Dehaven, E. J. Johnson and P. Davidovits, *J. Appl. Phys.*, **48**, 3551 (1977).
2) R. A. Olstad and D. R. Olander, *J. Appl. Phys.*, **46**, 1499 (1975).
3) H. Overeijnder, M. Szymonski, A. Haring and A. E. de Vries, *Rad. Effects*, **36**, 63 (1978).
4) M. L. Knotek, V. O. Jones and V. Rehn, *Phys. Rev. Lett.*, **43**, 300 (1979).

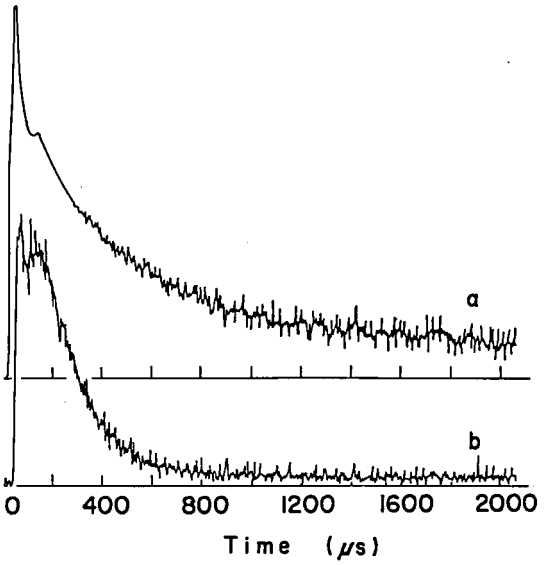

Figure 1. Time-of-flight spectra of Zn atom emitted from ZnO single crystal by N_2-laser. Curves a and b were measured at room temperature and at ~ 250°C, respectively.

III—E Study of Elementary Processes in Chemical Reaction

The purpose of the project is to perform a detailed study on the reactivity of molecules in vibrationally and/or electronically excited states and on the distribution of energy among the internal states of reaction products as well as the product kinetic energy distribution. Using a supersonic molecular beam combined with laser irradiation, we measured the reaction probability directly by observing the attenuation of parent beam upon laser irradiation.

III-E-1 IR-Multiphoton Dissociation of Trichlorethylene under the Collision Free Condition: A Direct Measurement of Dissociation Probability

Iwao NISHIYAMA and Ichiro HANAZAKI

IR multiphoton dissociation of trichloroethylene was investigated under a collision free condition using a supersonic molecular beam and a Q-pole mass spectrometric detection. An absolute dissociation probability was determined by measuring the attenuation of parent beam intensity upon irradiation with a CO_2 laser radiation. Laser-fluence and wavelength dependence of dissociation probability were examined. In Figure 1 is shown the time-of-flight spectrum of the parent ion showing a dip caused by the dissociation of parent molecules with pulsed laser irradiation. The dissociation probability was derived from the TOF spectrum by a computer simulation. Laser fluence dependence of dissociation probability is shown in Figure 2. It is rather striking to see that the dissociation is almost complete at the fluence as low as 1 Jcm^{-1}, although a static cell experiment shows generally a much steeper dependence on the laser fluence. It is also to be noted that the dissociation probability shows a linear dependence on the laser fluence at lower fluences. To our knowledge, this is the first observation of linear dependence in the IR-multiphoton process and suggests that the light absorption process itself is already saturated in this

region. In other words, the absorption of a single photon (probably at the top of barrier) is rate-determining in the multiphoton excitation process.

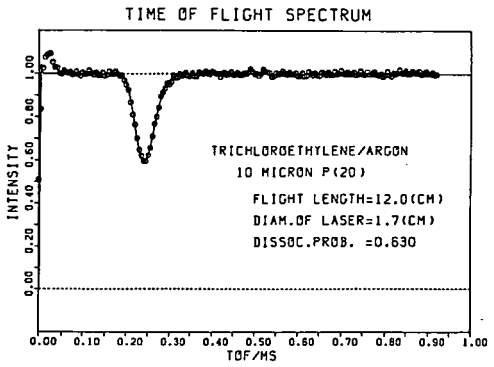

Figure 1. Observed (circles) and Calculated (solid line) TOF spectra of trichloroethylene showing a dip in the parent beam signal caused by the IR-multiphoton dissociation.

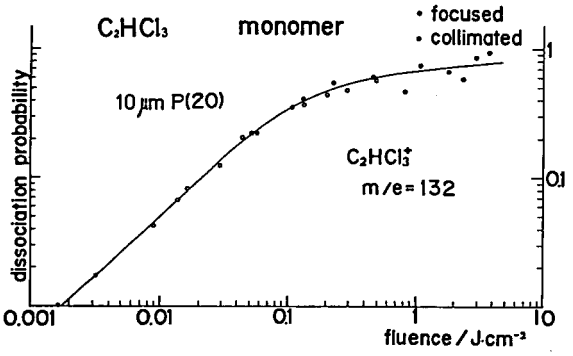

Figure 2. Laser-fluence dependence of the dissociation probability of trichloroethylene upon IR-multiphoton excitation.

III-E-2 Formation and IR-Multiphoton Dissociation of Hydrogen-Bonded Clusters and CT Complexes in a Supersonic Molecular Beam

Iwao NISHIYAMA, Taiji KITAGAWA,* and Ichiro HANAZAKI *(*Toyoma Medical and Pharmaceutical Univ.)*

Dissociation probabilities of hydrogen-bonded clusters and CT complexes excied by IR-multi photon excitation were measured by the method stated in III-E-1. About 30 to 40 photons are required to dissociate a normal bond by the IR-multiphoton excitation with a CO_2 laser. On the other hand only a few photons are required to dissociate the weakly bound complexes such as molecular clusters and CT complexes. These molecules might be expected to give some new features in the IR-MPD experiment because of their low binding energies. Clusters and CT complexes were formed by using a nozzle beam seeded in Ar gas. Acetic acid clusters of $n \leq 7$ and methanol clusters of $n \leq 10$ were detected by a Q-pole mass spectrometer in a form of protonated ion $M_{n-1}H^+$ which was formed in an electron impact ionizer. It was also found that weak CT complex such as benzene-I_2 could be formed easily in a supersonic molecular beam. Laser fluence and wavelength dependence of dissociation probability were measured for these complexes. Figure 1 shows fluence dependences for acetic acid clusters (n = 2 − 4) as examples. It is rather striking to see that the fluence of 0.1 − 1 Jcm^{-2} was required to complete dissociation in spite of their low binding energy. It was suggested from the wavelength dependence measurement that the light absorption cross section plays an important role in determining the dissociation probability.

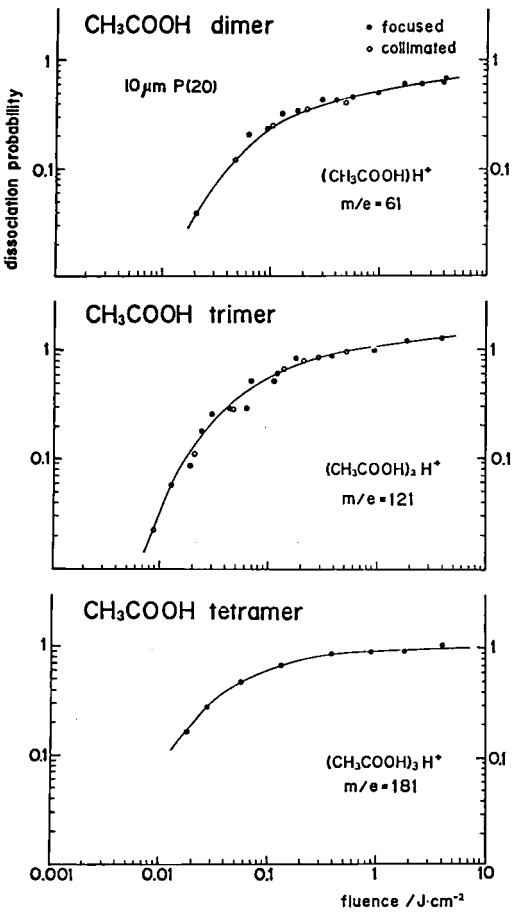

Figure 1. Laser-fluence dependence of dissociation probability of acetic acid dimer, trimer and tetramer upon IR-multiphoton excitaiton.

III-E-3 IF(B—X) Emission Induced by IR-Multiphoton Excitation of SF_6-I_2 Mixture; Observation of an Oscillatory Time-Dependent Reaction

Susumu KUWABARA, Masaaki BABA, Iwao NISHIYAMA, and Ichiro HANAZAKI

observed period of optoacoustic signal showed a good agreement with the reaction period. This fact indicates that the oscillation is caused by a pressure change and/or heating effect due to the standing wave produced in the cell upon laser irradiation.

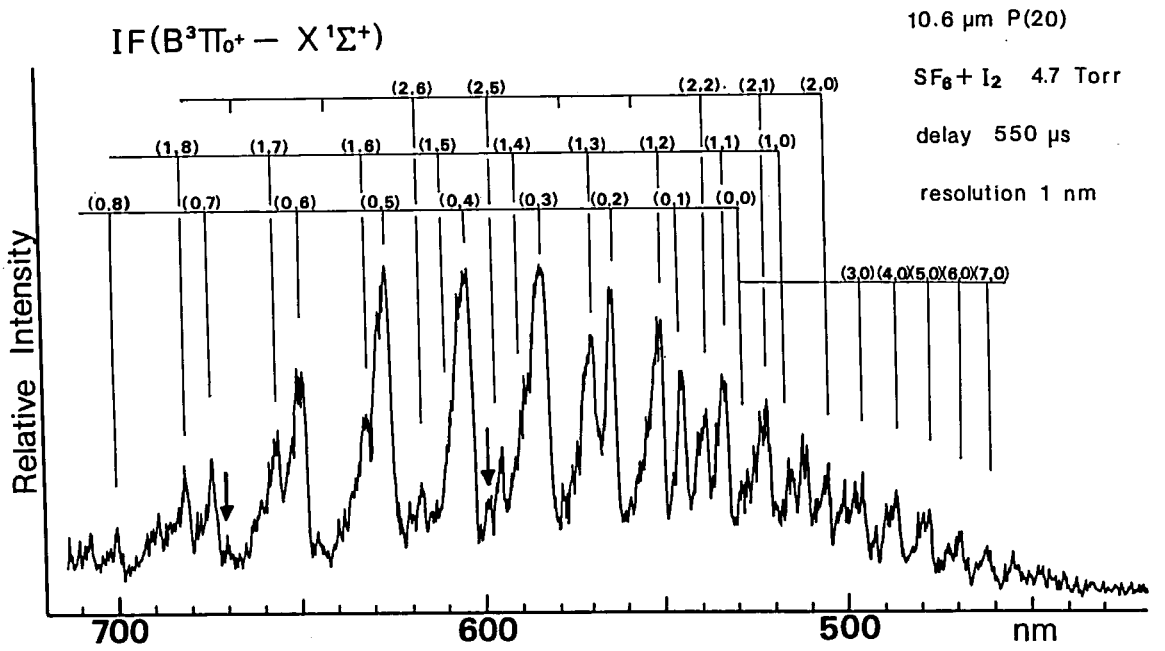

Figure 1. Emission spectrum of IF(B—X) observed upon irradiation of the SF_6 — I_2 mixture with CO_2 laser.

SF_6 is well known to produce F and SF_5 radicals in a primary process and finally F_2 and SF_4 molecules by the IR multiphoton excitation. We studied a subsequent reaction of these active species with iodine by emission spectroscopy. Bright emission observed in a visible region was assigned to IF(B—X) transition as shown in Figure 1. The IF(A—X) emission was also observed very weakly. Relative vibrational intensities of IF(B—X) emission agree with that observed in chemiluminescense caused by the F_2 + I_2 reaction. Figure 2 shows the time dependence of the total emission intensity. It shows a time-dependent oscillation with a time interval of 140 μs. A delay of 15 μs was observed in a rise of the first peak indicating that IF(B) was formed even after the laser irradiation. The shape of the time dependence was sensitive to pressure, laser fluence and emitting position in the cell. In order to resolve the cause of oscillation, we made a pressure-wave measurement using a microphone. The

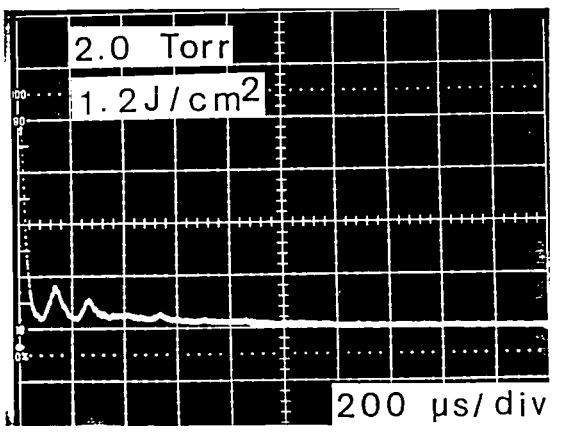

Figure 2. Time dependence of IF(B—X) emission.

III—F Chemical Reactions Through Highly Excited Vibratioal States

The nature of highly excited vibrational states has been a subject of increasing interest in the last decade. We are interested in their fundamental dynamical behaviour, especially in the vibrational energy transfer and coupling between highly excited vibrational modes and the chemical reaction channel. In this project, a spectroscopic study was made on the nature of highly excited vibrational overtones (local mode). A theoretical study was also made on the effect of laser beam focusing in the multiphoton excitation experiment.

III-F-1 Splitting of Methyl CH Stretching Vibrations in Higher Overtone Spectra of Methyl-substituted Unsaturated Hydrocarbons

Ryoichi NAKAGAKI and Ichiro HANAZAKI

[*Chem. Phys. Lett.*, in press]

CH stretching overtone spectra of methyl-substituted unsaturated hydrocarbons were measured in the liquid phase up to $\Delta v = 5$ or 6. A large splitting of CH stretching overtone was observed for sterically hindered methyl groups, *e.g.* those in *o*-xylene, *o*- and α-methylstyrene, and α-methylnaphthalene. Sterically unhindered methyl groups, *e.g.* those in toluene, *m*- and *p*-xylene, appear to show a small splitting. Splitting of this kind is attributed to conformationally inequivalent CH bonds, *i.e.* two out-of-plane and one in-plane CH bonds. The main cause for the splitting is attributed to the presence of an adjancet part of the molecule. It is also suggested that a small splitting in toluene arises from the interaction with the conjugated plane of the molecule.

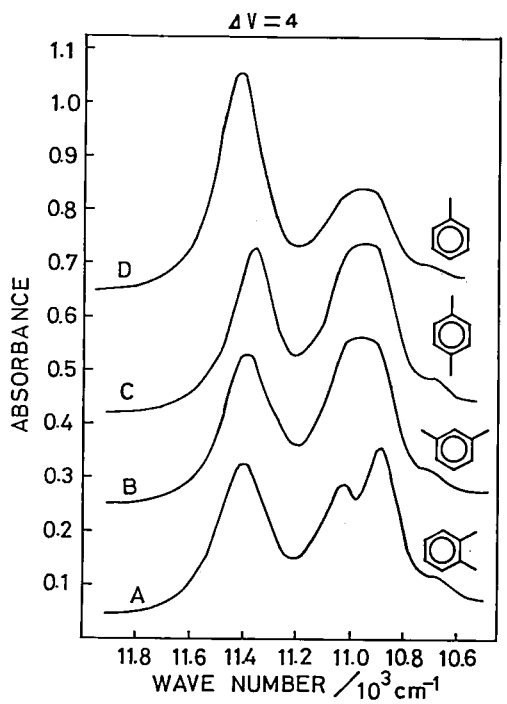

Figure 1. Liquid phase overtone spectra at room temperature in the region of $\Delta v(CH) = 4$ (*o*-xylene, *m*-xylene, *p*-xylene, and toluene). The high energy band (11,200–11,600 cm^{-1}) is due to the aromatic ring CH stretching modes, and the low energy band (10,800–11,200 cm^{-1}) due to the methyl CH stretching modes.

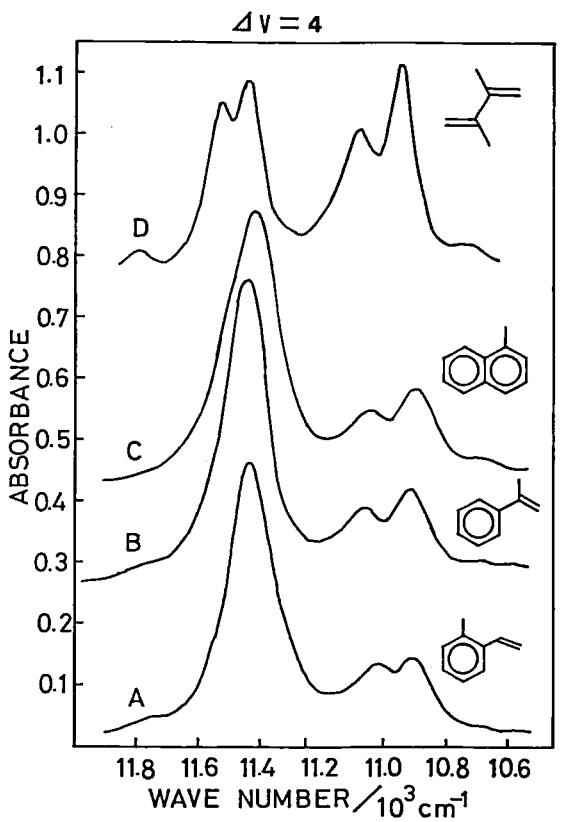

Figure 2. Liquid phase overtone spectra at room temperature in the region of $\Delta v(CH) = 4$ (*o*-methylstyrene, α-methylstryene, α-methylnaphthalene, and 2,3-dimethyl-1, 3-butadiene). The high energy band (11,200–11,600 cm^{-1}) is due to the $C(sp^2)$-H stretching modes, and the low energy band (10,800–11,200 cm^{-1}) due to the methyl CH stretching modes.

III-F-2 Doublet Structures in Higher CH Stretching Overtones of Organic Molecules Containing Methyl Groups

Ryoichi NAKAGAKI and Ichiro HANAZAKI

We have extended the previous work to the following compounds: 1,2,3-trimethylbenzene, 1,2,3,4-tetramethylbenzene, 1,2,4,5-tetramethylbenzene, pentamethylbenzene, 2-methylfuran, 2,5-dimethylfuran, 2- and 3-methylthiophene. Doublet structures similar to those in *o*-xylene and α-methylnaphthalene have been observed for the polymethylated benzenes, and smaller splittings have been also seen for the methylated five-membered hetrocycles. Eclipsed conformations are generally prefered by methyl groups directly bonded to π-electron conjugated systems, and there exist two conformationally inequivalent CH bonds in each methyl group, *i.e.* in-plane and out-of-plane orientations with respect to the molecular plane. The present work shows that conformationally inequivalent sites correspond to two distinct peaks in overtone spectra of CH stretching vibrations ($\Delta v(CH) \geqq 4$).

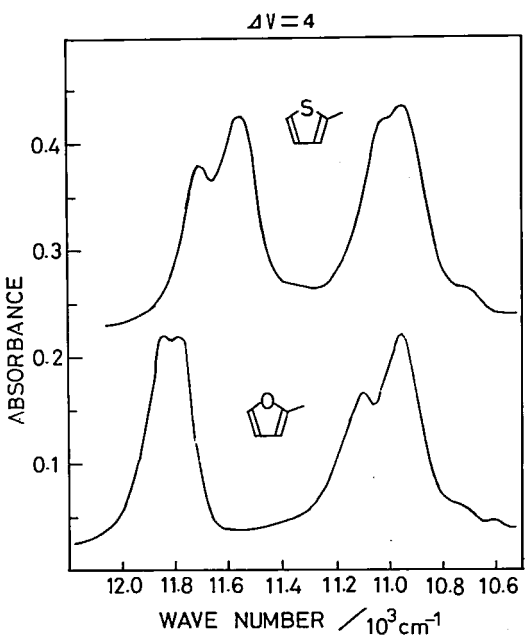

Figure 1. Liquid phase overtone spectra at room temperature in teh region of $\Delta v(CH) = 4$ (2-methylfuran and 2-methylthiophene). The high energy band (11,400–12,000 cm^{-1}) is due to the ring CH stretching modes and the low energy band (10,800–11,200 cm^{-1}) due to the methyl CH stretching modes.

III-F-3 Focusing Effect of Laser Beam on the Power Dependence of Multiphoton Processes

Ichiro HANAZAKI

[*Appl. Phys.*, **B26**, 111 (1981)]

Effect of focusing a laser beam on the intensity (I) dependence of multiphoton processes was examined. A general method is given to deduce a genuine intensity dependence from the focused-beam experiment. In addition, some typical examples were examined in detail. For the dependence of the type of I^n, an apparent relation of $I^{3/2}$ appears only when there is a change of dependence as $I^n \rightarrow I^m$, with $n > 3/2$ and $m < 3/2$ (Figure 1). A genuine intensity dependence can be obtained directly from the focused beam experiment if n does not change throughout the irradiated volume, or if the condition $n > 3/2 > m$ does not hold. The case of gradually decreasing n, as is common for the infrared multiphoton reaction probability (P), was also analyzed taking the Arrihenius-type dependence, $P \propto \exp(-\theta/I)$, as an example. A simple method is proposed to obtain a genuine relation between P and I for this type of intensity dependence.

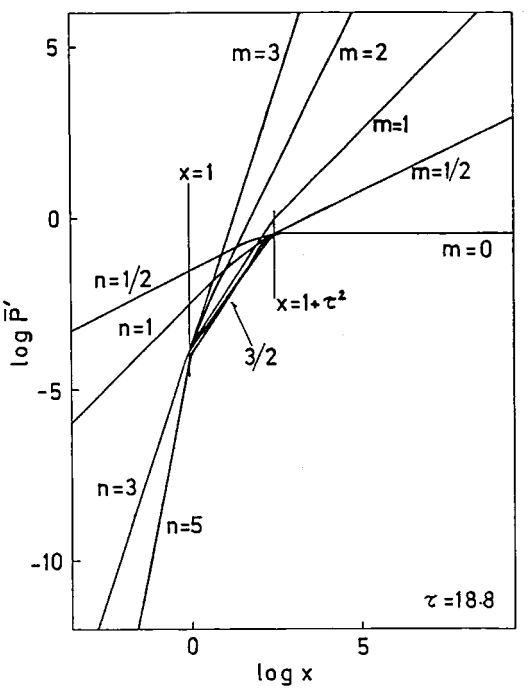

Figure 1. Apparent light intensity dependence for the change of intensity dependence as $I^n \rightarrow I^m$ at $I = I_t \cdot \overline{P'}$ is a normalized reaction probability, $x \equiv I_f/I_t$, where I_f is the light intensity at the focal point, and $\tau \equiv z_0/a$, where z_0 is the distance from the entrance window of the reaction cell and the focal point and a is the effective length of focal region.

III—G Study on Photochemical Processes Related to Planetary Space Chemistry

After $10^7 \sim 10^8$ years from the solar system formation, the sun is believed to be in the T. Tauri stage, when UV radiation is $10^3 \sim 10^4$ times as strong as the present luminosity. Although most of molecules in low density gas environment could be destroyed under such strong radiation, molecular aggregates on the dust surface or clusters in clouds may show different chemical processes from gas system. In the outer part of the solar nebula, ice particles had been condensed on cold dusts which grow to a comet-type nuclei. From a thermochemical equilibrium interpretation of the chemistry of C, N and O in the solar nebula, the condensation of H_2O-, CH_4-, and NH_3-bearing ice particles has been expected. Photochemistry and photophysics of low temperature molecular aggregates composed of solar nebula molecules have been developed by using molecular beam, ultra-high-vacuum and high sensitive mass spectrometric techniques. Here, we report the preliminary results on the two kinds of new experiments.

III-G-1 Photochemical Generation of N_xH_y Type Molecules from Low Temperature $(NH_3)_n$ Clusters

Hisanori SHINOHARA and Nobuyuki NISHI

Ammonia photochemistry in vacuum-ultra-violet region has received considerable experimental and theoretical attentions in recent years. This is due, in part, to the fact that ammonia has been found to play an important role in the chemistry of planetary atmospheres and comets. Multiphoton ionization (MPI) method is well suited for surveying complicated molecular systems such as ammonia clusters produced by expansion cooling in a supersonic molecular beam. Figures 1 and 2 present MPI mass spectra of ammonia, seeded in argon, supersonic nozzle beam with the excitation wavelength at 193 nm. Ammonia clusters are detected at the parent ions minus an NH_2, i.e., the dimer at mass number 18, the trimer at mass 35, and so forth. Except for NH_3 itself, the parent ions are not observed, presumably reflecting the greater stability for the ammonium ion analogues, $(NH_3)_{n-2}NH_4^+$, than for the parent $(NH_3)_n^+$ ions. We have found the clusters up to $(NH_3)_7H^+$ (Figure 2).

More interestingly, the two MPI spectra of ammonia in a nozzle beam reveal that relatively good amont of ions at m/e = 30, 32 and 58 are formed by the primary photochemical processes. The appearance of m/e = 30, 32 and 58 in the mass spectra of ammonia can be attributed to $N_2H_2^+$, $N_2H_4^+$ and $N_4H_2^+$, respectively. Since the spectra by the electron impact under identical conditions do not show such signals, we conclude that the generation of unsaturated "hydronitrogens" is characteristic to the photolytic process of ammonia clusters.

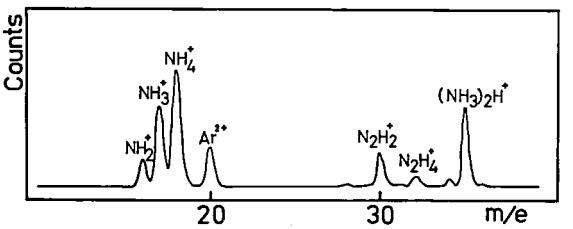

Figure 1. Supersonic molecular beam MPI spectrum of NH_3(30 Torr) seeded in Ar(730 Torr) using an ArF excimer laser. The ordinate scale is an unit mass resolution. The vertical scale for the spectrum is arbitrary.

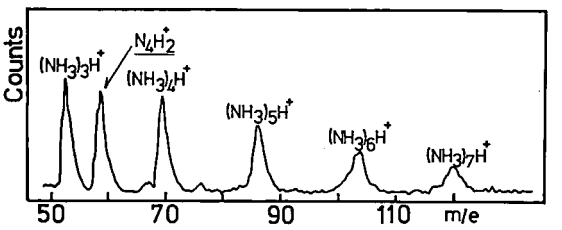

Figure 2. Supersonic molecular beam MPI mass spectrum of NH_3(40 Torr) seeded in Ar(720 Torr) obtained by an ArF excimer laser.

III-G-2 Photodissociation and Succeeding Reactions of Fragments on a Low Temperature Surface and in Its Inner Part of Methylamine Aggregate

Nobuyuki NISHI and Hisanori SHINOHARA

Methylamine, which has been proved to be generated by VUV light irradiation to the mixture of methane and ammonia,[1] is condensed on a quartz plate cooled at ~80 K in an UHV reaction chamber. A pulsed laser beam at 193 nm is used as an energy source to bring about photochemistry and to sputter the parent and product molecules which are detected directly by a quadrupole mass spectrometer in a detection chamber (Figure 1). At 193 nm, the following two kind of reactions are expected to occur in an isolated molecule.

$$CH_3NH_2 + h\nu \longrightarrow CH_3NH \text{ or } CH_2NH_2 + H \quad \Delta H = 4.1 \text{ eV} \quad (1)$$

$$CH_3NH_2 + h\nu \longrightarrow CH_3 + NH_2 \quad \Delta H = 3.0 \text{ eV}. \quad (2)$$

We observed the time-of-flight signals of the fragments, H and CH_3, and the photoproducts of HCN, HN_3, $CH_3CH_2NH_2$ and an unidentified compound with m/e = 58 (possibly, $CH_3N = NCH_3$ or $H_2NCH = CHNH_2$). Kinetic energy distributions of the parent and the product molecules are found to be thermarized at characteristic temperatures of 1000 ~ 1400 K. The translational energy distribution of the parent signal is almost independent of the photon density in the lower laser energy region than 100 mJ/cm^2. We conclude that the sputtering is due to a local excitation of molecular clusters including an energy trapped surface molecule and the surrounding molecules. More than two photons participate in the production and the sputtering of HCN. Atomic hydrogen is found to have an extremely high kinetic energy composed of the several components. In the solid, HN_3 is accumulated as a product. Removal of hydrogen and CH_3 to vacuum could yield nitrogen rich products in the solid.

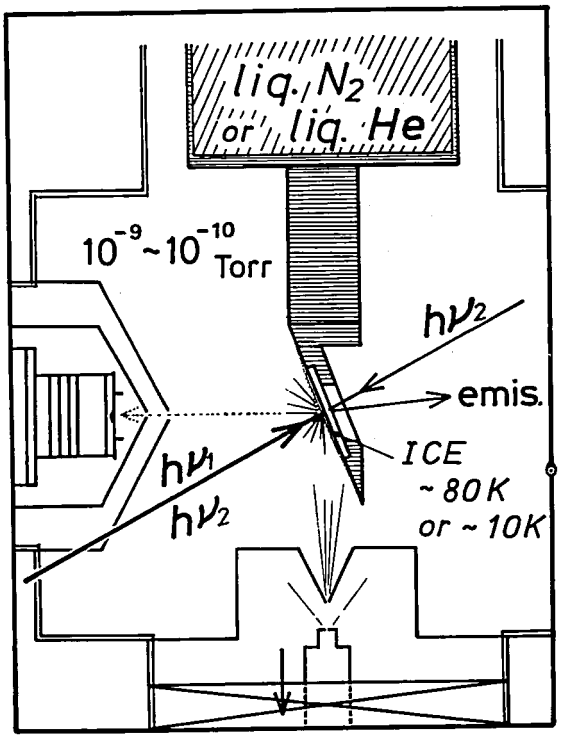

Figure 1. Illustration of time-of-flight experiment of the laser photolysis on condensed gas surface.

Reference

1) E. P. Gardner and J. R. McNesby, *J. Photochem.*, **13**, 353 (1980).

III-H Photodissociation Dynamics of Molecular Beam by Photofragment Spectroscopy

It has been recognized that knowledge of mechanisms and excess energy partitioning of photofragments is important to our understanding and modeling such diverse problems as chemical processes in interstellar space, the composition and kinetics of planetary atmospheres, and laser chemistry in general. Strong VUV lasers, together with technology of supersonic molecular beams, make the so-called photofragment spectroscopy a promising candidate for elucidating photodissociation dynamics. A photofragment spectrometer equipped both with a high peak power VUV excimer laser and a pulsed supersonic molecular beam enables us to characterize experimentally dissociation channels.

Due in large part, to experimental difficulties, photofragment spectroscopy has generally been applied to experiments involving diatomic or pseudo-diatomic molecules. In this case, "direct-dissociation" is often to result. As the polyatomic becomes larger, the number of internal state increases and accordingly

"predissociation" becomes dominant over direct-dissociation.

Studies in the past notwithstanding, unresolved problems remain concerning the mechanisms of predissociation in polyatomic molecules. In this project, we have undertaken a systematic investigation of predissociation and molecular elimination processes of some ethylene derivatives and several polyatomic molecules.

III-H-1 Photodissociation of Acrolein and Acrylonitrile upon Excitation to the Lowest $^1(\pi, \pi^*)$ States

Hisanori SHINOHARA and Nobuyuki NISHI

Pulsed supersonic molecular beams of acrolein (C_2H_3CHO) and acrylonitrile(C_2H_3CN) have been photodissociated by an ArF excimer laser at 193 nm in an ultra high vacuum chamber. Time-of-flight (TOF) spectra show that acrolein dissociates to give C_2H_3 and CHO radicals upon one-photon excitation to a $^1(\pi, \pi^*)$ state. The average translational energy of the fragments is 10.1 kcal/mol. The TOF spectra of acrolein also suggest that the molecule undergoes extensive photofragmentation into smaller fragments (e.g., C_2H_2) via two-photon excitation of 193 nm laser. Figure 1 shows the center-of-mass converted, total translational energy distribution of C_2H_2 fragment. On the other hand, TOF signals of acrylonitrile, observed at various mass numbers, confirm us that the molecule dissociates not only via the radical channel, $C_2H_3CN + h\nu \rightarrow C_2H_3 + CN$, but by means of the molecular elimination process, $C_2H_3CN + h\nu \rightarrow C_2H_2 + HCN$. The TOF spectra are analyzed as superpositions of two thermalized components at the characteristic temperatures of 2500 K and 6000 K for the dissociation and the molecular elimination processes, respectively (Figure 2).

Observed isotropic angular distributions imply that the molecules will live for certain period after the excitation which is relatively long as compared with the rotation period. It is concluded that the photodissociations at 193 nm are predissociative.

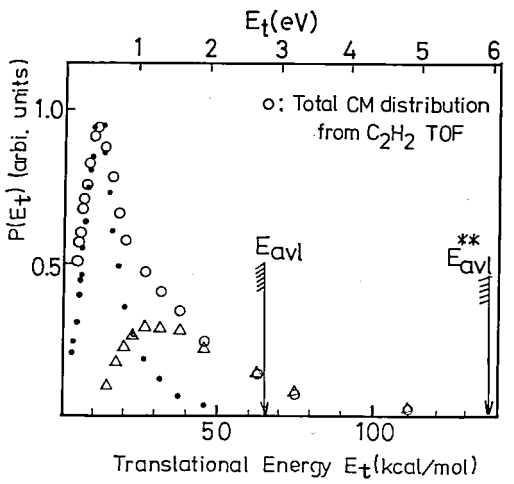

Figure 1. The center-of-mass converted, total translational energy distribution of C_2H_2 fragment. The open circles represent the total CM distribution converted from the C_2H_2 TOF spectrum. The triangles give the two-photon generated (directly from the parent molecule) C_2H_2 CM distribution. The closed circles stand for the CM distribution of C_2H_3 fragments. It should be noted that the open circles are given by the sum of the triangles and the closed circles. E_{avl}^{**} is the available energy and amounts to 138 kcal/mol (6.81 eV).

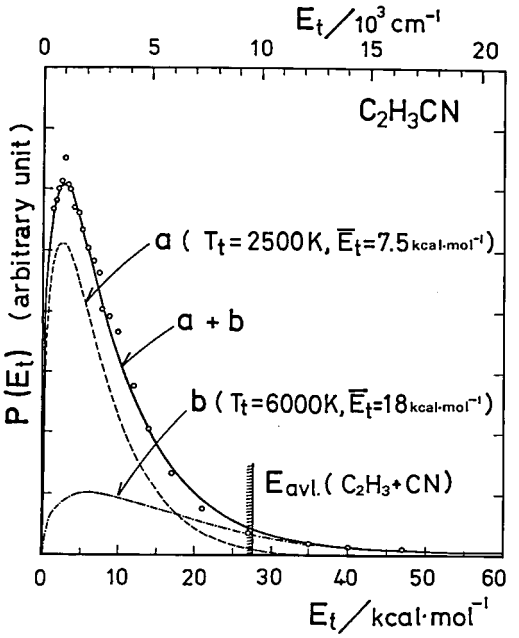

Figure 2. The distribution, $P(E_t)$, of total center-of-mass (c.m.) translational energy obtained by an approximate lab to c.m. transformation of the data at m/e = 27 analyzed as due to the dissociation process producing the two fragments with m/e = 27 and 26. The solid curve is a composit of the two thermalized components expressed by Maxwell-Boltzmann distribution functions with characteristic temperatures of 2500 K (broken line, a) and 6000 K (dotted line, b).

III-H-2 Molecular Elimination and Atomic Detachment Processes in Chloroethylenes

Masayuki UMEMOTO[1], Hisanori SHINOHARA, Nobuyuki NISHI, and Ryoichi SHIMADA
(Kyushu Univ.)

A photofragment spectrometer can directly detect both of the fragments, Cl and HCl, generated through independent events of photodissociation and molecular elimiantion channels in chloroethylenes. Upon the $\pi \rightarrow \pi^*$ excitation of monochloroethylene at 193 nm, the strong time-of-flight signals at m/e = 35 and 36 are observed as shown in Figure 1. They are attributed as due to the following reactions,

$$C_2H_3Cl + h\nu \rightarrow C_2H_3 + Cl$$
$$\Delta H = 85.6 \text{ kcal.mol}^{-1} \quad (1)$$

$$C_2H_3Cl + h\nu \rightarrow C_2H_2 + HCl$$
$$\Delta H = 23.6 \text{ kcal.mol}^{-1}. \quad (2)$$

The total translational energy distribution for the two reactions are substantially different as seen in Figure 2. They indicate that the reactions are not brought about directly from the (π, π^*) state. Reaction (1) shows a sharp distribution, while the HCl elimination process (2) reveals almost thermalized translational energy distribution. Table I summarizes fractions of the average translational energy to the available energy, $E_{avl.}$. The observed energy of the fragments of trans-dichloroethylene for Cl detachment process amounts to 44% of the available energy, whereas that for HCl elimination is about 13%. The later value is also found for other two dichloroethylenes, indicating that the elimination process is independent of the position of Cl atoms. Angular dependence of the signal intensity on the polarization direction of exciting light is found to be very large for reaction (1) in contrast to that for the molecular elimination process (2). It is

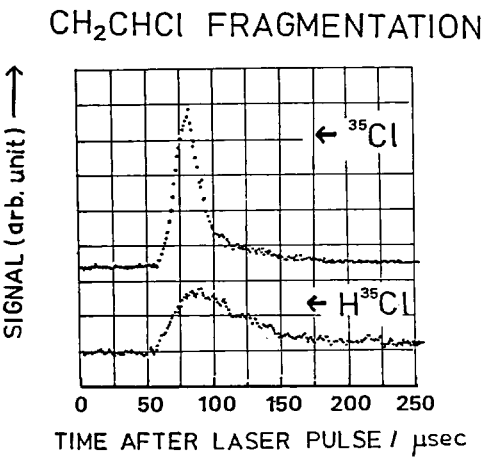

Figure 1. Time-of-flight signals at m/e = 35 (top) and 36 (bottom).

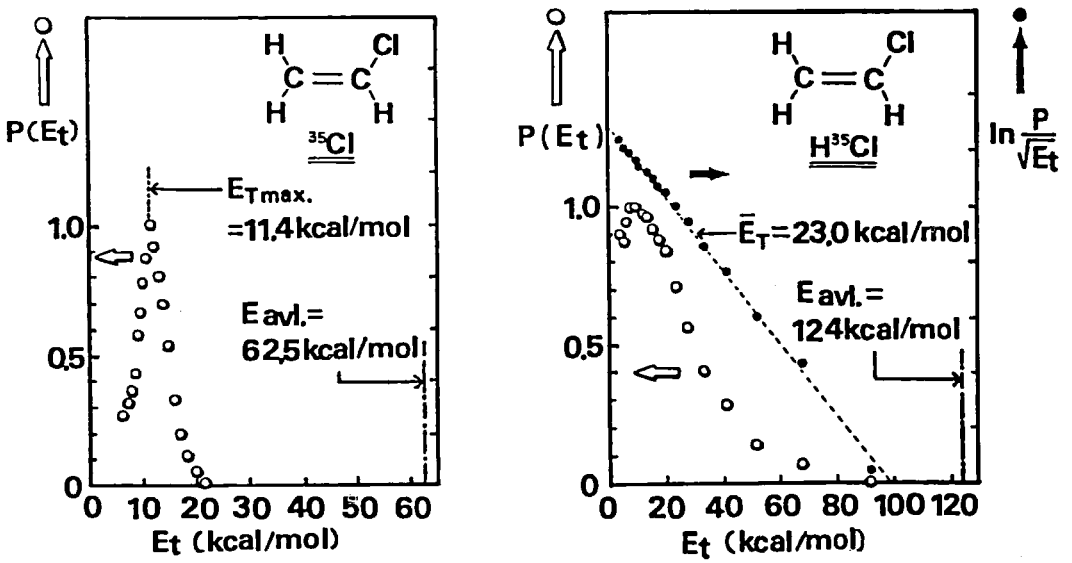

Figure 2. Total translational energy distributions for the Cl detachment process (left) and the HCl elimination process (right).

concluded that reaction (1) occurs faster than the rotational correlation time of ~1 ps from the (n, σ^*) state. However, the molecular elimination process is occured throgh vibrationally excited ground electronic state. The branching ratio of reaciton (1) to reaction (2) is about 1.3 : 1.

1) IMS Graduate Student 1980—1982 —— from Kyushu Univ.

Table I. Fractions of average translational energy, $\overline{E}_T$, to available energy, $E_{avl.}$

Parent	Cl atomic elimination			HCl molecular elimination		
	$E_{avl.}$ kcal/mol	$\overline{E}_T$ kcal/mol	$f_T \equiv \frac{\overline{E}_T}{E_{avl.}}$	$E_{avl.}$ kcal/mol	$E_{Tmax.}$ kcal/mol	$f_T \equiv \frac{E_{Tmax.}}{E_{avl.}}$
$CH_2 = CHCl$	62.5	11.4	0.182	124	23.0	0.185
cis-$CHCl = CHCl$	58.9	13.6	0.231	120	15.2	0.127
trans-$CHCl = CHCl$	59.4	26.1	0.439	120	16.6	0.138
$CH_2 = CCl_2$	58.5	21.2	0.362	120	15.3	0.128

III-H-3 Molecular Beam Photodissociation of Trimethylamine

Masahiro KAWASAKI*, Kazuo KASATANI*, Hiroyasu SATO *(*Mi'e Univ.)*, **Hisanori SHINOHARA, Nobuyuki NISHI, and Tohru IBUKI** *(Kyoto Univ.)*

The first and the second excited states of trimethylamine have been identified as n $\rightarrow$ $3S(\tilde{A}^1A''_2)$ and n $\rightarrow$ $3P(\tilde{B}^1E')$. These states predissociate into $CH_3 + (CH_3)_2N$. Upon the excitation to the second excited state at 193 nm, we observed the time-of-flight and angular distribution of the photofragments. The isotropic angular distribution observed indicates that the dissociative lifetime is much longer than the molecular rotation period. The high energy part of the observed translational energy distribution is well represented by the theoretical formula given by Marcus[1],

$$P(E_t) \propto E_t^{m^{\ddagger}-m} N_P(E_{avl} - E_t),$$

where $m^{\ddagger}$ refers to the number of rotational and vibrational degrees of freedom in the transition state, m to that in the products, N_P to the vibronic level density of the products and E_{avl} to the available energy. In this case, four active vibrations become adiabatic rotations in the products and thus $(m^{\ddagger} - m)$ is equal to two. The averaged translational energy was thirteen percent of available energy. This analysis of the translational energy leads us to conclude that the dissociation occurs through hot ground state. A diffuse fluorescence spectrum from S_1 was also observed at 193 nm excitation in a molecular beam. This fact indicates that the internal conversion, $S_2 \rightarrow S_1$, is very fast. Thus, the predissociation mechanism is proposed as follows,

$$S_2 \xrightarrow{\text{very fast}} S_1 \xrightarrow{10\ \text{ps}^{2)}} S_0^{\ddagger} \xrightarrow{\text{slow}} CH_3 + (CH_3)_2N.$$

References
1) R. A. Marcus, *J. Chem. Phys.*, **62**, 1372 (1975).
2) Y. Matsumi and K. Obi, *Chem. Phys.*, **49**, 87 (1980).

III-H-4 Photodissociation Dynamics of SO_2 Supersonic Molecular Beam at 193 nm

Masahiro KAWASAKI*, Kazuo KASATANI*, Hiroyasu SATO* *(*Mi'e Univ.)*, **Hisanori SHINOHARA, and Nobuyuki NISHI**

We have photodissociated sulfer dioxide in a supersonic molecular beam at 193 nm using an ArF excimer laser and measured the translational energy distribution of the photofragments. Figure 1 shows the center-of-mass converted translational energy. A broad translational energy distribution is observed

like Freedman et al. reported.[1] As the dissociation energy of SO_2 is 130 kcal/mol and its average internal energy at room temperature is 1.5 kcal/mol, the available energy at 193 nm (148 kcal/mol) is 19.5 kcal/mol. More than half of the available energy on the average is found as translation (E_t/E_{avl} = 0.68), with remainder being internal energy of the S-O fragment. We presume that the slanted area in Figure 1 represents the probability that molecules are in the vibrational state of v = 1. Figure 2 presents the comparison of measured vibrational state distribution shown as solid circles with the results of the calculated one shown as open circles. Both of the distributions peak at v = 2 and their agreement is fairly good except for the higher vibrational states (v = 3, 4) where the experimental error might become significant.

The angular distribution of fragments with respect to the polarization direction of the laser beam is found to be isotropic, which suggests that photodissociation of SO_2 at 193 nm is predissociation.

Reference

1) A. Freedman, S. C. Yang, and R. Bersohn, *J. Chem. Phys.*, **70**, 5313 (1979).

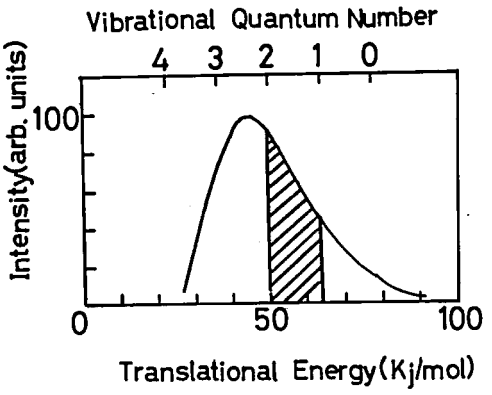

Figure 1. The center-of-mass converted, total translational energy distribution of SO fragments. The upper ordinate scale is the vibrational quantum number. The slanted area represents the probability that molecules are in the vibrational state of v = 1.

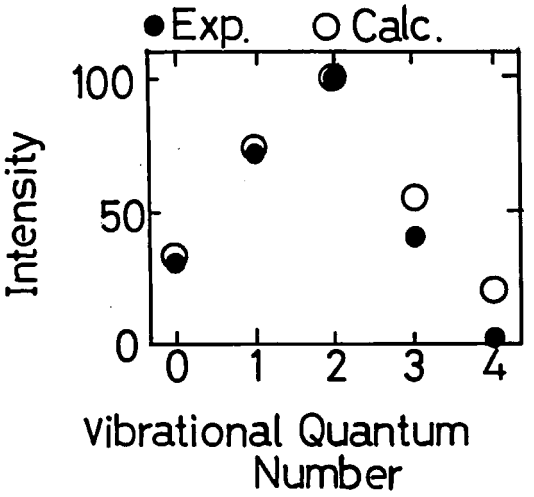

Figure 2. The comparison of measured vibrational state distribution with the calculation where the harmonic oscillator approximation is adapted in evaluating the Frank-Condon factors.

III—I Molecular Photofragmentations from Highly Excited Electronic States

Direct multiphoton excitation using a VUV laser creates superexcited states of polyatomic molecules which lie above the ionization thresholds. Nature of superexcited state is not known so precisely. Such a high electronic state must include multi-electron excitation configulations and, therefore, is expected to be unstable except for the states with excited electrons in s-type Rydberg orbitals.

Since the two photon energy of 193 nm light (12.8 eV) is more than twice of the bond energy for a C = C double bond and much greater than three times of that for a C − C single bond, molecular photofragmentation is expected to be observed upon strong laser irradiation. A high resolution spectrum of emission or laser induced fluoresence enables us to know internal energies of fragments. The selection rule for a sequential multiphoton excitation may enhance multi-electron excited species as compared to that for a single photon excitation to superexcited states.

III-I-1 VUV Laser Photofragmentations of Acrylonitrile Molecular Beam

Nobuyuki NISHI, Hisanori SHINOHARA, and Ichiro HANAZAKI

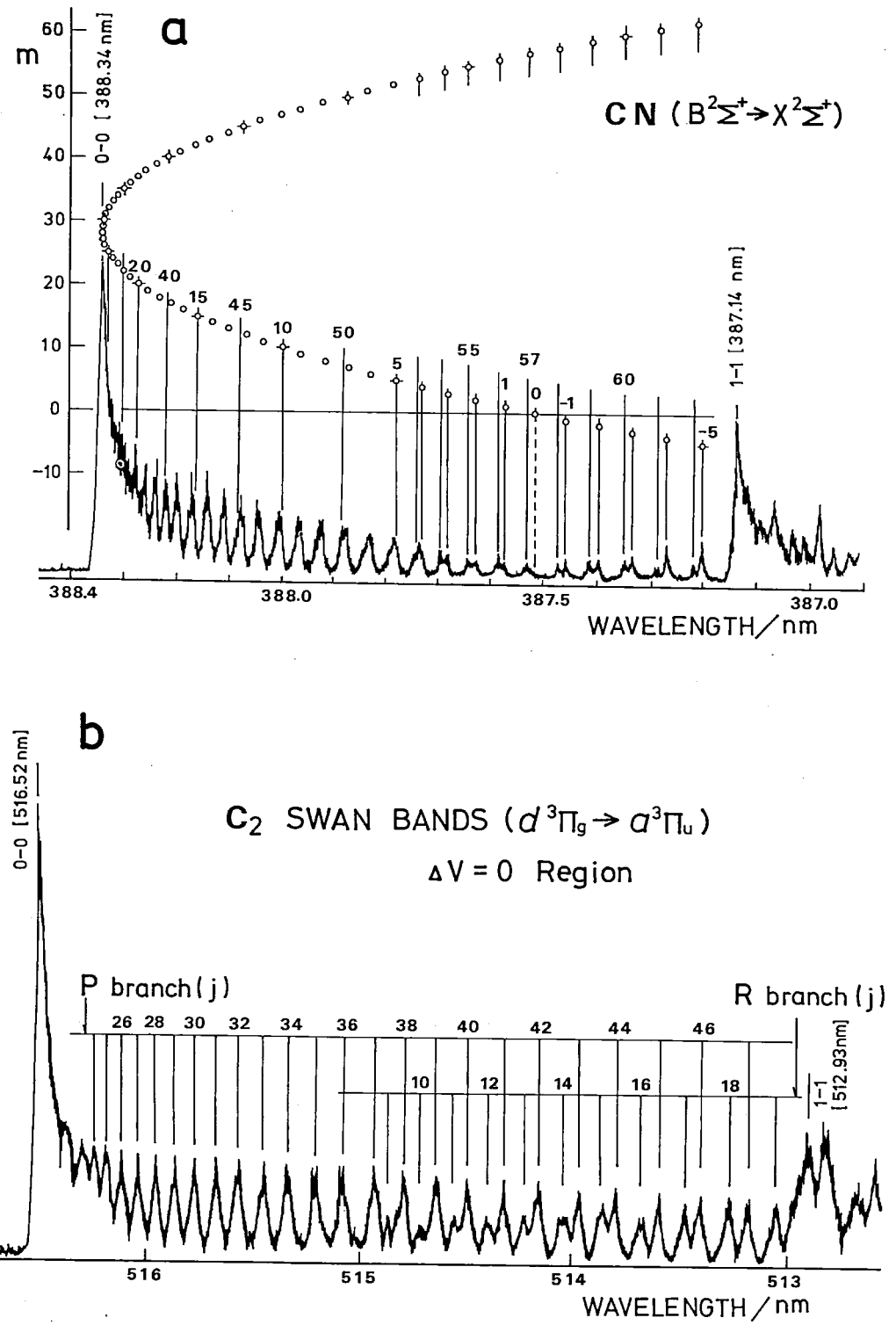

Figure 1. a: A portion of the CN($B^2\Sigma^+ \rightarrow X^2\Sigma^+$) spectrum for the rotational sequence in the $\Delta v = 0$ region produced by mildly focussed 193 nm laser photolysis of an acrylonitrile molecular beam. The running numbers m are shown for the P and R branches of the 0-0 band as a Fortrat parabola.

b: The 0-0 band of the C_2 Swan emission ($d^3\Pi_g \rightarrow a^3\Pi_u$) observed in the 193 nm laser photolysis of an acrylonitrile molecular beam. Only the integer part of the rotational quantum number j is shown for the P and R branches.

Photofragment emission from CH and C_2 is observed at the interaction region of an acrylonitrile molecular beam and an ArF laser beam. Power dependence experiment shows that the emission from $CH(B^2\Sigma^+)$ and $CH(A^2\Pi_i)$ are produced through two photon excitations of the parent and that from $CN(E^2\Sigma^+)$, $CN(F^2\Delta_r)$ and $C_2(d^3\Pi_g)$ are generated through three photon excitations. Parts of the CN and C_2 emission are shown in Figure 1. The fluorescence lifetimes in the beam condition agree very well with the values obtained from Stern-Volmer plots in static cell experiments, (e.g., $\tau[CN(A^2\Pi_i \rightarrow X^2\Sigma^+)] = 7.1 \pm 0.6$ μs).

The vibrational distribution in the $A^2\Pi_i$ state is found to be highly non-statistical with maximum population around v = 9 level which is close to the origin of the $B^2\Sigma^+$ state. However, the vibrational and rotational population of $CN(B^2\Sigma^+)$ are almost thermarized at characteristic temperatures of 5860 $\pm$ 420 K and 2830 $\pm$ 25 K, respectively. The vibrational temperature of $C_2(d^3\Pi_g)$ is observed to be 7150 $\pm$ 160 K and the rotational one to be 4960 $\pm$ 150 K. The $CN(A^2\Pi_i)$ radical, highly excited vibrationally, is succeedingly pumped by the third photon to the $F^2\Delta_r$ and the $E^2\Sigma^+$ states.

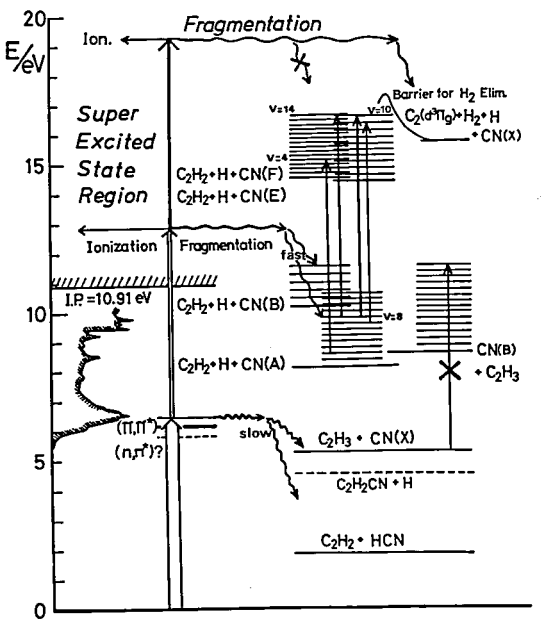

Figure 2. Excitation and fragmentation scheme observed in the ArF laser photolysis of acrylonitrile. Vertical arrows stand for the excitation processes observed. The main reaction process is the one-photon dissociation process generating the two radicals of C_2H_3 and CN. This process is sufficiently slow to distribute excess energy among various vibrational modes.

Figure 2 summarizes the excitation and fragmentation processes observed in the 193 nm laser photolysis of C_2H_3CN. None of the emissive fragments arise from the secondary excitations of the C_2H_3 and the CN radicals produced through the one photon dissociation process described in III-H-I. Superexcited states, generated by two or three photon excitation, are responsible for the fragmentations and they could be composed mainly of two or three electron excitation configurations. Appearance of the two CN species with different electronic structures may originate in different electronic configurations in the superexcited states.

III-I-2 VUV Laser Photofragmentation Dynamics of Acrolein Molecular Beam; Role of Charge-Transfer Character in Excited State

Hisanori SHINOHARA and Nobuyuki NISHI

Emission resulting from the photofragmentation of acrolein has been investigated by incorporating a pulsed supersonic free jet as a sample source. Strong emission from the $CH(A^2\Delta, B^2\Sigma^-, C^2\Sigma^+, \rightarrow X^2\Pi)$ systems and weak emission from the $C_2(d^3\Pi_g \rightarrow a^3\Pi_u)$ Swan system have been observed. The spectra arising from the fragmentation of a pure acrolein free jet by a focused ArF laser are shown in Figure 1. From the laser fluence dependence on the emission intensity, the excitations of the CH ($A^2\Delta$) and $C_2(d^3\Pi_g)$ states require the absorption of 2 and 3 photons, respectively.

According to a previous study,[1] the (π, π^*) state has charge transfer character from the electron-donating group(H_2C = CH) toward the electron-accepting group(HC = O). Sequential excitation from this state to a superexcited state is possible by another 6.4 eV photon. Doubly excited electron configurations are expected for the superexcited state, which include the similar (π, π^*) type configuration to the $S_2(\pi, \pi^*)$ state. Thus, the charge transfer character is considered to play an important role in the geometrical stability in the superexcited state from which acrolein undergoes fragmentation, viz.

$$C_2H_3CHO^{**} \longrightarrow CH^* + CH_3 + CO.$$

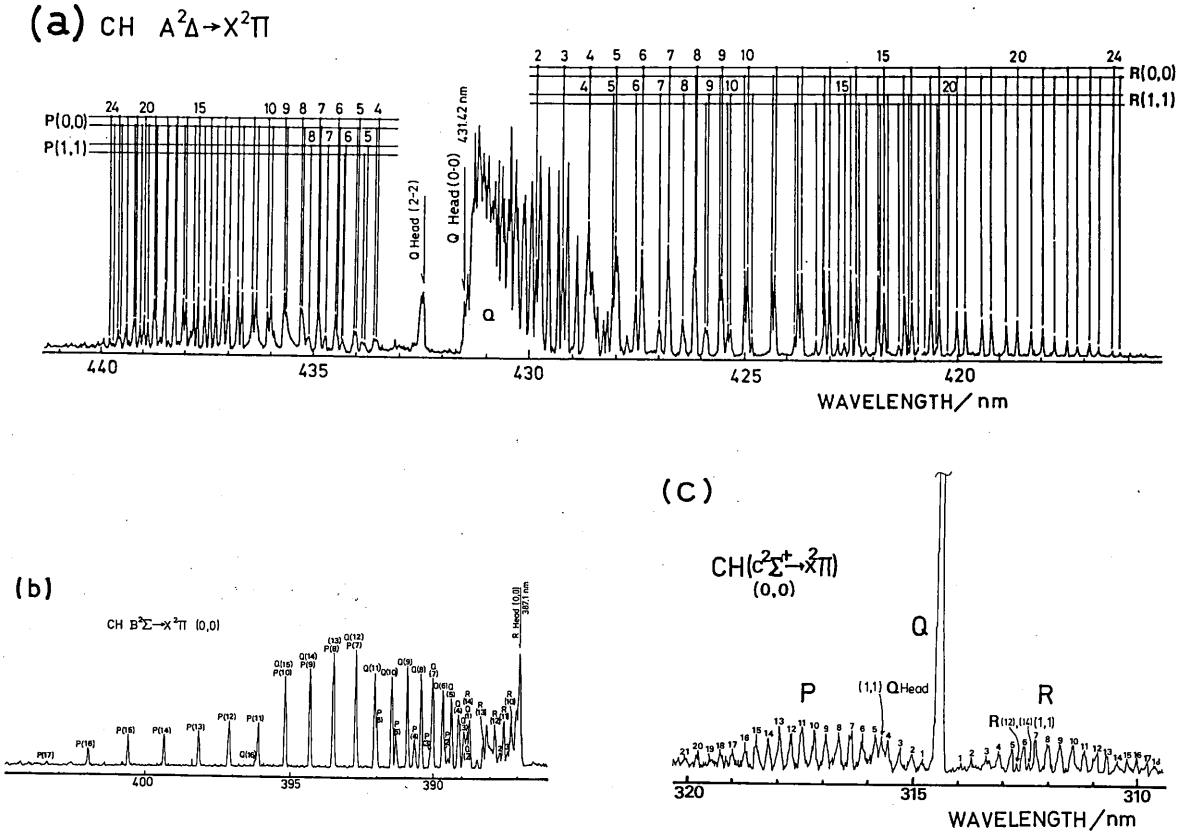

Figure 1. Emission spectra from CH (a) $A^2\Delta \rightarrow X^2\Pi$, (b) $B^2\Sigma^- \rightarrow X^2\Pi$ and (c) $C^2\Sigma^+ \rightarrow X^2\Pi$ systems arising from photodissociation of a pure acrolein supersonic free jet by focused ArF laser irradiation.
(a) The large Λ splitting, which originates from the CH ground state splitting and not from the A state, is obseved with partially overlapping (0,0) and (1,1) bands. The Q-head of the (2,2) band is also observed.
(b) The P(10) + Q(15), P(9) + Q(14), P(8) + Q(13) and P(7) + Q(12) groups are unresolved at the present resolution.
(c) The (0,0) R(8) − R(1) lines are strongly overlapped by the (1,1) R(18) − R(16) lines. The (1,1) Q lines, Q(1) − Q(20), are blended with the strong (0,0) P lines originating from N < 9.

Reference
1) S. Nagakura, *Mol. Phys.*, **3**, 105 (1960).

III-I-3 ArF Laser Photofragmentation of Substituted Benzenes

Masahiro KAWASAKI,* Kazuo KASATANI,* Hiroyasu SATO *(*Mi'e Univ.)*, **Hisanori SHINOHARA, and Nobuyuki NISHI**

The photodissociation pathways of substituted benzenes, involving the π electron system of the benzene ring, are characterized by indirect dissociation. Present work reports the results of photofragmentation of phenyl and benzyl compounds.

Multiphoton fragmentation of the aromatic compounds are examined by observing the emissions from photofragments. Banded emission of CN fragments was observed from C_6H_5CN, while that of CH was detected from $C_6H_5CH_2CN$. The results are summarized in Table 1. The fragments attached directly to the phenyl ring are electronically excited. As mentioned above, the photons excite a delocarized singlet state of the phenyl ring. Since the dissociation lifetime is expected to be fairly long for these molecules with substituents of weak spin-orbit coupling, the aryl ring can absorb the second photon to form electronically excited fragments.

$$S_0 \xrightarrow{h\nu} S_n(\pi,\pi^*) \xrightarrow{h\nu} S_m(\pi,\pi^*) \longrightarrow \text{Decomp.}$$

Since the π orbital of the CN substituent is overlapped with the π orbital of phenyl ring, the electronically excited CN* is formed. On the other hand, from benzyl cyanide, CN* is not formed but CH* is generated because of hyperconjugation. This is the case for $C_6H_5CH_2OH$, that is, CH* was detected but not OH.

Table 1. Observed Emission of Photofragments

Parent Molecule	Emission
C_6H_6	none
C_6H_5-CH_3	CH(A,B)
C_6H_5-CN	CN(B)
C_6H_5-CH_2-CN	CH(A,B)
C_6H_5-CH_2-OH	CH(A,B)

III—J Multiphoton Ionization Mass Spectroscopy of Cyclic Molecules

Use of mass spectrometry for the study of multiphoton ionization processes gives us direct informations on the dynamical properties in ionic state and intermediate electronic states. Fragmentation mechanisms of the ions produced photochemically are expected to be different from those found in the electron bombardment mass spectroscopy. Stepwise fragmentations of the ions are observed for planer and non-planer cyclic molecules. Relative abundance of the parent and fragment ions are dependent on the resonant electronic states or exciting wavelengths.

III-J-1 Role of Intermediate Excited State on the Multiphoton Ionization Processes of Cyclic Ketones and Acetone

Masaaki BABA, Hisanori SHINOHARA, Nobuyuki NISHI, and Noboru HIROTA *(Kyoto Univ.)*

The photochemistry of cyclic ketones and acetone in the gas phase has been the subject of active investigation using a variety of experimental techniques. Here, we present results of a study of the multiphoton ionization mass spectroscopy (MPIMS) of cyclic ketones and acetone obtained at unit mass resolution with the excitation wavelengths at 248 and 193 nm. Figure 1[(a), (b) and (c)] shows the MPIMS of acetone, cyclobutanone and

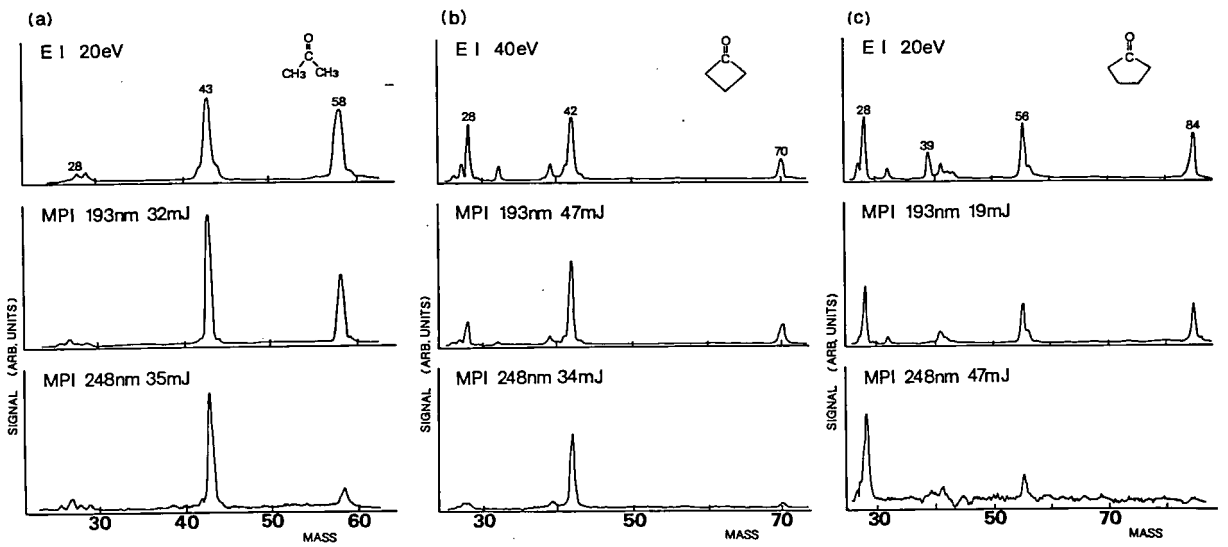

Figure 1. The electron impact (EI) and multiphoton ionization (MPI) mass spectra of acetone(a), cyclobutanone(b) and cyclopentanone(c) with ArF(193 nm) and KrF(248 nm) excimer laser excitations. Experimental conditions are identical both in the EI and MPI mass spectrum measurements.

cyclopentanone molecular beams, respectively. A comparison is also made of the MPIMS with electron impact mass spectrometry.

It has been found that the fragmentation pattern changes with the two different laser wavelengths. At each wavelength a mildly focused beam is used. In the present study, two possible MPI mechanisms are responsible for the fragmentation patterns. With 248 nm excitation to the lowest (n,π^*) state, the parent ion signal is considerably weak in contrast to the sharply peaked fragment ions. This is indicative of stepwise MPI processes in which the intermediate (n,π^*) states may play important roles in ion productions. On the other hand, direct excitations into photoionization continuums (or into superexcited states), which can generate not only fragment ions but parent ion itself, are efficient at 193 nm excitation where an (n,3s) Rydberg state dominates in absorption. Different MPI fragmentation patterns presumably reflect the stability for the intermediate states.

III-J-2 Ionization and Decomposition Processes in UV Multiphoton Excitation of Xylenes

Yoshiya TAKENOSHITA *(Kitakyushu Univ.)*, **Hisanori SHINOHARA, and Nobuyuki NISHI**

Multiphoton ionization (MPI) mass spectra of p- and o-xylenes are studied by irrdiating pulse lasers at 248 and 193 nm which are resonant with the first and the third $\pi \rightarrow \pi^*$ transitions, respectively. Figure 1 shows spectral differences which depend on the exciting wavelengths and laser power. None of MPI spectra coincide with the conventional electron impact (EI) mass spectrum with an ionization energy of 70 eV (Figure 1-c). MPI spectrum taken at 248 nm always shows the maximum peak for the parent ion with m/e = 106 in the laser power range below 120 mJ, although stronger light increases smaller fragments relatively. On the other hand, 193 nm light generates larger amount of the ion with m/e = 91, which lacks one methyl of xylene, than the parent ion. The intensities of the signals at m/e = 106 and 91 grow quadratically with the increment of the laser power at 193 nm. The signals at m/e = 77 and 65 behave almost in pairs for 193 nm light showing cubic power dependences.

Two photon energy of 248 nm light (10 eV) exceeds the ionization potential of p-xylene by 1.4 eV, which can produce only the parent ion. However, the double quantum energy of 193 nm light (12.8 eV) is even higher than the energetical threshold of 11.6 eV for the reaction,

$$CH_3\text{-}C_6H_4\text{-}CH_3 \rightarrow (C_6H_4\text{-}CH_3)^+ + CH_3 + e.$$

The spectra in Figure 1-a demonstrate that this process is more predominant than the simple ionization of the parent molecule for the 193 nm

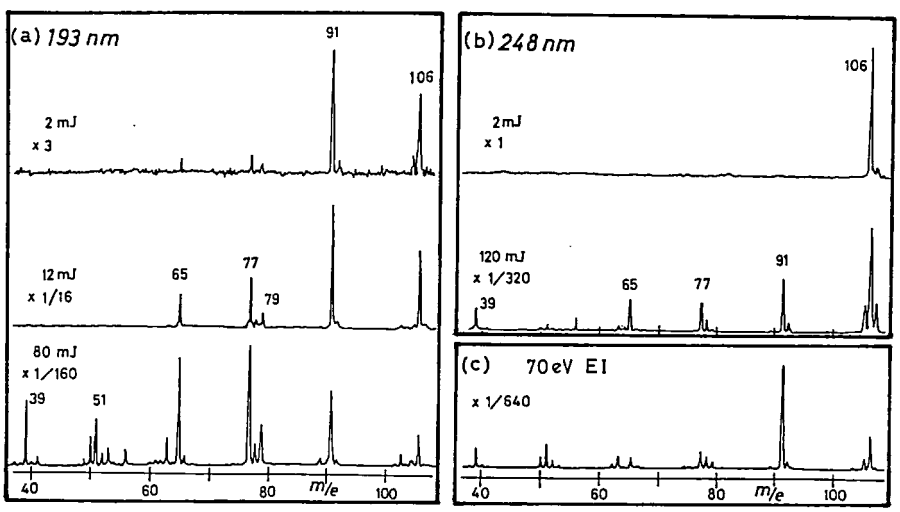

Figure 1. Multiphoton ionization mass spectra of p-xylene.

excitation. o-xylene shows very similar spectra to those of p-xylene except for the small intensity difference between pair signals. Further degradation processes are characterized by retro-Diels-Alder type reactions which snap off the acetylene fragment.

III—K Photoelectrolysis of Water under Visible Light with Doped $SrTiO_3$ Electrodes

Michio MATSUMURA *(Osaka Univ.)*, **Masahiro HIRAMOTO** *(Osaka Univ.)*, **and Hiroshi TSUBOMURA** *(Osaka Univ. and IMS)*

Various pieces of sintered strontium titanate doped with metal oxides were used as photoanodes in aqueous solutions. Some of them (having Ru, V, Cr, Ce, Co, Rh) caused photocurrents with light in the visible region (Figure 1). The production of oxygen at the semiconductor electrode and hydrogen at the counter electrode was confirmed. For the electrode doped with RuO_2, the quantum efficiency of the photocurrents with the visible light (400 − 500 nm) reached ca. 2% under anodic polarization. Based on these results and on the reflection and electroluminescence spectra of the sinter, it is concluded that the photocurrent arises from an electronic transition from a dopant level to the conduction band, the former lying a little above the valance band.

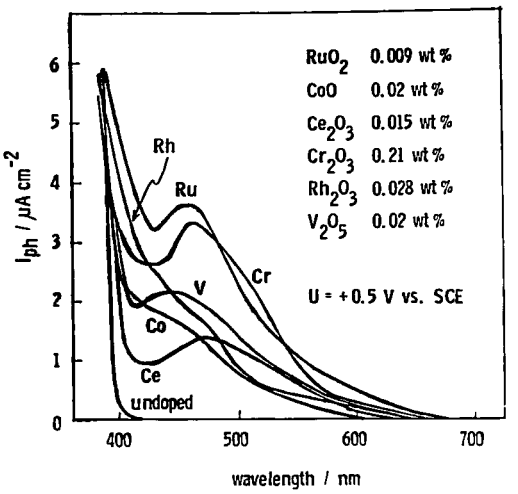

Figue 1. Action spectra of the photocurrents for the $SrTiO_3$ electrodes doped with metal oxides in aqueous solutions of pH 4.6 under the potential of 0.5 V vs. SCE.

III—L Studies on Electronic Structure, Energy Transfer, Dissociation and Recombination of Small Molecules

Absorption, fluorescence, and light scattering spectra of various small molecules are measured under a pressure 1 mTorr − 150 Atom and a temperature 77 − 1200 K. The electronic structure and the potential curve are studied by analyzing the transition energies and the intensity distribution of spectra. By exciting a molecule to the dissociative continuum or close to the dissociation limit or the level-crossing region, the mechanism of energy transfer, dissociation, and recombination of dissociated atoms are studied by relating to the intra- and intermolecular potentials.

III-L-1 Laser-Induced Fluorescence of the NaRb Molecule

Naohisa TAKAHASHI *(Kobe Univ.)* **and Hajime KATO** *(Kobe Univ. and IMS)*

[*J. Chem. Phys.*, in press]

Several series of laser induced fluorescence lines of the heteronuclear alkali dimer NaRb have been observed when a mixture of sodium and rubidium is irradiated by the He-Ne, Ar^+, or Kr^+ laser line. The spectroscopic constants of the X $^1\Sigma^+$ ground state have been determined and the potential energy curve has been calculated by the RKR methods. RKR potential curves for the excited B $^1\Pi$ and D $^1\Pi$ have been determined by comparing the

observed and calculated intensity distributions as well as the transition energies. The dependence of the transition dipole moment upon the internuclear distance has been estimated. The fluorescence of the D lines of Na and Rb atoms and a less intense fluorescence, which is assigned as a transition to the a $^3\Sigma^+$ state in NaRb, have been observed. From the measured vibrational spacing, which can be followed close to the dissociation limit, the dissociation energy D^e of the a $^3\Sigma^+$ state is determined to be 568 ± 5 cm^{-1}.

III-L-2 $Na_2(A\ ^1\Sigma_u^+ \rightarrow X\ ^1\Sigma_g^+)$ Fluorescence Accompaned by a Continuous Spectrum

Hajime KATO *(Kobe Univ. and IMS)*, **Tohru MATSUI** *(Kobe Univ.)*, **and Chifuru NODA** *(Kobe Univ.)*

[*J. Chem. Phys.*, in press]

A suitably adjusted single-mode line of the krypton ion laser at 5682 Å has been found to excited Na_2 to the single level A $^1\Sigma_u^+$ ($v' = 34$, $J' = 50$). Then, a series of resonance fluorescence to different vibrational levels of the ground state X $^1\Sigma_g^+$ have been observed up to the point of convergence. A continuous spectrum with banded diffraction structure has been contiguous to it and extended toward the small wave number region. The spectrum has been quantitatively accounted for by quantal calculations.

III-M-1 Phase and Velocity Changing Collisions of Na and Na_2 with Ar Studied by Backward Photon Echoes

S. ASAKA, H. YAMADA, M. FUJITA *(Kyoto Univ.)*, **and M. MATSUOKA** *(Kyoto Univ. and IMS)*

Argon induced photon echo decays and their phase and velocity changing collision-cross sections have been measured on the atomic sodium Na and the molecular sodium Na_2. The transition lines measured are the D_1 and D_2 lines of Na, and several isolated lines of the $X\Sigma$-$A\Sigma$ and $X\Sigma$-$B\Pi$ transitions of Na_2.

Echoes were studied by the three-pulse-backward-echo method. Decays of the echo intensity were measured carefully as a function of the pressure of Ar buffer gas. With the pulse separations of 3 to 8 nsec, the decays were mostly due to the phase changing collisions. Cross sections of the velocity changing collisions were measured in the same systems with increased pulse separations.

Table I shows a result of the phase-changing collisional cross sections.

Table I. Collision Cross Sections and Radii

	$\sigma(Å^2)$	r(Å)
$Na(D_1, D_2)$ + Ar	340 ± 10	10.4
$Na_2(A-X)$ + Ar	423 ± 17	11.6
$Na_2(B-X)$ + Ar	455 ± 19	12.0

RESEARCH ACTIVITIES IV
Division of Molecular Assemblies

IV—A Photoelectric and Optical Properties of Organic Solids/Liquids in Vacuum Ultraviolet Region

By means of various kinds of photoelectron spectrometer, quantitative information on the electronic properties of the organic materials at condensed phase, solid and liquid, has been obtained.

IV-A-1 Vacuum-UV Absorption Spectra of Molten Polyethylene

Shimpei HASHIMOTO *(Japan Synthetic Rubber Co.)*, **Kazuhiko SEKI, Naoki SATO, and Hiroo INOKUCHI**

We have been studying the electronic properties of polyethylene (PE) $-(-CH_2-CH_2-)_{\overline{n}}$ and long chain linear alkanes as its model compounds by means of vacuum-uv absorption spectra,[1] uv photoelectron spectroscopy,[2] and secondary electron emission.[3] To clarify the electronic properties of amorphous PE, the measurements of its molten state will be useful. In this work we measured the vacuum-uv absorption spectra of molten PE on a LiF substrate. Figure 1 shows the temperature dependence of the absorption spectra of high density PE (Showlex 7200) measured on a McPherson 225 1m normal incidence monochromator equipped with a H_2-discharge lamp and double beam attachment. Upon melting (m.p. ~ 130 °C), the absorption at $h\nu < 8.2$ eV increases, while that at $h\nu > 8.2$ eV decreases. Similar results were observed for low density PE and linear high molecular weight PE, although the spectra differed from that of high density PE in detailed features. These results suggest that the absorption of amorphous parts is shifted to the photon energy region lower than that of crystalline parts. The change of absorption edge on going from crystalline to amorphous state is now being studied.

References

1) S. Hashimoto, K. Seki, N. Sato, and H. Inokuchi, *IMS Ann. Rev.* **67** (1978).
2) K. Seki, S. Hashimoto, N. Sato, Y. Harada, K. Ishii, H. Inokuchi, and J. Kanbe, *J. Chem. Phys.* **66**, 3644 (1977).
3) N. Ueno, T. Fukushima, K. Sugita, S. Kiyono, K. Seki, and H. Inokuchi, *J. Phys. Soc. Jpn.*, **48**, 1254 (1980).

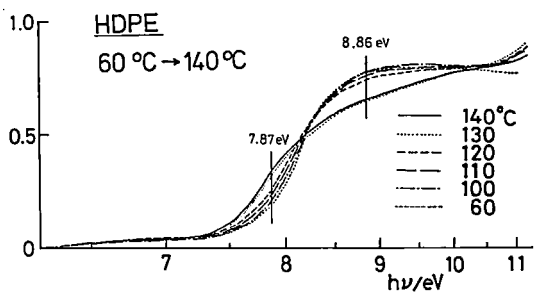

Figure 1. The temperature dependence of the vacuum-uv absorption spectra of high density polyethylene. The temperature was raised from 60 to 140°C.

IV-A-2 UV Photoelectron Spectroscopic Study of Melting of Long-chain Alkanes

Kazuhiko SEKI, Nobuo UENO,* Keisuke SAKAMOTO,* Kazuyuki SUGITA,* and Hiroo INOKUCHI *(*: Chiba Univ.)*

The photoelectron spectra of crystalline and molten tetratetracontane (n-$C_{44}H_{90}$) were measured by virtue of the low vapor pressure in molten state. Figure 1 depicts the comparion of the He I ($h\nu$ = 21.2 eV) photoelectron spectra. Features A—D in crystalline spectrum are assigned to those of conduction band.[1] Upon melting, these are completely smeared out. This change is recovered on cooling, but shows a hysteresis. Changes were observed above the melting point of bulk material. These results agree with those observed in

secondary electron emission.[2] The comparison with gas phase He I spectrum of n-$C_{36}H_{74}$ shows that the gross features in the molten state spectrum do not reflect the features of valence band clearly, but are determined by those of conduction band. The large change of conduction bands on melting is in contrast to the small difference between the valence bands of crystalline and gaseous state of n-$C_{36}H_{74}$. The change of the photoemission threshold on melting is now under investigation.

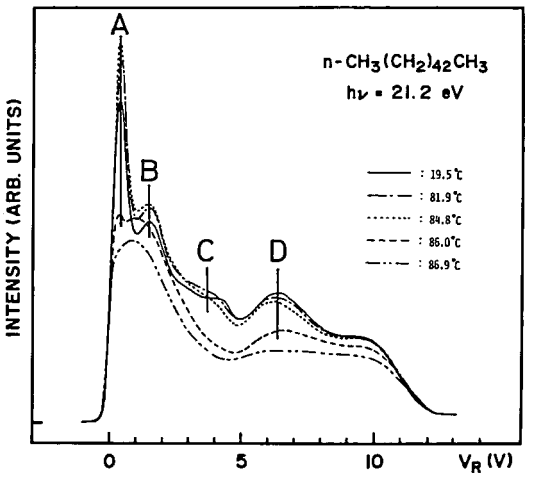

Figure 1. He I photoelectron spectra of crystalline and molten n-$C_{44}H_{90}$. Melting point of bulk material is about 86 °C.

References

1) K. Seki, S. Hashimoto, N. Sato, Y. Harada, K. Ishii, H. Inokuchi, and J. Kanbe, *J. Chem. Phys.* **66**, 3644 (1977).
2) N. Ueno and K. Sugita, *Solid State Commun.* **34**, 355 (1980).

IV-A-3 UV Photoelectron Spectroscopy of Poly-*p*-xylylene

Yoshiaki TAKAI,* Teruyoshi MIZUTANI,* Masayuki IEDA,* Kazuhiko SEKI, and Hiroo Inokuchi *(*: Nagoya Univ.)*

[*Polymer Photochem.* **1**, in press]

Poly-*p*-xylylene (PPX) —(—CH_2-*p*-C_6H_4—CH_2—)$_n$— is one of rare polymers where the energy of the top of the valence band can be measured by photoinjection of holes from electrode without much problem of contact. UV photoelectron spectroscopy (UPS) is an independent method to measure this quantity, and it is interesting to compare the results of these methods. Further, UPS gives the features of valence bands. We measured the UPS spectra of PPX prepared by thermal decompositon of paracyclophan. Figure 1 shows the photoelectron spectra. This gives the photoemission threshold energy of 6.9 eV, which agrees well with the result 6.84 eV obtained from photoinjection.[1] The features in the spectra correspond well with those of benzene, dibenzyl, and *p*-xylene in gas phase, showing that the photoemission can be described as the photoionization of the benzene ring in PPX.

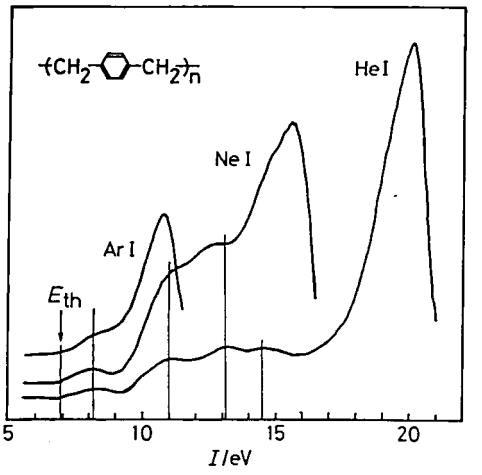

Figure 1. Photoelectron spectra of poly-*p*-xylyene with He I (21.2 eV), Ne I (16.8 eV), and Ar (11.7 eV) light sources.

References

1) Y. Takai, A. Kurachi, T. Mizutani, M. Ieda, K. Seki, and H. Inokuchi, submitted to *J. Phys. D.*

IV-A-4 Vacuum-UV Absorption Spectra of Evaporated Films of Volatile Aromatic Hydrocarbons

Shojun HINO *(Chiba Univ.)*, **Kazuhiko SEKI, Koichi OHNO,* Tamás VESZPRÉMI,* and Hiroo INOKUCHI** *(*: Univ. of Tokyo)*

Vacuum-uv absorption spectra of crystalline *p*-terphenyl and chrysene evaporated on LiF substrates were measured between 300 and 130 nm and compared with the spectra of gas phase and solution. In order to suppress the sublimation of the sample, which affects severely the absorption intensity of very thin films required for measurements, optically transparent Ar gas of about 10^5 Pa was filled in the sample chamber. The observed spectrum of *p*-terphenyl is shown in Figure 1 with

related results of other workers. The spectrum resemble the result obtained from electron energy-loss (EEL) spectra of a single crystal at room temperature,[1] but differs much from gas phase,[2] solution,[3] and low temperature solid[4] spectra. *p*-Terphenyl molecules are known to be coplanar in crystal above 178 K, while twisted in crystal below 178 K, gas phase, and solution. Such a structural change may be the origin of the difference among the spectra. The results of chrysene resemble to those of gas and solution, but the relative intensities of transitions are different, which was ascribed to the effect of orientation of molecules in crystalline state.

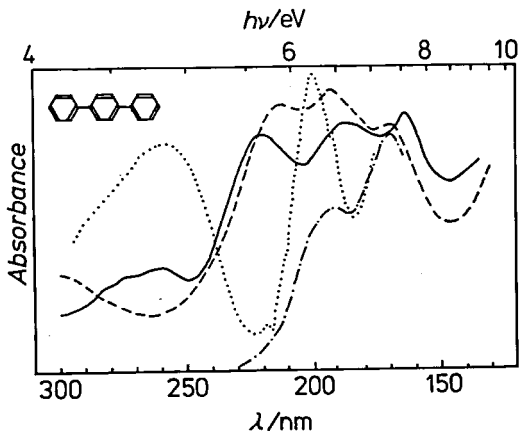

Figure 1. Absorption spectra of *p*-terphenyl. ——: evaporated polycrystalline film at room temperature (present work), –·–: polycrystalline film at 77 K (Ref. 4), ---: derived from electron energy-loss spectra of a single crystal (Ref. 1), and ····: gas phase (Ref. 2).

References

1) H. Venghaus and J.-J. Hinz, *J. Chem. Phys.*, **62**, 4937 (1980).
2) T. Kitagawa, *J. Molec. Spectrose.*, **26**, 1 (1968).
3) *UV-Atlas of Organic Compounds*, Butterworths, London (1966).
4) G. Milazzo and P. de Gasperis, *J. Chem. Phys.*, **65**, 1171 (1968)

IV-A-5 Temperature Dependence of the Photoelectron Spectra of an Evaporated Violanthrene A Film

Naoki SATO, Kazuhiko SEKI, Hiroo INOKUCHI, Yoshiya HARADA *(Univ. of Tokyo)* **and Takashi TAKAHASHI** *(Tohoku Univ.)*

A reversible temperature dependence of ultraviolet photoelectron spectra was observed for a polycrystalline violanthrene A thin film between 255 and 393 K as shown in Figure 1. A decrease in the linewidth of the lowest-energy peak with decreasing temperature was understood in terms of the interaction of the photoinduced molecular cations with low-energy vibrational modes in the solid film just as in the case of cumene studied by Salaneck *et al.*[1] On the other hand, the temperature dependence of the linewidth of the secondary-electron peak has an origin different from that of the valence peaks.

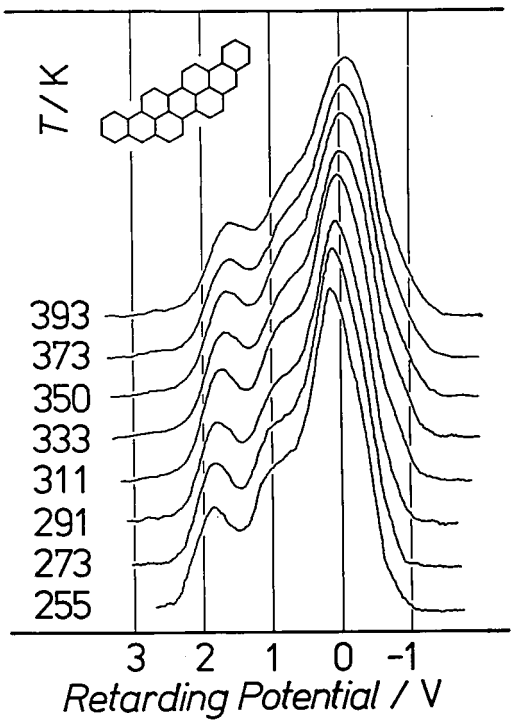

Figure 1. Temperature dependence of the photoelectron spectra of a violanthrene A film illuminated by $\lambda = 160$ nm light.

Reference

1) W. R. Salaneck, C. B. Duke, W. Eberhardt, E. W. Plummer and H. J. Freund, *Phys. Rev. Lett.*, **45**, 280 (1980).

IV-A-6 Electronic Structure of α-Chlorohemin Films

Naoki SATO and Hiroo INOKUCHI

Electronic structure of α-chlorohemin films was studied by means of ultraviolet photoelectron spectroscopy in order to obtain informations about electronic states of metalloporphyrin systems in various aggregated forms. An evaporated film and a film cast from a liquid solution of α-chlorohemin were prepared. Electronic absorption spectra and

X-ray powder patterns showed that α-chlorohemin suffered a chemical change during the thermal process of evaporation. Differential thermal analysis and elemental analysis supported this change. These results suggest that the valency of the central iron atom changed from trivalence to divalence through the thermal process.

Photoelectron spectra of the two films for the same-energy light were different. Figure 1 shows a comparison of the spectra of the two films illuminated by $\lambda = 135$ nm light. The abscissa is the retarding potential. Though the maximum kinetic energy of the emitted electrons are the same for both films, their energy distributions below the energy are remarkably different; the lowest three ionization energies are 6.3, 7.3 and 9.2 eV for a cast film and 5.3, 6.8 and 8.8 eV for an evaporated film. This difference suggests the change in the electronic structure concerning π-electron system of porphyrin rings through the evaporation. Further, the threshold ionization potentials were determined to be 5.3 and 4.6 eV for the cast and evaporated films, respectively. The latter value is extraordinarily low, which should be elucidated by more detailed investigation with comparison to the case of other biological systems.

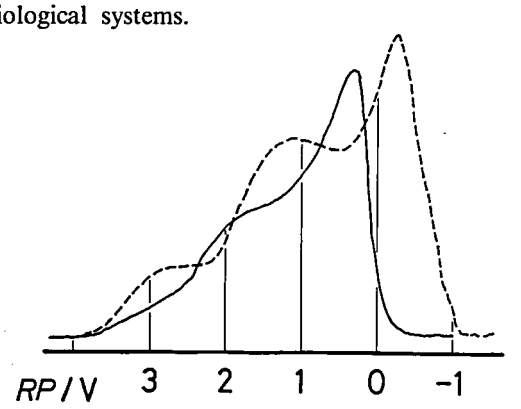

Figure 1. A comparison of the photoelectron spectra of α-chlorohemin films illuminated by $\lambda = 135$ nm ($h\nu \sim 9.18$ eV) light. The solid and dashed lines indicate the cast and evaporated films, respectively.

IV—B Photoconduction in Organic Solids

Using an ultra-high vacuum photoconduction apparatus (UHV-PCA), we have observed a photoconductive behaviour of organic semiconductors: The behaviour depends strongly on purity, crystallinity and surface states. In cooperation with joint research group (p175) and Chemical Materials Centre of IMS, very high purity polycyclic aromatic compounds, tetrabenzo[*a*, *cd*, *j*, *lm*]perylene, tetrabenzo[*de*, *hi*, *op*, *st*]pentacene and flavanthrene, are applying to observe their photoconductive character.

IV—C Structural Analysis and Electron Transfer in Cytochrome c_3

Through the structural analysis of cytochrome c_3, the arrangement of four hemes in cytochrome c_3 has been obtained. The peculiar electron transfer in cytochrome c_3 has been examined by electrochemical and thermal analysis.

IV-C-1 The Structure of Cytochrome c_3 at 2.5 Å Resolution

Y. HIGUCHI,* S. BANDO,* M. KUSUNOKI,* Y. MATSUURA,* N. YASUOKA,* M. KAKUDO,* T. YAMANAKA,* (* *Osaka Univ.*), T. YAGI *(Shizuoka Univ.)*, and H. INOKUCHI

[*J. Biochem.* **89**, 1659 (1981)]

The Structure of tetraheme cytochrome c_3 isolated from *Desulfovibrio vulgaris* Miyazaki has been determined at 2.5 Å resolution by an X-ray diffraction method. The mean figure of merit was 0.77. Four heme groups are exposed on the surface of the molecule. The overall dimensions of the molecule are approximately 33 × 39 × 34 Å. The arrangement of four hemes are as follows. Heme 1 is nearly perpendicular to Heme 4. Heme 2 and Heme 3 are also perpendicular to Heme 3 and Heme 4, respectively, while Heme 1 and Heme 3

are nearly parallel to each other. The heme-heme distances range from 11.3 Å to 18.1 Å. Each heme iron is coordinated by two imidazol groups of histidine residues.

IV-C-2 Electrocatalytic Four-Electron Reduction of Oxygen at the Cytochrome c_3-Adsorbed Electrode

K. NIKI,* Y. TAKIZAWA,* H. KUMAGAI,* R. FUJIWARA,* *(*Yokohama National Univ.)*, **T. YAGI** *(Shizuoka Univ.)*, **and H. INOKUCHI**

[*Biochem. Biophys. Acta*, **636**, 136 (1981)]

The electrocatalytic activity of cytochrome c_3 for the reduction of molecular oxygen was characterized from the studies of the adsorption of cytochrome c_3 and the coadsorption of cytochrome c on the mercury electrode by the a.c. polarographic technique. From these observation, cytochrome c_3 catalyzes the electrochemical reduction of molecular oxygen from the two-electron pathways vai hydrogen peroxide to the four-electron pathway at the mercury electrode in neutral phosphate buffer solution.

IV-C-3 Tetrahemoprotein, Cytochrome c_3 as Organic Conductive Material

Kenji ICHIMURA, Keisaku KIMURA, Yûsuke NAKAHARA *(Tech. College of Miyakonojo)*, **Tatsuhiko YAGI** *(Univ. of Shizuoka)* **and Hiroo INOKUCHI**

Cytochrome c_3 in *D. vulgaris*, having four hemes in one molecule, shows very low redox potential among biological materials. It is reduced with molecular hydrogen by a catalysis of hydrogenase even in the solid state. An electrical conductivity of cytochrome c_3 showed anusual temperature dependence and the conductivity of ferro form was better than that of ferri form.[1] Around the freezing point, the conductivity increases with the increment of hydrogen pressure. The electrical conductivity of cytochrome c_3 anhydrous film was measured in the region of temperature between 220 K and 330 K under the condition of high pressure of hydrogen. The minimum electrical resistivity reached to the order of 1×10^{-3} Ωcm at 293 K. The four hemes in a molecule are situated close to each other which make interact between neighboring hemes. It is reasonable to consider that intermolecular heme-heme interaction also exists in the solid state, causing the delocalization of the π electrons among the heme with the π electron systems, probably aromatic residues around hemes. These electron transfer may be a reason to the high electric conduction of cytochrome c_3.

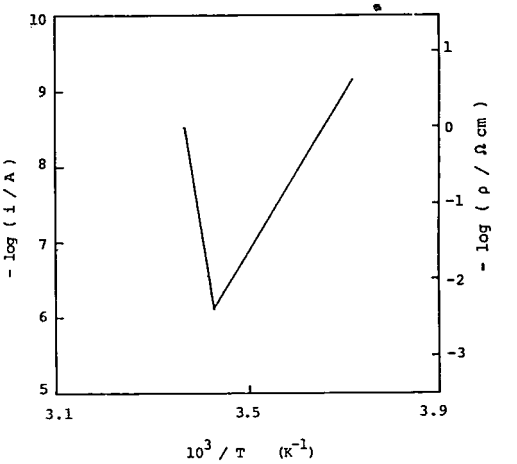

Figure 1. Current vs. Temperature of cytochrome c_3 anhydrous film under the conditions of P_{H_2} = 10 atm and E = 0.1 mV. The electric resistivity ρ is given as the following equation by the use of the value, thickness d = 82 nm, distance between electrode l = 1.0 mm, length of the film L = 5.0 mm, supplied voltage E = 0.1 mV.

Reference

1) Y. Nakahara, K. Kimura, H. Inokuchi and T. Yagi, *Chem. Phys. Lett.* **73**, 31 (1980).

IV-C-4 Kinetic Studies on Hydrogenase in Solution and on Anhydrous Film — Ortho-Para Hydrogen Conversion and Reduction of Cytochrome c_3

Kenji ICHIMURA, Keisaku KIMURA, Tatsuhiko YAGI *(Univ. of Shizuoka)* **and Hiroo INOKUCHI**

The kinetics of ortho-para hydrogen conversion and reduction of cytochrome c_3 catalyzed by *D. vulgaris* hydrogenase [H_2: ferricytochrome c_3 oxidoreductase] have been investigated in solution as well as on anhydrous deposited film.

From the proposed mechanism of reaction in solution, all the rate constants and equilibrium constants were evaluated. The rate constant of hydrogenase-hydrogen complex formation was in

good agreement with the previously reported value by T. Yagi *et al.* and with that of other enzyme complex formation in magnitude.[1] A simple collision theory also predicted well the values of ES complex formation rate constant by taking into account of the observed activation energy. The reaction energy scheme in solution and the model of the active site of hydrogenase were presented. Both ortho-para hydrogen conversion and reduction of cytochrome c_3 were found to be catalyzed even in the state of anhydrous film of enzyme. To the contrary in solution, a collision theory could not explain the observed rate constant, from which a conformational change in the protein was suggested.

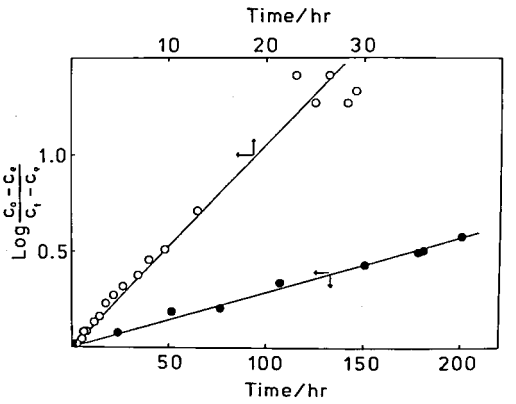

Figure 1. A first order plots of o-p hydrogen conversion and cytochrome c_3 reduction on anhydrous film.
●, o-p hydrogen conversion; ○, cytochrome c_3 reduction.

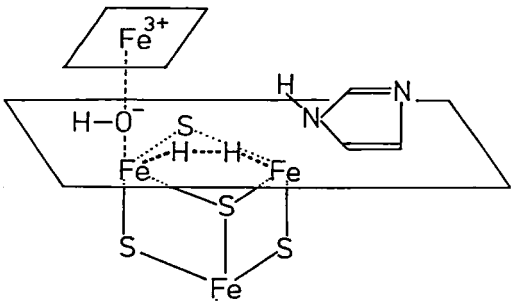

Figure 2. Active site model of hydrogenase.
Fe_4S_4 cube cluster stands for "Ferrodoxin Structure" of hydrogenase, Fe^{3+} in tetragon means heme of cytochrome c_3. Imidazole is a residue of Histidine of Hydrogenase.

Reference

1) T. Yagi, M. Tsuda and H. Inokuchi, *J. Biochem.*, **73**, 1069 (1973).

IV-C-5 Simultaneous Measurement of Specific Heat and Conductivity and Its Application to Cytochrome c_3

Kenji ICHIMURA, Toshiaki ENOKI, Keisaku KIMURA and Hiroo INOKUCHI

AC calorimetry is known as a new technique for the measurement of specific heat.[1] One of principal advantage of this method is that extremely small heat capacities are measured with accuracy. Therefore this method enables widely the calorimetry of biological materials. On the basis of AC calorimetric technique, a new vessel for simultaneous measurement of specific heat and conductivity was designed and constructed. The object of this study is to clarify the electric conduction mechanism of cytochrome c_3 by this method.

Cytochrome c_3 in solution containing a small proportion of hydrogenase was reduced under hydrogen atmosphere in glove box. A sample pellet was made of a cytochrome c_3 powder which was given by evaporating the solution under the same condition. Cytochrome c_3 was reduced with molecular hydrogen by a catalysis of hydrogenase in solid state as well as in solution, and hence hydrogen gas playing a role of a thermal conductive gas was used actively to a reaction gas. The time-course of change in specific heat suggests that the reduction of cytochrome c_3 proceeds in solid state. Figure 1 shows an anomalous behavior of specific heat in the region of temperature between 250 K and 310 K and the corresponding anomaly was found in the electric conductivity.

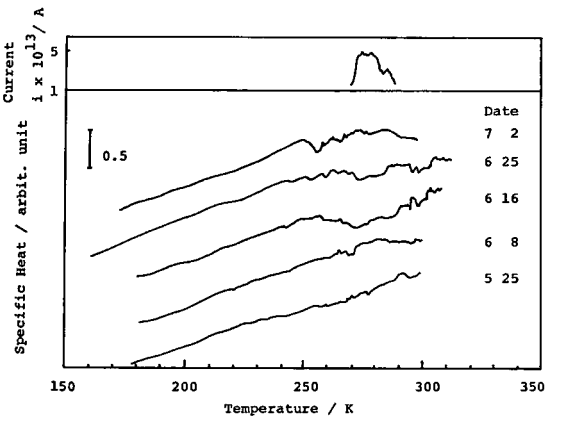

Figure 1. Time-course of change in specific heat and electric conductivity of cytochrome c_3 pellet.

Reference

1) P. E. Sullivan and G. Seidel *Phys. Review* **173**, 679 (1968).

IV—D Physics and Chemistry of Graphite Intercalates

Electronic characters and catalytic activities of graphite-alkalimetal and also graphite-hydrogen-alkalimetal system are being studied by the measurements of the electrical conductivity, the superconductivity and ESR. As graphite host material, new-type graphite filament prepared from graphite in argon flame is being used extensively.

IV—E Organic Metals

More than one hundred highly conducting charge-transfer (CT) complexes have been prepared since the discovery of the notable organic metal; tetrathiafulvalene·tetracyano-p-quinodimethane (TTF·TCNQ). Even some superconducting cation radical salts of tetramethyltetraselenafulvalene (TMTSF) have been discovered very recently. Numerous criteria for achievement of the metallic state in these systems have been forwarded to understand of the materials already in hand and to generate new such materials. Some of the criteria are concerning to the minimal on site Coulomb repulsive energies in the ionized component molecules. This criterion has been investigated as a continuous study of the requirements for an organic metal.

The discovery of superconductivity in $(TMTSF)_2X$; X = PF_6, AsF_6, TaF_6, and ClO_4 has renewed interest in the properties and syntheses of organic metals.[1] At ambient pressure $(TMTSF)_2X$; X = PF_6 and AsF_6 have metal to semiconductor (MS) transitions at 19 and 15K, however under moderate pressure these slats remain metallic with the onset of superconductivity at 0.9 and 1.2 K at 12 Kbar, respectively. The perchlorate salt in contrast does not show the MS transition down to 1.3-1.5 K and becomes superconducting at ambient pressure. Synthesis of other organic metals in which the MS transitions are suppressed is now desirable to design new organic superconductors and to understand the requirements for them.

Reference

1) K. Bechgaard, C. S. Jacobsen, K. Mortensen, H. K. Pedersen, and N. Thorup, *Solid State Commun.*, **33**, 1119 (1980); D. Jerom, A. Mazaud, M. Ribault, and K. Bechgaard, *J. Physique Lett.*, **41**, L95 (1980), K. Bechgaard, K. Carneiro, F. B. Rasmussen, and M. Olsen, *J. Am. Chem. Soc.*, **103**, 2440 (1981).

VI-E-1 Requirements for an Organic Metal: An Electrochemical Study into the Redox Behavior of π-Acceptors

Gunzi SAITO and Hiroo INOKUCHI

P-Quinones and TCNQs were the most frequently employed π-acceptors in the study of CT complexes and organic metals. These molecules were known to capture one and two electrons quite easily as indicated by their large half-wave reduction potentials (E^1 and E^2); $A^0 \xrightarrow[E^1]{e} A^{\cdot-} \xrightarrow[E^2]{e} A^{2-}$. Our previous observation of linear relationship between E^1 and E^2 values for F_nTCNQ (n = 0, 1, 2, 4) prompted us to exploit the relation more extensively and to inquire the dispropotionation energies (U) for the reaction $2A^{\cdot-} \longrightarrow A^0 + A^{2-}$.[1] This dispropotionation energies can be approximated by the on-site Coulomb energies in A^{2-} molecule. In Figure 1, E^2 values are plotted against E^1 values (vs. SCE, MeCN) for 25 p-quinones and 27 TCNQs using our data and also reported ones. The linear relationships are expressed as $-E^2 = -aE^1 + b$ in eV where a = 0.81 ± 0.05 and 0.83 ± 0.05 and b = 0.70 ± 0.03 and 0.40 ± 0.01 for p-quinones and TCNQs, respectively. In a solution, U values can be expressed as $U = E^1 - E^2 + \Delta G - \Delta F$, where ΔG and ΔF are the differences in free energies of solvation of $A^{\cdot-}$ and A^0, and those of solvation of A^{2-} and $A^{\cdot-}$, respectively. Using the Hedges and Matson's approximation[2] and employing ΔG of −2.29 eV result in the following relationships, p-quinones: $U = (0.19 \pm 0.05)E^1 + (5.28 \pm 0.40)$ eV and TCNQs: $U = (0.17 \pm 0.05)E^1 = (4.98 \pm 0.40)$ eV.

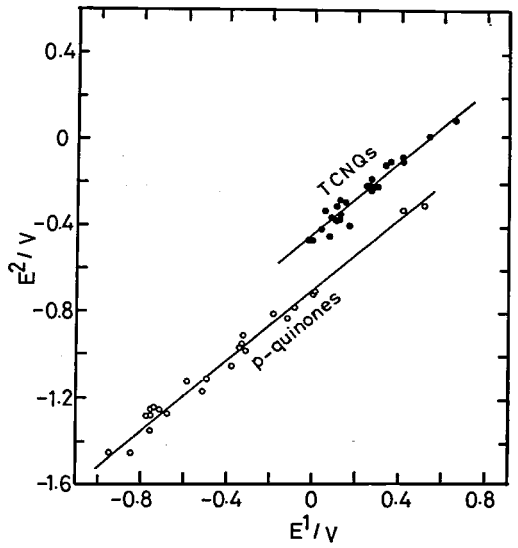

Figure 1. E^2 vs. E^1.

References

1) G. Saito and J. P. Ferraris, *J. C. S. Chem. Comm.*, 1027 (1979).
2) R. M. Hedge and F. A. Matson, *J. Chem. Phys.*, **28**, 950 (1958).

IV-E-2 Suppression of Metal to Semiconductor Transition by Chemical Modification

Gunzi SAITO, Toshiaki ENOKI, Koshiro TORIUMI, and Hiroo INOKUCHI

We have chosen the alkylthio substituted TTF(I) as a π-donor in the hope that chemical modification such as the extension of the TTF moiety and an increased polarizability will increase the conduction band width and decrease the on-site Coulomb repulsion in the cation radical salts resulting in a considerable enhancement of metallic character.

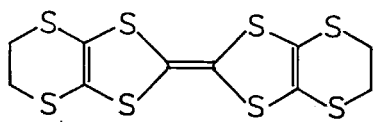

(I)

Two different forms (leaf and rod-like) of perchlorate salt of (I) were prepared by the electrocrystallization technique. Preliminary X-ray studies show that the two forms are identical despite the different appearance. They belong to the triclinic system with the unit cell parameters; a = 13.012, b = 18.640, c = 7.752Å, α = 79.31, β = 104.73, and γ = 110.85°. Though the two forms are crystallographically identical, they are different in their physical properties (conductivity, ESR) distinctly, may be due to the different phases induced by thermal motion of the six membered rings in (I) in the two forms. A thermal analysis is now performed to confirm this. In Figures 1 and 2 are depicted resistivity data for typical crystals of each forms along the elongated directions which are nearly perpendicular to the stacking axis. In the leaf-like crystals a distinct MS transition is not observed, probably due to the increased dimensionality. On the other hand, the temperature dependence of the resistivity of the rod is complicated and characterized by two MS transitions.

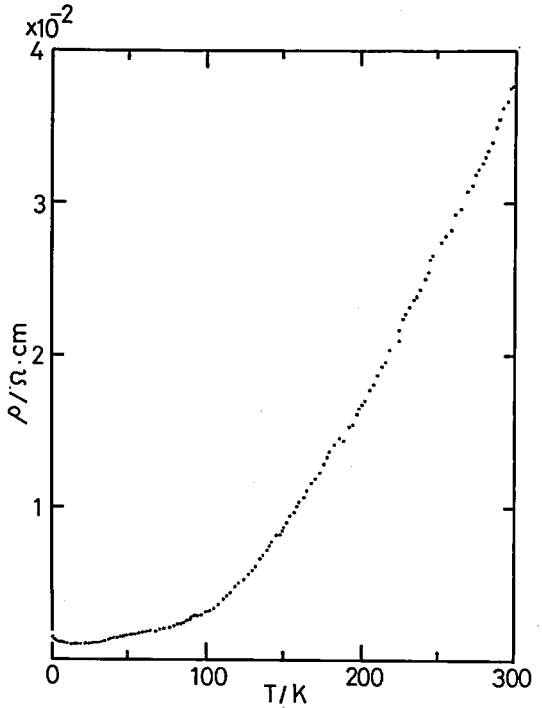

Figure 1. Temperature dependence of $\rho_{//a}$*, leaf-like form.

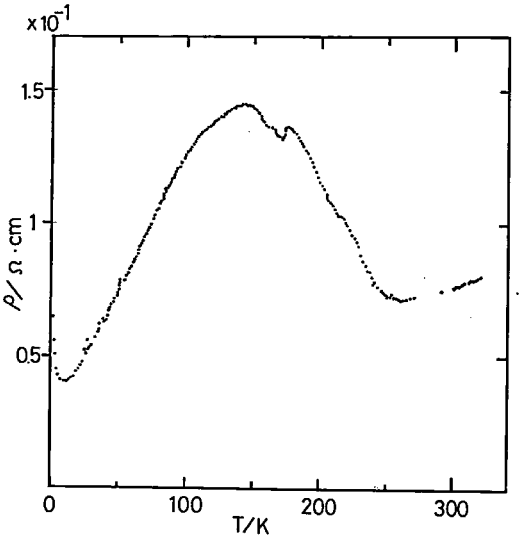

Figure 2. Temperature dependence of $\rho_{//a}$*, rod-like form.

IV—F Studies of Ion-Molecule Reactions by a Threshold Electron-Secondary Ion Coincidence (TESICO) Technique

The knowledge of the microscopic reaction cross sections for evolution of a system in a single reactant quantum state (translational, rotational, vibrational, and electronic) to a single product quantum state is essential for a complete understanding of a chemical reaction. In neutral-neutral reactions, approach to this "state-to-state" cross sections has been made possible by the advent of new techniques, such as molecular beams and lasers, which prepare and probe these states. In ion-molecule reactions, on the other hand, a different approach toward this microscopic cross sections is possible since ions can readily be prepared in various internal states in the initial ionization processes, such as photoionization, and the emitted photoelectrons provide information on the distribution among these states.

In this project, we study state-selected ion-molecule reactions by the use of a photoionization technique which utilizes the threshold photoelectron-secondary ion coincidence. The technique allows direct determination of $\sigma(i,v)$, i.e. the reaction cross section as a function of the internal and collisional energies of reactants. The selection of electronic, vibrational, rotational, and fine-structure states are possible by this technique.

IV-F-1 Vibrational-State Selected Reaction Cross Sections for $H_2^+(v) + Ar \rightarrow ArH^+ + H$, $Ar^+ + H_2$

Kenichiro TANAKA, Tatsuhisa KATO, and Inosuke KOYANO

[*J. Chem. Phys.* **75**, 4941 (1981)]

The **TESICO**[1] studies of the vibrational-state dependence of the reaction cross sections for each channel of the title reaction have been reported previously.[2] A considerable enhancement of the charge-transfer cross section at v = 2 of the H_2^+ ion was observed at a collision energy of 0.77 eV.[2] In the present study, a complete investigation of these reactions has been performed over a wide collision energy range and several interesting results have been obtained.

Experimental results at a collision energy of 0.48 eV are summarized in Figure 1 which shows the reaction cross sections for the proton-transfer (σ_1) and charge-transfer (σ_2) channels, as well as their sums ($\sigma_1 + \sigma_2$), as functions of the vibrational quantum number v. As exemplified by the figure, a salient feature observed at these low collision energies is that the hump in the charge-transfer cross section at v = 2 is accompanied by a corresponding dip in the proton-transfer cross section. This is to be contrasted with the results at higher collision energies (e.g., 0.8 and 1.5 eV), in which the proton-transfer cross sections remain

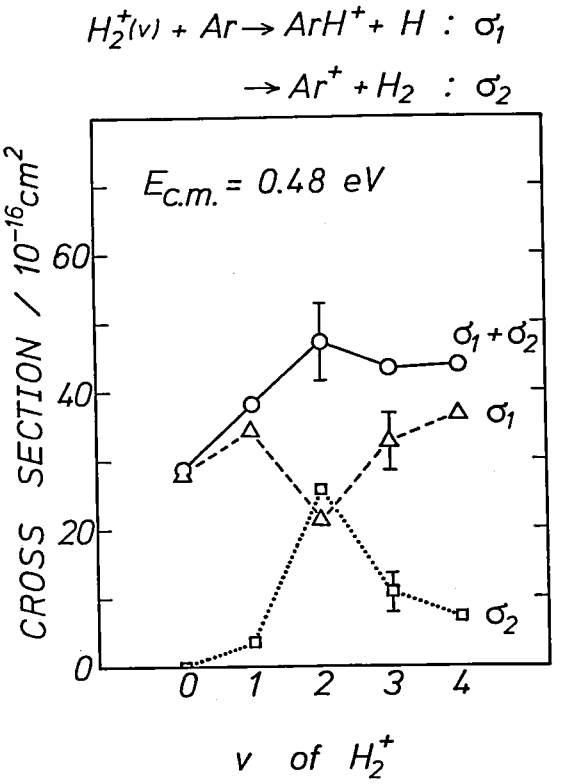

Figure 1. State seledcted cross sections for the two reactions as a function of vibrational quantum number v of H_2^+ obtained at 0.48 eV of collision energy.

almost independent of or a weakly increasing function of the vibraional quantum number. It has also been found that, at still higher collision energies (around 20 eV), the magnitude of the cross section for the charge-transfer process with v = 1 (which is endoergic by 0.06 eV) becomes comparable with that with v = 2, whereas the cross section for the same process with v = 0 (which is endoergic by 0.33 eV) still remains negligibly small.

References

1) I. Koyano and K. Tanaka, *J. Chem. Phys.* **72**, 4858 (1980).
2) K. Tanaka, T. Kato, and I. Koyano, *IMS Ann. Rev.* 93 (1980).

IV-F-2 State Selected Charge-Transfer Reactions of $Ar^+(^2P_{3/2}, {}^2P_{1/2})$ with N_2 and CO

Tatsuhisa KATO, Kenichiro TANAKA, and Inosuke KOYANO

While low energy charge-transfer reactions have most often been discussed in terms of the energy resonance and Franck-Condon factors, recent elaborate experiments have revieled that the mechanism in most cases is much more complicated than the simple model predicts. In order to investigate the roles of these factors in charge-transfer process, as well as the effect of spin-orbit couplings on it, we have studied the low energy charge-transfer reactions

$$Ar^+(^2P_J) + N_2 \rightarrow Ar + N_2^+ \quad (1)$$

$$Ar^+(^2P_J) + CO \rightarrow Ar + CO^+ \quad (2)$$

with separation of the two spin-orbit states (J = 3/2 and 1/2) of the reactant ion utilizing the **TESICO** technique.

The relative cross sections $\sigma(J)$ for both reactions were determined from the ratio of the coincidence counts of the primary and secondary ions at collision energies of 0.21 and 1.44 eV. The relative cross sections $\sigma(J)$ and the ratio of the cross sections $\sigma(1/2)/\sigma(3/2)$ obtained are listed in Table I.

As can be seen, the relative importance of the two spin-orbit states in charge transfer processes is inverted between the reactions with N_2 and CO at these collision energies. The ratio $\sigma(1/2)/\sigma(3/2)$, however, is dependent on the collision energy and tends to approach unity, in both cases, as collision energy decreases. This difference is of particular interest in view of the similarity of N_2 and CO in their mass and electronic structure.

Table I. Relative cross sections $\sigma(J)$ and the ratio of the cross sections $\sigma(1/2)/\sigma(3/2)$ obtained at collision energies of 0.21 and 1.44 eV.

E_{cm} = 0.21 eV

System	$\sigma(1/2)$	$\sigma(3/2)$	$\sigma(1/2)/\sigma(3/2)$
$Ar^+ + N_2$	3.9	5.2	0.8 ± 0.1
$Ar^+ + CO$	1.7	1.4	1.2 ± 0.2

E_{cm} = 1.44 eV

System	$\sigma(1/2)$	$\sigma(3/2)$	$\sigma(1/2)/\sigma(3/2)$
$Ar^+ + N_2$	4.7	8.0	0.6 ± 0.1
$Ar^+ + CO$	0.83	0.51	1.6 ± 0.4

Electronic and vibrational energy levels of Ar^+, CO^+, and N_2^+, shown in Figure 1, indicate that there is no apparent energy resonance in these reaction systems. The Franck-Condon factors between the ground states of CO and N_2 and possible product

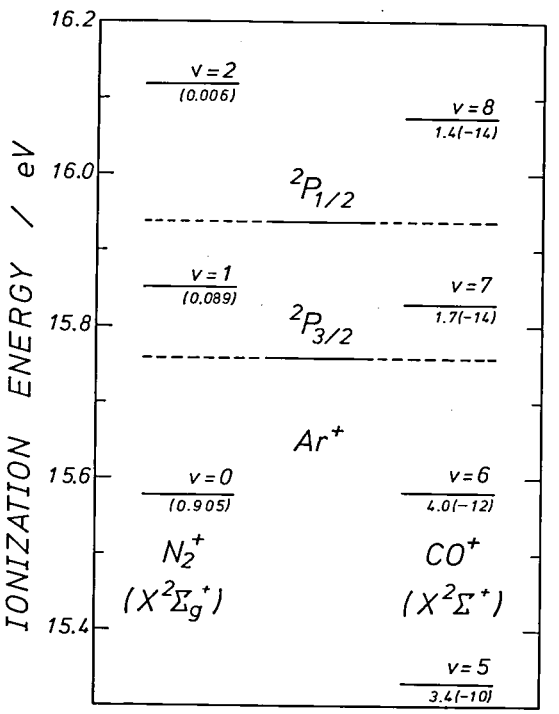

Figure 1. Electronic and vibrational energy levels of Ar^+, CO^+, and N_2^+.

states of CO^+ and N_2^+ (also shown in Figure 1 under the lines indicating vibrtational levels) indicate that charge transfer with CO is particularly unfavorable. In spite of all these facts, absolute values of the cross sections for both reactions with N_2 and CO were found to be fairly large (more than 10^{-1} and 10^{-2} of the respective Langevin value), indicating the failure of the near-resonance theory.

IV-F-3 Selection of Vibrational States of N_2^+ in the Charge-Transfer Reaction with Ar

Tatsuhisa KATO, Kenichiro TANAKA, and Inosuke KOYANO

In order to further investigate the mechanism of the low energy charge-transfer reaction $Ar^+ + N_2 \rightarrow Ar + N_2^+$ (see the preceding paper, IV-F-2), we have also studied the following reverse charge-transfer reaction,

$$N_2^+(v) + Ar \rightarrow Ar^+(^2P_J) + N_2 \qquad (1)$$

The reaction channel forming Ar^+ in $J = 3/2$ is endoergic by 0.182 eV for N_2^+ in $v = 0$ but is exoergic for $v \geqslant 1$. On the other hand, the reaction channel forming Ar^+ in $J = 1/2$ is still endoergic by 0.085 eV for $v = 1$ and is exoergic for $v \geqslant 2$.

While in usual He(I) photoionization there is no or very small probability to form N_2^+ ions in $v \geqslant 2$ due to unfavorable Franck-Condon factors, the **TESICO** technique, which utilizes threshold electron method, can prepare N_2^+ in a considerably wider range of vibrational states (up to $v = 4$) via resonance autoionization. This enabled us to determine the vibrational-state selected cross sections of Reaction (1) for $v = 0 - 3$ of N_2^+.

Experimental resuslts obtained at a collision energy of 0.3 eV are summarized in Figure 1. As

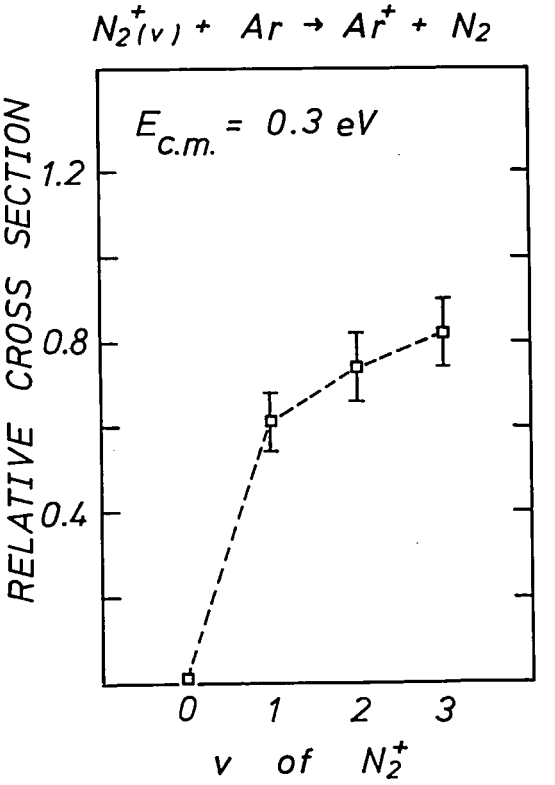

Figure 1. State selected cross sections for Reaction (1) as a function of vibrational quantum number v of N_2^+, obtained at 0.3 eV of collision energy.

can be seen from the figure, the cross section of Reaction (1) is dramatically enhanced at $v = 1$ and after that weakly increases with increasing vibrational quantum number. Similar v-dependence of cross sections is observed at other collision energies (0.76 and 1.53 eV). Very small cross sections obtained at $v = 0$ are probably due to the endoergic nature of this reaction. However, it should be noted that the endoergicity of this reaction is only 0.182 eV, and the collision energies used here are all sufficient to overcome this endoergicity. This indicates that transitional energy is much less effective than vibrational energy in promoting this endoergic reaction.

IV-G Photoionization Processes in Small Molecules

Two techniques have generally been used for the study of molecular photoionization processes, i.e., measurements of photoionization effeciency curves **(PIEC)** and photoelectron spectra **(PES)**. While PIEC yields a wealth of information on the ionizaiton processes and energy levels of ions and neutral molecules, difficulty is often encountered with this technique when autoionization obscures the step structure of the curve. In such a situation, we often resort to **PES** which provides precise locations of ionic states and

transition probabilities to these states. However, ionic states that can be studied by the ordinary (constant wavelength) **PES** are largely limited to the states which combine with the ground state of the parent molecule with favorable Franck-Condon factors.

Another type of photoelectron spectroscopy is the threshold electron spectroscopy **(TES)** which uses a variable wavelength light source and detects only the zero kinetic energy photoelectrons (threshold electrons). In this method, ionic states which are not favored by direct ionization are often observed through resonance autoionization.

In this project, we study photoionization processes in small molecules by simultaneous measurements of photoionization efficiency curves and threshold electron spectra. Furthermore, we find that the analysis of autoionizing transitions is possible utilizing charge-transfer processes of product ions. This technique is also incorporated.

IV-G-1 Photoionization Efficiency Curves of N_2 and the Analysis of their Autoionization Structure Utilizing Charge-Transfer Process with Ar

Kenichiro TANAKA, Tatsuhisa KATO, and Inosuke KOYANO

As one of the extensive studies on photoionization processes in small molecules, we have investigated the threshold electron spectrum **(TES)** and photoionization efficiency curve **(PIEC)** of nitrogen with the intention to analyze the autoionization structure. As shown in the preceding paper (IV-F-3), the charge transfer process of $v = 0$ state of N_2^+ with Ar has a negligible cross section, whereas those from higher vibrational states has fairly high values which are vibrational state dependent. We could utilize this fact to analyze the autoionization peaks by simultaneously measuring the charge-transfer process of the produced N_2^+ ions with Ar.

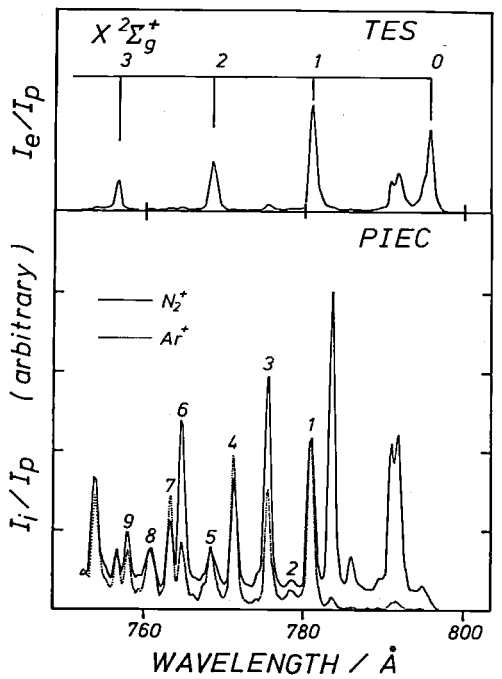

Figure 1. Threshold electron spectrum of N_2 (top) and photoionization efficiency curves (PIEC) for N_2^+ and Ar^+, taken with double chambers. The peaks in the PIEC numbered 1-9 are analyzed as shown in Table I.

Table I. Relative probabilities of forming N_2^+ in various vibrational levels at several autoionization peaks

# of peaks	Wavelength (Å)	v = 0	v = 1	v = 2
1	781.1	0.35 (0.29)[a]	0.65 (0.71)	
2	778.6	0.59	0.41	
3	775.8	0.67 (0.73)	0.33 (0.27)	
4	771.7	0.24 (0.36)	0.76 (0.64)	
5	768.4	0.33	0.24	0.43
6	764.9	0.79 (0.83)	0.12 (0.06)	0.09 (0.11)
7	763.6	0.16 (0.34)	0.62 (0.41)	0.22 (0.25)
8	760.8	0.33	0.14	0.53
9	758.3	0.51 (0.63)	0.18 (0.10)	0.31 (0.27)

[a] values in parentheses are results of Ref. (1)

Figure 1 shows the **TES** (top) and the **PIEC** (bottom) of nitrogen obtained in the threshold region. The solid curve in the **PIEC** represents **PIEC** for N_2^+ and the dotted curve that for Ar^+ produced by charge-transfer. It can be seen that the ratio of the Ar^+ intensity to that of N_2^+ varies considerably from one autoionization peak to another. Compare, for example, peaks labeled 3 and 4 in the **PIEC**. The ratio is much higher in peak 4, indicating that the percentage of autoionization going to the v = 1 state of N_2^+ is much larger in 4 than in 3.

Quantitative analysis has been performed for **PIEC** peaks numbered 1 to 9, and the results are summarized in Table I. It can be seen that the results are in good agreement with the Berkowitz Chupka's results (shown in the parenthesis) obtained by photoelectron analysis at these peaks.

References

1) J. Berkowitz and W. A. Chupka, *J. Chem. Phys.*, **51**, 2341 (1969).

IV—H Spectroscopy and Chemical Dynamics Using Supersonic Nozzle Beams

The usefulness of supersonic nozzle beams has increasingly been recognized in both spectroscopy and chemical dynamics. The capability of cooling internal degrees of freedom of molecules and the possibility of producing various kinds of molecular clusters are important properties of the technique. In this project, we aim at high resolution absorption and Raman spectroscopy, dynamical studies of cluster reactions, and their combinations, utilizing the above properties of supersonic nozzle beams.

IV-H-1 Production and Characterization of Ar_2 and $(H_2)_2$ in Supersonic Nozzle Beams

Kenichiro TANAKA, Tatsuhisa KATO, Koji TESHIMA *(Kyoto Univ.)* **and Inosuke KOYANO**

A cluster beam source has been constructed for the purpose of studying ion-neutral cluster reactions[1] and the characterization of such beams has been made. The formation of neutral clusters generally takes place during supersonic expansion of a gas flow into vacuum from a high pressure source. The sizes and intensities of clusters are strongly dependent on the source conditions such as pressure, temperature, size and shape of the orifice (nozzle).

In the present study a temperature-variable beam source with a nozzle of 30 μm in diameter was used to produce dimers of Ar and H_2. Detection and characterization of dimers were performed by time-of-flight (T.O.F.) mass spectrometry. The typical T.O.F. spectra of Ar and Ar_2 are shown in Figure 1. These spectra were obtained in a beam of Ar obtained by expanding 5 atm source gas through a room temperature nozzle. From the position and FWHM of the T.O.F. peak of Ar, we obtained the speed ratio of 20.7 which agrees with other literature values.[2]

In the case of H_2, no $(H_2)_2$ dimers were detected in the H_2 beam when a room temperature nozzle

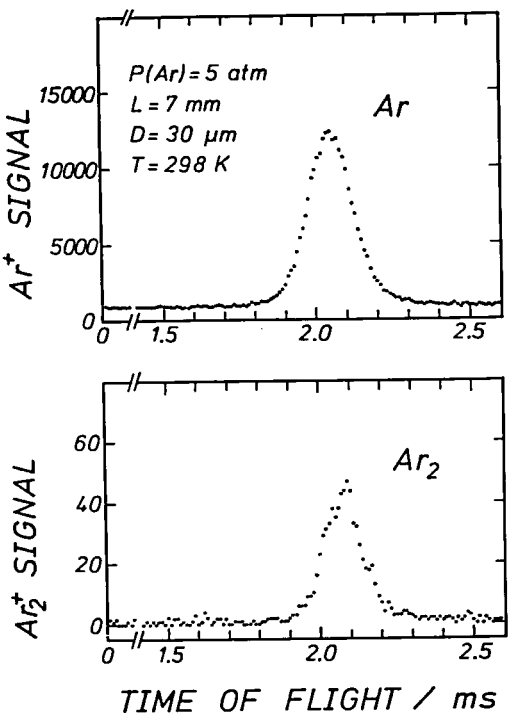

Figure 1. Time-of-flight spectra of Ar and Ar_2 in the supersonic nozzle beam of Ar.

was used. At 77°K, however, $(H_2)_2$ dimers were easily formed and their relative population in the beam increased from 0.5 to 2% with increasing source pressure of H_2 between 2 and 6 atm. These results indicate that sufficient dimer intensities are obtained with this source to study bimolecular reactions of neutral dimers with ions (ion-neutral cluster reactions).

References

1) Y. Mori, K. Tanaka, T. Kato and I. Koyano, *IMS Ann. Rev.*, 96 (1980).
2) J. B. Anderson and J. B. Fenn, *Phys. Fluids*, **8**, 780 (1965).

IV—I Several Topics in HeI Photoelectron Spectroscopy

Molecular photoelectron (PE) spectroscopy with the HeI resonance line is now a well-established technique to determine ionization potentials of well-established technique of valence electrons. For the last decade it has been employed for studying a variety of problems associated with electronic structures of organic and inorganic molecules in the gaseous phase. There still remain many interesting subjects to be studied by HeI PE spectroscopy. Firstly, we are now in the position to assign HeI spectra systematically on the basis of *ab initio* SCF MO calculations for many fundamental organic molecules. It seems quite appropriate to compile a handbook which covers HeI spectra of fundamental organic compounds together with their *ab initio* MO assignments. Secondly, quantitative measurements of PE intensities are important from the analytical and theoretical point of view, in order to establish a method to determine reliable PE intensities. Intensity-defined PE spectra may be quite useful for analytical purposes. On the other hand, PE band intensities are closely related to partial photoionization cross sections associated with specific ionic states.

IV-I-1 Compilation of HeI Photoelectron Spectra of 200 Fundamental Organic Molecules—Ionization Energies, Ab Initio Assignments, and Valence Electron Structure

Katsumi KIMURA, Shunji KATSUMATA,* Yohji ACHIBA, Tomoko YAMAZAKI* *(*: Hokkaido Univ.)*, **and Suehiro IWATA** *(Keio Univ.)*

Very recently we have published a handbook entitled "*Handbook of HeI Photoelectron Spectra of Fundamental Organic Moelcules*" from *Japan Scientific Societies Press and Halsted Press (John Wiley & Sons)*. This consists of two parts: In part I we describe some important principles of photoelectron spectroscopy as well as the experimental and theoretical methods to derive the photoelectron spectra and ionization energy data compiled. In part II we have compiled the HeI photoelectron spectra, ionization energies, theoretical assignments for many fundamental molecules. Here, we demonstrate an example which shows various information in a compact form. The book has the following characteristics. 1) For each of the 200 molecules, a complete set of ionization energy data below ca. 20 eV is tabulated. So far no such complete data have been published. 2) For about 150 out of the 200 compounds, all the ionization energies are interpreted systematically in terms of *ab initio* SCF MO calculations and Koopmans' theorem. In addition, for about 50 basic compounds, we have studied ionic states of about 50 basic molecules in terms of configuration interaction calculations of ionic states. 3) Valence molecular orbitals for about 150 molecules are schematically illustrated. 4) The intensity-normalized photoelectron spectra are also included for 25 molecules in Appendix. In the footnotes of the tables, we have mentioned references to papers published by other workers, references to papers of up-to-date molecular structures, SCF total energies, etc.

(159) HCOOH Formic Acid

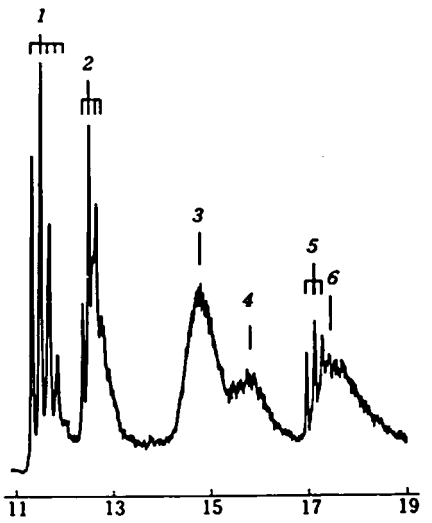

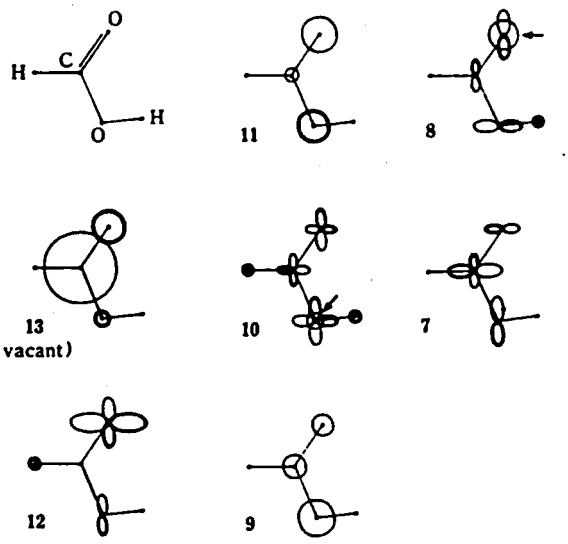

	Exptl.[a]	SCF MO [6-31 G][b]			CI (Ionic State) [6-31 G][c]		
	I_v(eV)	$-\varepsilon$(eV)	MO	Character	E(eV)	State	Configuration
1	11.51	12.96	$10a'(12)$	$n_{O(C-O)}$	10.99	$1^1A'$	$0.94(12^{-1})$
2	12.50	13.43	$2a''(11)$	$\pi_{C-O}, n_{O(OH)}$	11.98	$1^1A''$	$0.93(11^{-1})-0.16(9^{-1})$ $+0.10(9^{-1},11^{-1},13^1)_\beta$
3	14.78	16.23	$9a'$ (10)	$\sigma_{C-O}, \bar{n}_{O(OH)}$	14.17	$2^1A'$	$0.93(10^{-1})$
4	15.76	17.44	$1a''$ (9)	$\pi_{C-O}, n_{O(OH)}$	15.50	$2^1A''$	$0.90(9^{-1})$ $-0.23(12^{-1},13^1)$ $+0.16(11^{-1})$
5	17.29	19.26	$8a'$ (8)	σ_{OH}	16.82	$3^1A'$	$0.88(8^{-1})$ $-0.27(7^{-1})$ $-0.12\{(10^{-1},11^{-1},13^1)_\alpha$ $+(10^{-1},11^{-1},13^1)_\beta\}$
6	17.49	19.93	$7a'$ (7)	σ_{C-O}	17.88	$4^1A'$	$0.87(7^{-1})+0.28(8^{-1})$ $-0.16(10^{-1},11^{-1},13^1)_\beta$ $+0.14(10^{-1},11^{-1},13^1)_\alpha$

a) Kimura *et al.* (132). See also other works: Brundle *et al.* (52); Turner (213); Turner *et al.* (215); Potts *et al.* (183); Watanabe *et al.* (220, 221); and Carnovale *et al.* (57b).
b) We used the molecular structure determined from MW data (A 99); symmetry C_s. $E_{SCF}=-188.6621$ hartree. In 4-31 G calculations, $E_{SCF}=188.4721$ hartree and $-\varepsilon$(eV)=12.93, 13.39, 16.18, 17.40, 19.21, and 19.88.
c) CI-II'. (13)=$3a'$. $|N\rangle=0.97$ (SCF).
CI-I: E(eV)=11.38, 11.90, 14.42, 15.50, 17.17, and 17.98.

IV-I-2 Vacuum UV Photoelectron Intensity of Gaseous Compounds. II. Experimental Processes of Determination of Differential and Partial Photoionization Cross Sections

Yohji ACHIBA, Tomoko YAMAZAKI *(Hokkaido Univ.)*, **and Katsumi KIMURA**

[*Bull. Chem. Soc. Jpn.*, **54**, 408 (1981)]

Experimental processes recently developed to determine differential and partial photoionization cross sections of molecules are described in detail, based on photoelectron intensity measurements using a gaseous binary mixture of a sample with a standard gas. The quantities obtained here in these processes are 1) relative photoelectron peak heights, 2) normalized photoelectron spectra, 3) relative photoelectron band areas, and 4) differential and partial photoionization cross sections. Corrections are made for electron collection efficiency. In

connection with the photoelectron intensity determination, we propose here a method of obtaining the mole ratio of the componenets of binary mixture entered into the ionization chamber of a photoelectron spectrometer. Satisfactory results on partial photoionization cross sections have been obtained for several test samples.

IV-I-3 Re-Measurements of Partial Photoionization Cross Sections of CH_4, NH_3 and H_2O at 58.4 nm by He(I) Photoelectron Spectroscopy

Yohji ACHIBA, Tomoko YAMAZAKI *(Hokkaido Univ.)*, **and Katsumi KIMURA**

[*J. Electron Spectrosc. Relat. Phenom.*, **22**, 187 (1981)]

Kimura *et al.*[1] have previously described a gas-phase photoelectron method that uses a binary mixture of a standard and a sample in order to obtain partial photoionization cross-sections of molecules. We have recently improved this method with the aid of a minicomputer-based data-processing system. In this communication, we report some results of our re-measurements of differential and partial photoionization cross-sections of CH_4, NH_3 and H_2O.

Reference

1) K. Kimura, Y. Achiba, M. Morishita, and T. Yamazaki, *J. Electron Spectrosc. Relat. Phenom.*, **15**, 269 (1979).

IV—J Studies of Molecular Complexes and Clusters by HeI Photoelectron Spectroscopy

Various inter-molecular species such as van der Waals molecules, hydrogen bonded species and electron-donor-acceptor (EDA) complexes in the gaseous phase are interesting species to be studied by HeI photoelectron spectroscopy, because changes in ionization energies by the formation of such species can be directly studied. It is, however, difficult to detect such inter-molecular species in ordinary photoelectron measurements, since the concentration is usually too low. In order to obtain a measurable density of such a species, it is necessary to introduce a supersonic molecular beam in a photoelectron spectrometer with a high-speed pumping system. The gaseous EDA complex of $(CH_3)_2O$ with BF_3 has recently been studied by a HeI photoelectron spectrometer which we previously constructed using a gas inlet system of effusive nozzle type. On the other hand, in order to measure a more weakly bound inter-molecular species, we have newly designed and constructed a HeI photoelectron spectrometer with a high-speed pumping system and a supersonic molecular beam source. The HeI photoelectron spectrum of water dimer has been measured by this spectrometer.

IV-J-1 Photoelectron Spectrum of Water Dimer

Shinji TOMODA, Kenji SATO, Yohji ACHIBA, and Katsumi KIMURA

Photoelectron spectrum of the first band of water dimer is observed by means of a nozzle beam photoelectron spectrometer with a HeI light source.[1] In figure 1. the spectrum of a mixture of H_2O and $(H_2O)_2$ obtained from the nozzle source at 82°C ($P_o \approx 390$ torr) is compared with that of H_2O from an effusive source. The maximum of the broad band (I_v) yields the vertical ionization energy of water dimer, 12.1 ± 0.1 eV, which is slightly (0.5 eV) smaller than that of monomer. It is concluded that this ionization energy should be ascribed to the ionization from the out-of-plane nonbonding orbital of the proton donor according to *ab initio* SCF MO calculations.[2] The adiabatic ionization energy and the dissociation energy of $(H_2O)_2^+$ are also estimated and listed in Table I. They are in good agreement with the values reported by Ng *et al.*[3]

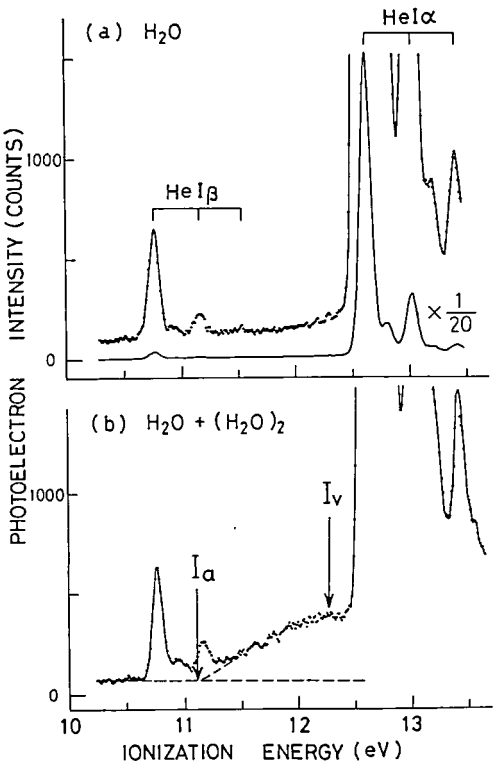

Table I. Ionization energies of $(H_2O)_2$ and dissociation energy of $(H_2O)_2^+$. Values are in eV units.

	This work	Ng *et al.* (Ref. 3)
I (vertical)	12.1 ± 0.1	
I (adiabatic)	11.1	11.21 ± 0.09
Dissociation energy	1.7	1.58 ± 0.13

References

1) S. Tomoda, K. Sato, Y. Achiba, and K. Kimura, *IMS Ann. Rev.*, 99 (1980).
2) Coputations were carried out at the Computer Center , Institute for Molecular Science, using IMS Gaussian-70 package.
3) C. Y. Ng, D. J. Trevor, P. W. Tiedemann, S. T. Ceyer, P. L. Kronebusch, B. H. Mahan, and Y. T. Lee, *J. Chem. Phys.*, 67, 4235 (1977).

IV—K Photoelectron-Mass Spectroscopy of Multiphoton Ionizaiton

In this project, a new attempt is made to extend molecular photoelectron spectroscopy to recently developed multiphotoionization spectroscopies using a tunable dye laser. We are still constructing a new photoelectron spectrometer for this purpose. (*IMS Annual Review* 1980, p. 100) On the other hand, we have been obtaining some preliminary results of multiphoton ionization photoelectron spectra by combining a laser source and a photoelectron spectrometer already available in our laboratory. Since state-selected molecular ions may be possibly produced by using a multiphoton ionization technique with a tunable dye laser, the photoelectron-mass spectroscopy will also become a powerful experimental method for studying dissociation processes of molecular ions.

IV-K-1 Construcion of a Time-of-Flight Electron Analyzer for Laser Ionizaiton Photoelectron Spectroscopy

Yohji ACHIBA, Kenji SATO, Yoshio SHINDO *(Hokkaido Univ.)*, **and Katsumi KIMURA**

An efficient electron kinetic energy analyzer based on the time-of-flight (TOF) method has been constructed for laser ionization photoelectron spectroscopy. Conventional photoelectron spectrometers have mainly used electrostatic deflective electron analyzers. Such analyzers have high resolving capabilities, but are intrinsically inefficient for laser experiments, because only electrons in narrow energy ranges are collected at one time. A time-of-flight electron analyzer permits entire energy spectrum to be analyzed simultaneously, so that it is not necessary to correct relative intensities for fluctuations in sample pressure and laser beam intensity.

Figures 1 and 2 show schematic drawings of our photoelectron apparatus and data aquisition system. A Nd-YAG pumped dye laser (Quanta Ray, DCR-1A, PDA-1) was used as a light source (Δt = 5 ns) at a repetition rate of 10 Hz. Photoelectrons which travel over a 12 cm field free region are detected by a channeltron electron multiplier. The time-of-flight was measured with a 500 MHz transient recorder (Biomation 6500), and each signal was transfered to

a microcomputer data accumlating system, in which the data was added untill a good S/N ratio is obtained. From a total time resolution of 12 ns and flight path of 12 cm, the energy resolution of the TOF analyzer was estimated to be 20 meV and 80 meV for 0.4 eV and 1.0 eV electrons, respectively. Several experimental results obtained by the present apparatus will be described in the following sections.

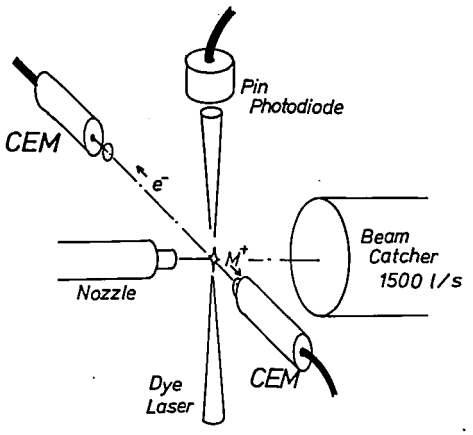

Figure 1. Schematic view of a MPI time-of-flight electron analyzer. CEM means a channeltron electron multiplier. Molecular beam is differentially pumped out with a 1500 l/s oil diffusion pump.

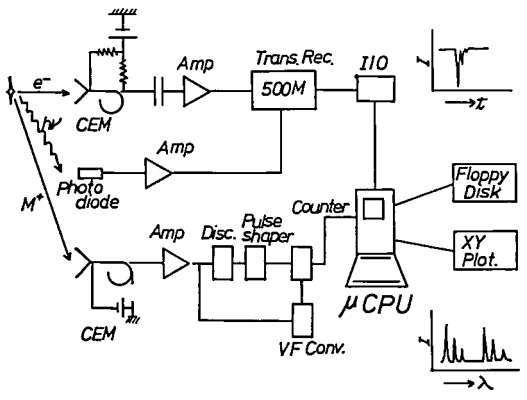

Figure 2. Schematic diagram of the experimental set-up for a time-of-flight electron energy analysis. CEM; channeltron electron multiplier, AMP; high speed preamplifier, I/O; input-output interface. The lower part of the diagram shows a system to measure a conventional MPI spectrum.

IV-K-2 Four-Photon Ionization Photoelectron Spectra of NH_3 and NO

Yohji ACHIBA, Kenji SATO, Kosuke SHOBATAKE, and Katsumi KIMURA

We have studied multiphoton ionization (MPI) photoelectron spectra of NH_3 and NO molecules following four-photon ionization resonant with various vibrational levels of electronic excited states. Figure 1 shows a series of the time-of-flight (TOF) photoelectron spoectra obtained by excitation of NH_3 through single vibrational level of the three-photon allowed $\tilde{C}'$ state.[1] Such MPI photoelectron spectra are completely different in pattern from available HeI photoelectron spectra.

In the case of NH_3, the MPI photoelectron spectra are considered to depend on the Franck-Condon factors between the $\tilde{C}'$ state and the ground state ion. Since the potential curves of the two states are considered to be very similar to each other, the Franck-Condon factors must be significant only for the $\Delta v = 0$ transition. Assuming that the ion is produced by the $\Delta v = 0$ ionization, the main peaks appear at the values indicated in Figure 2. It is seen from Figures 1 and 2 that the experimental electron energies are in good agreement with the calculated ones.

Generally speaking, most of the higher excited states of simple molecules must be Rydberg like in

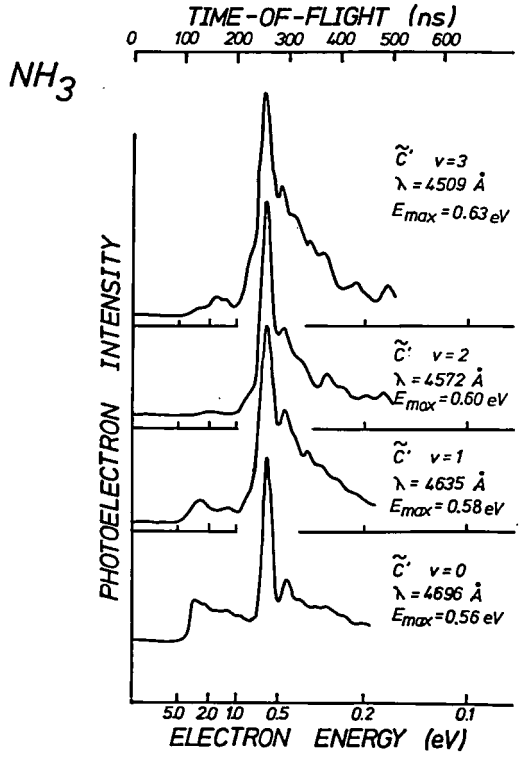

Figure 1. TOF photoelectron spectra following four-photon ionization resonant with four vibrtational levels of the $\tilde{C}'$ state of ammonia.

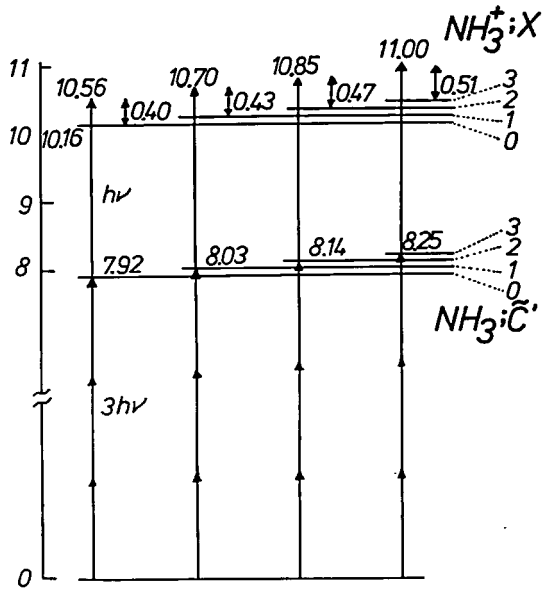

Figure 2. Energy level diagram showing the three-photon resonant, four-photon ionization of ammonia via various vibrations of the $\tilde{C}'$ state. The final four-photon energy in the continuum and the expected electron energy resulting from direct ionization is given in electron volts (eV).

character, so that such spectral features seem to characterize a general MPI photoelectron spectrum which substantially differs from that of an one-photon ionization. A similar situation was also observed in the case of NO, and its spectra are almost consistent with those reported by Miller and Compton.[2)]

References

1) J. H. Glownia, S. J. Riley, S. D. Colson, and G. C. Nieman, *J. Chem. Phys.*, **73**, 4296 (1980).
2) J. C. Miller and R. N. Compton *J. Chem. Phys.*, **75**, 22 (1981).

IV-K-3 Multiphoton Ionization Photoelectron Spectrum of Benzene

Yohji ACHIBA, Kenji SATO, Kosuke SHOBATAKE, and Katsumi KIMURA

Recent mass-resolved measurements of the ions formed by multiphoton ionization (MPI) have shown that an extensive fragmentation occurs in the ionization process. In the case of benzene, a variety of fragment ions, namely $C_1^+ \sim C_6^+$ have been reported.[1,2)] Such dissociative ionization may in principle be caused by absorption of additional photons either from neutral autoionization states or the ground state of the parent ions. Several studies of theoretical treatments have also recently appeared to explain such an anomalous fragmentation of MPI.[3)] In the present work, we have measured photoelectron kinetic energy distributions by MPI of benzene to obtain direct information on the ionization process.

A Nd-YAG pumped dye laser was used to ionize benzene molecules through the four-photon process resonant with $^1B_{2u}$ (14_0^1, $14_0^1 1_0^1$) intermediate states. Photoelectron kinetic energies were measured using a time-of-flight (TOF) technique described in the previous section.

Figure 1 shows the TOF photoelectron spectra obtained by excitation of benzene to two single vibronic levels in the two-photon resonant $^1B_{2u}$ state. Although these spectra are a little different in spectral patterns from each other, the main peaks observed here can be rationalized by considering that the four-photon direct ionization occurs to give the benzene ions in its electronically ground state.

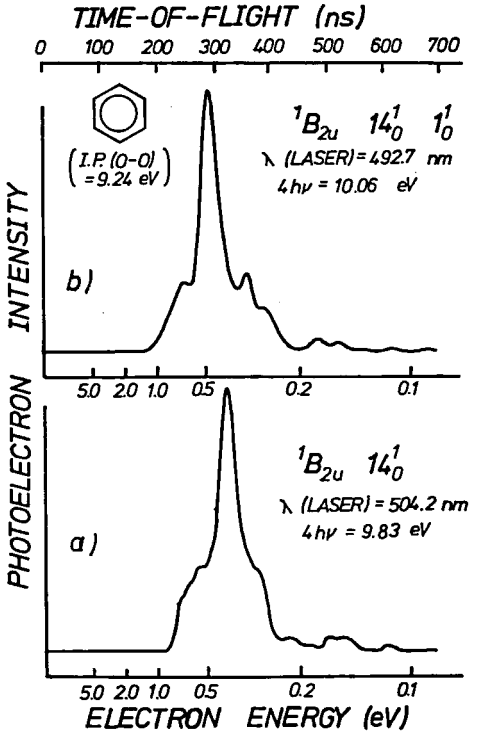

Figure 1. Four-photon ionization photoelectron spectra of benzene; a) excitation at $^1B_{2u}$, 14_0^1 state, b) excitation at $^1B_{2u}$, $14_0^1 1_0^1$ state.

The fragmentation mechanism deduced here, in which ion fragmentations occur following the subsequent absorption of additional photons by parent ions, is consistent with that proposed by Boesl *et al.*[2] from a MPI mass spectrometric study.

References

1) L. Zandee and R. B. Bernstein, *J. Chem. Phys.*, **71**, 1359 (1979).
2) U. Boesl, H. J. Neusser, and E. W. Schlag, *J. Chem. Phys.*, **72**, 4327 (1980).
3) J. Silberstein and R. D. Levine, *Chem. Phys. Lett.*, **74**, 6 (1980).

IV—L Production, Characterization, and Spectroscopic Studies of Molecular Complexes and Clusters

There are several techniques to investigate the physics and chemistry of molecular complexes and clusters. One of the most powerful techniques for the production of such weakly bound compounds is the supersonic expansion of a high pressure gas through a small nozzle hole, by which one can obtain a very large number of exotic complexes. However, the identification and characterization of these complexes is difficult because of its weak bonding character.

In the present project we are developing new types of supersonic beam sources to investigate the UV, VUV and IR absorption spectroscopy, laser induced fluorescence spectroscopy and electron bombardment and multiphoton ionization mass spectroscopy of van der Waals complexes, molecular complexes and clusters. Then we plan to characterize these complexes by these spectroscopic means.

We pay a great interest in finding what would happen after weakly bound molecular complexes are brought to vibrationally and/or electronically excited states and obtaining information on the predissociation dynamics of these molecules in relation to the intermolecular potential between the component molecules.

IV-L-1 Molecular Beam Apparatus with Optical Spectroscopic Detection

Kiyohiko TABAYASHI, and Kosuke SHOBATAKE

A multipurpose molecular beam apparatus-I as shown in Figure 1 is near completion. This apparatus has a fixed beams and rotatable detector configuration.[1] The scattering chamber is a rectangular stainless steel box with inner dimensions 79 × 86 × 54 cm having three side flange holes (F) of 34.0 cm in diameter and one rectangular cover flange port (not shown) as shown in Figure 2. For spectroscopic studies of van der Waals molecules a beam source chamber (B) with a supersonic nozzle source (N) is snugly inserted and the probe laser is irradiated through the bottom hole (H). In the detector compartment (D) attached to the cryostat (C), either a liguid He cooled bolometer[2] or a

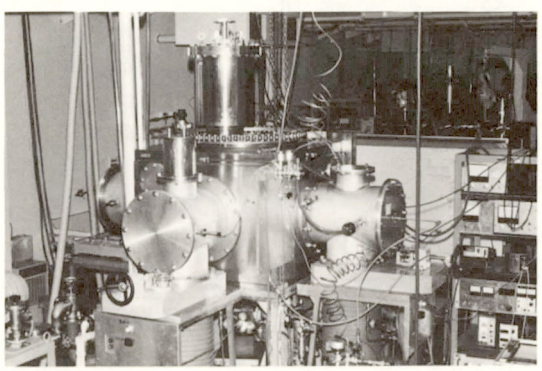

Figure 1. Molecular beam apparatus-I with optical spectroscopic detection.

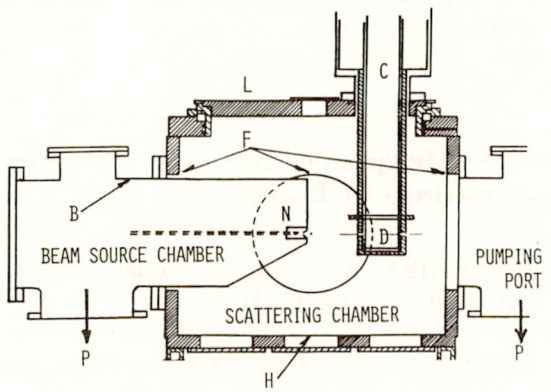

Figure 2. Schematic side view of the molecular beam apparatus-I.
B: Beam Source Chamber, C: Cryostat, D: Detector Compartment, F: Side Flange Hole, H: Bottom Hole, L: Rotatary Lid, N: Nozzle Beam Source, P: Diffusion Pump.

photomultiplier is mounted depending on the type of experiment carried out. The cryostat mounted on a rotatry lid (L) can be rotated by as much as 110 degrees around the vertical axis.

This apparatus also enables us to study crossed beams reactive scattering with additional reactive atomic or radical beam source in place on the remaining port. An arc-heated nozzle beam source for producing very reactive species is under construction at the Development Workshop.

References

1) Y. T. Lee et al., *Rev. Sci. Instrum.* **40**, 1402 (1969).
2) T.E. Gough, R. E. Miller, and G. Scoles, *Appl. Phys. Lett.*, **30**, 338 (1977).

RESEARCH ACTIVITIES V

Department of Applied Molecular Science

V—A Nature and Its Chemical Consequences of Interaction between Benzene Rings in Bridged Aromatic Compounds

Electronic interactions in the ground as well as excited states between the benzene rings in a fixed three dimensional molecular framework are the subject of our continued interest. As a chemical consequence of the excitonic interaction between the three benzene rings held at an angle of 120° each other, triptycenes undergo photochemical bridging between the benzene rings to give the monocentric diradical species, i.e., carbenes and nitrenes, due to one of the bridgehead atoms. Mechanistic delineation of the photochemical reaction of 1-azatriptycene has been made. The excited singlet state responsible for the reaction was well characterized. The dynamic behavior of the *o*-(9-fluorenyl)phenylnitrene intermediate was elucidated by time-resolved spectroscopy in collaboration with Prof. Yoshihara's group.

V-A-1 The Behavior of Excited States of 1-Azatriptycene

Tadashi SUGAWARA and Hiizu IWAMURA

Quantum yields of fluorescence and intersystem crossing, a life-time, and quenching rate constants have been determined for the excited singlet state of 1-azatriptycene (**1**) in order to fully characterize this state from which *o*-(9-fluorenyl)phenylnitrene (**2**) is generated in a high efficiency.[1] The fluorescence spectrum of **1** showed a broad emission maximum at 292 nm at ambient temperature in a fluid solution (Φ_f = 0.1 and τ_f = 2.4 ns), whereas in a rigid matrix (2,2-dimethylbutane/n-pentane, 8:3) it had a structure with a splitting of 1,000 cm^{-1} (281 and 287 nm), presenting a mirror image of the excitation spectrum (Figure 1). A similar feature was obtained on hydrocarbon triptycene, which ruled out the possibility of a solvent effect involving the nitrogen atom of **1**. The results are best interpreted in terms of deformation from C_{3v} symmetry of the molecular skeleton in the S_1 state. Since the mode of the distortion would be coupled with the reaction coordinate from the S_1 state, studies to elaborate this coupling mechanism is in progress.

Fluorescence of **1** was quenched both by diethylamine and tetracyanoethylene. From the Stern-Volmer plots, the quenching rate constants in an acetonitrile solution were obtained as $k_q = 4.1 \times 10^9$ and $\sim 2 \times 10^{10}$ l mol^{-1} for the added electron-donor and acceptor, respectively.

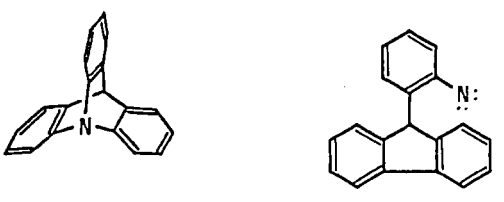

1 2

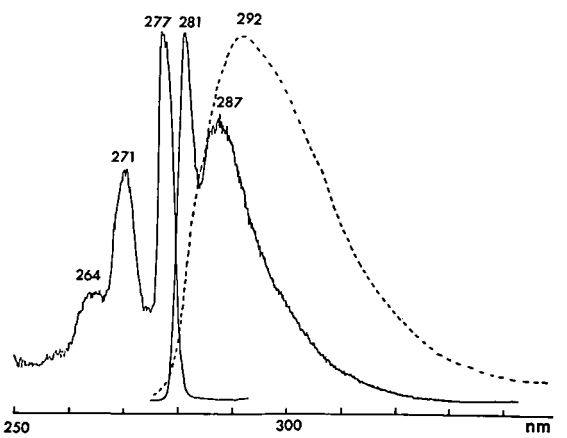

Figure 1. Fluorescence and excitation spectra of 1-azatriptycene in a rigid matrix at 77K. Fluorescence spectrum at ambient temperature is shown by a dotted curve.

Reference
1) T. Sugawara and H. Iwamura, *J. Am. Chem. Soc.*, **102**, 7134 (1980); *IMS Ann. Rev.*, 103 (1980).

V-A-2 The Dynamics of *o*-(9-Fluorenyl)-phenylnitrene Generated by Photorearrangement of 1-Azatriptycene

Tadashi SUGAWARA, Hiizu IWAMURA, Nobuaki NAKASHIMA,[1] and Keitaro YOSHIHARA[1]

Photolysis of 1-azatriptycene (**1**) to give *o*-(9-fluorenyl)phenylnitrene (**2**)[2] was monitored by UV-absorption spectroscopy at low temperature (4 ~ 77 K). Absorption bands due to nitrene **2** were observed at 288, 302 and ~ 370 nm. An additional broad band centered at 340 nm was assigned to azanorcaradiene **3** which was presumed to be formed *via* the singlet nitrene and could be considered as a key intermediate for a number of reaction products identified previously.[2]

The kinetic behavior of **2** was investigated by time-resolved spectroscopy using a KrF eximer laser with an emission at 248 nm (pulse width of 10 ns; power of 100 mJ) as excitation light and a xenone flash lamp as monitor light. Typical transient absorption spectra obtained with delay times of 100 and 450 ns are reproduced in Figure 1. The rise of the 340 nm band was found to be expressed by the sum of two kinetic processes (k_a = 4.2×10^6 s^{-1} and $k_b = 4.2 \times 10^5$ s^{-1}). Addittion of xenone (1.4 atm) supressed the formation of **3**, while that of triplet nitrene **2** was kept almost constant. A detailed reaction scheme which satisfies above observations is proposed as in Figure 2.

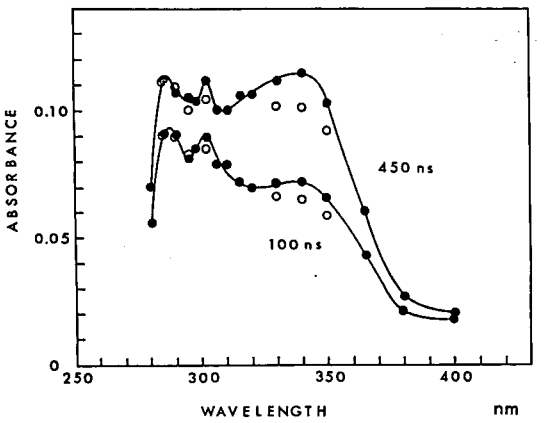

Figure 1. The time-resolved transient absorption spectra during photolysis of 1-azatriptycene (**1**). Delay times are 100 and 450 ns.

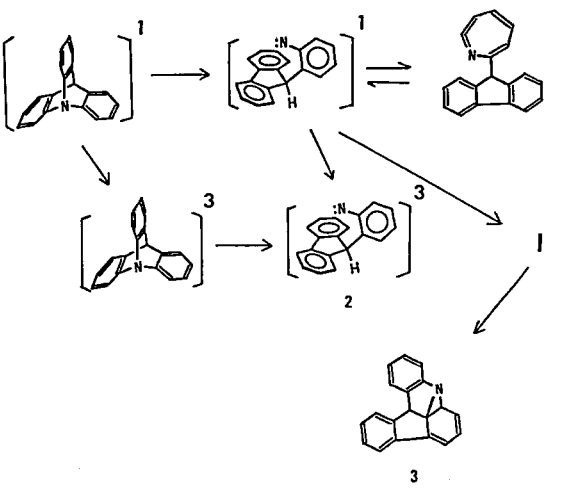

Figure 2. Reaction scheme related to *o*-(9-fluorenyl)phenylnitrene (**2**).

References
1) Department of Electronic Structure.
2) T. Sugawara and H. Iwamura, *J. Am. Chem. Soc.*, **102**, 7134 (1980); *IMS Ann. Rev.*, 103 (1980).

V-B Stereochemical Consequences of the Non-bonded Interaction in Overcrowded Molecules

We have been interested for some time in the unexpectedly high potential energy barrier to rotation around the bond extending out of the bridgehead carbon of triptycene molecules. The uniqueness of the molecules has been shown to be derived from the high s character of the bond and the ideal disposition of the peri-hydrogens on the benzene rings serving as an effective picket for the three fold barrier.

In order to see how far the internal rotation around two or more bonds within a molecule can be correlated and what stereochemical consequences would be brought about from the coupled rotation, a series of two-top molecules Trip-X-Trip in the shape of a bevel gear has been designed by combining two triptycene molecules with a central atom X. One of the most dramatic demonstrations of the conformational mobility in

overcrowded molecules was thus made. An effort to verify a perfect correlation of the rotation around the two bridgehead-X bonds has now given birth to a new concept of phase isomerism in gear shaped molecules.

In one example of the reaction of 1-triptycyllithium with carbon dioxide, steric hindrance to the mutual approach of the two reagents produced an unprecedented case of an electron transfer to CO_2 followed by recombination of the radical pair to give the carbonation product.

V-B-1 Bis(4-chloro-1-triptycyl) Ether. Separation of Phase Isomers of Labeled Bevel Gears

Yuzo KAWADA and Hiizu IWAMURA

[*J. Am. Chem. Soc.*, **103**, 958 (1981)]

In order to ascertain a high degree of correlation, and to rule out the possibility of a non-correlated pathway, in the rapid gear rotation in bis(1-triptycyl) ether,[1] we have synthesized and separated "phase isomers" of labeled bevel gear, bis(4-chloro-1-triptycyl) ether (**1**). 1-Bromo-4-chlorotriptycene

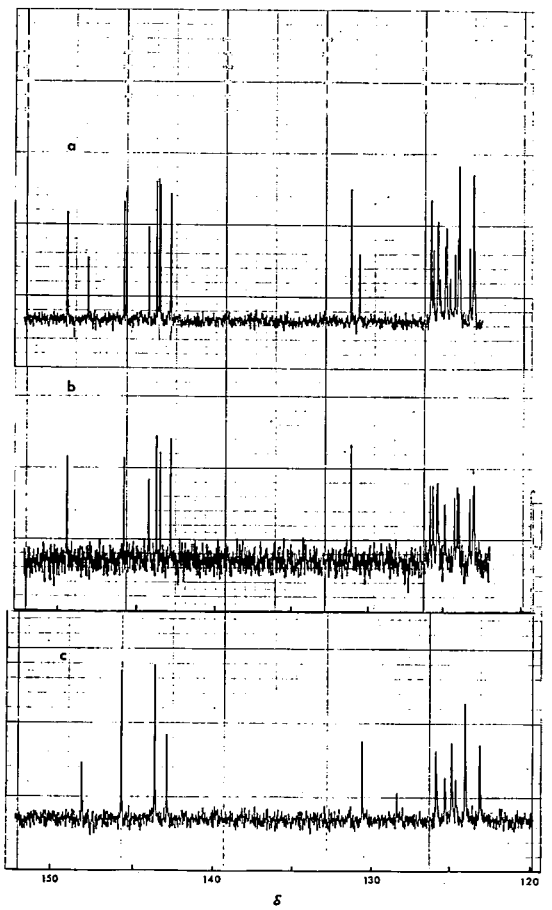

Figure 1. 25.15 MHz ^{13}C NMR spectra of **1** (aromatic region only). (a) The sample before fractionation, (b) dl isomer, and (c) meso isomer.

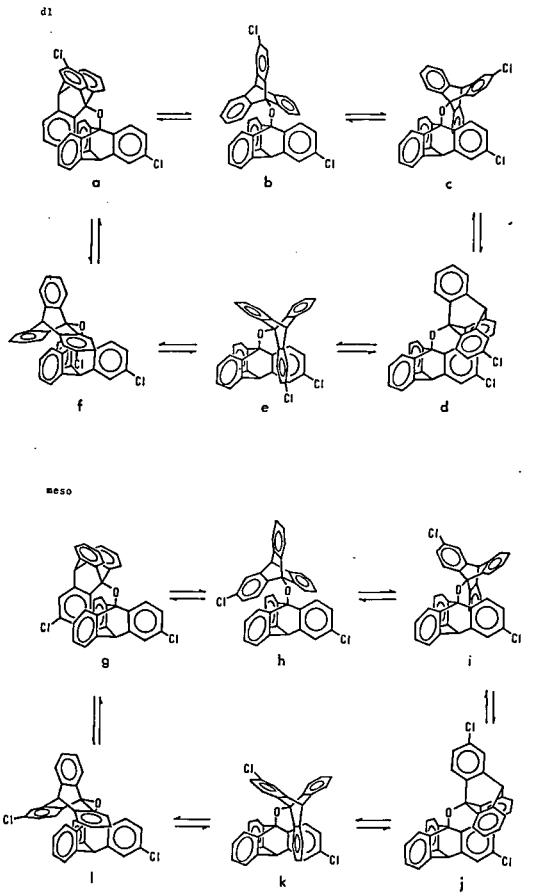

Figure 2. Phase isomers dl and meso of bis(4-chloro-1-triptycyl) ether (**1**). They do not interconvert unless rotation around the C-O bonds gets out of gear.

Scheme 1

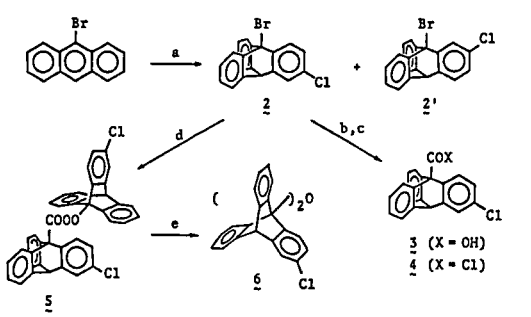

(2) was treated with butyllithium to give the 1-lithio derivative which was then converted to the 1-carbonyl chloride (4) on the one hand and to the lithium 1-hydroperoxide on the other. They were coupled to give peroxy ester (5). Thermolysis of 5 at 150 °C in perfluorodecalin gave in good yield 1 (≡6) (Scheme 1). High resolution ^{13}C NMR spectra of 1 (Figure 1a) showed the presence of two isomers in a two to one ratio. The mixture was subjected to HPLC on a μ-porasil column to give separate isomers, dl, mp 397 °C and meso, mp 383 °C. In the dl isomer the labeled cogs can bite each other during each 360° rotation and each conformer is chiral (Figure 2a). Thus the two unsubstituted benzene rings were shown by its ^{13}C NMR spectrum to be mutually diastereotopic (Figure 1b). In the meso isomer the labeled teeth are one phase apart and never come next to each other (Figure 2b). Its conformers have either the plane of symmetry or both dl pairs and are therefore achiral (Figure 1c). HPLC analyses of the melts showed the interconversion between the two isomers at these temperatures.

Reference

1) Y. Kawada and H. Iwamura, *J. Org. Chem.*, **45**, 2547 (1980); *IMS Ann. Rev.*, 107 (1980).

V-B-2 Phase Isomerism in Gear-shaped Molecules

Yuzo KAWADA and Hiizu IWAMURA

[*Tetrahedron Lett.*, **22**, 1533 (1981)]

In the preceding paper we have shown that, when one of the cogs on each wheel is labeled in perfectly geared molecules, a phase relationship is established with respect to the labeled cogs and the phase isomers can be produced in spite of rapid rotation of the gear.[1]

In order to generalize this concept of phase isomerism, a bevel gear in Figure 1 is taken as representing the molecules in question. It is summarized in Table I how many ways of labeling one cog in each wheel are possible and if the labeling patterns are, in effect, achiral or chiral.

Our bis(1-triptycyl) ether (1) and di-(1-triptycyl)-methane in which one of the benzene rings of each triptycene moiety is equally labeled provide the case N = 3. One achiral and one dl isomers should be present as verified experimentally in the previous paper. A possible correlated rotation in 1-benzyltriptycenes (2) reported by Yamamoto and Ôki corresponds to the example of m = 3 and n =

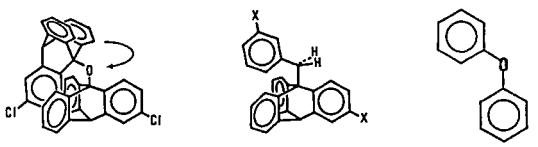

1 2 3

2.[2] There is no common divisor and one of the wheels carries an odd number of teeth. Therefore, no phase isomerism emerges in this system, although it is necessary for the Ph-CH_2 and 1-triptycyl-CH_2 bonds to rotate by 3 × 360° and 2 × 360°, respectively, to get back to the original conformation. Stable conformations and intercon-

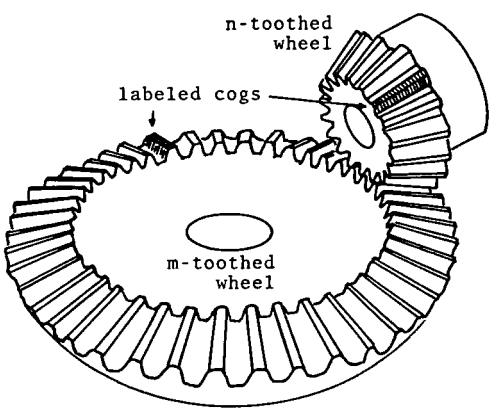

Figure 1

Table I. The number of the phase isomers possible for a bevel gear (Figure 1) carrying the m- and n-toothed wheels

the greatest common divisor of m and n		achiral	dl
N	odd	1	$\frac{N-1}{2}$
	even	0	$\frac{N}{2}$
none	one or both of m and n odd	1	0
	both m and n even	0	1

version between them of diphenyl ether (**3**) were the subject of classical works by Morino and Higashi.[3] When suitable substituents are introduced in this molecule so that one side of the phenyl ring may be labeled and rotation around the C-O bond may get hindered, there is a chance of having a case of N = 2. As long as tetracoordinated carbon atoms are employed as materials for constructing the gear, it would be difficult to envisage a molecule in which $N > 3$. Effective use of the corner of octahedral metal complexes or some carboranes could produce gear-shaped molecules with $N > 3$ and our rule would be operationally extended.

References

1) Y. Kawada and H. Iwamura, *J. Am. Chem. Soc.*, **103**, 958 (1981).
2) G. Yamamoto and M Ôki, *Chemistry Lett.*, 1251, 1255 (1979).
3) K. Higashi and S. Uyeo, *Bull. Chem. Soc. Jpn.*, **14**, 87. (1939); H. Shimizu, S. Fujiwara, and Y. Morino, *J. Chem. Phys.*, **34**, (1961); **37**, 1565 (1962)

V-B-3 Effect of the Central Atoms on the Tightness of the Molecular Bevel Gear

Yuzo KAWADA and Hiizu IWAMURA

A series of di-(1-triptycyl)-X compounds (**1**) has been prepared to realize an extreme case of the precisely coupled rotation around the two C-X bonds in the molecule. The chlorine atoms on the benzene rings served as a label on the cogs of the bevel gear and we were able to isolate from each compound the phase isomers in which only the phase relation between the labeled cogs was different.

It is naturally expected that at elevated temperature the smoothly geared cogs could get stripped and, as a result, the phase isomers would interchange each other. The interconversion was carried out at 100 ~ 350°C and the activation energy for throwing the di-(1-triptycyl)-X molecules out of gear was obtained as summarized in Table I. The ethers offered the bevel gear tighter than that of the methanes by *ca.* 10 kcal mol^{-1}. The results are interpreted in terms of shorter C-O bond length and larger deformation force constant of the C-O-C moiety. The indifference of the activation energy values to the position of the chlorine substitution is consistent with the deformed transition state structure.

Table I. Activation Parameters for Throwing the Di-triptycyl Molecules (**1**) out of Gear

X	Y	Z	E_a/kcal mol^{-1}	log A	K ($\frac{dl}{meso}$)
O	Cl	H	42.7 ± 0.7	12.6 ± 0.1	1.92 ± 0.02
O	H	Cl	43.0	12.4	1.95 ± 0.01
CH_2	Cl	H	31.8	11.9	1.70 ± 0.01
CH_2	H	Cl	32.9	12.2	1.86 ± 0.01

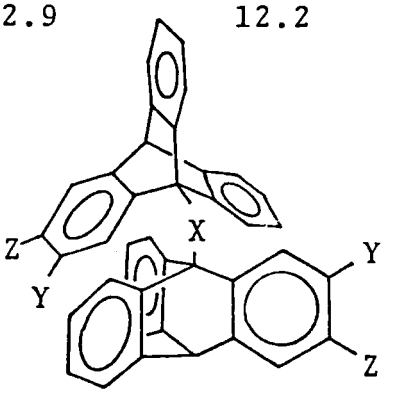

1

V-B-4 Carbonation of 1-Triptycyllithium Taking Place *via* Electron Transfer-Recombination Mechanism

Yuzo KAWADA and Hiizu IWAMURA

[*J. Org. Chem.*, **46**, 3357 (1981)]

Whereas there is considerable evidence to indicate that the addition of organometallic reagents to the carbonyl compounds proceeds *via* an electron transfer pathway, no definitive example of the one-electron transfer mechanism has been shown to be important in the carbonation of organometallic reagents with CO_2 which has relatively high reduction potential, $E_{1/2} = -2.3$ V *vs.* SCE in CH_3CN. We now report and discuss evidence for one electron transfer from 1-triptycyllithium (**1**) to carbon dioxide taking place in a non-polar solvent.

The reaction of **1** with CO_2 in benzene/ether (1:2) gave 1-triptoic acid (**2**) (85 ~ 27%), 1-(1-triptycyl)ethanol (**3**) (trace ~ 23%), and triptycene (15 ~ 48%). As the rate of introduction of CO_2 gas was decreased, the yields of **3** and triptycene increased at the expense of **2**. The results are explained in terms of formation of the 1-triptycyl radical by one electron transfer from **1** to CO_2. The reactions of **1** with CH_2O, CH_3CHO, Ph_2CO and adamantanone gave the normal products and showed no sign of significant contribution of the electron transfer mechanism. Steric hindrance to the electrophilic approach of the linear CO_2 to the reaction center of **1** with C_{3v} symmetry (see Figure 1) is considered to be relieved by one electron transfer to give bent $CO_2^{\cdot}$ (see Figure 2).[1]

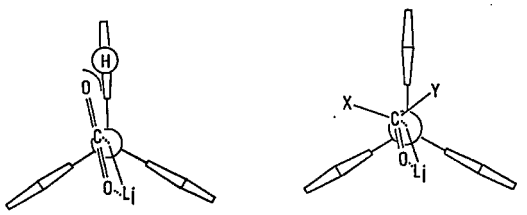

Figure 1. Newman projection of two models for the approach of 1-triptycyllithium to (a) linear CO_2 and (b) trigonal ketones. Note that the approach between the trigonal reaction center of **1** and the linear CO_2 molecule is hindered by one of the three peri-hydrogens on the triptycene moiety.

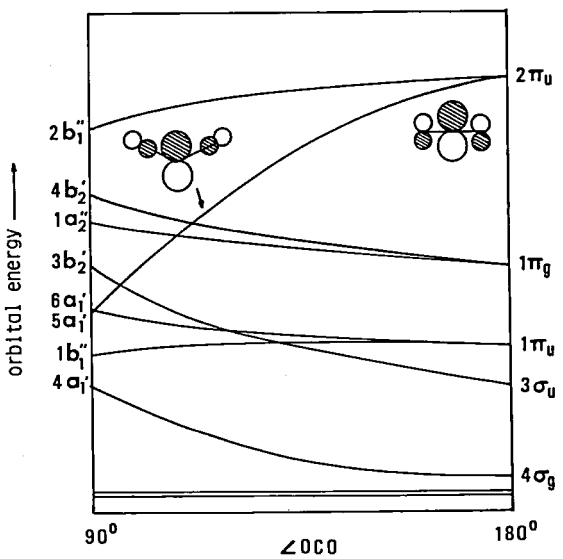

Figure 2. Walsh diagram showing how linear CO_2 with 16 valence electrons $(\cdots(1\pi_u)^4(1\pi_g)^4)$ tends to the bent structure in $CO_2^{-\cdot}$ with 17 valence electrons $(\cdots(1a_2'')^2(4b_2')^2(6a_1')^1)$.

References

1) A. D. Walsh, *J. Chem. Soc.*, **1953**, 2266; R. J. Buenker and S. D. Peyerimhoff, *Chem. Rev.*, **74**, 127 (1974)

V—C Structural and Mechanistic Studies by Means of NMR of the Less Common Nuclei

Structural and mechanistic studies with the aid of NMR of ^{17}O, ^{35}Cl and ^{77}Se have been carried out on a Varian FT-80A spectrometer. Diastereomeric differentiation of the two oxygen atoms in sulfones has been observed for the first time and will prove to be useful in stereochemical studies of sulfones. Chemical shifts for more metal carbonyls have been determined to delineate the chemical bonding in these compounds. We have developed and critically evaluated a new method of ^{17}O labeling coupled with ^{17}O NMR determination which may replace the conventional ^{18}O tracer technique widely used to elucidating structures and reaction mechanisms. Oxygen scrambling in the decomposition reaction of peroxybenzoates was used as an example. ^{35}Cl NMR line width studies on some chloride salts in aqueous organic solvents and in the presence of a

crown ether have been carried out in collaboration with Prof. Fujiyama's group (see II-D-7) and offered interesting insight into the ion-pairing and solvation in these systems. ^{77}Se NMR spectra have been determined for some fundamental and new organoselenium compounds. Chemical shifts were given as a chart and correlation of chemical shifts, spin coupling constants and relaxation rates with the chemical structure of organoselenium compounds was reviewed.

V-C-1 Diastereomeric Differentiation of Sulfone Oxygens by ^{17}O NMR Spectroscopy

Keiji KOBAYASHI *(Univ. of Tokyo)*, **Tadashi SUGAWARA, and Hiizu IWAMURA**

[*J. C. S., Chem. Commun.*, **1981**, 479]

The magnetic non-equivalence of geminal groups close to a center of molecular asymmetry has been observed in ^{1}H, ^{13}C, and ^{19}F NMR spectra and widely recognized as a useful probe in stereochemical problems.[1] Thus it was of interest to see if there is magnetic non-equivalence observable for the two oxygen atoms of a sulfone by ^{17}O NMR spectroscopy.

We prepared a diastereomeric pair of sulfones in which one of the oxygens was enriched stereospecifically with the ^{17}O-isotope. Oxidation of phenyl 1-phenylethyl sulfide with iodobenzene dichloride and $H_2[^{17}O]$ (10 atom%) in pyridine gave the diastereomeric [^{17}O] sulfoxides, (*RR/SS*)-**1** and (*RS/SR*)-**1** of known configuration. Further oxidation of these sulfoxides with *m*-chloroperoxybenzoic acid gave the corresponding [^{16}O, ^{17}O] sulfones, (*RR/SS*)-**2** and (*RS/SR*)-**2**. Phenyl 1-phenylpropyl sulfones **3** were prepared similarly.

Distinct chemical shift non-equivalence for the diastereotopic oxygens of these sulfones was found as summarized in Tabel I. The higher shielding of the oxygens in (*RR/SS*)- as compared with (*RS/SR*)-compounds can be rationalized in terms of the γ-effect induced by the methyl group. Preferred conformation (Figure 1) is concluded not to be significantly altered on changing from the sulfoxide to the sulfones.

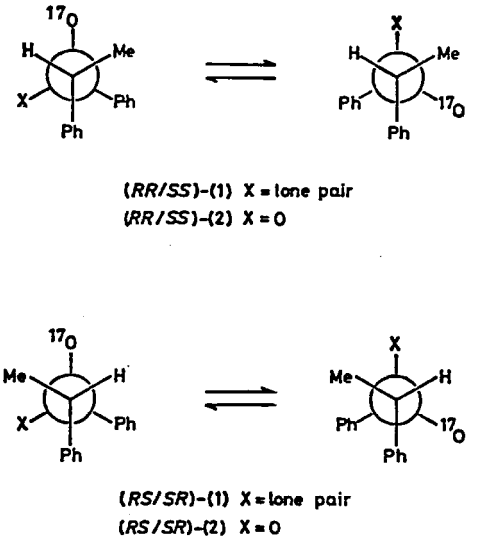

Figure 1. Preferred conformations of (*RR/SS*)- and (*RS/SR*)-sulfoxides and sulfones.

Table I. ^{17}O NMR Chemical Shift and Chemical Shift Non-equivalence (Δ) for Diastereomeric Phenyl 1-Phenylethyl and 1-Phenylpropyl Sulfones.[a]

	C_6H_6	$CHCl_3$	MeOH	CF_3CO_2H
(*RR/SS*)-**2**	137	134	132	127
(*RS/SR*)-**2**	141	139	137	133
Δ	4	5	5	6
(*RR/SS*)-**3**	136	134	132	124
(*RS/SR*)-**3**	142	140	139	134
Δ	6	6	7	10

[a] The exact Larmor frequency for water relative to which all chemical shifts are expressed in ppm was 10.783170 MHz with D lock frequency (external D) at 12.210 MHz. Chemical shifts are accurate to ± 1 ppm.

Reference

1) For a review, see: W. B. Jennings, *Chem. Rev.*, **75**, 307 (1975).

V-C-2 Oxygen-17 Nuclear Magnetic Resonance Spectra of Mononuclear Manganese and Dinuclear Group VI Metal Carbonyl Complexes[1]

Satoru ONAKA *(Nagoya Inst. of Tech.)*, **Tadashi SUGAWARA, Yuzo KAWADA and Hiizu IWAMURA**

[*J. Chem. Soc., Dalton Trans.*, in press]

Oxygen-17 magnetic resonances have been measured for two series of metal carbonyl derivatives, $RMn(CO)_5$ (R = H, CH_3, and Br), and $[MM'(CO)_{10}]^{n-}$ (n = 0 for M = M' = Mn; n = 1 for M = Mn, M' = Cr, Mo and W; n = 2 for M = M' = Cr, Mo, and W), at natural ^{17}O abundance. The chemical shift data are collected in Table I and typical spectra are reproduced in Figure 1.

Oxygen-17 chemical shifts for mononuclear $RMn(CO)_5$ are explained in terms of substituent electronegativity which would be expected to increase the paramagnetic shielding as the charge density at the oxygen 2p orbitals decreases. For the dinuclear metal carbonyls, an electron density argument supplemented by the carbonyl stretching force constants appears not to be enough to explain the observed trend in ^{17}O chemical shifts. The diamagnetic shielding effect due to the metal-metal bond may be responsible for a subtle change in the ^{17}O resonance frequency.

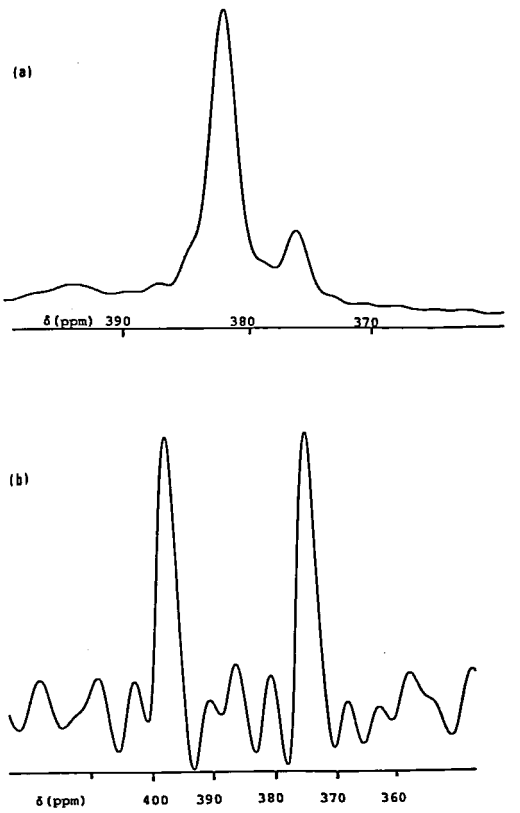

Figure 1. ^{17}O NMR spectra (10.78MHz) of (a) $HMn(CO)_5$ in toluene and (b) $(Et_4N)[CrMn(CO)_{10}]$ in nitromethane.

Reference

1) For a previous paper, see: Y. Kawada, T. Sugawara, and H. Iwamura, *J. C. S., Chem. Commun.*, **1979**, 291; *IMS Ann. Rev.*, 113 (1979).

Table I. ^{17}O NMR Chemical Shift and the Relevant Force Constant Data

Compound	$\delta(^{17}O)$/ppm [a] equatorial	axial	$\underline{k}$(M-M) mdyn Å^{-1}	$\underline{k}$(CO)/mdyn Å^{-1} equatorial	axial
$HMn(CO)_5$ (1)[b]	382	376			
$CH_3Mn(CO)_5$ (2)[b]	381	372			
$ClMn(CO)_5$ (4)	378.7	386.7 [3]			
$BrMn(CO)_5$ (3)[c]	386	392			
$Mn_2(CO)_{10}$ (5)[d]	387	367	0.59[i]	16.33	16.06[k]
$(Et_4N)[MnCr(CO)_{10}]$ (6)[d]	{398[e] 375[f]		0.50[j]	{15.89[e] 15.14[f]	{15.21[e] 14.27[f],j
$(Et_4N)[MnMo(CO)_{10}]$ (7)[d]	{400[e] 368[g]		0.60[j]	{15.83[e] 15.31[g]	{15.15[e] 14.34[g],j
$(Et_4N)[MnW(CO)_{10}]$ (8)[d]	{393[e] 358[h]		0.71[j]	{15.91[e] 15.14[h]	{15.24[e] 14.23[h],j
$(Et_4N)_2[Cr_2(CO)_{10}]$ (9)[d]	367	382	0.60[13]	14.70	12.00[1]
$(Et_4N)_2[Mo_2(CO)_{10}]$ (10)[d]	390	365	0.68[13]	15.30	13.10[1]
$(Et_4N)_2[W_2(CO)_{10}]$ (11)[d]	380	342	0.73[13]	15.30	13.10[1]
$Cr(CO)_6$ (12)[d]		376			
$Mo(CO)_6$ (13)[d]		367			
$W(CO)_6$ (14)[d]		357			

[a]Chemical shifts from $H_2{}^{17}O$. [b]In toluene. [c]In CH_2Cl_2. [d]In nitromethane. Solvent effects are less than 1 ppm for the Mn carbonyl derivatives. [e]$Mn(CO)_5$ part. [f]$Cr(CO)_5$ part. [g]$Mo(CO)_5$ part. [h]$W(CO)_5$ part. [i]C. O. Quicksall and T. G. Spiro, Inorg. Chem., 1969, 8, 2363. [j]J. R. Johnson, R. J. Ziegler, and W. M. Risen, Jr., ibid., 1973, 12, 2349. [k]F. A. Cotton and R. M. Wing, ibid., 1965, 4, 1328. [l]S. Onaka, unpublished results.

V-C-3 Thermal Decomposition of ^{17}O-Labeled *t*-Butyl *o*-Methylthio- and *o*-Phenylthioperoxybenzoates Studied by ^{17}O NMR. The Sulfuranyl Radical Structure of the *o*-Thiobenzoyloxy Radicals

Warô NAKANISHI *(Wakayama Univ.)*, **Toshihiko JO** *(Wakayama Univ.)*, **Kunio MIURA** *(Wakayama Univ.)*, **Yoshitsugu IKEDA** *(Wakayama Univ.)*, **Tadashi SUGAWARA, Yuzo KAWADA and Hiizu IWAMURA**

[*Chemistry Lett.*, 387 (1981)]

In order to differentiate between structures **1a** and **1b** for the intermediate radicals formed by thermal decomposition of *t*-butyl *o*-thioperoxybenzoates,[1] the fate of the oxygen label at the carbonyl group of the starting material was studied by ^{17}O NMR spectroscopy.

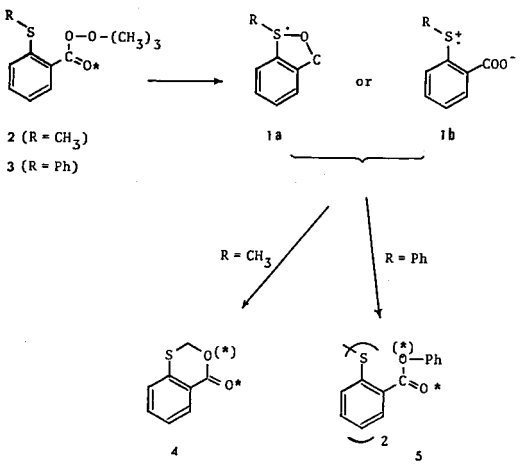

t-Butyl *o*-methylthio- and *o*-phenylthioperoxybenzoates (**2** and **3**) enriched with ^{17}O (5 atom%) selectively at the carbonyl group were prepared. The ^{17}O NMR spectrum of the lactone product **4** from the decomposition of **2** in chlorobenzene at 76.0°C is given in Figure 1. The low-field signal (365 ppm from external D_2O) was assigned to the carbonyl oxygen and the highfield one (159 ppm) to the ether oxygen. They were found to be in the integration ratio of 66:34. Population of the ^{17}O label at the carbonyl oxygen of **4** increased to 69 and 74% as the temperature of decomposition was lowered to 62.0 and 40.0°C, respectively. Thus the identity of the carbonyl oxygen can be kept through the reaction path to **4** and there is a competitive channel available for the scrambling of the oxygen label. In product **5** obtained by decomposition of **3** at 52.0°C, the ^{17}O label was retained 71% at the carbonyl oxygen. Sulfuranyl radical structure **1a** for the *o*-thiobenzoyloxy radical is thus concluded.

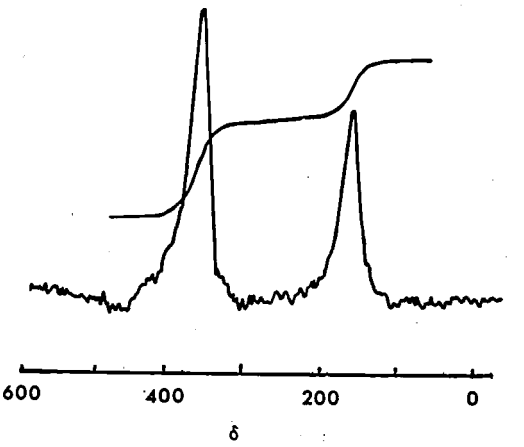

Figure 1. ^{17}O NMR spectrum (10.782 MHz) of **4** derived from the thermal decomposition of **2** at 76.0°C.

Reference

1) W. Nakanishi, S. Koike, M. Inoue, Y. Ikeda, H. Iwamura, Y. Imahashi, H. Kihara, and M. Iwai, *Tetrahedron Lett.*, 81 (1977).

V-C-4 Crown-Ether-KCl Complexes in Solution Studied by ^{35}Cl NMR Line Width

Tadashi SUGAWARA, Yukihiro YOKOYAMA,[1] Hiizu IWAMURA, Masako YUDASAKA,[2] and Tsunetake FUJIYAMA[2]

The ^{35}Cl NMR line widths have been determined for the KCl/18-crown-6 complex (**1**) in various solvents. The plots of the line width $\Delta\nu_{1/2}^{obs}$ *vs.* KCl concentration gave a kind of titration curve (Figure 1) which was simulated by theoretical equation:[3]

$$\Delta\nu_{1/2}^{obs} = \frac{\Delta\nu_{1/2}^{p} - \Delta\nu_{1/2}^{f}}{1 + f/p} + \Delta\nu_{1/2}^{f} \qquad (1)$$

based on the ion pair formation between the free chloride ions and K^+ incorporated in the crown ether as:

$$K^+ + \text{18-crown-6} \overset{K_2}{\rightleftharpoons} \textcircled{K}^+ \qquad (2)$$

$$\textcircled{K}^+ + Cl^- \overset{K_3}{\rightleftharpoons} \textcircled{K}^+ \cdots Cl^- \qquad (3)$$

The best fit was obtained when log $K_3 = 0.3 \pm 0.5$ (Figure 2) and the intrinsic line width ($\Delta\nu_{1/2}^{p}$) due to the ion pair was 90 ± 20 Hz.

In acetonitrile the line width due to **1** was narrow, concentration-dependent, and can be considered as a "naked anion". The line widths in other organic solvents were also determined and found to be narrower than those of tetramethylammonium chloride in the same solvents, showing more abundant population of the paired species in the ammonium salt solution.

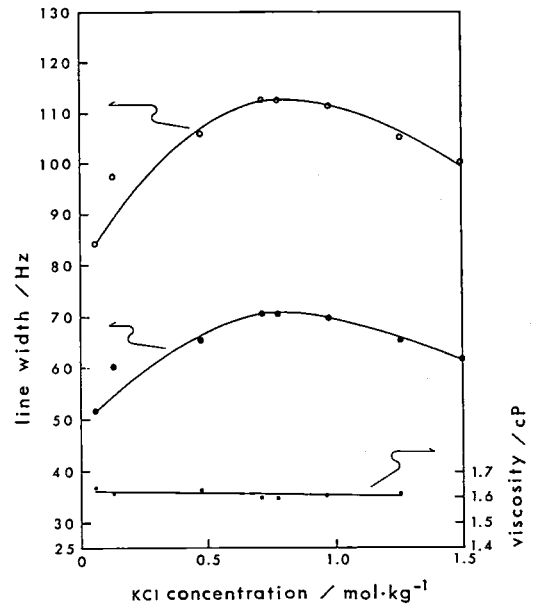

Figure 1. Plots of ^{35}Cl NMR line width due to aq. KCl in the presence of 18-crown-6 (0.808 mole/kg) *vs.* the KCl concentration at 29°C; ○: the observed line width, ●: the viscosity-corrected line width, and •: the viscosity of the solution.

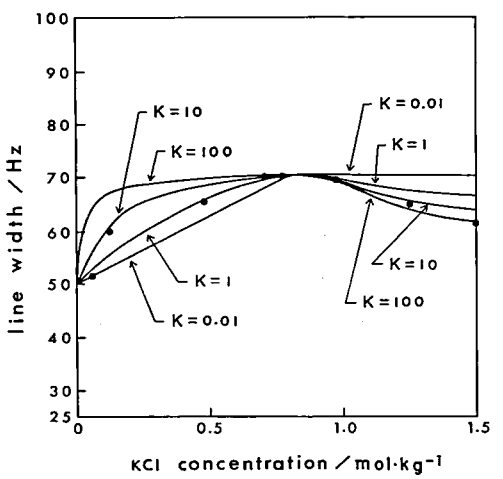

Figure 2. The theoretical curves (Eq. 1) describing the relation between the ^{35}Cl NMR line width and the KCl concentration. The curves are from top to bottom for $K_3 = 0.01$, 1, 10 and 100, the amplitude being normalized to fit the line width parameters experimentally observed as in Figure 1.

References

1) IMS Graduate Student from Nagoya Inst. of Tech. for 1981.
2) Department of Molecular Structure.
3) f and p stand for the free and paired chloride ions, respectively.

V-C-5 Recent Application of ^{77}Se NMR Spectroscopy in Organoselenium Chemistry

Hiizu IWAMURA and Warô NAKANISHI
(Wakayama Univ.)

[*J. Synth. Org. Chem. Jpn.*, **39**, 795 (1981)]

Recent development in ^{77}Se NMR spectroscopy is reviewed and the information available therefrom is critically discussed. After brief discussion on the technical problems inherent in the measurement, an NMR chart is given which illustrates relationship between structures and chemical shifts having the range as wide as 2,000 ppm (Figure 1). Spin-spin coupling constants pertaining to ^{77}Se can be informative of stereochemistry. Contribution of dipolar interaction between nuclear spins to the total spin-lattice relaxation is negligible in ^{77}Se NMR. Spin rotation and/or chemical shift anisotropy are shown to be important here. Recent high research activity in organoselenium chemistry will be strongly aided by this new methodology.

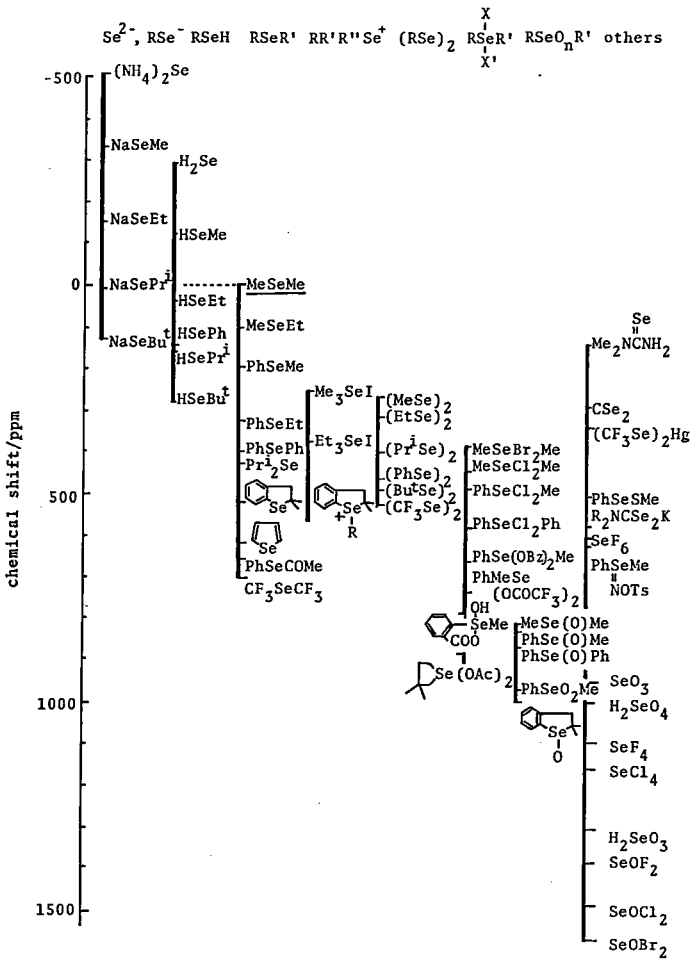

Figure 1. ^{77}Se NMR chemical shifts.

V-C-6 On the Structure of 2-Carboxyphenyl Methyl Selenoxide and Its Sodium Salt in Solution Studied by ^{1}H, ^{13}C, and ^{77}Se NMR Spectroscopy

Warô NAKANISHI *(Wakayama Univ.)*, **Shigekazu MATSUMOTO** *(Wakayama Univ.)*, **Yoshitsugu IKEDA** *(Wakayama Univ.)*, **Tadashi SUGAWARA, Yuzo KAWADA and Hiizu IWAMURA**

[*Chemistry Lett.*, 1353 (1981)]

As the carboxyl group in the neighborhood of the Se-O bond can play the role of a fourth ligand to form a selenurane, it has been a standing puzzle in organoselenium chemistry whether 2-carboxyphenyl methyl selenoxide (**1**) would be present as selenoxide **1a** or cyclic selenurane **1b**. ^{1}H, ^{13}C, and ^{77}Se NMR spectra of **1**, its sodium salt (**2**) and the related compounds have now been measured to disclose their structures in solution.

It is concluded from the upfield shift of ^{77}Se resonance and smaller one-bond coupling constant in **1** (see Table I) that **1** has structure **1b** whereas **2** is acyclic selenoxide **2a**. The driving force for the selenurane formation in **1** appears not necessarily to be crystal packing in solid,[1] but its advantageous free energy of formation even in solution. Selenuranes are known to be stabilized by strong electronegative ligands at the apical positions. The oxygen anion of **2b** may not be enough to stabilize the selenurane structure because of the electron rich character of the ligand.

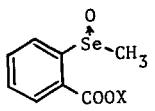

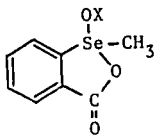

1a (X = H) 1b

2a (X = Na) 2b

Table 1. ^{77}Se NMR Data.

	$\delta(^{77}Se)^a$	$^1J(^{77}Se - ^{13}C)^b$
	ppm	Hz
1	799	65.1
2	830	81.4

a Referred to $(CH_3)_2Se$.
b Carbon of the methyl group.

References

1) B. Dahle'n, *Acta Crystallogr.*, **B 29**, 595 (1973).

V-C-7 A Facile Formation of Cyclic Selenuranes and a Cyclic Selenurane Oxide in the Reaction of 2-Methylseleno- and 2-Phenylselenobenzoic Acids and Their Derivatives with *t*-Butyl Hydroperoxide

Warô NAKANISHI *(Wakayama Univ.)*, **Satoru MURATA** *(Wakayama Univ.)*, **Yoshitsugu IKEDA** *(Wakayama Univ.)*, **Tadashi SUGAWARA, Yuzo KAWADA, and Hiizu IWAMURA**

[*Tetrahedron Lett.*, **22**, 4241 (1981)]

In view of the striking effect of a neighboring sulfur atom in the homolytic O-O bond cleavage of *t*-butyl 2-thioperoxybenzoates,[1] it seemed of interest to investigate a similar anchimeric assistance of the neighboring selenium atom in the decomposition of *t*-butyl 2-selenoperoxybenzoates (**1a** and **1b**). The reaction of 2-methylselenobenzoic acid with 1,1'-carbonyldiimidazole followed by addition of *t*-butyl hydroperoxide gave cyclic selenuranes **2a** and **3a**, suggesting the intramolecular insertion of the neighboring selenium atom into the O-O bond of **1a**. When the reaction was monitored by ^{13}C NMR spectroscopy, intermediary formation of **1a** was indicated by the appearance of the Se-methyl signal at δ 6.2 which eventually was replaced by a signal at δ 37.0 of **2a** in a few hours. The observed efficient conversion of **1a** to **2a** would be the O-O bond cleavage assisted by the neighboring selenium atom. The rate enhancement factor for the 2-methylseleno group is estimated to be about ten times as large as that of the 2-methylthio group in the decomposition of *t*-butyl peroxybenzoates.

A mixture of two compounds **2b** and **4**, mp 154-155°C; ^{77}Se NMR($CDCl_3$) δ(from CH_3SeCH_3) 785, were obtained from the reaction of 2-phenylselenobenzoyl chloride with *t*-butyl hydroperoxide.

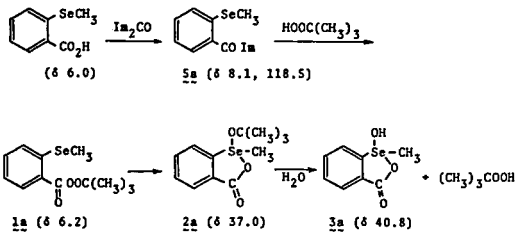

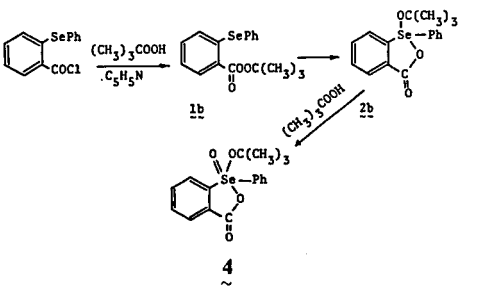

References

1) W. G. Bentrude and J. C. Martin, *J. Am. Chem. Soc.*, **84**, 1561. (1962); C. W. Parkins, J. C. Martin, A. J. Arduengo, W. Lau, A. Alegria, and J. K. Kochi, *J. Am. Chem. Soc.*, **102**. 7753 (1980); W. Nakanishi, S. Koike, M. Inoue, Y. Ikeda, H. Iwamura, Y. Imahashi, H. Kihara, and M. Iwai, *Tetrahedron Lett.*, 81 (1977); W. Nakanishi, T. Jo, K. Miura, Y. Ikeda, T. Sugawara, Y. Kawada, and H. Iwamura, *Chemistry Lett.*, 387 (1981).

V—D Exciton Coupled Circular Dichroism and Applications to Organic and Bioorganic Stereochemistry

The circular dichroic exciton chirality method, a nonempirical method based on the coupled oscillator theory, has been successfully used in various organic compounds for the determination of absolute configurations. In this project, the excition coupled circular dichroism of chiral triptycene derivatives and allylic benzoates was studied, and their absolute configurations were unambiguously determined. Furthermore, the CD and VIS spectra of anthocyanin aggregates, flower color pigments, were theoretically studied in order to clarify the mechanism of flower color variation.

V-D-1 Exciton Coupled Circular Dichroism of Chiral Triptycene Derivatives

Nobuyuki HARADA *(Tohoku Univ. and IMS)*

The CD spectra of (5*S*, 14*S*)-(+)-1,17-diethynyl-5,14-dihydro-5,14[1′,2′]benzenopentacene (**1**) and related compounds were quantitatively calculated on the basis of chiral exciton coupling between three chromophores, i.e., one anthracene and two ethynylbenzene chromophores. The numerical calculations were performed by the SCF-CI-dipole velocity molecular orbital method including the interchromophoric homoconjugation. The calculated spectra were in excellent agreement with the observed ones, establishing the absolute stereochemistry in a nonempirical manner (Figure 1).[1,2]

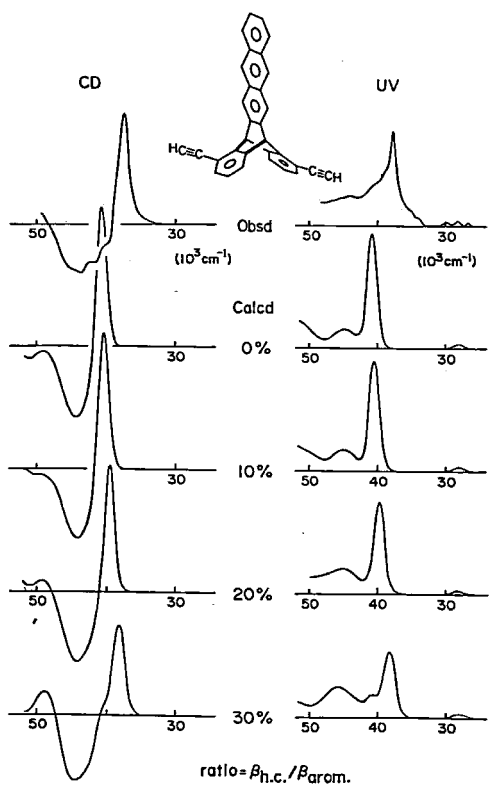

Figure 1. The CD and UV spectra of (5*S*, 14*S*)-(+)-1,17-diethynyl-7,14-dihydro-7,14[1′,2′]benzenopentacene (**1**) calculated by the SCF-CI-DV MO method. The top curves are the observed spectra.

References

1) N. Harada, Y. Tamai, Y. Takuma, H. Uda, *J. Am. Chem. Soc.*, **102**, 501 (1980).
2) N, Harada, Y. Tamai, H. Uda, *J. Am. Chem. Soc.*, **102**, 506. (1980).

V-D-2 A Chiroptical Method for Determining the Absolute Configuration of Allylic Alcohols

Nobuyuki HARADA *(Tohoku Univ. and IMS)*, **Jun IWABUCHI** *(Tohoku Univ.)*, **Yoichi YOKOTA** *(Tohoku Univ.)*, **Hisashi UDA** *(Tohoku Univ.)*, **and Koji NAKANISHI** *(Columbia Univ.)*

[*J. Am. Chem. Soc.*, in press]

A new chiroptical method for determining the absolute configuration of allylic alcohols is described. The CD exciton chirality method can be extended to the system of allylic alcohol benzoates, nondegenerate systems composed of two different chromophores, i.e., benzoate with an allowed $\pi \rightarrow \pi^*$ transition at 230 nm and C-C double bond with an allowed $\pi \rightarrow \pi^*$ transition around 195 nm. Since these $\pi \rightarrow \pi^*$ transitions are both polarized along the long axes of the chromophores, the

exciton theory predicts that if the two long axes of benzoate and double bond chromophores constitute a positive exciton chirality, i.e., right-handed screwness, the first Cotton effect at longer wavelengths (230 nm benzoate Cotton effect) is positive. On the other hand, if the allylic benzoate constitutes a left-handed screwness, the 230 nm benzoate Cotton effect should be negative (see Figure 1). The present method was confirmed by the CD spectra of a number of steroidal allylic alcohol benzoates and monoterpene alcohol *p*-nitrobenzoates, and also by the theoretical calculation using the SCF-CI-DV MO method.

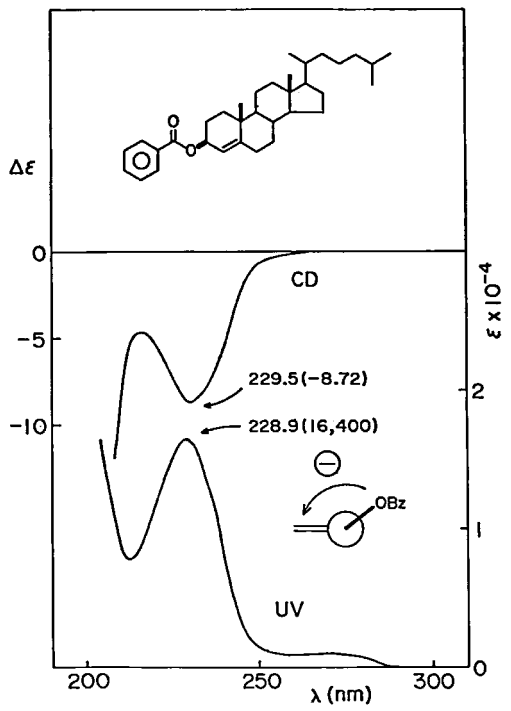

Figure 1. CD and UV spectra of cholest-3-en-3β-yl benzoate in ethanol.

V-D-3 Angular Dependence of UV λ_{max} of Exciton Coupled Systems

Nobuyuki HARADA *(Tohoku Univ. and IMS)*

When two identical chromophores couple with each other, the CD spectra exhibit split Cotton effects of opposite signs, which enables one to determine the absolute configuration of exciton coupled systems. On the other hand, the UV spectra reflect the relative stereochemistry of the chromophoric systems. Namely, UV λ_{max} of exciton coupled systems depends on the angle between the two dipole moments; when the angle is less than 90°, the UV spectrum exhibits a blue shift, in comparison with the λ_{max} of monomer. When the angle is larger than 90°, the UV spectrum shows a red shift.

The UV data of pertinent bis(*p*-dimethylaminobenzoates) with various dihedral angles and distances are listed in Table I; as the dihedral angle increases, UV λ_{max} gradually shifts to longer wavelengths. The numerical calculation by the SCF-CI-DV MO method also corroborated the above results.

Table I. Angular Dependence of UV λ_{max} of *p*-dimethylaminobenzoates.

compound	λ_{max} (nm)	solvent[a]
monobenzoate		
	311.0	D/E
dibenzoate		
0° (1,2-)	304.9	EtOH
60° (1,2-)	307, 308, 308, 309.4	EtOH
60° (1,4-)	309, 309.3, 310.0, 310	EtOH
60° (1,5-)	310, 310	EtOH
90° (1,3-)	310.5, 311.8	EtOH
180° (1,3-)	313.9	D/E
180° (1,2-)	314.8	EtOH

[a] D/E: 1% dioxane in EtOH

V-D-4 Chiral Exciton Coupled Stacking of Anthocyanins: Interpretation of the Origin of Anomalous CD Induced by Anthocyanin Association

Tsutomu HOSHINO *(Tokyo Coll. Pharmacy)*, **Ushio MATSUMOTO** *(Tokyo Coll. Pharmacy)*, **Nobuyuki HARADA** *(Tohoku Univ. and IMS)*, **and Toshio GOTO** *(Nagoya Univ.)*

[*Tetrahedron Lett.*, in press]

Natural anthocyanidin 3,5-diglucosides show exciton coupled CD Cotton effects in neutral aqueous solutions, indicating the chiroptical stacking of anthocyanidin chromophores. For example, the CD curve of cyanin quinonoidal base split into a pair of positive and negative Cotton bands (Figure 1). These split CD Cotton effects belong to

the typical exciton coupling type; areas of the positive and the negative Cotton effects are nearly equal, and both bands are found in the visible absorption band region of each of the anthocyanins. Thus, two or more anthocyanidin chromophores must stack in a right-handed or left-handed screw axis to cause this type of split bands. The magnitudes of CD in each of the anthocyanins are strongly intensified by increasing concentration, thus indicating the formation of stacked molecules more in the more concentrated solutions.

Shifts of the visible spectra towards longer or shorter wavelengths by formation of the chiral aggregates are also noted. Thus, the stacking affects variation of the flower colors that consists of such anthocyanins.

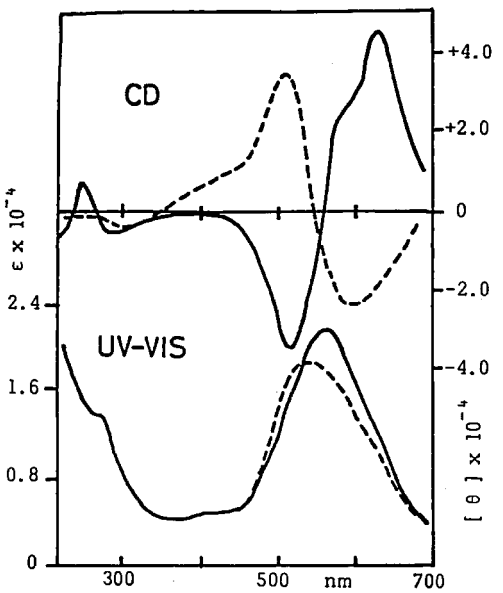

Figure 1. Electronic and CD spectra of cyanin and delphin in aqueous solution at pH 7.0: —— Cyanin; ---- Delphin (5×10^{-4}M).

V-D-5 Circular Dichroic Power of the Exciton Coupled Aggregate of Anthocyanins

Nobuyuki HARADA *(Tohoku Univ. and IMS)*

The CD spectra of dimeric aggregate of anthocyanins, flower color pigments, were numerically calculated by the SCF-CI-DV MO method. When the dimeric aggregate adopts the molecular association structure with positive exciton chirality as shown in Figure 1, the calculated CD spectrum was in agreement with the observed one. Furthermore, the red shift of λ_{max} of visible absorption spectrum was also reproduced by the calculation. The theoretical calculation thus also indicates that the UV-VIS spectra of anthocyanins which govern variation of flower color depend on the stereochemistry of molecular association of pigments.

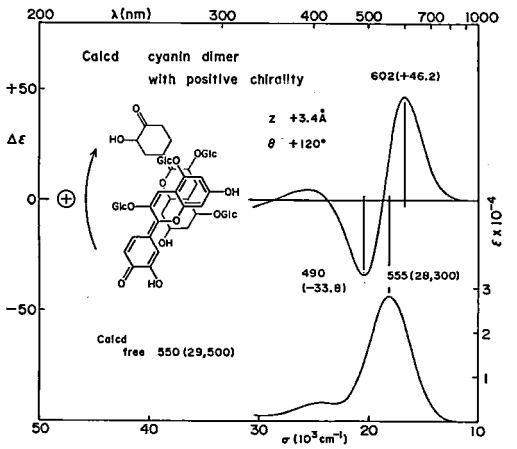

Figure 1. The CD and VIS spectra of a cyanin dimer with positive chirality calculated by the SCF-CI-DV MO method.

V—E Structural Studies of Tetraazamacrocyclic Complexes in Unusual Oxidation States

One dominant characteristics of macrocyclic ligands is the stability which they impart to the resulting metal complexes. In some cases, stable compounds of metal ions in unusual oxidation states have been isolated. In this study, structures of nickel(III) and silver(II) complexes of 1, 4, 8, 11-tetraazacyclotetradecane have been determined.

V-E-1 The Structure of *Trans*-dichloro (1, 4, 8,11-tetraazacyclotetradecane)nickel(III) Perchlorate

Tasuku ITO, Masako SUGIMOTO, Koshiro TORIUMI, and Haruko ITO *(Aichi Kyoiku Univ.)*

A trivalent nickel complex of the title ligand, $[Ni^{III}Cl_2L](ClO_4)$, crystallizes in orthorhombic space group $P2_12_12_1$ with unit cell parameters of a = 13.228(2), b = 19.804(3), c = 6.468(1) Å and U = 1694.4(6) Å^3 (Z = 4, D_c = 1.68, D_m = 1.68 Mg m^{-3}). The structure was refined to give R = 0.031 for 2023 independent reflections ($2\theta_{MoK\alpha} < 60°$, $|Fo| > 3\sigma(|Fo|)$). The Ni in this compound is surrounded octahedrally by a square-planar array of four nitrogens and two chlorine atoms occupying the axial positions, and the fourteen-membered marcrocyclic ligand adopts the most stable conformation (Figure). The total sterochemistry is the same as the corresponding Ni(II) analog, *trans*-$[Ni^{II}Cl_2L]$.[1] However, the coordination bond lengths of the trivalent complex are significantly shorter than those in the divalent analog. The average Ni-N and Ni-Cl distances are 1.970(4) and 2.452(4) Å for *trans*-$[Ni^{III}Cl_2L]^+$, and 2.058 and 2.492 Å for *trans*-$[Ni^{II}Cl_2L]$, respectively. There are some arguments on the authenticity of the Ni(III) state: some of so-called Ni(III) complexes are more properly described as a Ni(II) stabilized ligand radical, a mixed valence complex of Ni(II) and Ni(IV), or a partially oxidized Ni(II) complex. The Ni in the present compound is in the trivalent state in view of the structural parameters about the Ni and the normal bond lengths and angles within the organic ligand.

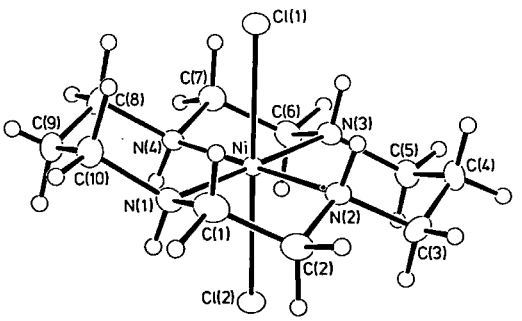

Reference

1) B. Bosnich, R. Mason, P. J. Pauling, G. B. Robertson, and M. L. Tobe, *J. Chem. Soc., Chem. Comun.*, **1965**, 97.

V-E-2 The Structures of Both the Kinetic and Thermodynamic Isomers of 1,4,8,11-Tetraazacyclotetradecanesilver(II) Perchlorate as Determined by X-ray Analyses

Tasuku ITO, Haruko ITO *(Aichi Kyoiku Univ.)*, **and Koshiro TORIUMI**

Kinetically controlled structural isomerism was found with the title silver(II) complex, $[AgL](CLO_4)_2$. Reaction of $AgNO_3$ with the title marcrocyclic ligand (L) produces red-orange needles of $[AgL](CLO_4)_2$.[1] Slow recrystallization of the needles from 10^{-3} mol dm^{-3} $HClO_4$ gave a small amount of yellow block crystals along with a large amount of needles. Successive slow recrystallization resulted in an increase in the amount of the blocks. With successive recrystallizations, the color of the needles turned orange from red-orange. Elemental analyses for both the crystals gave satisfactory results. The structure of the block crystal was described previously.[2] Crystal data for the needle crystal: orthorhombic, Pbnm, a = 13.024(2), b = 14.510(1), c = 9.594(1) Å, Z = 4, D_c = 1.87, D_m = 1.86 Mg m^{-3}, R = 0.039 for 2159 independent reflections ($2\theta_{MoK\alpha} < 65°$, $|Fo| > 3\sigma(|Fo|)$). The needle crystal consists of $[AgL](CLO_4)_2$ having two disordered isomeric structures (Figure 1). The main component (75%) has a basket type configuration (type 1) shown in Figure 2. The total stereochemistry of the minor component (25%) was essentially the same as that in Figure 3, which illustrates the structure found in the block crystal (type 2). In the needle, no axial interaction was found and the Ag in the type 1 structure is displaced 0.24 Å below the N_4 plane. On the other hand, in the block, the Ag sits in the N_4 plane and weak axial interactions with perchlorate oxygens result in a distorted octahedral coordiantion in which Ag-O is 2.788(2) Å.

Isomarization of the type 1 complex to the type 2 in solution was confirmed spectrophotometrically. The basket type structure would be favored for the formation of the Ag(II) complex, since the formation reacton proceeds *via* disproprtionation of Ag(I)[1] and the basket type structure can provide a large vacant site for the reaction. It is most reasonable to consider the observed basket type stereochemistry to be a result of kinetic control.

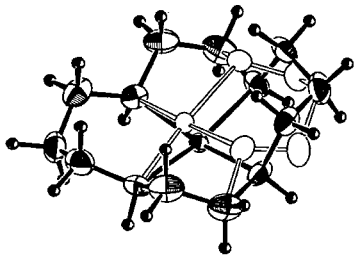

Figure 1.

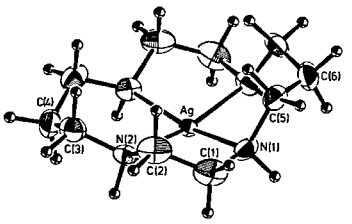

Figure 2.

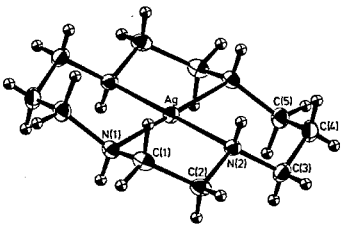

Figure 3.

Figure 1. Two disordered isomeric structures of $[AgL]^{2+}$ in the needle crystal.

Figure 2. A perspective view of $[AgL]^{2+}$ in the main component of the two disordered structures in the needle crystal (Type 1 structure). The silver sits in a crystallographic mirror plane bisecting the two six-membered chelate rings and through the silver. The Ag-N distances average 2.192(11) Å.

Figure 3. A perspective view of $[AgL]^{2+}$ in the block crystal (Type 2 structure). The silver sits on a crystallographic center of symmetry. the Ag-N distances average 2.158 (2) Å.

The type 1 is kinetically formed initially while the type 2 structure is clearly the thermodynamically more stable isomer. The color change of the needles from red-orange to orange upon recrystallization may be caused by a decrease in the relative amount of the basket type structure.

References

1) K. Barefield and M. T. Mocella, *Inorg. Chem.*, **12**, 2829 (1973).
2) T. Ito, K. Toriumi, and H. Ito, *IMS Ann, Rev., 113, (1980).*

V—F Tetraaza Macrocyclic Complexes Having a Middle Size Chelate Ring —— Highly Strained Metal Complexes

Middle size (8 to 11-membered) chelate rings have been reported to involve severe ring strain in the analogy with cycloalkanes and thereby to be hardly formed. In this study, a series of novel nickel(II) complexes having 7-, 8-, or 9-membered chelate ring have been successfully synthesized, using new tetraazamacrocyclic ligands. Molecular structures of some of these complexes have been determined by the X-ray analyses. The macrocyclic effect, "Multiple Juxtapositional Fixedness", plays an important role on the formation of such chelate rings. The complexes having 8- or 9-membered ring are highly strained sterically and electronically.

V-F-1 Tetraaza Macrocyclic Nickel(II) Complexes Having Seven-, Eight-, and Nine-Membered Chelate Rings. I. Synthesis and Characterization of Nickel(II) Complexes with 1,4,7,10-Tetraazacyclotetradecane, 1, 4, 7, 10-Tetraazacyclopentadecane, and 1,4,7,10-Tetraazacyclohexadecane.

Masako SUGIMOTO,[1] **Matsuo NONOYAMA** *(Nagoya Univ.)*, **Tasuku ITO, and Junnoske FUJITA** *(IMS and Nagoya Univ.)*

Three new tetraazamacrocyclic ligands, $N_4$7, $N_4$8, and $N_4$9, were prepared by a method similar to that for other analogous tetraazacycloalkanes in fairly good yields (60 — 90%). The ligands form orange Ni(II) complex perchlorates by reacting with $Ni(ClO_4)_2 \cdot 6H_2O$ in methanol. All the perchlorates are square-planar 4-coordinate complexes, $[NiL](ClO_4)_2$, which have three 5- and one 7-, 8-, or 9-membered chelate rings. The 4-coordinate complexes afford six-coordinate octahedral complexes $[NiX_2L]$ by treating with appropriate potassium salts such as KCl, KBr, or KSCN. These new complexes were characterized in a usual way. As is the case for analogous tetraazamacrocyclic Ni(II) complexes, all the present complex perchlorates give equilibrium mixtures of violet to green paramagnetic 6-coordinate $[NiL(H_2O)_2]^{2+}$ and yellow diamagnetic

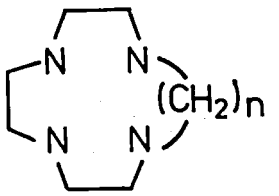

$[NiL]^{2+}$ in water. The equilibrium constants and the thermodynamic parameters were determined at ionic strength of 0.1 ($NaClO_4$) from temperature dependence of the electronic spectra. In the case of the $N_4$8 system, the equilibrium is shifted strongly toward the 4-coordinate species owing to the stereochemical consequence of the 8-membered ring. Ligand field spectra of the 6-coordinate complexes show a remarkable ring size effect.

Reference

1) IMS Graduate Student from Nagoya Univ. (1980).

V-F-2 Tetraaza Macrocyclic Nickel(II) Complexes Having Seven-, Eight-, and Nine-Membered Chelate Rings. II. X-ray Structural Studies of *Trans*-dichloro(1,4,7,10-Tetraazacyclotetradecane)nickel(II) Monohydrate, 1,4,7,10-Tetraazacyclopentadecanenickel(II) Perchlorate, and *Trans*-dichloro(1,4,7,10-Tetraazacyclohexadecane)nickel(II).

Masako SUGIMOTO, Haruko ITO *(Aichi Kyoiku Univ.)*, **Junnosuke FUJITA** *(Nagoya Univ. and IMS)*, **Koshiro TORIUMI, and Tasuku ITO**

Molecular structures of the title three compounds, *trans*-$[NiCl_2(N_4 7)]\cdot H_2O$, $[Ni(N_4 8)](ClO_4)_2$, and *trans*-$[NiCl_2(N_4 9)]$, have been determined (see the structural formulae in the preceding section for the abbreviations). Pertinent crystallographic data are summarized in Table I and perspective views of the complexes are shown in Figures 1-3. The 7-

Table I Crystallographic Parameters

	compound		
	trans-$[NiCl_2$-$(N_4 7)]\cdot H_2O$[a]	$[Ni(N_4 8)]$-$(ClO_4)_2$[b]	*trans*-$[NiCl_2$-$(N_4 9)]$[c]
formula	$NiCl_2N_4C_{10}H_{24}H_2O$	$NiN_4C_{11}H_{26}Cl_2O_8$	$NiCl_2N_4C_{12}H_{28}$
fw	347.95	471.96	357.98
space group	$P2_1/n$	$Pc2_1n$	C2/c
a, Å	12.102(1)	14.357(2)	16.747(5)
b, Å	16.803(2)	16.109(1)	10.390(2)
c, Å	7.672(2)	8.248(1)	11.708(5)
α, deg	90	90	90
β, deg	96.54(1)	90	126.16(1)
γ, deg	90	90	90
V, Å^3	1549.9 (3)	1907.9 (4)	1644.6 (9)
Z	4	4	4
d_c, g cm^{-3} (calcd)	1.49	1.64	1.45
d_m, g cm^{-3} (obs)	1.46 (at 24°C)	1.63	1.42 (at 16°C)
cryst size, mm	0.40 × 0.33 × 0.33	0.48 × 0.44 × 0.22	0.40 × 0.44 × 0.26
scan range	1.3 + 0.5tanθ	1.1 + 0.5tanθ	1.3 + 0.5tanθ
μ, cm^{-1}	1.59	1.34	1.49
2θ range, deg	2-60	2-65	2-65
no. of data	3836	2071	3213
$\|F_o\| > 3\sigma(\|F_o\|)$	3770	2068	3088
no. of variables	268	340	148
R	0.049	0.048	0.028
R_w	0.075	0.057	0.038

[a] Diffraction data were measured at −114°C. Unit cell parameters at 20°C are: a = 12.181(1), b = 16.874(2), c = 7.764(1) Å, β = 96.64(1)°, V = 1585.1(3) Å^3, d_{calcd} = 1.46 g cm^{-3}. [b] Data at 21°C. [c] Diffraction data were measured at −109°C. Unit cell parameters at 20°C are: a = 16.857(4), b = 10.437(2), c = 11.752(4) Å, β = 125.89(2)°, V = 1675.2(8) Å^3, d_{calcd} = 1.42 g cm^{-3}.

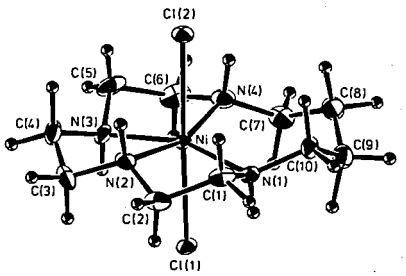

Figure 1.
A perspective view of *trans*-[$NiCl_2(N_47)$].

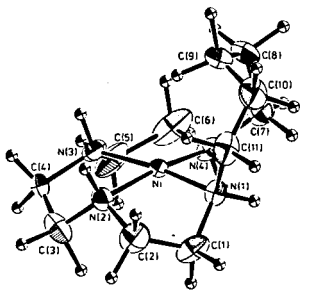

Figure 2.
A perspective view of $[Ni(N_48)]^{2+}$.

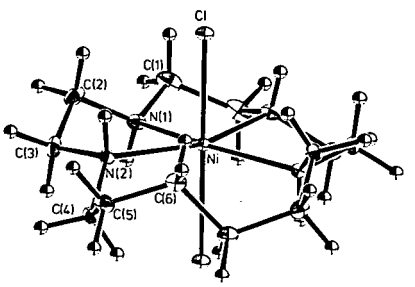

Figure 3.
A perspective view of *trans*-[$NiCl_2(N_49)$].

membered chelate ring in *trans*-[$NiCl_2(N_47)$] adopts a skew(h) conformation with a mean Ni-N distance of 2.07(2) Å. The 8-membered ring of $[Ni(N_48)]^{2+}$ takes an intermediate structure between crown and boat-boat in terms of cyclooctane conformer with a mean Ni-N distance of 1.909(8) Å. The 9-membered ring of *trans*-[$NiCl_2(N_49)$] adopts a structure very similar to twist-boat-chair conformation in terms of cyclooctane conformer with a Ni-N distance of 2.236(1) Å. A macrocycle in each compound adopts a rather contorted conformation in order to minimize angular, torsional, and bond length strain within the middle size chelate ring and about the metal. Considerable chelate ring strain has been noted in structural parameters of the 8- and 9-membered chelate rings. For the complexes of *trans*-$NiCl_2N_4$ type including reported analogous complexes, a "*cis effect*" was observed: a Ni-Cl distance decreases as a Ni-N distance increases. The nature of the *cis* effect must be electronic in origin since the spacial orientation of the ligands indicate no obvious intramolecular steric interactions of the same nature.

V—G A Pressure Effect on the Photo-induced Electron Transfer Reactions between *Tris*(2,2′-bipyridine)ruthenium(II) Ion and Variously Charged Metal Complex Ions

Fumio B. UENO,[1] **Tasuku ITO, Yoichi SASAKI** *(Tohoku Univ.)*,
Kazuo SAITO *(Tohoku Univ.)*

Triplet state lifetime of $[Ru(bpy)_3]^{2+}$ ion in water was not affected by pressure, although a remarkable pressure effect was observed in some organic solvents. The electron-transfer quenchings of photo-excited $[Ru(bpy)_3]^{2+}$ by $[Mo(CN)_8]^{4-}$ and Eu_{aq}^{2+} gave large positive and negative activation volumes ($\Delta V^{\neq}$ = +24.7 and −10.2 $cm^3\ mol^{-1}$), respectively, whereas those by some other quenchers having rate constants more than $10^9\ M^{-1}\ s^{-1}$ showed a small pressure effect regardless of the charge of a quencher. Figure shows an example of the Stern-Volmer plots. The data are summarized in Table I. The activation volumes of the quenching reactions cannot be explained simply by the charge of quenchers or the free energy of the quenching reactions.

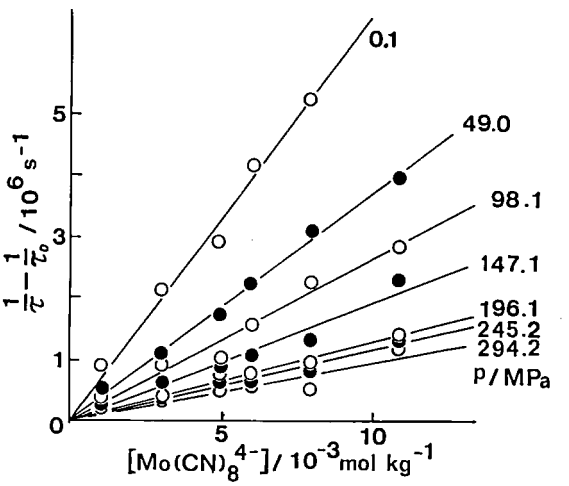

Table I Activation volume and rate constant for the quenching of photo-excited $[Ru(bpy)_3]^{2+}$.

	Quencher	Product [a]	$\Delta V^{\neq}$/cm^{3}mol^{-1}	k_q/10^{9}M^{-1}s^{-1} [b]
1	$[Fe(CN)_6]^{3-}$ [c]	$[Ru]^{3+}$ + Q^-	0.0 ± 0.1	5.6
2	$[(en)_2\overset{NH_2}{\underset{O_2}{}}Co(en)_2]^{4+}$ [d]	$[Ru]^{3+}$ + Q^-	0 ~ + 1.0	1.9
3	$[(NH_3)_5Co\text{-}O_2\text{-}Co(NH_3)_5]^{5+}$ [d]	$[Ru]^{3+}$ + Q^-	+1 ± 2	1.9
4	$[(CN)_5Co\text{-}O_2\text{-}Co(CN)_5]^{5-}$ [c]	$[Ru]^{3+}$ + Q^-	0 ~ +1.2	4.8
5	Tl^{3+} [e]	$[Ru]^{3+}$ + Q^-	+0.2 ± 0.1	1.02
6	$[Mo(CN)_8]^{4-}$ [c]	$[Ru]^{+}$ + Q^+	+24.7 ± 0.6	0.63
7	$[Os(CN)_6]^{4-}$ [c]	$[Ru]^{+}$ + Q^+	+6.8 ± 2.0	0.84
8	$[Fe(CN)_6]^{4-}$ [c]	$[Ru]^{+}$ + Q^+	−5.4 ± 0.5	0.27
9	$[IrCl_6]^{3-}$	$[Ru]^{+}$ + Q^+	+1.1 ± 0.5	0.83
10	Eu_{aq}^{2+} [f]	$[Ru]^{+}$ + Q^+	−11.0 ± 1.0	0.0082
11	$[Fe(H_2O)_6]^{2+}$ [d]	$[Ru]^{+}$ + Q^+	−0.6 ± 0.6	0.01
12	$[Co(NH_3)_5(H_2O)]^{3+}$ [d]	$[Ru]^{2+}$ + *Q	−2.6 ± 0.6	0.14

[a] $[Ru]^{3+}$ + Q^-, quencher is reduced by $*[Ru]^{2+}$; $[Ru]^{+}$ + Q^+, quencher is oxidised by $*[Ru]^{2+}$; $[Ru]^{2+}$ + Q^+, quencher is sensitized by $*[Ru]^{2+}$ (see, V. Balzani, L. Moggi, M. F. Manfrin, and F. Bolletta, *Coord. Chem. Rev.*, 1975, **15**, 347). [b] k_q, bimolecular quenching rate constat at 25°C, 1 atm. [c] 0.1 M HCl, I = 0.25 M(NaCl). [d] 0.05 M H_2SO_4, I = 0.25 M(NaCl). [e] 4.75 M $HClO_4$. [f] 0.5 M $HClO_4$.

Reference

1) IMS Graduate Student from Tohoku Univ. (1980-)

V—H Structural Studies of Some Tetraaza Macrocyclic Nickel(II) Complexes

V-H-1 The Structure of *Cis*-diisothiocyanato-(1, 4, 7, 10-Tetraazacyclotetradecane)nickel(II). Electronically Controlled *Cis*-Coordination.

Masako SUGIMOTO, Haruko ITO *(Nagoya Univ.)*, **Koshiro TORIUMI, and Tasuku ITO**

This study was undertaken in order to investigate a "*cis effect*" (see Research Activity V-F-2). Crystal data: $Ni(NCS)_2(C_{10}H_{24}N_4)$, orthorhombic, $Pbn2_1$, a = 11.399(1), b = 16.231(2), c = 9.503(2) Å, U = 1758.1(4) Å^3, Z = 4, D_c = 1.42, D_m = 1.41 Mg m^{-3}, R = 0.042 for 2033 independent reflections ($2\theta_{MoK\alpha} < 70°$). The complex is of *cis*(NCS) type with the titled macrocyclic ligand folded. On the other hand, the dichloro complex having the same macrocyclic ligand, $NiCl_2(C_{10}H_{24}N_4)$, has a coordination geometry of *trans*-$NiCl_2N_4$ type (see Research Activity V-F-2). It is most reasonable to consider the observed *cis* stereochemistry to be a result of the electronically controlled *cis effect*, in view of the strong ligand field of NCS^- and the hole size of the tetraazamacrocyclic ligand.

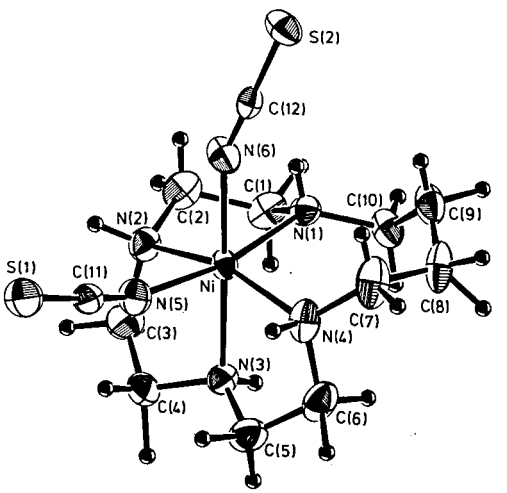

V-H-2 The Molecular Structure of 1*R*, 2*R*, 4*S*, 7*S*, 8*R*, 9*R*, 11*S*, 14*S*-Octametyl-1, 4, 8, 11-tetraazacyclotetradecanenickel(II) Perchlorate

Tasuku ITO, Haruko ITO *(Nagoya Univ.)* **and Koshiro TORIUMI**

[*Acta Crystallogr.*, **B37**, 1412 (1981)]

The title compound crystallizes in tetragonal space group $P4_32_12$ with unit cell parameters of a = 8.872(1), c = 33.368(2) Å, U = 2626.5 Å^3, Z = 4, D_c = 1.44, D_m = 1.44 Mg m^{-3}. The structure was refined to R = 0.034 for 2343 independent reflections ($2\theta_{CuK\alpha} < 155°$). The fourteen-membered macrocyclic ligand adopts a basket type configuration with all the four NH groups on the same side of the coordination plane. The absolute configurations of the eight chiral centers were determined. The total sterochemistry was exactly the same as deduced from a previous NMR study including a novel observation of intramolecular Nuclear Overhauser Effect combined with stereospecific deuteration and strain energy calculation.[1]

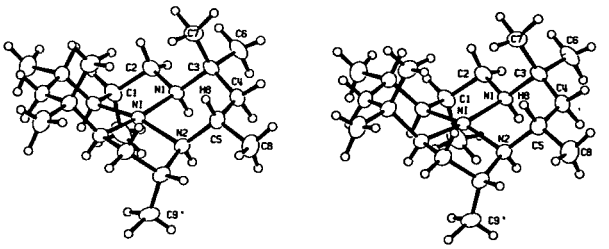

Reference

1) T. Ito and D. H. Busch, *J. Am. Chem. Soc.*, **95**, 7528 (1973).

V—I Structural Studies of Some New Cobalt(III) Complexes Having a Co-P Bond

V-I-1 The Crystal and Molecular Structures of Diisothiocyanatobis{(2-aminoethyl)diphenyl phosphine}cobalt(III) Ions, *trans*(NCS,NCS),*cis* (P, P)-$[Co(NCS)_2\{NH_2CH_2CH_2P(C_6H_5)_2\}_2]Br \cdot 3H_2O \cdot (CH_3)_2CO$ (1), *trans*(NCS, NCS), *cis*(P, P)-$[Co(NCS)_2\{NH_2CH_2CH_2P(C_6H_5)_2\}_2](PF_6)_{1/3} \cdot (F)_{2/3} \cdot (PF_5)_{1/3} \cdot H_2O$ (2), *cis*(NCS, NCS),*trans*(P, P)-$[Co(NCS)_2\{NH_2CH_2CH_2P(C_6H_5)_2\}_2]Br \cdot CH_3OH$ (3)

Masamichi ATOH *(Nagoya Univ.)*, **Kazuo KASHIWABARA** *(Nagoya Univ.)*, **Haruko ITO** *(Nagoya Univ.)*, **Junnosuke FUJITA** *(Nagoya Univ. and IMS)* **and Tasuku ITO**

Pertinent crystallographic data are given in Table I and perspective drawings of the complexes **1** - **3** are shown in Figures 1-3, respectively. Each of the *trans*(NCS,NCS) and *cis*(NCS,NCS) complexes gives only one isomer of two and three possible geometrical isomers, respectively. The phosphorus atoms in both **1** and **2** occupy the *cis* positions, and the P-Co-P angle of 102-103° widens remarkably owing to steric repulsions among the bulky phenyl groups. The average Co-NH_2 distance of 2.011 Å is longer than that of $[Co(en)_3]^{3+}$ (en = $NH_2CH_2CH_2$-NH_2, 1.979 Å), the *trans effect* of the phosphorus donor atom operating on the Co-NH_2 bond. Complex **3** has the *cis*(NCS,NCS), *trans*(P,P) configuration, and the Co-NH_2 distance of 1.979 Å is similar to that of $[Co(en)_3]^{3+}$.

Table I

Complex	1	2	3
Crystal system	Monoclinic	Rhombohedral	Triclinic
Space group	$P2_1/a$	$R\bar{3}$	$P\bar{1}$
a Å	23.094(3)	26.003(2)	13.158(2)
b Å	17.513(3)	26.003(2)	14.138(2)
c Å	9.755(2)	27.080(5)	9.723(1)
α °	90	90	104.99(1)
β °	105.23(1)	90	97.41(1)
γ °	90	120	103.6(2)
U Å^3	3806(1)	15857(3)	1663.1(5)
Z	4	18	2
μ(Mo $K\alpha$) cm^{-1}	18.19	8.28	20.58
R %	4.39	5.58	4.46
R_w %	5.99	9.53	5.06

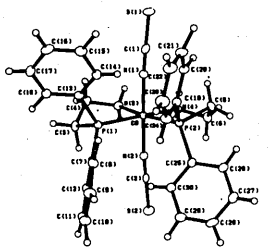

Figure 1.
A perspective view of the complex **1**.

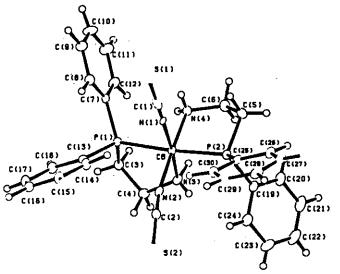

Figure 2.
A perspective view of the complex **2**.

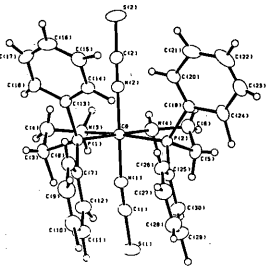

Figure 3.
A perspective view of the complex **3**.

V-I-2 The Molecular Structure of *Cis*-β-{(2-Aminoethyl)dimethylphosphine}{N,N'-bis(2-aminoethyl)-1,3-propanediamine} cobalt(III) Bromide Dihydrate, $[Co\{NH_2CH_2CH_2P(CH_3)_2\}(NH_2CH_2CH_2NHCH_2CH_2CH_2NHCH_2CH_2NH_2)]Br_3 \cdot 2H_2O$

Tomoji OISHI,* Kazuo KASHIWABARA,* Haruko ITO,* Junnoske FUJITA *(Nagoya Univ. and IMS)*, **Koshiro TORIUMI, Tasuku ITO** *(* Nagoya Univ.)*

The title compound crystallizes in monoclinic space group $P2_1/a$ with unit cell parameters of a = 17.719(2), b = 8.776(1), c = 14.966(1) Å, and β = 108.01(1)° (U = 2213.2, Z = 4, D_c = 1.80, D_m = 1.80 Mg m^{-3}). The structure was refined to R = 0.043 for 3687 independent reflections ($2\theta_{MoK\alpha} < 60°$). The complex ion adopts a *cis*-β type geometry with the six-membered chelate ring in the chair form. The phosphorus atom occupy the *cis* position of two terminal NH_2 groups of 2,3,2-tet ligand. The *trans effect* of the phosphorus donor atom operates on the Co-N(2) bond, the distance of which lengthens to 2.029(4) Å.

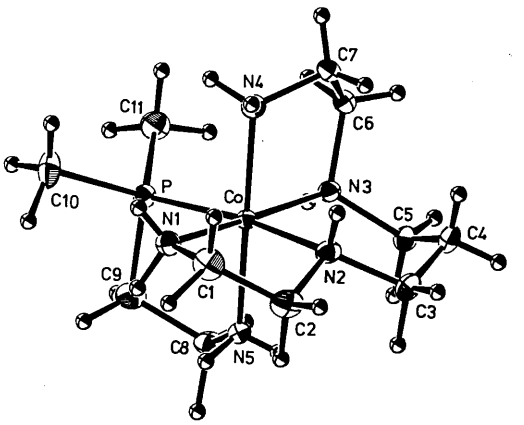

V—J Structural Studies of Some Coordination and Organic Compounds of Interest

V-J-1 The Crystal Structure of $[Pt(NH_3)_4][Pt(NH_3)_4Br_2](HSO_4)_4$

Masako TANAKA,* Koshiro TORIUMI, Tasuku ITO, and Ikuji TSUJIKAWA* *(* Kyoto Univ.)*

The title compound was obtained by the oxidation of $[Pt(NH_3)_4][PtBr_4]$ in 62% sulfuric acid solution. Lustrous light green needle crystals were grown by standing for the solution. The crystal structure of the compound was determined by single crystal X-ray diffractometry. The complex crystallizes in the monoclinic space group $P2_1/a$ with cell dimensions, a = 10.654(1), b = 10.282(1), c = 5.505(1) Å, β = 93.17(1), and Z = 2. The final R value is 0.029 for 1448 reflections. The complex units are stacked in chains along c, along which Pt and Br are located alternately. Br atoms are distributed over two half-occupied positions near the center of symmetry (0, 0, 1/2). These two positions are 0.55 Å aparts, the two Pt-Br distances being 3.029(2) and 2.476(1) Å, respectively. These values can be compared with the corresponding distances in the ethylamine derivative of 3.12 and 2.46 Å. In contrast to Wolffram's salt analogues, Weissenberg photographs of this compound showed

no evidence for a one-dimensional superstructure along the Pt-Br–Pt chain. This can be explained by supposing random distribution of Pt^{II} and Pt^{IV} along the chain.

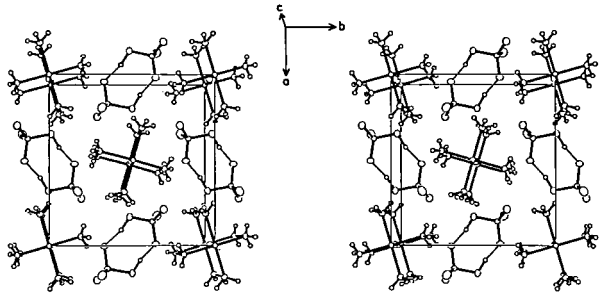

V-J-2 The Crystal and Molecular Structure of Flavanthrene

Koshiro TORIUMI, Kinko KOYANO *(Aichi Kyoiku Univ.)*, **Naoki SATO, Hidemasa TAKAYA, Tasuku ITO, and Hiroo INOKUCHI**

[*Acta Cryst.*, **B38** (1982), in press]

Flavanthrene was obtained by the reduction of flavanthrone. Single crystals were grown by sublimation in *vacuo* at 270°C. Crystals are monoclinic, space group $P2_1/a$, a = 16.179(2), b = 3.7996(2), c = 15.818(1) Å, β = 119.192(6)° and Z = 2. The Crystal structure was determined by single crystal X-ray diffractometry. The final R is 0.041 for 1441 observed amplitudes. Flavanthrene molecule is planar, the maximum deviation from the plane being 0.023(1) Å. As shown in Figure, the molecules are stacked to form a roof-top type structure. Interplanar spacing between molecules is 3.4711(5) Å. The proportion of overlapped area of molecular plane is about 54%.

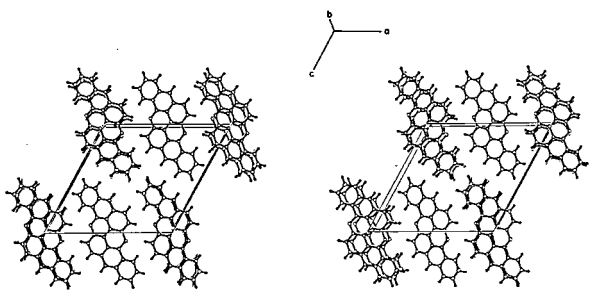

V-J-3 A Structure of an Important Metal Complex in the Asymmetric Synthesis of α-Amino Acids. The Crystal Structure and Absolute Configuration of (-)$_{546}$-β_2-[(*R*)-alaninato{6(*R*), 8(*R*)-6,8-dimethyl-2,5,9,12-tetraazatridecane}cobalt(III)] Bromide Trihydrate,(-)$_{546}$-β_2-{Co(*R*-ala)(1,5*R*,7*R*,11-Me$_4$-2,3,2-tet)}$Br_2 \cdot 3H_2O$

Masanobu AJIOKA,* Shigenobu YANO,* Sadao YOSHIKAWA,* Koshiro TORIUMI, and Tasuku ITO *(* Univ. of Tokyo)*

The crystal and molecular structure of (-)$_{546}$-β_2-[Co(*R*-ala)(1,5*R*, 7*R*, 11-Me$_4$-2, 3, 2-tet)]$Br_2 \cdot 3H_2O$ which was derived from [Co(AMM) (1,5*R*, 7*R*, 11-Me$_4$-2,3,2-tet)]$^+$ on decarboxylation has been determined from three-dimensional X-ray data collected by the diffractometer method, where AMM is α,α-aminomethylmalonate. The compound forms orthorhombic crystals with a = 11.713(1) Å, b = 20.301(2) Å, c = 10.113(2) Å, and Z = 4, in space group $P2_12_12_1$. The calculated density of 1.60 g cm^{-3} for four formula units in the unit cell agrees with the observed density of 1.61 g cm^{-3}. The structure has been solved by the heavy-atom method and refined by full-matrix least-squares methods with anisotropic temperature factors to give an R value of 0.054 for 2168 independent reflections with $Fo > 3\sigma(Fo)$. A detailed view of the complex cation is given in Figure. The absolute configuration of the complex cation is Λ, the conformations of the two five-membered chelate rings for the tetramine are δ, and the central six-membered ring adopts the chair conformation with one methyl group axial and the other equatorial. The secondary nitrogen atoms have *S* chirality except for one terminal nitrogen atom, the absolute configuration of which is *R*. The N-methyl group in the "out-of-plane" five-membered ring is equatorial, whereas the other in the "in-plane" five-membered ring has an axial disposition. The alanine coordinates to the cobalt *via* N and O atoms in the β_2 form. The absolute configuration around the carbon center of the alanine is found to be *R*.

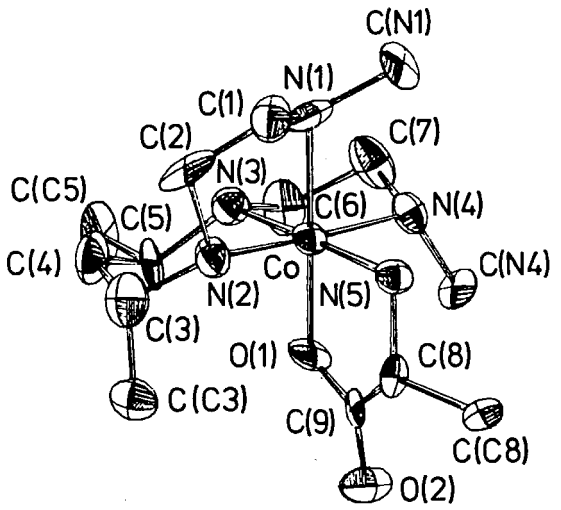

V-J-4 The Absolute Configuration of (-)$_{589}$-2,2'-bipiperidine — The Crystal Structure of (-)$_{546}$-*trans*-Dinitrobis{(-)$_{589}$-2,2'-bipiperidine}cobalt(III) *d*-3-Bromocamphor-9-sulfonate Tetrahydrate

Mitsunobu SATO,* Yoichi SATO,* Shigenobu YANO,* Sadao YOSHIKAWA,* Koshiro TORIUMI, and Tasuku ITO *(* Univ. of Tokyo)*

The stereochemistry of octahedral metal complexes containing N-alkyl group substituted polyamines has been of much interest. Although the diamines with aliphatic heterocyclic ring belong to N-alkylated polyamines, there is very limited information concerning their stereochemical behaviour to transition metal ions. Recemic 2,2'-bipiperidine (2,2'-bpp), which has two six-membered heterocyclic rings, was resolved into optical isomers through its *trans*-dinitrobis(diamine)cobalt(III) complex, by using ammonium *d*-3-bromocamphor-9-sulfonate (NH_4 *d*-BCS). The crystal structure of the title compound was determined from three-diemnsional X-ray counter data. Figure shows a perspective drawing of the complex cation. The complex cation has approximate C_2 symmetry. The absolute configurations around the asymmetric carbon atoms are both *R* for (-)$_{589}$-2,2'-bpp, and the conformations of the two five-membered chelate rings are both λ. The four six-membered heterocycles involving the secondary nitrogen atoms adopt the chair conformation. The absolute configurations about the four secondary nitrogen atoms are all *S*. It seems that water molecules of crystallization play an important role in the diastereomeric discrimination of the complex cation by *d*-BCS.

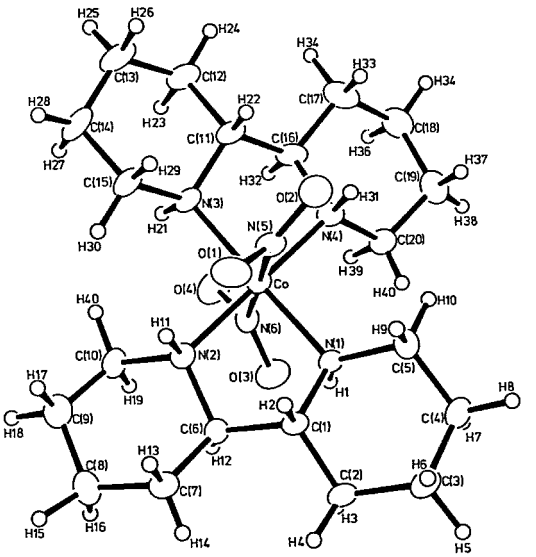

V-J-5 The Crystal Structure of Bis(ethylenediamine)oxalatocobalt(III) dicyanobis(glycinato)cobaltate(III) Trihydrate

Masao SEKIZAKI,* Shuhei FUJINAMI,* Koshiro TORIUMI and Tasuku ITO *(* Kanazawa Univ.)*

In the course of the spectroscopic and configurational investigations of $[Co(CN)_2(N)_2(O)_2]^-$ series, the crystal structure of the title compound, $\Delta(-)_{589}$-$[Co(ox)(en)_2](+)^{CD}_{500}[Co(CN)_2(gly)_2]\cdot 3H_2O$, was determined by X-ray diffrectometry. Crystals are orhtorhombic with the space group of $P2_12_12_1$, a = 10.967(3), b = 26.116(5), c = 7.807(2) Å, and Z = 4. The structure was refined to give R = 0.027 for 3073 independent reflections. The structure of the anion is shown in Figure. The structure and the absolute configuration of the cation were coincident with those reported by Aoki *et al.*[1] The absolute configuration of the anion was derived by comparison with the cation. The anion, $(+)^{CD}_{500}[Co(CN)_2(gly)_2]^-$, has slightly distorted octahedral geometry with the Δ configuration. Each glycinato ion coordinates through the nitrogen and the oxygen atoms, and the remaining positions are occupied by the two CN^- ions. Thus the arrangement of the

ligating atoms around the cobalt is *cis*(C), *cis*(N), and *cis*(O). The cations are connected to one another by hydrogen bonds to form a layer parallel to the (010) plane. The anions and water molecules exist between the layers and combine these layers by hydrogen bonds.

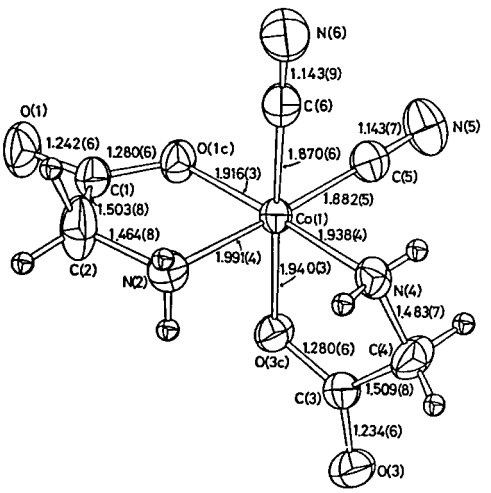

Reference

1) T. Aoki, K. Matsumoto, S. Ooi, and H. Kuroya, *Bull. Chem. Soc. Jpn.*, **46**, 159 (1975).

V-J-6 The Crystal and Molecular Structure of *Cis*-dichlorobis(1,10-phenanthroline)molybdenum(III) Chloride Tetrahydrate

Koshiro TORIUMI and Tomoji S. MORITA,* Tasuku ITO and Kazuo SAITO* *(* Tohoku Univ.)*

In recent years, chemistry of molybdenum compounds have attracted much attension. In this study, the structure of the titled new molybdenum-(III) compound has been determined by X-ray diffractometry. Crystals of the title compound are monoclinic, space group C2/c, a = 15.791(3), b = 13.806(2), c = 12.664(2) Å, β = 100.25(1)° and Z = 4. The crystal structure has been refined to give an R value of 0.050 for 2817 observed reflections. As shown in Figure, the complex cation has C_2 symmetry. The molybdenum has coordination geometry of *cis*-$MoCl_2N_4$ type. The Mo-Cl distance is 2.396(2) Å, and the Mo-N distances average 2.164(5) Å.

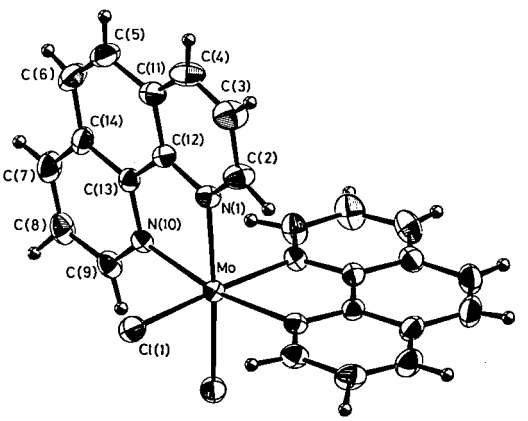

V—K An Analysis of Thermochromism of Some Iron(III) Spin-state Equilibrium Systems in Solution by SALS

Hiroaki NAKAYAMA *(Kagawa Nutrition College)*, **Masako SUGIMOTO, and Tasuku ITO**

The temperature dependence of the electronic spectra of spin-state equilibrium systems, $[Fe^{III}(Sal_2trien)](NO_3)$ in H_2O (**1**) and $[Fe^{III}(3\text{-MeO})\text{-}Sal_2(3,2,3\text{-tet})](NO_3)$ in methanol (**2**), were investigated throughly by means of a nonlinear least-squares program SALS.[1] The system (**1**) shows remarkable thermochromism around the midpoint of the equilibrium, while the system (**2**) shows small one. In order to determine thermodynamic parameters ΔH and ΔS, and spectra of high- and low-spin species, values of T_i, ΔH, $-RlnK_s$, Fs_j and Dec_j were parametrized so as to lessen the correlation between each two of parameters, where T_i denotes i-th temperature, K_s the equilibrium constant K =

[low-spin]/[high-spin] at Ts (Ts = 298.16 K used as an internal constant), Fs_j the absorbance at Ts and at j-th wavelength, $Dec_j = (\epsilon_{Lj} - \epsilon_{Hj})/\Delta H$, and ϵ_{Lj} and ϵ_{Hj} molar extinction coefficients of low- and high-spin species at j-th wavelength. The data were about 500 in number for each system. Figures 1 and 2 show the resolved spectra of the low- and high-spin species for the systems (**1**) and (**2**), respectively, for which ΔH (in kcal mol^{-1}), ΔS (in eu), and Ks were −4.9(5), −16.3(16), and 1.03(3), and −6.2(22), −19.3(88), and 2.3(10), respectively. The precision was fairly high for the equilibrium constants (K) despite of relatively large uncertainty in ΔH, which propagates to the standard deviations of ΔS, ϵ_{Lj}, and ϵ_{Hj} ($\sigma_{\epsilon Lj} = \sigma_{\epsilon Hj}/Ks = \sigma_{\Delta H} \cdot Dec_j/(\Delta H)^2(1 + Ks)$, see Figures 1 and 2). It should be mentioned that the reliable solution was obtained even for the system (**2**), which show so small thermochromism, because of the close resemblence of the spectra of the high- and low-spin species, that it seems difficult to analyze the equilibrium by conventional methods formerly used.

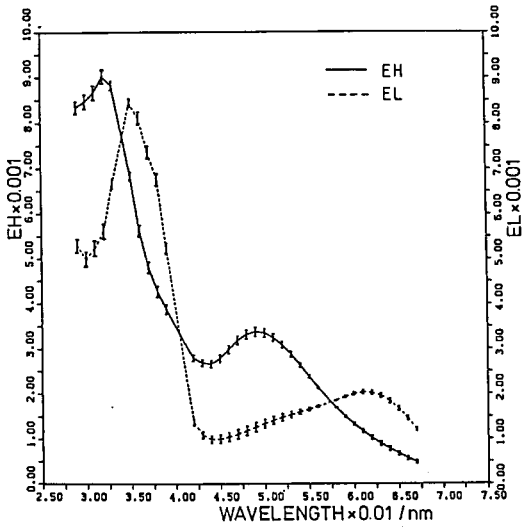

Figure 1. Calculated electronic spectra for high-(—) and low-spin (····) $[Fe^{III}(Sal_2trien)]^+$.

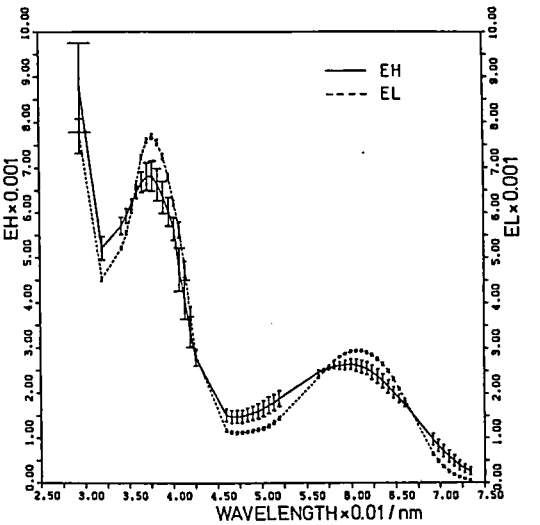

Figure 2. Calculated electronic spectra for high-(—) and low-spin (····) $[Fe^{III}\{(3\text{-MeO})Sal\}_2(3,2,3\text{-tet})]^+$.

Reference

1) T. Nakagawa and Y. Oyanagi, "Saishojijoho Hyojun Program SALS Riyonotebiki", the Computer Center of the University of Tokyo (1979).

RESEARCH ACTIVITIES VI

COMPUTER CENTER

VI—A Theoretical Investigations of Metalloporphyrins and Charge-Transfer Complexes by the Ab Initio SCF MO Method

Metalloporphyrins and charge-transfer complexes are interesting polyatomic systems because of their complicated electronic structure and because of their catalytic function. Heme and flavin are prominently important as an active center of energy conversion processes in biological systems. In this project the electronic structure and the fundamental functions are studied for several complexes by performing ab initio MO computations.

VI-A-1 Theoretical Studies of Electronic States and Mössbauer Spectra of High-, Intermediate-, and Low-Spin Fe(II)-Porphyrin Complexes by Ab Initio MO Calculations

Shigeru OBARA and Hiroshi KASHIWAGI

It is known empirically that there is a relation of isomer shift (IS) and quadrupole splitting (QS) observed from Mössbauer experiment to oxidation number and spin of complex. One of our interests is to investigate the origin of this relation from a theoretical analysis of Fe-porphine (FeP), Fe-porphine-pyridine (FeP(py)) and Fe-porphine-pyridine-carbonmonoxide (FeP(py))CO) by ab initio method.

We have plotted V_{zz}, the component perpendicular to the porphine plane of electric field gradient (EFG) tensor, on which QS depends, obtained from ab initio method and from a simple estimation with an atomic 3d orbital and formal occupation numbers. All points are nearly on three straight lines, as in Figure 1, expressed as flollows: $V_{zz} = \sum_i n_i \cdot A_i + C$. It should be stressed that the coefficient of the first term is unity for all three ferrous complexes. The second term C is constant and depends on each complex. The large positive C value of FeP, which means that the charge distribution around the Fe nucleus is distorted from spherical to oblate, comes from that FeP has no axial ligands and has four ligated nitrogen atoms with one half of excess negative charge. In FeP(py) the C value is reduced by the weak ligation of pyridine. C is close to zero in FeP(py)CO because of the strong axial ligand CO. It can be said that complexes with the same oxidation number and the same spin do not necessarily have a similar QS value if they have different types of ligands. The QS value of Fe-porphyrin complexes are determined by two factors, the formal d-electron configuration and the species of axial ligands.

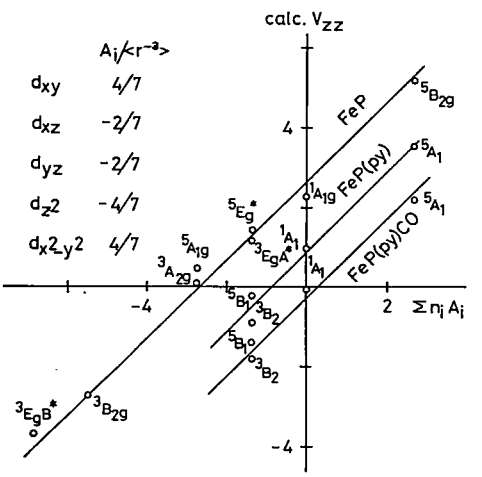

Figure 1. The calculated V_{zz} versus $\Sigma\, n_iA_i$, where n_i is a formal occupation number and A_i is V_{zz} value of an atomic 3d orbital. In the estimation of V_{zz}, the value of the radial integral $\langle r^{-3}_i\rangle$ is 4.7791 a.u., using the atomic 3d orbital of ^5D state of Fe atom.

VI-A-2 Ab Initio SCF Calculations on Oxyhemoglobin and Oxymyoglobin Models

Tsunenori NOZAWA *(Tohoku Univ.)*, **Masahiro HATANO** *(Tohoku Univ.)*, **Unpei NAGASHIMA** *(IMS Graduate Student 1980- from Hokkaido Univ.)*, **Shigeru OBARA, and Hiroshi KASHIWAGI**

The nature of the iron-oxygen bond in oxyhemoglobin and oxymyoglobin are still undetermined. X-ray data from a model and oxymyoglobin support the bent Fe-O_1-O_2 geometry proposed by Pauling. However, questions concerned with the details of the bonding and the charge on the oxygen have not been resolved.

We have tried *ab initio* LCAO SCF MO calculations to predict energy levels and Mössbauer parameters on a model oxyheme shown in Figure 1. Table I shows the calculated SCF energy for the three groups of states with different configurations. The lowest states in the SCF energy were found to be the configuration $(d\epsilon)^5(\pi_g^a)^2(\pi_g^b)^1$ whose electronic structure can be expressed as Fe(III)-O_2^-. Calculated Mössbauer parameters of those states are in good agreement with experiments for oxyhemoglobin, while those of the closed-shell singlet state $(d\epsilon)^6(\pi_g^a)^2$ are inconsistent with experiments. The Fe-O_1 overlap populations indicate bonding nature for the former states and nonbonding for the latter state. It was suggested from the consideration of the configuration mixing that there exists a low-lying triplet state of Fe(III)-O_2^- structure just above the singlet ground state.

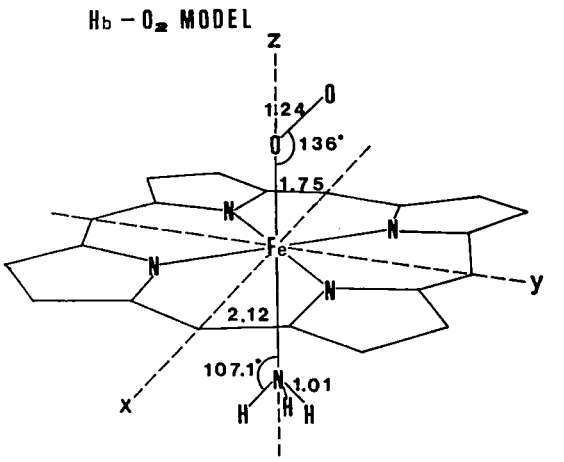

Figure 1. The relative orientation and bond lengths (Å) of the dioxygen and distal ammonia molecules in the model oxyheme.

Table I. SCF Total Energies and Mössbauer Parameters Calculated for Various Electronic Configurations of Model Oxyheme.

State	Formal occupation number							SCF	Mössbauer parameter		
	Fe					O_2		total	ΔE_Q	η	Direction
	$d_{x^2-y^2}$	d_{xz}	d_{yz}	d_{z^2}	d_{xy}	π_g^a	π_g^b	energy			of largest V_{ii}[a]
	a′	a′	a″	a′	a″	a′	a″				
$^1A'$	2	2	2	0	0	2	0	−2444.6630	0.64	0.50	zz
b^5A''	2	2	1	0	1	1	1	.6674	3.60	0.15	zz
a^5A''	1	2	2	1	0	1	1	.6951	−4.19	0.15	zz
b^5A'	1	2	2	0	1	1	1	.7056	0.97	0.36	zz
a^5A'	2	2	1	1	0	1	1	.7064	1.42	0.68	yy
$^1A''C$	2	1	2	0	0	2	1	.7508	−1.19	0.72	yy
b^3A''	2	1	2	0	0	2	1	.7520	−1.21	0.65	yy
a^3A''	1	2	2	0	0	2	1	.7526	0.93	0.01	xx
$^3A'$	2	2	1	0	0	2	1	.7512	−1.17	0.53	xx
						observed			−2.10	0.23	xx or yy

a) The symbols x, y, and z denote molecular axes in Figure 1.

VI-A-3 Ab Initio MO Study of the Stacking Complexes, Flavin-Tyrosine, Flavin-Tryptophan, and Flavin-NADH

Yoshitaka WATANABE*, Kichisuke NISHIMOTO* and Hiroshi KASHIWAGI (*: *Osaka City Univ.*)

In the previous paper, it is pointed out that the ab initio SCF MO method based on STO-3G basis set is not appropriate for the calculations of the charge transfer complexes. In order to investigate the charge transfer interaction, an extended basis set such as the 4-31G must be used. The charge transfer interaction between aromatic systems mainly comes from the π-electron interaction. Therefore, one approach is to use a split basis set for π-orbitals and STO-3G for σ-one's. We found that this approach works satisfactorily for benzen + TCNE (tetracyanoethylene) and naphthalene + TCNE complexes.

The STO-3G π-split basis set might be recommended for the ab initio SCF MO calculation of the very large stacking complex. We calculated the planar stacking interaction with the maximum phase overlapping geometry of HOMO of electron donor, and LUMO of electron acceptor (Figure 1). Since FMN, FAD, tryptophan, tyrosine and NADH are too large molecules for the ab initio MO calculation, we used lumiflavin, skatole, p-cresol and N-methyl-1, 4-dihydronicotinamide instead of them. The distance between the flavin plane and the plane of the stacking molecule is put to be 3.5 Å.

The calculated results are summarized as follows: Aromatic residue behaves as a weak electron donor and the flavin plays as a weak electron acceptor in the stacking interaction (Figure 2). When the aromatic residue of protein has a stacking interaction with the hydrophobic part of flavin in models (I) and (III), the π-electron population of hydrophilic part in flavin nucleus is varied. However, if the aromatic residue interacts with the hydrophilic part of flavin in model (II) and (IV), the hydrophobic part is not influenced by this interaction. The stacking interaction produces some amount of induced dipole moment in flavin complex as shown in Table I.

Table I. Lumiflavin-p-cresol, lumiflavin-skatole, and lumiflavin-N-methyl-1, 4-dihydronicotinamide complexes. (Intermolecular distance R = 3.5 Å)

Basis set	Geometry	Binding energy (Kcal/mol)	Total differential dipole moment (Debye)
STO-3G	I	−2.489	0.393
π-split	II	−2.071	0.564
	III	−2.358	0.533
	IV	−1.850	0.805
	V	−0.415	0.610

Using a threshold for overlap integral $|S_{ij}|$; 1×10^{-3} and a threshold for exchange integral $(ij|ij)^r$; 1×10^{-6} a.u.

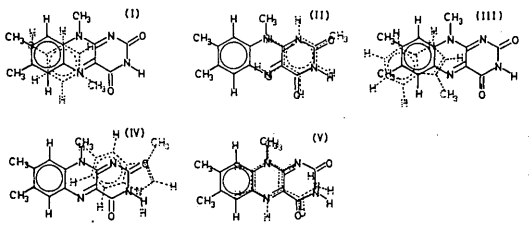

Figure 1. The geometries of the complexes of lumiflavin with the aromatic compounds.
(I) FMN-tyrosine complex model in *Desulfovibrio vulgaris* flavodoxin. (lumiflavin-p-cresol)
(II) FMN-p-cresol complex model in old yellow enzyme. (lumiflavin-p-cresol)
(III) FMN-tryptophan complex modle in *Desulfovibrio vulgaris* flavodoxin. (lumiflavin-skatole)
(IV) FMN-tryptophan complex modle in *Clostridium* MP flavodoxin. (lumiflavin-skatole)
(V) FAD-NADH complex model in glutathione reductase. (lumiflavin-N-methyl-1, 4-dihydronicotinamide)

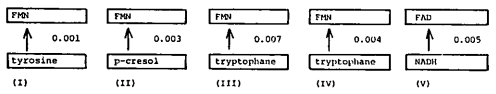

Figure 2. The charge flux diagram in flavoprotein.

VI-A-4 Ab Initio MO Study on Hydrogen Bonding in Lumiflavin-Water Complexes

Yoshitaka WATANABE*, Kichisuke NISHIMOTO*, Hiroshi KASHIWAGI, and Kunio YAGI** (*: *Osaka City Univ.*) (**: *Nagoya Univ.*)

In order to elucidate further the detailed effects of hydrogen bonding on the electronic structure of

the isoalloxazine nucleus of flavins, we carried out ab initio MO calculations of lumiflavin-water complexes, models of hydrogen bonded flavin in flavoprotein. Since the geometry of hydrogen bonded lumiflavin has never been determined experimentally, the equilibrium structure was calculated by geometry optimization. The structures of lumiflavin-water complexes are shown in Figure 1. Ab initio MO calculation was made on these complexes with the semiorthogonalized orbitals, using the program JAMOL3. The data are shown in Table I. The charge transfer in hydrogen bonding at each site can be quantitatively represented by charge migration (ΔQ). The strongest charge tranfer is occurring at O(14). It is noted that the value ϵ(LUMO)-ϵ(HOMO) obtained in the present study runs parallel with the value obtained previously by the P-P-P method. The order of the magnitude of the stabilization energy of hydrogen bonding was N(3)H > O(12) > N(5) > N(1) > O(14). The magnitude of the effect of hydrogen bonding on the electron acceptability of N(5) is in the order of N(5) > O(14) > N(1) > O(12) > N(3)H.

The calculated data were analyzed and difference charge density maps were delineated. From these results the following conclusions were obtained. (I) The polarization is delocalized over the polar part of flavin. An interesting fact is that C(8) is rather sensitive to the delocalization through π-type polarization. (II) The hydrogen bonding at O(14) or N(5) promotes significantly the electron acceptability of N(5). (III) The electron acceptability of C(4a) increases upon formation of the hydrogen bonding at N(3)H or N(5), but decreases upon formation of the hydrogen bonding at N(1) or O(12).

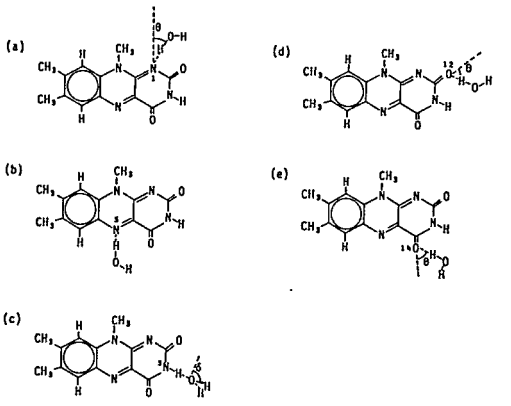

Figure 1. Possible structures of lumiflavin-water complexes. (a): N(1)-hydrogen bonding (R = 3.1 Å, θ = 30°); (b): N(5)-hydrogen bonding (R = 3.0 Å, θ = 0°); (c): N(3)H-hydrogen bonding (R = 2.6 Å, δ = 37.7°); (d): O(12)-hydrogen bonding (R = 2.77 Å, θ = 60°); (e): O(14)-hydrogen bonding (R = 2.7 Å, θ = 60°).

Table I. The calculated results on lumiflavin-water complexes

Hydrogen bonding	NO	N(1) (R = 3.1 Å) θ = 30°	N(5) (R = 3.0 Å) θ = 0°	N(3) (R = 2.6 Å) δ = 37.7°	O(12) (R = 2.77 Å) θ = 60°	O(14) (R = 2.7 Å) θ = 60°
ΔQ	——	−0.021	−0.026	+0.074	−0.038	−0.046
ΔE	——	5.64	5.78	7.81	6.25	5.51
LUMO energy	0.1345	0.1271	0.1237	0.1478	0.1283	0.1258
HOMO energy	−0.2209	−0.2306	−0.2275	−0.2079	−0.2292	−0.2267
HOMO-LUMO energy	−0.3553	−0.3577	−0.3511	−0.3557	−0.3575	−0.3525
Coefficient of LUMO at						
N(5)	0.5426	0.5478	0.5524	0.5323	0.5452	0.5504
C(4a)	−0.4214	−0.4123	−0.4299	−0.4284	−0.4107	−0.4169

ΔQ: calculated charge migration, ΔQ = Q(lumiflavin, hydrogen bonding) − Q(lumiflavin, free)

ΔE: hydrogen bonding energy (kcal/mol)

VI-A-5 Theoretical Study of Degree of Covalency in Some CoF_6(n-) Complexes (n = 4, 3, and 2)

Eisaku MIYOSHI *(Fukuoka Dental Coll.)*, **Shigeru OBARA, Toshikazu TAKADA** *(NRCC)*, **Hiroshi KASHIWAGI, and Kimio OHNO** *(Hokkaido Univ.)*

In the previous paper[1], we have reported the results of ab initio LCAO SCF MO calculations on the ground and d-d transition states of $CoF_6(n-)$ (n = 4, 3, and 2). The emphasis was placed on trasition energies.

The object of the present research is to make some analysis of the degree of covalency or ionicity of the Co-F bonding in the ground state of these complexes based on our LCAO SCF MO calculations of the $CoF_6(n-)$ complexes. These calculations are carried out with a basis set of triple zeta quality for valence orbitals. The degree of covalency or ionicity of Co-F bond in the $CoF_6(n-)$ complexes has been discussed in terms of several quantities.

The Co-F bond in $CoF_6(4-)$ is usually regarded as an ionic bond. The degree of covalency of the Co-F bond increases when the valency (or oxidation number) of the central metal increases. It has been shown that the overlap population of the Co-F bond, degree of the MO delocalization, the charge density around the bond region, degree of the charge deformation around the F atoms, the difference between SCF and point-charge-model orbital energies, and degree of the shortening of the equilibrium Co-F distances (Table I) change with the valency of the central metal in the complexes. All of these changes are consistent with the idea that covalency increases with valency of Co.

The Co-F distance of a high-spin state, which has a larger occupation of the antibonding $4e_g$ orbital, is longer than that of the corresponding low-spin state within the same complex.

Table I. Equilibrium Co-F distances (Å).

complex	state	configuration (t_{2g} e_g)	calc.	expt.
$CoF_6(4-)$	$^4T_{1g}$	5 2	2.40	2.035
$CoF_6(4-)$	^2E_g	5 1	2.09	
$CoF_6(3-)$	^5E_g	3 3	2.01	
$CoF_6(3-)$	$^5T_{2g}$	4 2	1.99	1.89
$CoF_6(3-)$	$^3T_{1g}$	5 1	1.97	
$CoF_6(3-)$	$^1A_{1g}$	6 0	1.94	
$CoF_6(2-)$	$^6A_{2g}$	3 2	1.87	
$CoF_6(2-)$	$^2T_{2g}$	5 0	1.79	1.73

Reference

1) E. Miyoshi, T. Takada, S. Obara, H. Kashiwagi, and K. Ohno, *Int. J. Quantum Chem.* **19**, 451 (1981).

VI—B A Color Graphic System CANVAS and its Application's

Satoshi INA and Hiroshi KASHIWAGI

We have developed a color graphic system CANVAS and have applied for displaying MO's and electron density differences in the analysis of ab initio SCF calculations. As seen from Figure 1, a color graphic display (GRAPHICA M506) is connected to minicomputer (HITAC-20) with DIO (Digital Input/Output) interface and DMA (Direct Memory Access) interface. HITAC-20 is connected to host computer (HITAC M-200H) with DXC (Digital data eXChange) interface. Figure 2 shows the whole view of the hardware system. A high speed channel interface between M-200H and M506 has not been supported, so HITAC-20 was installed to act as a go-between. The specifications of M506 is shown in Table I. M506 can display about 260,000 colors.

CANVAS is a FORTRAN callable subroutine package, containing about 60 routines. CANVAS is applicable to CAD (Computer Aided Design), animation, computer art, and graphic design etc. We have applied CANVAS to investigate the electronic structures of molecules. Figure 3 shows the 3-dimensional view of the electron distribution of $3d_z^2$ orbital (Fe) at density 0.0001 electron/(Bohr)^3. Figure 4 shows the distribution of the electron density difference for Fe-porphine. Using CANVAS, the conversational and speedy display of the electron density with pseudo colors is helpful for heuristic approach to investigate the result of ab initio SCF calculations. It looks like "super electron microscope".

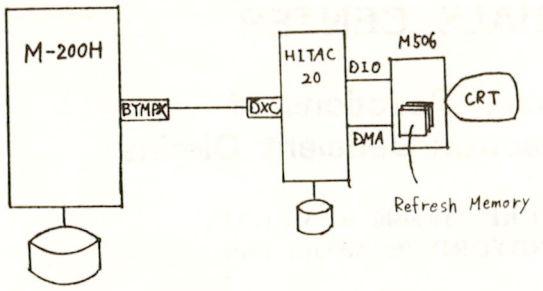

Figure 1. The hardware configuration.

Figure 2. The whole view of the hardware.

Table I. The specifications of M506

CRT Type	High resolution RGB color monitor
CRT Size	20 inch
Visible Raster	28 cm × 28 cm
Resolution	512 × 512
Grey Legvel (R, G, B)	64 levels (6 bits)
Color	262,134 colors
Hardware Option	Light pen
	Cross hair cursor

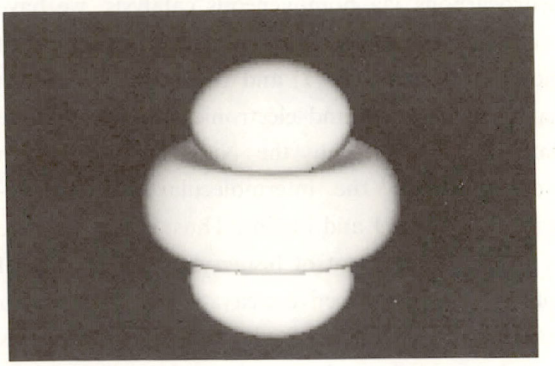

Figure 3. The three-dimensional view of electron distribution ($3d_{z^2}$ orbital).

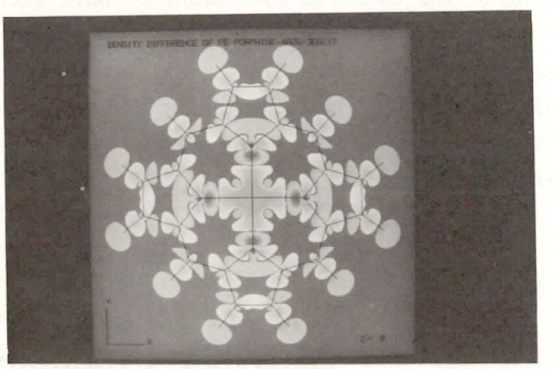

Figure 4. The electron density difference for Fe-porphine.

CHEMICAL MATERIALS CENTER

VI—C Nickel(0)-Catalyzed Reactions of Bicyclo[2.1.0]pentane and Electron-Deficient Olefins

Hidemasa TAKAYA, Takatoshi SUZUKI*, Yasushi KUMAGAI*,
Masashi YAMAKAWA, and Ryoji NOYORI* (*: *Nagoya Univ.*)

[*J. Org. Chem.* **46**, 2846 (1981)]

In connection with the activation of saturated hydrocarbons via homogeneous catalysis, we have examined transition metal catalyzed reactions of bicyclo[2.1.0]pentane (**1**) and its derivatives, which have unique steric and electronic structures.[1,2] We have found that only the Ni(0) catalyst system induces facilely the intermolecular coupling reacitons between **1** and olefins. Thus, in the presence of a catalytic amount of bis(acrylonitrile)nickel(0),**1** suffers from the selective cleavage of the central σ bond and cycloadds to electron-deficient olefins such as methyl acrylate and acrylonitrile to give bicyclo[2.2.1]heptanes in good yields (eq 1). Dimethyl maleate and fumarate also entered into the catalytic cycloadditions with retention of the olefin configurations. The stereochemistry and mechanism of the catalyzed cycloadditions have been elucidated by use of deuterated bicyclo[2.1.0]pentanes. Especially noteworthy is the fact that the stereochemistry of the cycloaddition is virtually the reverse of that encountered in the purely thermal reaction (Scheme I).

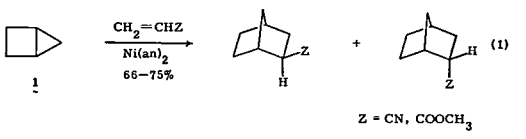

(1)

Scheme I

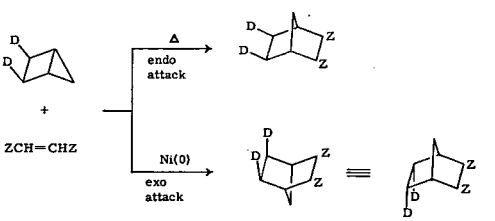

References

1) R. Noyori, T. Suzuki, and H. Takaya, *J, Am, Chem. Soc.*, 93, 5896 (1971).
2) R. Noyori Y. Kumagai, and H. Takaya, *J. Am. Chem. Soc.*, 96, 634 (1974).

VI—D Nickel(0)-Catalyzed Reaction of Bicyclo[1.1.0]butanes. Geminal Two-Bond Cleavage Reaction and the Stereospecific Olefin Trapping of the Carbenoid Intermediate

Hidemasa TAKAYA, Takatoshi SUZUKI*,
Yasushi KUMAGAI*, Masaharu HOSOYA*, Hiroyoshi KAWAUCHI*,
and Ryoji NOYORI* (*: *Nagoya Univ.*)

[*J. Org. Chem.* **46**, 2854 (1981)]

In spite of the high strain energy, bicyclo-[1.1.0]butane (**1**) is rather thermally stable, but it experiences skeletal change quite facilely by the aid of transition-metal catalysts. In most cases, the

products are 1,3-dienes. We have found that zerovalent nickel complexes such as bis(acrylonitrile)nickel(0) or bis(1,5-cyclooctadiene)nickel(0) catalyze the reaction of bicyclo[1.1.0]butanes and electron-deficient olefins such as methyl acrylate and acrylonitrile to give the corresponding allylcyclopropane derivatives in excellent yields (eq 1). The reaction of 3-deuterio-1,2,2,-trimethylbicyclo-[1.1.0]butane indicates that the two-bond cleavage occurs at the central σ bond and one of the four peripheral bonds of bicyclo[1.1.0]butanes to generate an allylcarbene-nickel complex as the reactive intermediate. The reaction of bicyclo[1.1.0]butane with (*Z*)-β-deuterioacrylate or a pair of *E* and *Z* 1,2-disubstituted olefins proceeded with a high degree of stereospecificity. The mechanism of cycloaddition is discussed.

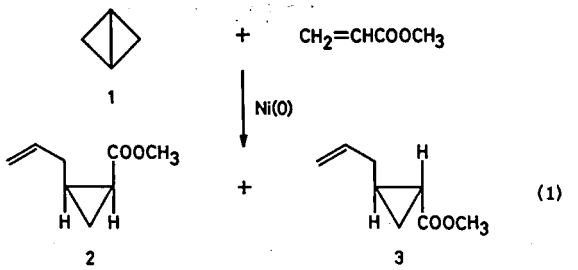

(1)

References

1) R. Noyori, T. Suzuki, Y. Kumagai, and H. Takaya, *J. Am. Chem. Soc.*, **93**, 5894 (1971)
2) R. Noyori, H. Kawauchi, and H. Takaya, *Tetrahedron Lett.*, 1949 (1974).

VI—E Reaction of Bicyclo[1.1.0]butanes with Pt(II) Complexes. Isolation and Characterization of New Platinacycle Compounds

Akira MIYASHITA, Mikio TAKAHASHI,* and Hidemasa TAKAYA (*: *Nagoya Univ.*)

[*J. Am. Chem. Soc.*, **103**, 6257 (1981)]

Transition-metal catalyzed isomerizations of strained cyclic hydrocarbons have been a subject of recent interests. Although much efforts have been done so far for the elucidation of the mechanism of the catalysis, numerous questions still remain to be answered. We have done the first isolation of transition metal complexes of **1** and revealed their unique chemical behaviors.

Reaction of the Zeise's dimer, $[PtCl_2(C_2H_4)]_2$, with excess bicyclo[1.1.0]butane (**1**) in acetone at −45°C for 48 h afforded a polymeric complex $[PtCl_2(C_4H_6)]_n$ (**2**) in 97% yield (eq 1). Treatment of suspension of **2** in CH_2Cl_2 with 2 equiv of pyridine at −50°C gave 2-[bis(pyridine)dichloroplatina]bicyclo[1.1.1]-pentane (**3**), mp 160−162°C (dec), in 94% yield (eq 2). The similarity of products obtained in the thermal decomposition of **3** with those given in the catalysis with **3** suggested that **3** is an important intermediate in the Pt(II) catalyzed isomerization of **1**. The origin of the remarkable temperature dependence of the NMR spectra of **3** was discussed.

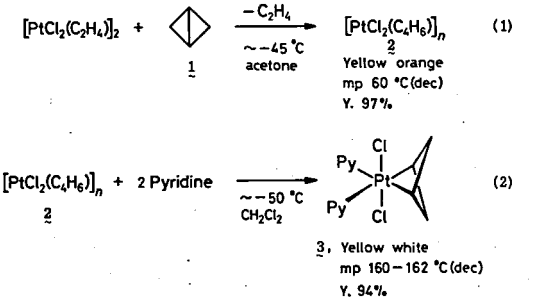

VI—F Reactions of Nickel—Carbene Complexes Generated From Nickelacycle Complexes

Akira MIYASHITA and R. H. GRUBBS*
(: California Institute of Technology)*

[*Tetrahedron Lett.*, **22**, 1255 (1981)]

Nickelacyclobutane complex **1** is believed to be in equilibrium with olefin-coordinated nickel-carbene complex **2** on the basis of the available experimental evidence.

When **1** in toluene was pyrolyzed in the presence of H_2, methane (32%), 2-methylpropane (37), 1,1-dimethylcyclopropane (19), and 2,2-dimethylpropane (8) were produced. The reaction of **1** with CO resulted in the formation of ketene dimer (11%) and 2-methylpropene. No cyclobutanone was obtained. The reaction is most reasonably interpreted in terms of a nucleophilic attack of the carbenic carbon in **2** to the coordinated CO molecule to form nickel-ketene complex **3**. Carbon monoxide was converted into ethanol (14% per Ni) by the reaction with **1** in the presence of H_2 followed by hydrolysis. The above results suggest that other Fischer-Tropsch type reactions may also proceed by way of metal-ketene complexes.

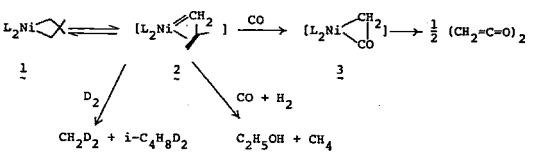

VI—G Nickel(0)-Catalyzed [2 + 2] Cross-Addition of Bicyclo[2.2.1]heptene Derivatives with Electron-Deficient Olefins

Hidemasa TAKAYA, Masashi YAMAKAWA, and Ryoji NOYORI* *(*: Nagoya Univ.)*

[*Bull. Chem. Soc. Jpn.* in press]

We have studied a Ni(0) catalyzed reaction of several bicyclo[2.2.1]heptene derivatives that are structurally related to norbornadiene, and electron deficient olefins. In the presence of bis(acrylonitrile)nickel(0) or bis(1,5-cyclooctadiene)nickel(0), exo cyclopropanated compound **1** cycloadds to acrylonitrile or methyl acrylate to give **2** and **3**, or the corresponding methoxycarbonyl derivatives **4** and **5** (eq 1). The [2 + 2] cross-addition proceeds with complete selectivity and no byproducts were detected. The cycloaddition with dimethyl maleate proceeds with retention of olefin configuration. Benzonorbornadiene also enters into the [2 + 2] reaction, while endo isomer of **1**, norbornene, and 5-methylenebicyclo[2.2.1]heptene are unreactive. Origins of the observed selectivities of the reactions and reactivities of the strained olefins in the catalyzed reaction are discussed.

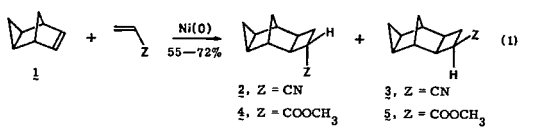

INSTRUMENT CENTER

VI—H Intramolecular Electronic Relaxation and Photochemical Reaction in Organic Compounds

A study of vapor-phase fluorescence characteristics especially under a collision-free condition allows us to examine the nature of the *intramolecular* electronic relaxation. The photophysical processes in the isolated molecule often include an important part of a photochemical reaction scheme. The radiationless transitions are responsible for conveying the molecule to the reactive electronic surface as well as for providing necessary activation energy to reactants. A collision-free experiment enables the consideration of the primary photochemical reaction in which only elementary individual process appears. Such an experiment requires experimental tools capable of detecting very weak fluorescence and/or transient absorption of low intensities. Along this line, we have constructed a time-correlated, photon-counting fluorimeter equipped with a synchronously pumped, cavity-dumped dye laser as an excitation pulse source.

VI-H-1 Subnanosecond Time-Resolved Fluorescence Spectrometer Equipped with Synchronously Pumped, Cavity-Dumped Dye Laser

Toshiro MURAO, Takaya YAMANAKA, Iwao YAMAZAKI and Keitaro YOSHIHARA

[*Bunko Kenkyu*, in press]

For purposes of measuring fluorescence decays and time-resolved fluorescence spectra with subnanosecond time resolution, a time-resolved fluorescence spectrometer has been constructed. The system consists of a synchronously pumped, cavity-dumped dye laser, a time-correlated photon-counting system, and a microcomputer system. A schematic diagram is shown in Figure 1. The dye laser (Spectra Physics 375 and 344S) is operated with a mode-locked Ar^+ laser (Spectra Physics 171-18). A repetition rate of the laser is 800 kHz and a pulse width at half maximum is 8 ps. The fluorescence emission is detected by a microchannel plate photomultiplier (Hamamatsu R1294U). The output pulses are fed into the time-to-amplitude

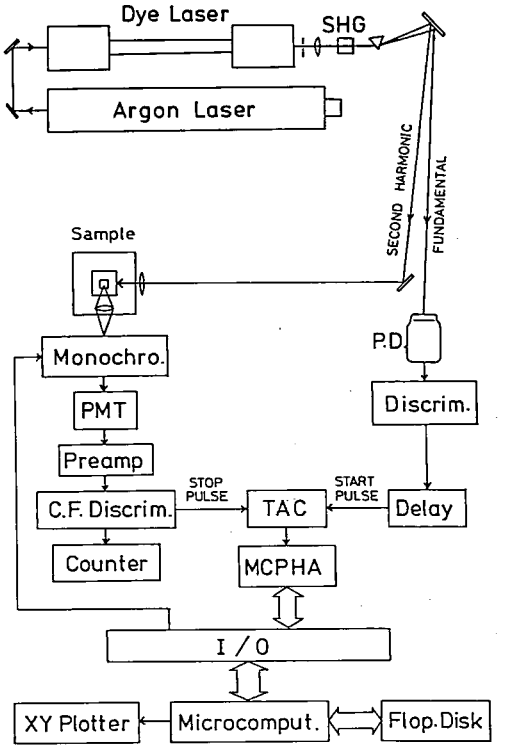

Figure 1. Schematic diagram of the laser system and the time-correlated photon-counting system

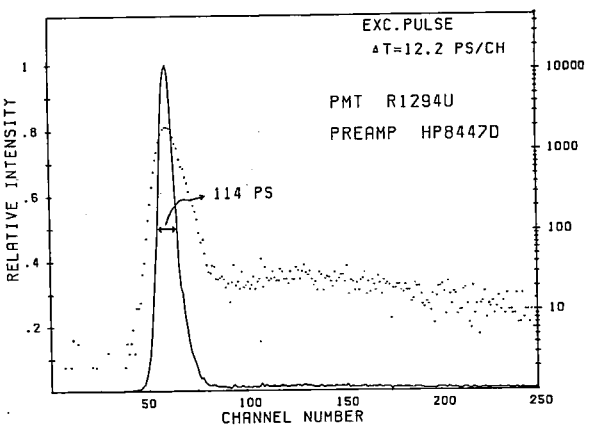

Figure 2. Laser pulse profile obtained with the time-correlated photon-counting system

converter to obtain fluorescence decay curves on the multichannel pulse-height analyzer which is controlled by a microcomputer system. Figure 2 shows a representative curve of a laser pulse profile. Fluorescence lifetimes and time-resolved spectra can be measured with a time resolution of 20–50 ps by the convolution method.

VI-H-2 Intramolecular Electronic Relaxation and Photoisomerization of Azabenzene Vapors

Iwao YAMAZAKI, Toshiro MURAO, and Keitaro YOSHIHARA

[*Chem. Phys. Lett.*, in press]

Azabenzenes such as pyridine, pyrazine, and pyrimidine are the molecules of special significance in view of a dynamical aspect of the electronic structure in the excited state. The present study is designed for the two problems of the azabenzenes (cf. Figure 1): (1) A variation of the intramolecular nonradiative decay rate upon excitation of different vibronic levels in the S_1 vibrational manifolds and (2) dynamical aspects of the intramolecular photoisomerization that occurs in the S_2 state.

By using the time-resolved fluorescence spectrometer mentioned in the previous section, we can directly measure the subnanosecond fluorescence lifetimes. The lifetime data are compared with the emission quantum yields obtained previously,[1] to deduce rate parameters for nonradiative processes. It has been suggested that, when pyrazine is excited at wavelengths corresponding to the $S_2 \leftarrow S_0$ absorption, the molecule undergoes photoisomerization into pyrimidine through a benzvalene-type of molecule as a reaction intermediate.[2] Studies on the wavelength-dependent fluorescence and the transient absorption would give a firm mechanism of this photochemical reaction. The final goal is to get a general picture of the intramolecular photoisomerization of azabenzenes in relation to the third channel problem of the parent hydrocarbon, benzene.

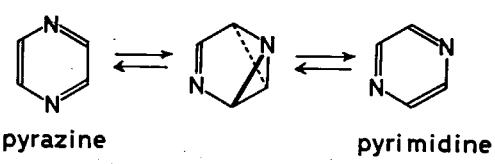

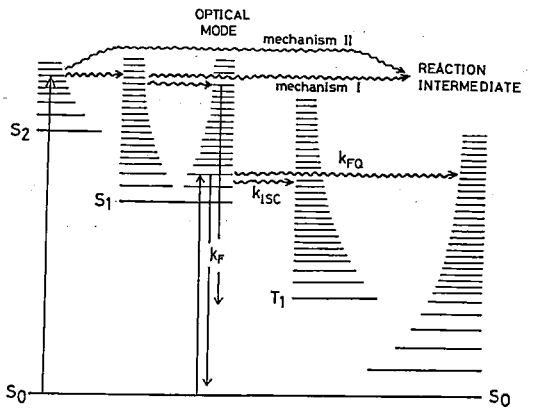

Figure 1. A scheme of photophysical and photochemical processes in the isolated azabenzene molecule.

References

1) I. Yamazaki, M. Fujita, and H. Baba, *Chem. Phys.* **57**, 431 (1981).
2) F. Lahmani and N. Ivanoff, *J.Phys. Chem.* **76**, 2245 (1972).

VI—I Time-Resolved Fluorescence Spectroscopy of Photosynthetic Organisms: Blue-Green Algae *Anacystis Nidulans* and *Anabaena Cylindrica*

Iwao YAMAZAKI, Toshiro MURAO, Keitaro YOSHIHARA, Mamoru MIMURO *(NIBB)*, **and Yoshihiko FUJITA** *(Univ. of Tokyo and NIBB)*

Photosynthetic organisms have evolved a light harvesting antenna system for light absorption and energy transfer to the reaction center. In blue-green algae, the system consists of phycobiliproteins and chlorophyll *a* ; the phycobiliproteins form an aggregate, phycobilisome, on the surface of thylakoid membrane, and chlorophylla *a* is directly connected to the reaction center. The light energy

absorbed by phycobiliproteins is transferred to the reaction center in thylakoid membrane, as shown in Figure 1. In the course of energy transfer processes, fluorescence is emitted from each pigment, and is used as an index of the energy transfer.

The present study has been initiated with purposes of getting detail information on the energy transfer processes by means of a time-resolved spectroscopic technique. Figure 2 shows a typical example of the time-resolved fluorescence spectra that was observed with *Anacystis nidulans*. This shows on the whole that the photon energy initially absorbed by phycocyanin migrates ultimately to chlorophyll *a* whose fluorescence gives intensities at a longer wavelength region. A kinetic analysis of the fluorescence provides us with information on the structure of the pigment system of blue-green algae.

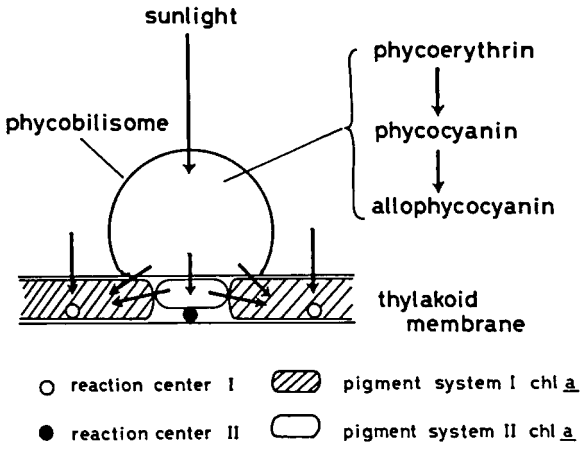

Figure 1. Pigment system in blue-green algae and pathways of the energy transfer.

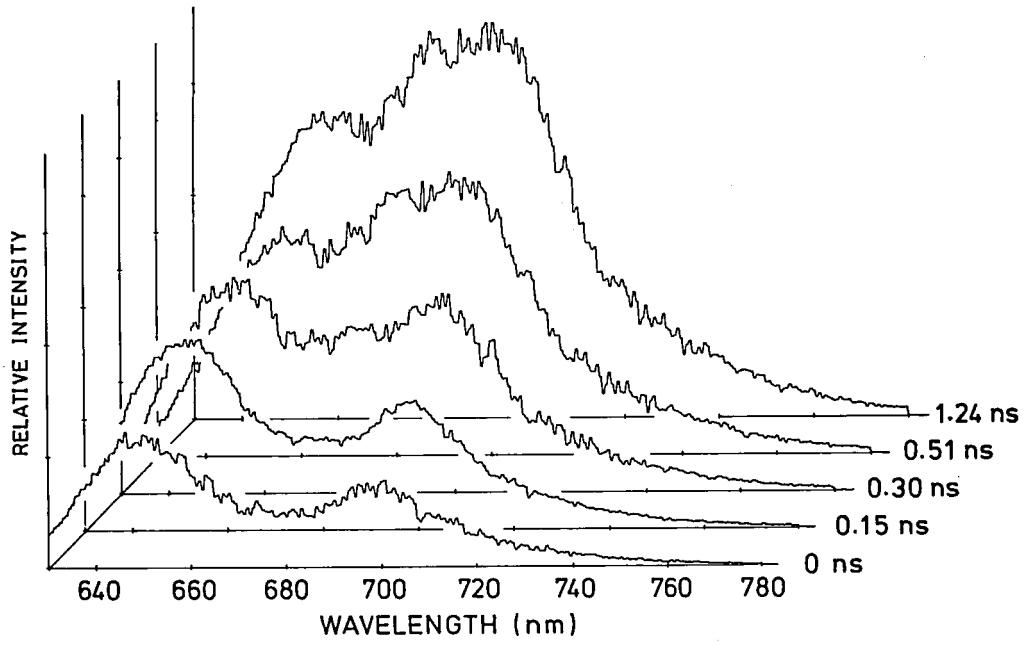

Figure 2. Time-resolved fluorescence spectra of *Anacystis nidulans* obtained with the subnanosecond time-resolved spectrometer by using a synchronously pumped, cavity-dumped dye laser as an excitation pulse source.

VI—J A Cryostat for Electric Conductivity Measurement

Shunji BANDOW and Keisaku KIMURA

There are many kinds of cryostat for electric conductivity measurement, but few examples for considering on chemical reaction. We will show a design of cryostat which enables the atmosphere of the sample port to control freely. The characteristic of the present apparatus is in situ measurement of conductivity under the controlled condition of gas phase reduction, oxidation and chemical adsorption. The time course of the reaction can be also monitored by a conductivity measurement.

Figure 1 shows the cryostat in which a sample compartment is doubly sealed with In wire and is independent from a vacuum chamber. We can measure a low temperature photoconductivity with the use of top quartz window. Two irises determine the precise irradiation position. The extention of the measurement to the magnetoresistance is also possible.

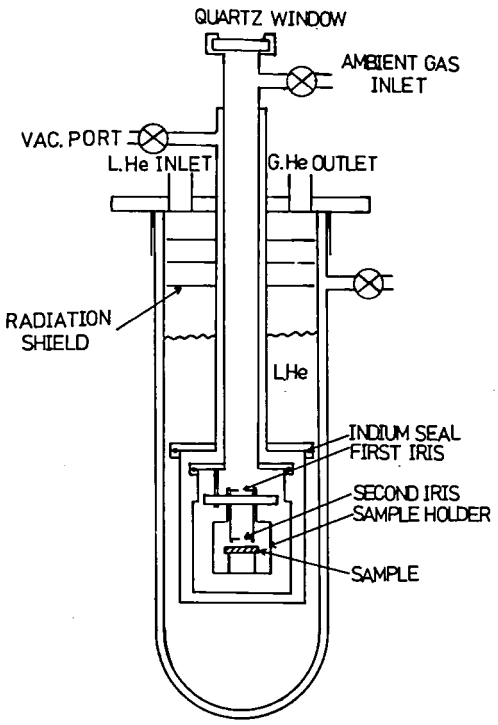

VI—K Molecular and Solid State Properties of Cytochrome c_3

The reduction mechanism of cytochrome c_3 was analysed from the observation of hydrogen pressure dependence and from kinetics of induction period. From the EPR measurement, the g-tensors of four hemes are analysed and related to axial distortion and rhombic distortion parameters. The anusual electron transport properties of cytochrome c_3 anhydrous film was investigated as a function of constituent ratio. An interpretation based on a percolative conduction was proposed to this observation.

VI-K-1 Percolative Conduction of Cytochrome c_3 Anhydrous Film

Keisaku KIMURA and Hiroo INOKUCHI

Cytochrome c_3 is known to have four hemes and is undergone the oxidoreduction under the catalytic action of hydrogenase.

$$\text{ferricyt } c_3(Fe^{3+}) + 2H_2 \longleftrightarrow \text{ferrocyt } c_3(Fe^{2+}) + 4H^+$$

Therefore it is possible to control the ferro to ferri content successively as a function of time. A d.c. conductivity was measured in the atmosphere of hydrogen at room temperature. Figure 1 shows the semilogarithmic plot of conductivity as a function of reduction ratio. A current abruptly increased at n = 0.95. This impressing findings was explained by a percolative conduction of cytochrome c_3 anhydrous film. The content of fully reduced ferrocytochrome c_3 is 0.85 at n = 0.95. The critical concentration 0.85 is good agreement with a calculated value 0.80 taking the coordination number z being 12 in amorphous case and with 0.85 taking z equals 6 from single crystallographic data of cytochrome c_3. The solid line in the figure is an empirical curve and expressed as

$$I = \frac{10 \cdot n^{1.5}}{1 + 4.5 \cdot n^{1.5}} \text{ pA}$$

This was interpreted by an impurity scattering combined with heme-heme contribution.

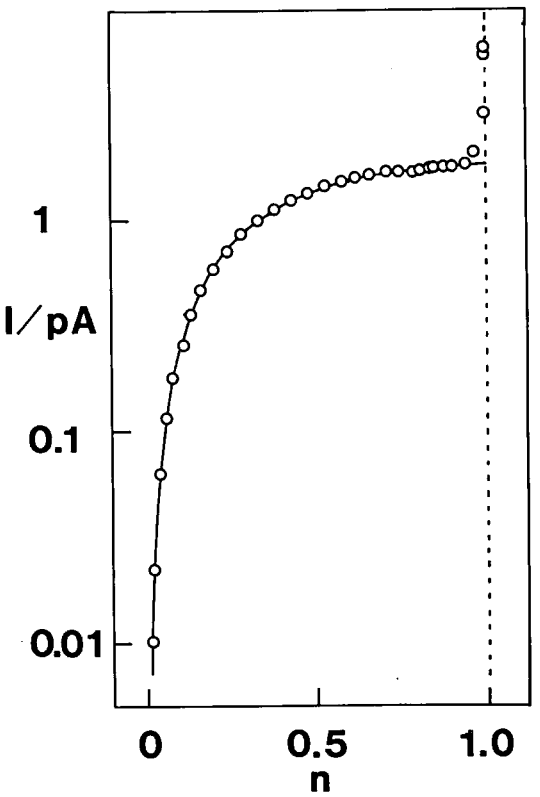

Figure 1. The semilogarithmic plot of current as a function of reduction ratio.

VI-K-2 Equilibration of Cytochrome c_3 Oxidoreduction as a Function of Hydrogen Pressure

Keisaku KIMURA, Hiroo INOKUCHI and Tatsuhiko YAGI *(Shizuoka Univ.)*

In a research series of enzymic activities in the dry state, we have revealed that hydrogenase had enzymic activities for orthoparahydrogen conversion, H_2-D_2 exchange reaction and oxidoreduction of cytochrome c_3 with hydrogen as well as those in solution. Of these reactions, the oxidoreduction of cytochrome c_3 in dry state is very important in order to understand the mechanism of electric conduction in a cytochrome c_3 anhydrous film. In solution, cytochrome c_3 undergoes one electron transfer between hydrogenase[1] as well as on dropping mercury electrode.[2] Figure 1 shows the time course of the absorption of cytochrome c_3 at 552 nm as a function of hydrogen pressure. The optical density at equilibrium is indicated by an arrow. From these readings, the reduction ratio Y was plotted as a function of logarithm of P as shown in Figure 2. Solid line is a calculated curve with $Y = KP/(1 + KP)$ where K is 0.4. It should be noticed that the power of P is unity but not one half as in the case of solution. Therefore the number of electron transferred was concluded to be two in the dry system against one in solution.

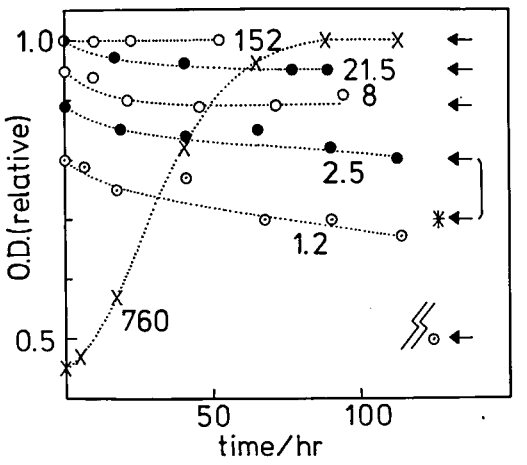

Figure 1. Time course of absorption at 552 nm. The numbers in the figure are pressure of hydrogen in Torr. The intensities are normalized to that of 760 Torr. An arrow indicates the value at infinite time. An asterisk at 2.5 Torr is an estimated value. For 1.2 Torr, it was determined by the reading after two weeks.

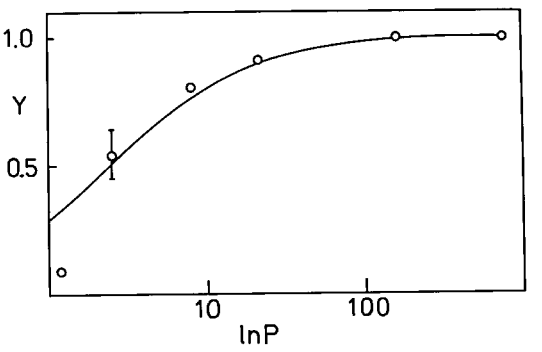

Figure 2. Reduction ratio as a function of ln P. Solid line is a calculated curve with two electron transfer process.

References

1) T. Yagi and K. Maruyama, *Biochim. Biophys. Acta*, **243**, 214 (1971).
2) K. Niki, T. Yagi, H. Inokuchi and K. Kimura, *J. Electrochem. Soc.*, **124**, 1889 (1977).

VI-K-3 Reduction Kinetics of Cytochrome c_3 Anhydrous Film

Keisaku KIMURA, Hiroo INOKUCHI and Tatsuhiko YAGI *(Shizuoka Univ.)*

It was observed[1] in the time course of the reduction of cytochrome c_3 anhydrous film with hydrogen that there was an induction period as shown in Figure 1. The induction period was scaresly observed in the normal reaction procedure. Figure 2 shows the logarithmic plot of the time dependence of the reduction process of ferricytochrome c_3 in the initial reaction stage. From the figure, it was concluded that the concentration of ferrocytochrome c_3 is a function of $\exp[-kt^2]$. In order to explain this functional relation, we postulate the following reaction scheme,

$$E + H_2 \longrightarrow EH_2$$

$$EH_2 + \text{ferricytochrome } c_3 \longrightarrow E + 2H^+ + \text{ferrocytochrome } c_3$$

where E denotes hydrogenase and EH_2 is a ES complex. The two electron transfer process of the second step was confirmed by the measurement of the hydrogen pressure dependence of cytochrome c_3. Under an appropriate assumption, it was derived based on the above reaction scheme that the $\ln a/a_0$ is proportional to the square of time coincided with the result of Figure 2.

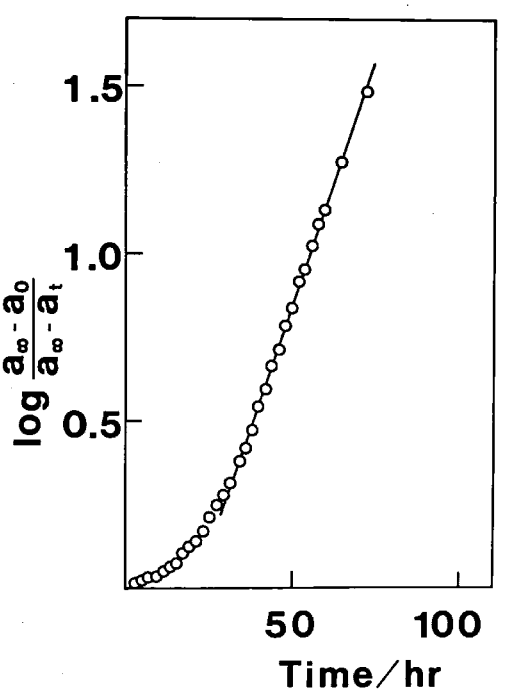

Figure 1. The time course of the ferrocytochrome c_3 content in the first order kinetics.

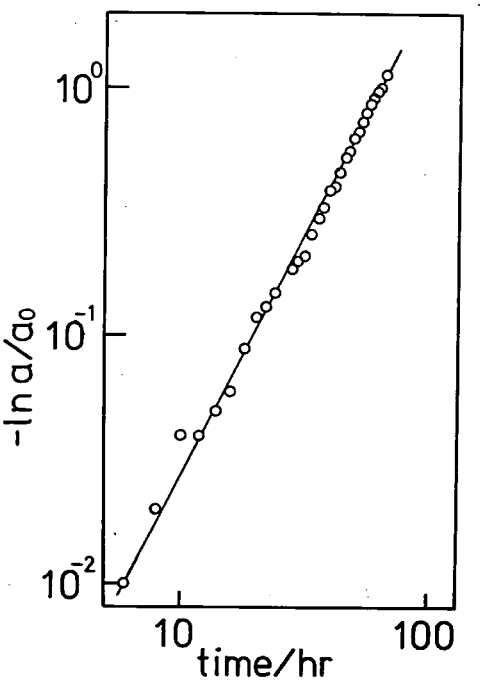

Figure 2. A logarithmic plot of the time dependence of the reduction of ferricytochrome c_3. a is a concentration of ferricytochrome c_3 and a_0 is that of the sum of ferri and ferrocytochrome c_3.

Reference

1) K. Kimura, A. Suzuki, H. Inokuchi and T. Yagi, *Biochim. Biophys. Acta*, **567**, 96 (1979).

VI-K-4 Electron Paramagnetic Resonance Study of Cytochrome c_3

Keisaku KIMURA and Hiroo INOKUCHI

Cytochrome c_3 has four heme in a single polypeptide chain. Due to this multiheme structure, it shows four redox potentials at pH 7. These are −226, −278, −298, and −339 mV vs NHE obtained from detailed electrochemical analyses of deffer-ential pulse polarography and cyclic voltammetry. Redox potential is believed to reflect an environment of heme in protein. Therefore it is interesting to find relations between redox potential and other

physicochemical properties. Ferricytochrome *c* has three *g*-values through spin orbit coupling of Fe *d*-orbitals in porphyrin. The *g*-values are related to the splitting of 3*d* orbilals. At very low temperature, ferricytochrome c_3 showed nine different peaks/shoulders in the EPR spectrum coming from four hemes. Table I summarizes three principal *g*-values of four hemes at 14.5 K. In protein, porphyrin loses its D_{4h} symmetry and this reflects to *g*-value. According to Griffith,[1] the axial distortion parameter Δ and rhombic distortion parameter ∇ are calculated and also listed in Table I. For heme I, II, III, the absolute value of Δ is larger than ∇. It seems that there are some relation between ∇ and E'_0 for this heme group.

Reference

1) J. S. Griffith, The Theory of Transition-metal Ions, Cambridge Univ. Press. 1971,

Table I. *g*-Values and Distortion Parameters of Ferricytochrome c_3

Heme	g_x	g_y	g_z	Δ/λ	∇/λ	E'_0/mV
I	1.395	2.294	3.411	−3.82	1.59	−226
II	1.538	2.294	2.981	−3.39	1.95	−278
III	1.633	2.294	2.782	−3.41	2.34	−339
IV	2.020	2.294	2.458	−4.28	4.52	−298

λ is a spin-orbit coupling constant. Δ and ∇ are the energies of axial distortion and rhombic distortion respectively.

LOW-TEMPERATURE CENTER

VI—L Spin Concentration of Violanthrone-B

Kenichi IMAEDA, Toshiaki ENOKI, Hiroo INOKUCHI, and Junji AOKI *(Toho Univ.)*

Violanthrone-B (VOB) is one of the condensation products obtained from the alkali fusion of benzanthrone. The oxidation product (VEBO) of violanthrene-B is also considered to have a violanthrone-B structure. They show strong ESR absorptions of Lorentzian lineshape due to unpaired electrons of the structure Ib shown in Figure 1. The results of spin concentration measurements of powdered samples at room temperature in air are listed in Table I, which are determined by a comparison of the integrated ESR absorption with that of 2,2-diphenyl-1-picrylhydrazyl (DPPH). From the fact that spin concentrations of VOB and VEBO are about 20 ~ 30%, we assume that they are the mixture of Ia and Ib.

Table I. Spin concentration of VOB

sample	spin concentration %	linewidth G	g-value
VOB	20	3.2	2.003
VEBO	30	3.1	2.003

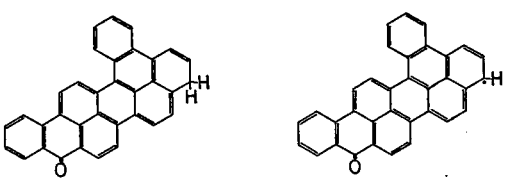

Ia Ib

Figure 1. Structure of VOB.

VI—M Hydrogen Absorption of Polycyclic Aromatic Hydrocarbon - Alkali Metal Complexes

The complexes between polycyclic aromatic hydrocarbons and alkali metals have catalytic activities for hydrogen. These activities are considered to be caused by the occlusion properties of hydrogen in these complexes. We are investigating the solid state properties of these complexes under hydrogen atmosphere in order to make clear the absorption mechanism of hydrogen and the static and dynamical behaviors of hydrogen in the complexes.

VI-M-1 ESR of Tetracyanopyrene-Cesium and its Hydrogen Absorption Complex.

Toshiaki ENOKI, Kenichi IMAEDA, Hiroo INOKUCHI, and Satoshi IWASHIMA *(Meisei Univ.)*

Tetracyanopyrene-Cs complex has a catalytic activity for H-D exchange reaction.[1] ESR of this complex is investigated under hydrogen atmosphere just after the introduction of hydrogen in order to reveal the absorption mechanism of hydrogen into the complex. The time dependence of the line width and the amplitude of the first derivative of ESR is shown in Figure 1. The line width ΔH is slightly lowered in the time course of hydrogen absorption, while the amplitude h is enhanced for about 10h and goes to a steady state value. The narrowing of the line width means the enhancement of interactions between spins due to the absorbed hydrogen. The increase of the amplitude shows the enhancement of spin concentration in the complex with the absorbed hydrogen. These findings are similar with the case of triphenylene-potassium complex under hydrogen atmosphere.[2]

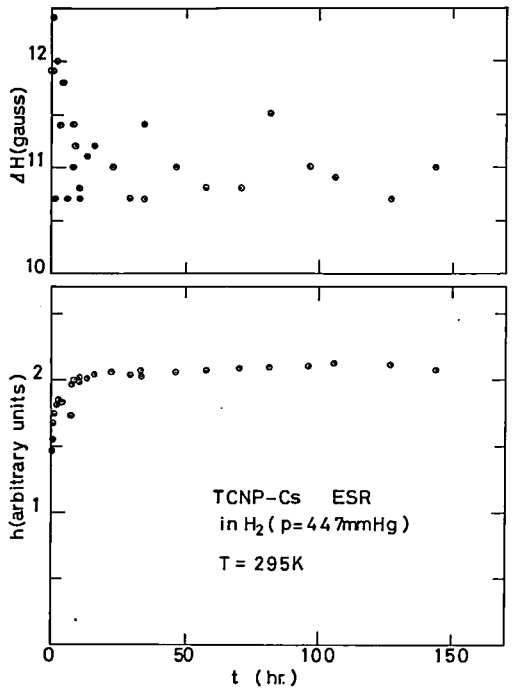

Figure 1. The time dependence of ESR of TCNP-Cs complex after the introduction of hydrogen. h denotes the amplitude of the first derivative of the absorption spectrum.

References

1) T. Kondow, H. Inokuchi and N. Wakayama, *J. Chem. Phys.* **43**, 3766 (1965).
2) T. Enoki and H. Inokuchi, *J. Chem. Phys.* **74**, 6440 (1981).

VI-M-2 Paramagnetic Resonance of Graphite-Alkali Metal-Intercalation Compounds and the Absorption of Hydrogen

Toshiaki ENOKI, Mizuka SANO *(Univ. of Electro-Communications)* **and Hiroo INOKUCHI**

Conduction electron spin resonance (CESR) of the first and second stage graphite-potassium-intercalation compounds, C_8K and $C_{24}K$, is investigated under hydrogen atmosphere in order to make clear the absorption mechanism of hydrogen in the gap between graphite layers. These two compounds show Dysonian line shapes of electron spin resonance because of their metallic properties as shown in Figure 1. In the case of C_8K, the enhancement of the amplitude of CESR signal and the slowing down of electron diffusion are found at the first step of hydrogen absorption. This fact might be explained by the dissociation of hydrogen molecules in the compound as well as the case of

triphenylene-potassium complex under hydrogen atmosphere.[1] At the steady state in a long time after the introduction of hydrogen, the intensity is lowered and the diffusion time of electrons is shortened. These facts are due to the electron transfer from graphite to absorbed hydrogen and the acceleration of the c-axis hopping of the conduction electrons through hydrogen anion $H^{\delta-}$. In $C_{24}K$, asymmetry parameter A/B goes down across the slow diffusion limit and the linewidth becomes large after the introduction of hydrogen. These findings are explained by the fluctuation of the internal field due to the absorption of hydrogen at random sites in the gaps between graphite layers.

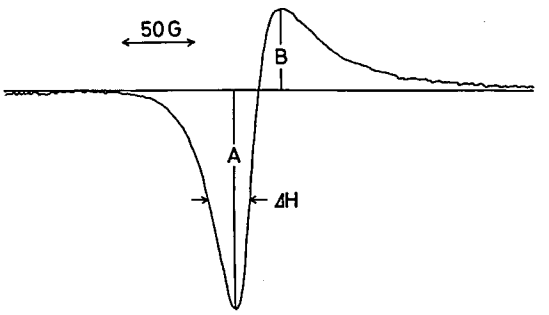

Figure 1. CESR of C_8K at T = 291K.

Reference

1) T. Enoki and H. Inokuchi, *J. Chem. Phys.* **74**, 6440 (1981).

VI—N Synthesis and Electrical Conductivity of CT Complexes of 2,7-Bis(dimethylamino)tetrahydropyrene with Several Acceptors

Naomi NISHIKAWA, Yoshiteru SAKATA, Soichi MISUMI
(Osaka Univ.), **Toshiaki ENOKI, Gunzi SAITO, and Hiroo INOKUCHI**

In connection with our synthetic studies on highly conductive compounds, six charge transfer complexes of 2,7-bis(dimethylamino)tetrahydropyrene 1 with TCNQ derivatives and chloranil were prepared.

Electrical resistivities of the complexes were measured on single crystals except for 1-Me_2TCNQ and 1-chloranil. They show semiconductive behavior in the temperature range measured. The results are summarized in Table I.

In view of these results, there is a trend that the introduction of substituents on the TCNQ molecule results in a decrease of the conductivities of the complexes, apart from the nature of the substituents. This fact suggests that the incomplete charge transfer from a donor to an acceptor plays an important role for the high conductivity in the charge transfer complexes.

Table I. Electrical Resistivity (ρ) and Activation Energy (Ea) of the Complexes

Complex	ρ (Ωcm)	Ea(eV)
1-TCNQ$(F)_4$[a]	1.45×10^5	0.37
1-TCNQ(F)[a]	9.52×10^1	0.53
1-TCNQ[a]	2.79	0.50
1-TCNQ$(Me)_2$[b]	1.04×10^6	——
1-TCNQ$(OMe)_2$[a]	4.21×10^5	0.31
1-Chloranil[b]	1.23×10^9	——

[a] single crystal
[b] compressed pellet

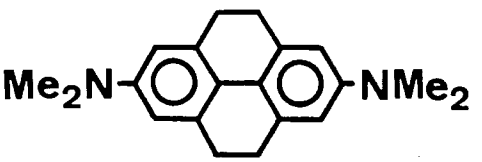

1

DEVELOPMENT WORKSHOP

VI—O Construction of UVSOR (Ultraviolet Synchrotron Orbital Radiation) Light Source

Makoto WATANABE, Akira UCHIDA, Osamu MATSUDO, Kusuo SAKAI, Kiyoshi TAKAMI,* Takeshi KATAYAMA, Katsuhide YOSHIDA,** and Motohiro KIHARA*****

*(*Kyoto Univ., **Univ. of Tokyo, ***Nat. Lab. High Energy Phys. and IMS)*

UVSOR light source is a 600 MeV electron storage ring dedicated to synchrotron radiation research, the injector of which is a 600 MeV synchrotron with a 15 MeV linac. Design study of the UVSOR light source was made in 1979 and 1980. In 1981, its construction is started. At present, the design of all parts of the synchrotron, such as the linac, injection beam line, injection system, magnets, RF cavity and generator, vacuum doughnut, extraction system, control and cooling system, has been completed and most of them are under construction. The summary and the present status of the UVSOR facility are given in "Large Scale Research Equipments" in this issue.

VI—P Picosecond Optical Parametric Oscillation and Amplification with High Efficiencies in Visible and near Infrared Regions

Yoshihiro TAKAGI, Minoru SUMITANI, Nobuaki NAKASHIMA, and Keitaro YOSHIHARA

Optical parametric oscillation (OPO) and amplification (OPA) are useful processes for obtaining a widely tunable coherent light in the visible and near infrared regions. The spectral range can be extended to the UV region by frequency mixing or harmonic generation. Thus we can produce coherent source for entire region from the near IR to UV region. In spite of its generarity, there are amazingly few examples of the practical use of OPOA.

Optical pulses with high enough peak power to induce OPO with a single-pass are obtainable in the picosecond domain. In order to receive the highest conversion efficiency, the optical characteristics of the nonlinear crystal and the geometrical configuration must be considered in detail.

We constructed a picosecond continuously tunable laser system based on OPOA and investigated about how to extract high output power. The system uses a mode-locked YAG laser and crystals for second, third, and fourth harmonic generation and OPOA (see LARGE SCALE RESEARCH EQUIPMENTS in this issue for the actual experimental set-up). Experimental results and conditions of OPOA are summarized in Table I. Spectral range from 4.4 μm to 420 nm was covered by three kinds of crystals: $LiNbO_3$, KD*P, and ADP. In all cases a pair of crystals were used. The first crystal worked as a parametric oscillator and the second one as an amplifier. During the amplification (except for the temperature-controlled OPOA in ADP with 90°-cut) "walk off" in the first crystal was canceled because of the symmetric configuration of the crystals with respect to their optical axes. In comparison with the past experiments[1)2)3)] remarkably high conversion efficiencies have been obtained in OPOA using KD*P(TYPE-II, 99%-deuterated) pumped by the second and third harmonic light of the YAG laser. The efficiencies reached 25% and 35%, respectively.

Table I. Experimental results and conditions of OPOA.

Crystal	$LiNbO_3$	KD*P	KD*P	ADP
pumping wavelength	1064 nm	532 nm	354.7 nm	266 nm
OPO output wavelength	1.4-4.4 μ	860-1400 nm	460-1550 nm	430-700 nm
OPO output energy (max)	6 mJ	3 mJ	2 mJ	0.4 mJ
Conversion efficiency	10 %	25 %	35 %	10 %
spectral width	16-140 cm^{-1}	<10 Å	5 Å (ordinary)	<5-20Å (signal)
tuning	angle	angle	angle	temperature
cutting	47° (TYPE I)	61° TYPE II)	61° TYPE II)	90° TYPE I)

These are 28% and 40%, respectively, if we consider the Fresnel losses. In each case the pumping beam was tightly focussed on the amplifier crystal by a cylindrical lens of a 50-cm focal length. The power density of the pumping wave reached about 10 GW/cm^2 at the beam waist, but it did not seem to give any damage in the crystal. The spectral width was almost constant in the entire wavelength range for each OPOA process. Figure 1 shows observed tuning curves and output energies as functions of

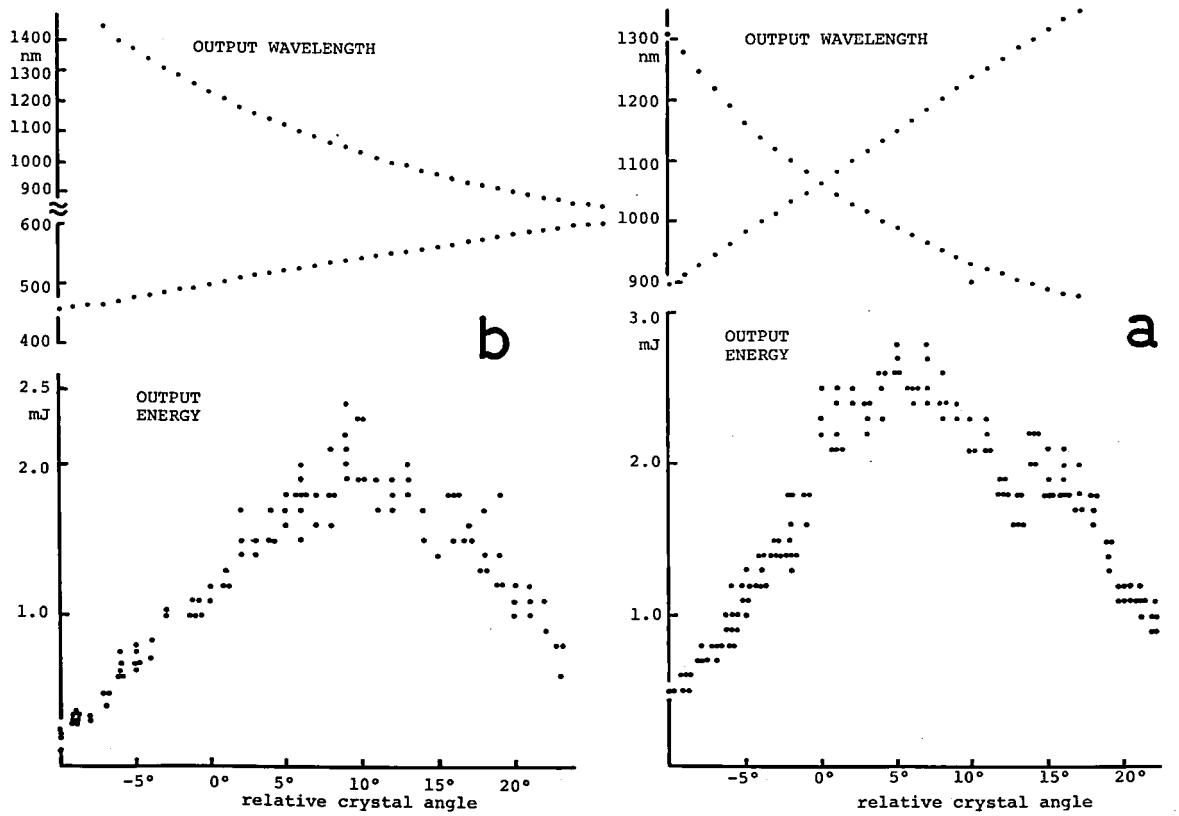

Figure 1. Dependences of wavelengths and energies on the rotation angle of the KD*P crystal.
a) OPOA pumped by the second harmonic light.
b) OPOA pumped by the third harmonic light.

the crystal angle.

Although OPOA using KD*P of TYPE-II will be an excelent picosecond tunable light source with respect both to the energy and the spectral purity, it does not cover the entire visible wavelength (Fig. 1). Then we used an induced Raman process in order to pump OPOA covering the spectral gap shown in Figure 1. The Raman output at 416 nm was obtained with H_2 gas by the third harmonic light. The energy was about 1 mJ, but the beam quality was not good enough to induce OPOA efficiently. Practically a use of KD*P of TYPE-I pumped by the fourth harmonic light will be better. It covers the ranges of 400-450 nm and 600-800 nm which are missing in OPOA by the third harmonic light.

References

1) R. Danelyus, V. Kabelka, A. Piskarskas, and V. Smil'gyavichus, Sov. J. Quantum electron. **8**, 398 (1978).
2) P. G. Kryukov, Yu. A. Matveets, D. N. Nikogosyan, and A. V. Sharkov, Sov. J. Quantum Electron. **8**, 1319 (1978).
3) Y. Takagi and K. Yoshihara, IMS Ann. Rev. 137 (1979)

VI—Q Optically Induced Magnetization Using a Broad Band d-d Transition in Ruby and Chrome Alum

Yoshihiro TAKAGI

Experiments of optically induced magnetization in paramagnetic materials started in the 1950s in the study of optical pumping.[1] Alkali atom vapors were magnetized by irradiation of the light. Powerful pulsed lasers could produce the magnetization in a solid at room temperature having much shorter relaxation time than that of gaseous media.[2] Recently using a mode-locked ruby laser an impact excitation of the transverse magnetization has been made and the precessing magnetization in an external magnetic field was observed.[3] Particularly, the technique in Ref. 3 can be considered as an optical method of the high speed pulsed ESR because the fast free induction decays (nanosecond order) were observed. Instead of using microwave pulses a circularly polarlized light was tuned to an absorption band in a sample.

In order to apply this technique to many paramagnetic materials we should have a tunable pulsed laser and should investigate about how the optical excitation of the magnetization depends on the structure of optical transitions. In the above case a weak forbidden transition which is just the ruby laser line was excited. Then, can other transition lines be used for the excitation of the magnetization?

First, we tried to excite the U-band ($^4T_2 \leftarrow {}^4A_2$) in ruby, and then excited the same line in a single crystal of chrome alum using a second-harmonic light (532 nm) of a mode-locked YAG laser. According to the selective transitions between Zeeman sublevels in the ground and excited states, population differences were produced in the ground state and probably in the excited state accompanied by an extremely fast relaxation. So, the magnetization observed is the one due to the population differences in the ground state. Figure 1 shows decays of the induced voltages in a pick-up coil wound around the sample. The decay with a time constant of about 70 nsec corresponds to the spin-lattice relaxation at room temperature. Figure 1 (b) is a FID signal with a decay time of 2-nsec. The result that the decay constants are shorter than those in Ref. 3 is probably due to a difference in the degree of spin-spin interaction or cross relaxation because the concentration of Cr^{3+} ions in the present sample is ten times larger than in Ref. 3.

The same experiment was made on a single crystal of chrome alum which is similar to ruby with respect to the structure of optical transitions. The signal was detected as shown in Figure. 2. It can be understood as a time derivative of the rapidly decaying magnetization. The relaxation rate was so rapid that our detection system could not follow it.

We are applying this technique to various transition-metal ions in aqueous solutions and in solids. As the excitation sources we are using a

picosecond tunable laser based on the optical parametric oscillation and amplification besides the harmonic light of the YAG laser.

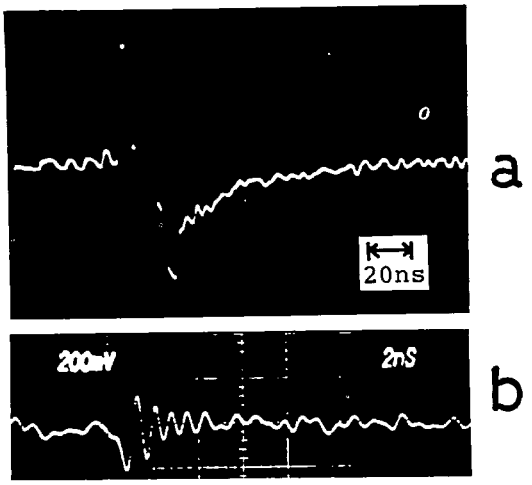

Figure 1. Magnetizations induced by a second-harmonic light of a mode-locked YAG laser.
a) Longitudinal magnetization.
b) Precessing magnetization in an external magnetic field of 250G. Frequency of the oscillation is about 1.4 GHz.

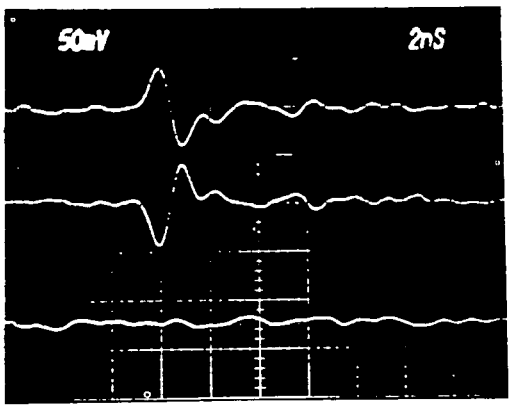

Figure 2. Optically induced magnetizations in chrome alum. Excitations were made by circularly polarized lights of opposite senses (top and middle) and a linearly polarized light (bottom).

References

1) R. A. Bernheim, in *Optical Pumping*, Benjamin, New York (1965).
2) J. P. van der ziel and N. Bloembergen, *Phys. Rev.* **138**, A1287 (1965).
3) Y. Takagi, Y. Fukuda, K. Yamada, and T. Hashi, *J. Phys. Soc. Japan*, **50**, 2762 (1981).

VI—R An Instrumentation for the Optical Method of Pulsed ESR

Yoshihiro TAKAGI

In the experiments on the optically induced magnetization behaviors of instantaneously produced magnetization were observed with a resolution time of less than one nanosecond.[1)2)] A wideband amplifier was used and photographs of the oscilloscope traces were taken. However the signal-to-noise ratio was limited by radio frequency noises and was not good enough for complete data analysis. If the repetition rate of our laser had been more than 10 Hz, we could have used a fast sampling oscilloscope. In our case of the low repetition rate (1Hz) the best way is probably to use a fast oscilloscope including a scan-converter tube. We shall be able to take out the data from it electrically. But it is very expensive. Consequently, we decided to attach a TV camera to an oscilloscope and process the video signal. For this pourpose we disigned a microcomputer-based video processor. It degitizes the video signal, stores the data into IC memories dividing the TV frame into 256 × 256 picture elements, and makes graphic displays on a TV screen. It is a modified type of the one used previously for the measurement of time-resolved spectroscopy using a streak camera.[3)] In the previous case the streak image was digitized by an 8-bit AD converter and the intensity profile of the image was analyzed, while the present processor has only to possess a one-bit AD converter since traces on the oscilloscope are treated. Figure 1 (a) and (b) are graphic displays of the oscilloscope traces of the precessing magnetizations excited one and 100 times, respectively. The software of the processor was written by a machine language and it treats the data quickly. The processor works by itself, but can be interfaced to another computer for more complicated analysis.

Recently, we introduced CAMAC standard, which is used commonly in the large scale

experiments in high energy physics. Although it is often combined to a large scale computer, we connected it with a desk computer and with the video processor. We designed their interfaces in the module types inserted to a CAMAC crate. With the help of the CAMAC system data of the sample temperature and of the excitation power as well as the data from the video processor were collected to the controller simultaneously. Thus the CAMAC system is conveniently used in such a multi-measurement in our labolatory.

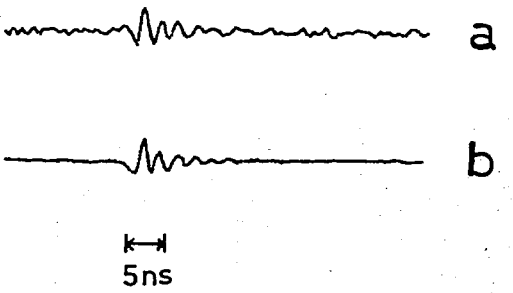

Figure 1. Graphic displays of oscilloscope traces.
a) single excitation.
b) after accumulation of 100 times.

References

1) Y. Takagi, Y. Fukuda, K. Yamada, and T. Hashi, *J. Phys. Soc. Japan*, **50** 2762 (1981).
2) Y. Takagi, *IMS Ann. Rev.*, VI-A, (1981).
3) Y. Takagi, M. Sumitani, and K. Yoshihara, *Rev. Sci. Instrum.*, **54** 54 (1981).

RESEARCH FACILITIES

Computer Center

The Computer Center began its service in January 1979 with two HITAC M-180 computers. One of them was replaced by a HITAC M-200H in April 1980. M-200H and M-180 have a processing capacity of over 10 and 4 million instructions per second, respectively. Both of the processors use 32 bit words and are essentially IBM-compatible at both the hardware and software levels. They have 12 and 4 mega byte main memory, 7150 and 3340 mega byte disk memory, respectively, and other I/O devices. The computers are used not only by the research staff at IMS but also by the staff at nearby National Institutes as well as by scientists outside the Institutes in the related fields. As of March 1981 the number of project groups was 203 consisting of 426 users. In the twelve month period ending March 1981, 183840 jobs were processed with 5405 hours of the CPU time (The base of speed is M-200H).

Unattended operation of the Computer Center in the night and on holidays has been carried on since September 1979, using the automated operation system developed by the Center and Hitachi Ltd. the hardware consists of many sensors (smoke, heat, water, temperature, humidity, and earthquake), alarm systems, and automatic fire extinguishers. The software returns preassigned responses to operator calls from the system. The system sends alarms and terminates itself, airconditioners and the power supply in an emergency. It can also automatically stop the operation or freeze running jobs when preassigned conditions are satisfied. The system has been providing an uninterrupted, unmanned week long service.

A program library for molecular science has been established under a unique library management system, with which users can search on their TSS terminal whereabouts and guides of wanted programs. Many programs have already been registered and are being used frequently. All of the QCPE programs has been obtained and will be so on the continued basis. An arrangement has been made to introduce programs supported by the National Resource for Computation in Chemistry at Berkeley, Calfornia.

In June 1979 the center began its service of QCLDB (Quantum Chemistry Literature Data Base), a file of references of ab initio molecular orbital calculations. Users now can search for references on their TSS-terminals under ORION, a data base management system supported by Hitachi. References can be found using keywords such as compounds, journals, and authors.

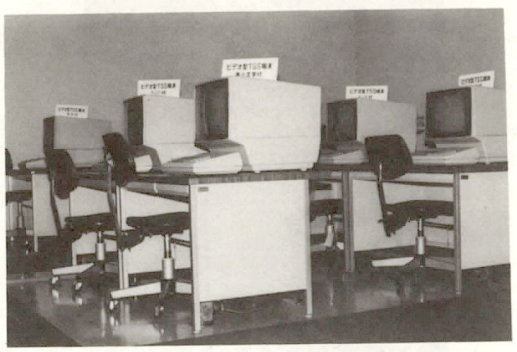

TSS Terminals

Open Magnetic Tape Drivers

Low-Temperature Center

Low-Temperature Center supplies coolants such as liquid nitrogen and liquid helium. The staff of this Center also develops cryogenic techniques in close cooperation with research divisions and other centers.

The Center building (1430m^2, 2 stories and 1 basement) was completed in March 1979. It consists of three machine rooms, ten laboratories, a machine shop and also a control room for a helium liquefaction and recycling system. The floor and the walls of the machine rooms for compressors and kinney vacuum pumps were separated from the rest of the building to avoid the propagation of mechanical vibrations of the heavy machines.

The laboratories are to be equipped with spectroscopic, magnetic and calorimetric instruments for low temperature measurements. Seven laboratories are located in the basement in order to keep a well regulated environment. Especially, one of them is the shielded room where the attenuation rate of electromagnetic disturbance is 80 dB. One can use two Kinney vacuum pumps in the laboratories when he experiments below 4.2K.

A helium liquefier (CTI-1410) with capacity of 40 l/h runs to supply liquid helium to research groups. The main laboratory building and the research facilities are equipped with the recycling pipings for helium gas. Helium gas used for experiments is recovered to Low-Temperature Center and is purified up to 99.99% purity. The flowsheet of the helium liquefaction system is as follows:

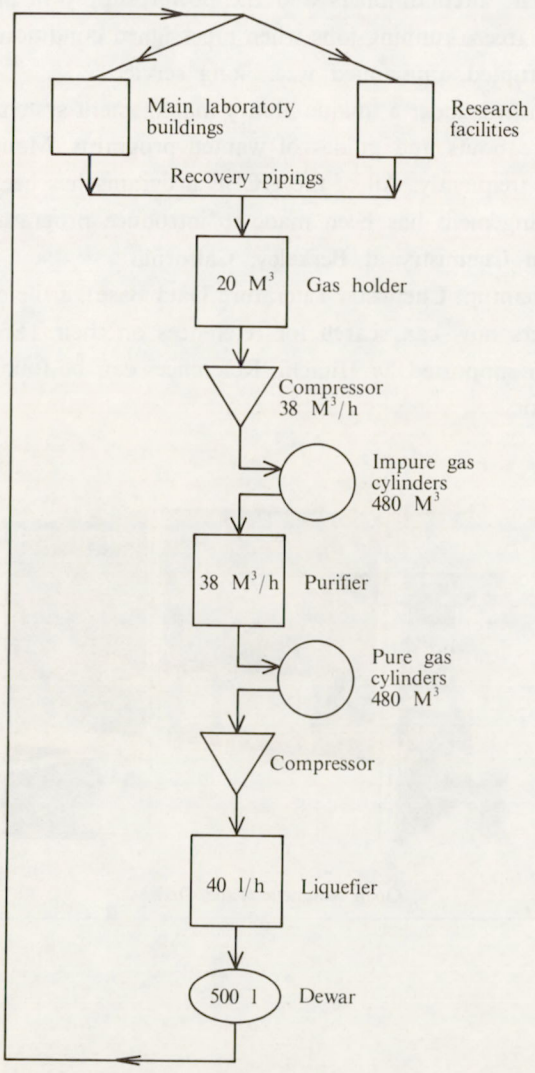

Major equipments are:

Helium Liquefier	CTI 1410
Helium Purifier	OSAKA SANSO UlO-1394-5
Cold Converter of Liquid Nitrogen	OSAKA SANSO CO-3
Helium Leak Detector	ULVAC DLMS-33
Rare Gas Purifier	BOC MK-3
Optical Measurement Cryostat	OXFORD 204
12T Superconducting Magnet	IGC MIDI-BRUTE-120
5T Superconducting Magnet	VMC SM-5075Q

Compressors of Helium Liquefaction System

Chemical Materials Center

The chemical materials center plays an important role in the preparation of chemical substances in IMS. The scientists and technicians of this facility carry out works on synthesis and purification of organic and inorganic compounds and preparation of single crystals. They develop new synthetic procedures to obtain interesting substances in pure forms and in large quantities. They also carry out their own researches on synthesis of new interesting chemicals, developments of new selective chemical transformations, elucidation of reaction mechanisms, and application of new methodologies developed in IMS to the analysis of chemical substances and reactions (see Research Activities VI-C ~ G). They participate in taking charge of and disposition of waste chemicals and solvents. The stockroom stores more than eight hundred chemicals and solvents.

Major equipments are:

Gas Chromatograph-Mass Spectrometer	JEOL JMS D300 equipped with EI, CI, and FD ion sources, and JMA-2000 mass data analysis system
NMR Spectrometer	Varian EM-390
High Performance Liquid Chromatographs	JASCO TRI ROTAR and JASCO FAMILIC-1000
Inert Atmosphere Glove Box	Vacuum Atmospheres Co. MO-40-2V DRI-TRAIN
CO_2 TEA Laser	LUMONICS 203
Infrared Spectrometer	Hitachi 295
Equipment for Crystal Growth	Assembled in IMS
Automatic Waste Fluid Disposition Apparatus	Yanaco YWT-1
Polarimeter	JASCO DIP-4
Zone Refiners	Shibayama SS-960 and Instruments Assembled in IMS
Auto Annular Teflon Spinning Band	Perkin-Elmer 251
Spaltrohr-Column Microdistillation System	Fischer HMS 300

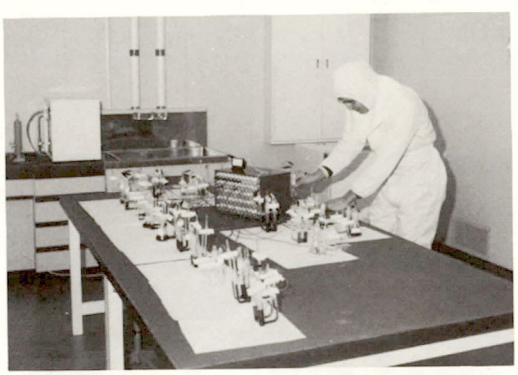

Clean Room Class 10000

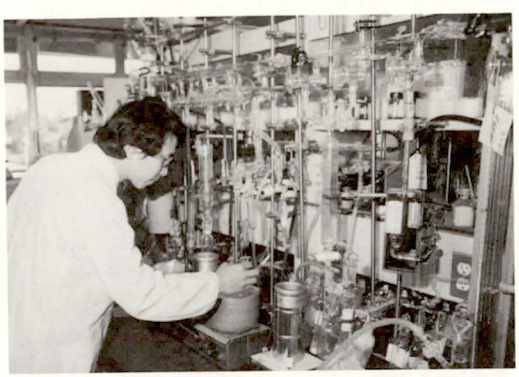

Research Laboratory

Instrument Center

For the efficient use of instruments, the Instrument Center is equipped with instruments for general use as listed below. The Center also lends out the total of some eighty electronic and optical instruments, such as oscilloscopes, amplifiers, signal averagers, function generators, electrometers, power supplies, recorders, monochromators, which are used inside the campus of IMS.

The Center had many visiting research scientists and graduate students from universities and the number of users of this facility amounted to 1800 in the fiscal year of 1980.

The Center staffs operate and do the maintenance work for these instruments and also conduct their own research by developing new instrumental techniques.

The major instruments are as follows:

Spectrophotometer	CARY 17
Dual-wavelength Spectrophotometer	HITACHI 556
Fourier-Transform IR Spectrophotometer	JEOL JIR-10
Fourier-Transform IR Spectrophotometer	NICOLET 7199A
Automatic Recording Spectropolarimeter	JASCO J40C
Emission Spectrophotometer	SHIMADZU RF-502
1-Meter VUV Scanning Monochromator	GCA MCPHERSON 225
Laser-Raman Spectrophotometer	JEOL JRS-400T
Subnanosecond Time-Resolved Fluorescence Spectrometer	SPECTRA PHYSICS 171-18, 375, 344S + ORTEC 6240B + NEC BS/80
Electrochemistry System	PAR 370-4
Argon Ion Laser	SPECTRA-PHYSICS 164-05
Helium-Neon Laser	SPECTRA-PHYSICS 125A
CW Dye Laser	SPECTRA-PHYSICS 375-90
Pulsed Dye Laser	MOLECTRON UV-24 + DL14
Pulsed Dye Laser	CHROMATIX CMX-4
X-ray Diffractometer	RIGAKU DENKI GEIGER FLEX 2027
Single Crystal Automatic Four Circle X-ray Diffractometer	RIGAKU DENKI AFC-5
Surface Roughness Tester	SLOAN DEKTAK
Thermal Analyzer	DUPONT 990

ESR Spectrometer

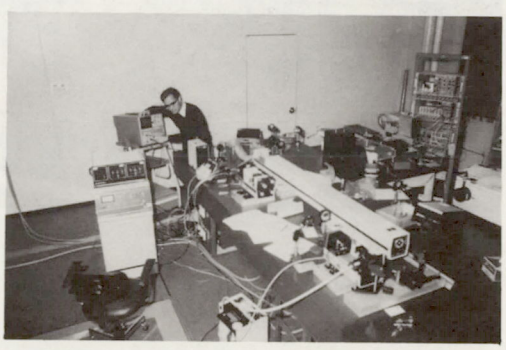

Subnanosecond Time-Resolved Fluorescence Spectrometer

High Vacuum Evaporator	ULVAC EBH-6
Scanning Electron Microscope	HITACHI S-450
Magnetic Balance	OXFORD
Fourier-Transform NMR Spectrometer	JEOL JNM-FX 100
ESR Spectrometer	VARIAN E-112/E-900
High Speed Refrigerated Centrifuge	KUBOTA KR-180A

Development Workshop

Development Workshop is expected to play a unique and important role in research activities at IMS. It designs and constructs instruments based on IMS's own ideas. It also improves existing research equipments. Technicians are making interplay with scientific staff members to support activities of the Workshop. Technical meetings are regularly held twice a year, which provide opportunities for technicians to exchange information and to discuss technical problems with those from other institutes and universities.

Development Workshop consists of machine shop, electronic shop, and glass-blowing shop.

1) Machine Shop

The facilities constructed or to be constructed at IMS include high-vacuum apparatus, lasers, microwave spectrometers as well as various types of equipments operated at the liquid-helium temperature. All these are of high performance and thus require very fine engineering to prepare their parts. Therefore, in addition to lathes, milling machines, drilling machines, and grinders of common use we have installed the following special machines:

(i) NC Lathe (OKUMA TEKKOSHO LS-N). This computer-controlled lathe has been used to prepare microwave lenses with spherical and/or paraboloidal surfaces, made of Teflon, TPX, or metals. It also made spherical collectors for electron spectroscopy. None of these parts can be constructed with a normal lathe. The electronic shop develops microcomputer facilities to feed tapes in the NC lathe.

(ii) Spark erosion machine (MAKINO SODICK GP-20L). This has been used to make a 50 mm diameter stainless steel cylinder can of 0.025 mm thickness, which is to support an optical window in a low-temperature apparatus. It has also been used to drill a very fine slit (0.04 mm wide and 30 mm long).

(iii) Electron-beam welder (NEC EBW). This can weld tightly two different kinds of metals (e.g. copper and stainless steel). This welding eliminates possible leakage in a vacuum apparatus operated at very low temperatures, especially in those parts that suffer from frequent changes in temperature. We can use a beam of 10 mA accelerated at a voltage of 150 kV under the pressure of 5×10^{-2} Pa or less. The maximum beam power is 1.5 kW.

(iv) Helium/nitrogen leak detector (ULVAC DLM 33). This detects a leakage in an ultra-high vacuum apparatus as small as 3×10^{-9} l·Pa/s. It may even detect the nitrogen gas. This machine consists of a detector combined with a vacuum system designed by the Machine Shop. It is equipped with a microcomputer that automatically eliminates backgrounds and noise signals.

(v) NC Milling Machine (MAKINO KGNCC-70). This has been used for some complicated fabrication which was not possible with a normal milling machine. The electronic shop develops microcomputer facilities to feed tapes in this machine.

(vi)Face Lathe (SEIBU KOKI LHS-3616). This lathe is employed in making large parts of equipments which can be as large as 1.6 m and 1.8 m in diameter and length, respectively, such as large-sized flange and vacuum chamber.

2) Electronic Shop

The major instruments installed are:

Oscilloscope	TEKTRONICS 7904 (500 MHz)

Oscilloscope	TEKTRONICS 475 (200 MHz)
Storage oscilloscope	HEWLETT PACKARD 1741A (100 MHz)
Sampling oscilloscope	IWATSU SAS-610B (12.4 GHz)
Spectrum analyzer	TAKEDA RIKEN 4110M (200 Hz – 1.3 GHz)
Frequency counter	TAKEDA RIKEN 5502C (≦ 1.4 GHz)
Lock-in amp	PAR 124
Boxcar integrator	PAR 162
LCR meter	HEWLETT PACKARD 4262A
Teletype	CASIO 502
Minicomputer system	NIHON MINICON ECLIPSE S-130

The Electronic Shop has designed and constructed a high-precision wavelength meter for infrared diode laser, a data processing system for a magnetic balance, and a microcomputer-controlled picture analyzer for a picosecond streak camera. It is also setting up a laser wavelength conversion unit utilizing parametric oscillation and also an interface for spectroscopic measurements in the vacuum ultraviolet region.

3) Glass-blowing Shop

We have installed the following machines:

Glass lathe	RIKEN SEIKO RGL-4DLH (max. diameter of the glass pipe is 20 mm)
Spot welder	NIPPON AVIOTRONICS NW-29 DS (100 W)
Water welder	FUJI BUSSAN S51-4 (oxygen/hydrogen evolving rate is 170 *l*/h)
Glass grinder	SANWA DIAMOND SDK 20-B (diamond disk 300 mmϕ with an angle holder)
Glass cutter	ITO DP-3 (diamond disk 200 mmϕ with an angle holder)
Ultrasonic microboring machine	CHO-OMPA KOGYO UM-2-7B
Ultrasonic soldering machine	ASAHI GLASS SUNBONDER USM-II

The shop has constructed, among others, high vacuum glass apparatus and laser tubes.

Electronic Shop

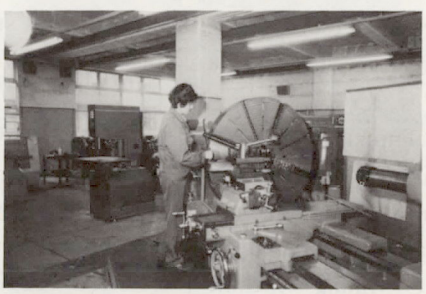

Machine Shop (Face Lathe)

Glass-blowing Shop

LARGE SCALE RESEARCH EQUIPMENTS

1) Picosecond Continuously Tunable Laser from UV to IR

The system consists of a mode-locked Nd:YAG laser with multistage amplifiers, crystals for second, third, and fourth harmonic generations, single-pass optical parametric oscillators (OPO) and amplifiers (OPOA), and crystals for second harmonic generation and frequency mixing. Four optical lines are constructed depending on the wavelength range as shown in Figure 1. Observed output wavelengths of OPOA in each line are shown in Figure 2 as a function of the phase-matching angle of the crystals. In the lines 2 and 3, which use KD*P crystals of TYPE II, the energy conversion efficiencies from pumping waves reached 25% and 35%, respectively. Such high conversion efficiencies or high peak powers in the OPOA enabled us to extend wavelengths efficiently into the UV region. Second harmonic generation of OPOA in the line 3 and up-conversions by frequency mixings of OPOA with pumping waves in the lines 2 and 3 are also shown in Figure 2. In the line 4 cascaded ADP crystals were pumped separately because otherwise, their low optical transmittances diminished the pumping power and obstructed the effective amplification in the second crystal.

Gaps in the tuning range in Figure 2 with the above methods can be convered in the line 4 by replacing the ADP crystals with KD*P crystals of TYPE I which have a wider tuning range and a higher transmittance.

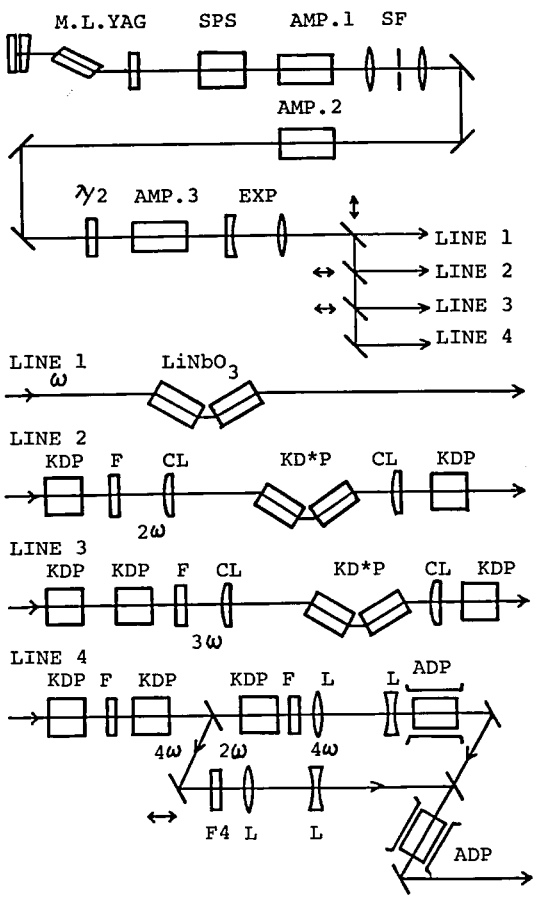

Figure 1. Optical arrangement of the system. M.L.YAG: mode locked YAG laser, SPS: single pulse selector, SF: spatial filter, λ/2: half wave plate, EXP: beam expander, F: filter, CL: cylindrical lens, and L: lens.

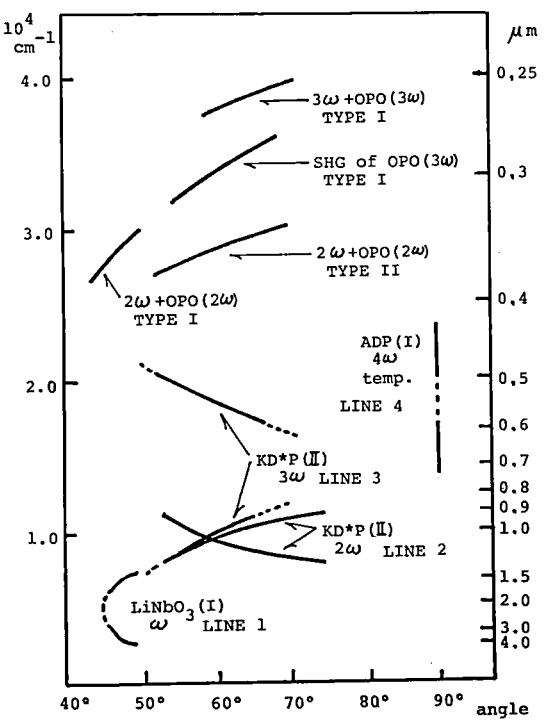

Figure 2. Output wavelengths of the OPOA and further frequency conversions.

2) High Resolution Spectroscopy

The system consists of two cw tunable lasers with high spectral purity, one in the visible region and the other in the infrared region.

2-a) Dye lasers in the visible region

Dye lasers and pump Ar^+ lasers remain the same as in the last year [IMS Ann. Rev. 135 (1980)]. They have been used in exciting fluorescence of unstable molecules (II-A-2, II-A-13), and also in microwave optical double resonance of HNO (II-A-3) and infrared optical double resonance of NH_2 (II-A-4). Professor K. Takagi *(Toyama Univ.)* and Dr. T. Amano *(Univ. of Tokyo)* have contributed, respectively, to the HNO and NH_2 works under a Joint Studies Program of IMS. Dr. N. Ohashi *(Kanazawa Univ.)* is continuing a study on singlet methylene, and Professor F. Shimizu *(Univ. of Tokyo)* and his coworker have observed two-photon signals of Na. Professor T. Yagi and Dr. A. Sakai *(Kyushu Univ.)* have attempted to observe linewidths of Rayleigh scattering spectra of a dielectric compound around a phase transition point. All these three works were also sponsored by the IMS Joint Studies Program.

2-b) Diode lasers in the infrared region

Laser diodes have been supplied by the Laser Analytics and also by the Fujitsu Laboratories. At present more than 20 diodes are working in the region from 580 cm^{-1} to 2860 cm^{-1}. The spectroscopic system essentially remains the same as in the last year [*IMS Ann. Rev.* 136 (1980)]. A discharge-current modulation technique has been developed to observe diamagnetic transitions of unstable molecules (II-B-1).

The spectrometer has been mainly used for detecting transient molecules or metastable atoms (II-A-1, II-A-5, II-A-7, II-A-8, II-A-11, II-A-12). S. Sofue et al. measured absorption intensities of the CHF_3 ν_4 band, which they have recently analyzed again using the same diode laser spectrometer [*Bull. Chem. Soc. Japan* **54**, 897 (1981)]. Professor Mr. Tsuboi *(Univ. of Tokyo and IMS)* and Dr. Y. Hamada *(Univ. of Tokyo)* are continuing observations and analyses of the NH_2NH_2 antisymmetric NH_2 wagging and the $^{15}NO_2$ ν_2 bands. Mr. H. Kuze *(Univ. of Tokyo)* is working on the C = 0 stretching band of formic acid. Dr. M. Takami has nearly completed the analysis of the CF_4 ν_3 band, except for a part of it perturbed by $2\nu_4$. He is extending similar studies to other tetrahedral molecules. All these works are sponsored by the IMS Joint Studies Program.

3) High Resolution Spectroscopic System in the Far-Infrared Region

Millimeter-wave sources have been installed, and have thus extended frequency coverage beyond 180 GHz. Six klystrons oscillate in the region up to 221 GHz (with a gap from 203 to 218 GHz), and a backward-wave oscillator in a higher-frequency region, 285–305 GHz (i.e. around 1 mm). These sources have been successfully incorporated with a microwave spectrometer already set up, with replacement of a Schottky-barrier diode by an InSb helium-cooled detector, and have been used to observe rotational spectra of PH_2 (II-A-15), CCl (II-A-6), SF [*IMS Ann. Rev.* 46 (1980)], and DO_2 (II-A-10). Applications of the system have also been made by Dr. M. Tanimoto (*Sagami Chem. Res*] *Center*) to rotational spectra of NO_2 in excited vibrational states (II-C-1) and by Dr. Y. Hamada (*Univ. of Tokyo*) to rotational spectra of $^{15}NO_2$ in the ground state under the IMS Joint Studies Program.

A CO_2-laser pumped far-infrared (FIR) laser has also been completed, and at present gives laser lines in the region from 70 μm to 500 μm. This laser has been combined with an absorption cell placed between the pole pieces of an electromagnet, to form a FIR laser magnetic resonance (IMR) spectrometer. Although an InSb detector under use works best at the 1 mm region, we have confirmed that about 10^{-5} of the input laser power can be detected at 163 μm.

4) Ultraviolet Synchrotron Orbital Radiation (UVSOR) Facility

The proposal for constructing a dedicated synchrotron radiation facility as one of the large scale equipments at IMS was approved in the 1980 fiscal year[1] and its construction is now in progress.

The facility, deliberately designed by the members of the UVSOR working group, consists of a 600 MeV storage ring, a 600 MeV injector synchrotron with a 15 MeV linac, experimental stations, and several experimental support facilities in a 2700 m^2 building.[2,3] The storage ring has a circumference of 53.2 m, consisting of eight bending magnet sections, four short straight sections, and four long straight sections. The radius of the bending magnet is 2.2 m, making the use of radiation down to 10 Å feasible at 600 MeV of electron energy (λ_c = 56.9 Å). The layout of the linac, synchrotron, storage ring, and beam channels is shown in Figure 1. The whole facility is expected to be completed by the end of March 1984 and the service for users will be available in April 1984.

In the 1980 fiscal year, a starting budget was granted for experimental equipments. Two 1-m vertical-dispersion Seya-Namioka monochromators and a standard ultrahigh vacuum chamber for use in the gas-phase experiments have been constructed with it. The construction of the light source itself has been started this year commencing with the injector synchrotoron and linac. Considerable efforts have thus been devoted this year to the design of the synchrotron and linac. The details of the design studies are published elsewhere.[4] The synchrotron, with energy and current of 600 MeV and 50 mA, respectively, has a circumference of 26.6 m consisting of six bending magnet sections and six straight sections (perodicity is 6). The radius of the bending magnet is 1.8 m. At each straight section, a doublet of quadrupole magnets is installed. Also installed in appropriate straight sections are an inflector for injection, an RF cavity, and a set of a fast kicker and a deflector for extraction. The maximum repetition rate is 3 Hz with the rise time of 0.15 s.

Design of a plane grating monochromator for use in the solid state photoemission experiments has also been completed this year and its construction is going on. Design of the UVSOR building has almost been completed in cooperation with the Building and the Equipment Divisions and the ground breaking is expected to be held in October.

References

1) IMS Ann. Rev., 136 (1980).
2) M. Watanabe, A. Uchida, O. Matsudo, K. Sakai, K. Takami, T. Katayama, K. Yoshida, and M. Kihara, IEEE Trans. NS-28, 3175 (1981).
3) I. Koyano, Y. Achiba, H. Inokuchi, E. Ishiguro, R. Kato, K. Kimura, K. Seki, K. Shobatake, K. Tabayashi, Y. Takagi, K. Tanaka, A. Uchida, and M. Watanabe, Nucl. Instrum. Methods, (1982), to be published.
4) M. Watanabe, A. Uchida, O. Matsudo, K. Sakai, K. Takami, T. Katayama, K. Yoshida, and M. Kihara, UVSOR-7, (1981) (in Japanese).

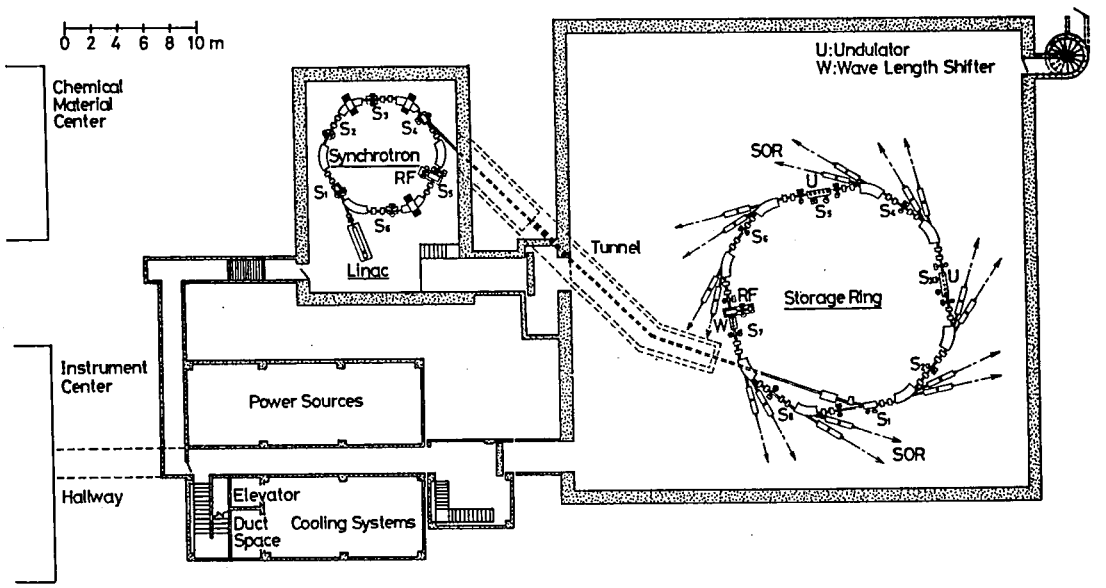

Figure 1. Layout of the UVSOR light source and beam channels.

SPECIAL RESEARCH PROJECT

IMS has special research projects supported by national funds. Two projects presently in progress under the second five year plan (1980–1985) are:
(1) The development and control of molecular functions,
(2) Energy transfer and energy conversion through molecular processes.
These projects are being carried out with close collaboration between research devisions and facilities. Collaborators from outside also make important contributions. Research fellows join these porjects. In this report, the results in 1980 are reviewed.

(1) The Development and Control of Molecular Functions

Spectroscopic Studies of Gaseous Molecular Complexes and Clusters

Katsumi KIMURA,* Kosuke SHOBATAKE,* Yohji ACHIBA, Kiyohiko TABAYASHI, Shinji TOMODA, and Kenji SATO

Supersonic free jet expansion is useful for production of molecular complexes and clusters in the gas phase as well as for lowering the translational and internal temperatures of the expanded gas. In order to elucidate the bonding characters and ammonia and NO (see RA IV-K-2). For molecular complexes and clusters we have performed the present project. Spectroscopic techniques applied are HeI photoelectron spectroscopy (PES), laser multiphoton ionization (MPI) spectroscopy and high resolution infrared spectroscopy, and the gaseous molecules and molecular complexes were produced by the free jet expansion.

To begin with we have studied the HeI PES of water dimer (see Research Activities IV-J-1) and the resonant MPI-PES of benzene (see RA IV-K-3) and ammonia and NO (see RA IV-K-2). For the high resolution infrared spectroscopy of molecular complexes we purchased a color center infrared laser – Burleigh Model FCL-20 with 1 MHz band width. Development of an infrared laser-bolometer system is in progress.

Molecular Designing of Novel Cyclic Compounds and Their Interaction with Metals

Hiizu IWAMURA,* Tasuku ITO,* Tadashi SUGAWARA, Koshiro TORIUMI, Yuzo KAWADA, and Masako SUGIMOTO

A series of cyclic organic compounds has been designed, prepared and analyzed to develop novel physico-chemical properties of their metal complexes. A stable silver(II) salt was found to be formed when complexed with a 14-membered tetraaza macrocyclic ligand. X-ray crystallography has revealed the presence of two isomeric structures for the salt. Difference in the degree of strain between the two molecules is discussed in relation to their interesting properties (see Research Activities V-E-1, V-E-2, V-F-1, and V-F-2). The solution structure of potassium chloride incorporated in the crown ethers has been studied by the line widths of ^{35}Cl NMR. The ion-pairing constants of the chloride ion which are intimately related to the transport phenomena of alkali halides in the living cell and to the nucleophilic reactivity of Cl^- were explicitly obtained (see Research Activities V-C-4).

Transition Metal Catalyzed Rearrangements of Small Ring Organic Molecules. Interception and Characterization of Unstable Intermediates

Akira MIYASHITA and Hidemasa TAKAYA*

Highly strained organic molecules rearrange upon exposure to a variety of transition metal complexes. This type of reaction is recently of great interest as a chemical conversion process of solar energy. Although extensive efforts have been done

so far, very little has been known for the mechanism of the catalysis. We have studied the reaciton of bicyclo[1.1.0]butane (1) with transition metal complexes.[1] First isolation of transition metal complexes of 1 have been successfully done by the reaction of 1 and Pt(II) complexes.[2] The interesting chemical behaviors and the remarkable temperature dependence of the NMR spectra of the complexes were found. The results are summarized in VI-C~G.

References

1) H. Takaya, T. Suzuki, Y. Kumagai, M. Hosoya, H. Kawauchi, and R. Noyori, *J. Org. Chem.*, **46**, 2854 (1981).
2) A. Miyashita, M. Takahashi, and H. Takaya, *J. Am. Chem. Soc.*, in press.

Optical Method of FTEPR in the Ground and Excited States in Molecules

Yoshihiro TAKAGI

Optical excitation of Zeeman coherence in paramagnetic or even in diamagnetic molecules provides us with a novel technique in the pulsed EPR.[1] We have succeeded in observing optically induced Zeeman coherence in the ground state of some paramagnetic materials. Our main pourpose now is to produce the Zeeman coherence in the excited state in molecules. In order that the Zeeman sublevels are well separated under the magnetic field and that the thermal broadening is sharpened, we designed a superconducting magnet with four optical windows. Its specifications are as follows. Maximum field strength: 3.5T. Liquid helium consumption: 0.65 *l*/hour. Hold-time of liquid helium: 10 hours. Sample temperature range: 1.6–300 K. Bore: 30 mm. Split: 28 mm.

The magnet is soon assembled to the experimental system. (see Research Activities VI-Q, R)

Reference

1) Y. Takagi, Y. Fukuda, K. Yamada, and T. Hashi, *J. Phys. Soc. Japan*, **50**, 2762 (1981).

Development of Picosecond Light Sources for Photon Echo Studies of Molecular Vibrational Relaxations

Masahiro MATSUOKA* *(Kyoto Univ. and IMS)*, **Masayuki FUJITA, and Shuji ASAKA** *(Kyoto Univ.)*

Development of a picosecond laser-amplifier system has been continued since 1979. A synchronously pumped mode-locked dye-laser (Spectra Physics) and three-stage YAG-laser-pumped dye-amplifires produced 1 MW pulses with 7 psec pulse-width, and were used previously for picosecond photon echoes on atomic and molecular systems (Ann. Rev. 1980).

During the year, we have improved the performance of the above amplifiers in order to produce picosecond UV-pulses out of the amplifier output. The program was delayed by more than eight months due to a glass tube break-down of the Ar ion laser. Increasing the dye cell length from 1.5 to 4 cm, and inserting saturable absorber filters between the stages, we have obtained near 100 times amplification in each stage.

(2) Energy Transfer and Energy Conversion through Molecular Processes

Theoretical Studies of Photosynthesis Systems and Solid Surfaces as Energy Conversion Systems

Hiroshi KASHIWAGI,* Shigeru OBARA, Unpei NAGASHIMA, Masaru TSUKADA,* Chikatoshi SATOKO, and Toshiharu HOSHINO

Theoretical studies of chlorophille and Fe-porphyrin complexes provide essential information for understanding of the mechanism of energy transfer in biological system. For the first step of this research, we carried out to make clear some important electronic states of chlorophille monomer and some Fe-porphine complexes by using ab initio SCF-MO method.

Two graphic displaying subroutine packages,

JAPIC1 and JAPIC2, were coded for drawing an electron density contour map of obtained from these calculations. The program packages are connected with JAMOL3. And the contour map drawn by JAPIC1 or JAPIC2 are very useful to understand the electron distribution result of MO calculation. Some part of a program system JASON for multiconfiguration SCF(MCSCF) calculation was developed.

A wide variety of energy conversion processes take place on the interfaces between the solid and the gas or the liquid phases. Theoretical elucidation of surface reaction mechanisms is crucially important for the design of efficient energy conversion system. Toward this goal, we studied static and/or dynamic chemisorption mechanisms as well as basic electronic properties of solid surfaces. Some impotant theoretical methods have been developed including the LCAO-Xα direct force method, the improved chemical pseudopotential method and Haselgrov multi-dimensional integration method.

Picosecond Fluorescence Studies of P700-Enriched Particles of Spinach Chloroplasts

Keiji KAMOGAWA, John M. MORRIS, Yoshihiro TAKAGI, Nobuaki NAKASHIMA, Keitaro YOSHIHARA,* and Isamu IKEGAMI *(Teikyo Univ.)*

Dynamic properties were investigated on the picosecond fluorescence of highly enriched reaction center particles of photosystem I prepared from spinach. The number of photons to excite chlorophyll molecules per reaction center was controlled from 0.06 to 80. The 1/e lifetime was ca. 25 ps, which is much shorter than the ones already known for photosystem I particles. The local structure of the particle and the mechanism of energy transfer were discussed in terms of fluorescence lifetime, exciton-exciton annihilation, time-resolved fluorescence spectroscopy, and effect of heat-treatment on fluorescence decay. (see III-C-2).

Photoelectrochemical Decomposition of Water and Chemical Conversion of Solar Energy

Kazuhito HASHIMOTO, Tomoji KAWAI, Tadayoshi SAKATA,* and Hiroshi TSUBOMURA* *(Osaka Univ. and IMS)*

We have demonstrated an efficient hydrogen production from water and various organic materials by using surface modified semiconductor (mainly TiO_2) photocatalysts. To exploit a new photocatalyst which works efficiency with visible light, the photocatalytic activity of various kinds of semiconductors was examined extensively. Among a number of photocatalysts, CdS/Pt was found to be most active. The fundamental properties of powdered semiconductor photocatalysts were explained based on the photochemical diode model. The electronic structure of particle semiconductor/metal diode, a small-particle effect on hydrogen evolution, an intimate correlation between hydrogen evolution and the irreversibility of oxidation of substrate molecules, and the suporting effect of Pt on powdered semiconductors were investigated. The photocatalytic redox reactions of carbohydrates, organic acids, alcohols, etc., were being investigated from the view point of organic synthesis.

Hydrogen evolution was successfully attained by using the dye sensitization effect of semiconductors, even though the efficienceis were not high. Efficient hydrogen evolution was also succeeded in by using fluorescein derivatives as new photocatalysts and the mechanism was discussed (see III-D).

The doping effect of $SrTiO_3$ electrode was studied by using various metals. Among them a $SrTiO_3$ doped with Ru was demonstrated to decompose water with visible light (see III-K).

Measurements of Translational Energy Distributions of Fragments Produced by the IR-Multiphoton Dissociation of Trichloroethylene

Iwao NISHIYAMA and Ichiro HANAZAKI*

As descrived in III-E-1, the IR multiphoton dissociation of trichloroethylene proceeds efficiently under the collision free condition. The fragment produced in a primary process and its translational energy distribution were measured by a time-of-flight technique using a supersonic nozzle beam and a mass spectrometric detection. C_2Cl_2 fragment was observed with the highest intensity among expected fragments, indicating that the main branch of

reaction was HCl elimination. Translational energy distribution of C_2Cl_2 in a center of mass system was estimated from the time-of-flight spectrum by a computer simulation. The average translational energy was estimated to be 0.74 kcal/mol.

Optical Generation of High Energy Reactant by VUV Multiphoton Excitation

Nobuyuki NISHI* and Hisanori SHINOHARA

A high power VUV laser can generate energetically rich reactants by multiphoton excitation of simple polyatomic molecules. An electronically excited reactant usually shows much greater reaction rate than a ground state species. Molecular beams of vinyl compounds(C_2H_3X, X = CHO, CN, Cl and Br) have been irradiated with an ArF laser to generate high energy reactants. The maximum yield of the two-photon generation of the excited fragments through the reaction, $C_2H_3CHO \rightarrow C_2H_2^* + CO^* + 2H$, is estimated to be ~ 25% relative to that of the one-photon process yielding $C_2H_3 + CHO$ with the laser power of 150 mJ collected in the area of 2×7 mm^2. Since two-photon process increases quadratically to the laser power, in principle, the two-photon reaction is expected to become domonant over one-photon processes in the power range higher than 3.2 J/cm^2 (450 mJ in 2×7 mm^2 or 150 mJ in 2×2.3 mm^2). A large part of the excess energy of 6.0 eV in this reaction must be left as the internal energy of the C_2H_2 fragment.

In the photolysis of acrylonitrile(C_2H_3CN), we detected the extremely high energy CN radical in the v = 14 level of the $F^2\Delta_r$ state. Three photons of 193 nm light are enough to produce this species. The yield of multiphoton generated reactant is a function of molar extinction coefficient at a given laser wavelength. The high yields of multiphoton excitations in the vinyl compounds are attributed to the large extinction coefficients (~ 5000) at 193 nm.

OKAZAKI CONFERENCES

"Okazaki Conferences" are principal symposia at IMS, which are held on the subjects related to the "Special Research Projects". They are held usually twice a year, with a moderate number of participants around 50, including several invited foreign speakers. The formal language for the conference is English. Ten conferences have been already held successfully. Outlines of the eleventh and twelfth conferences are as follows:

The Eleventh Okazaki Conference

The Molecular Potential Function — Present Status and New Aspects

(December 3—5, 1980)

Organizers: T. Fujiyama *(IMS)* **and M. Tatsumi** *(Tokyo Univ.)*
Invited Speakers: I. M. Mills *(Univ. of Reading)*, **G. Zerbi** *(Istituto di Chimica Industriale del Politecnico)*, **A. C. Albrecht** *(Cornell Univ.)*, **and R. N. Jones** *(Tokyo Inst. Tech.)*.

The purpose of this conference was, firstly, to ascertain the present status of potential function studies and, secondly, to find out new aspects which we should attack in the near future. The topics which were discussed in this conference may be classified into four categories.

1) Accurate Analyses of Potential Functions.

We devoted the first day of this conference to the discussion of the determination of accurate potential functions. It was only natural to include a consideration of large amplitude vibration problems, tunneling problems, and anharmonicity problems. We were certainly glad to have an opportunity to ascertain the present status and future aspects of the *ab initio* calculation of force constants.

For these topics, we have invited Professor Ian

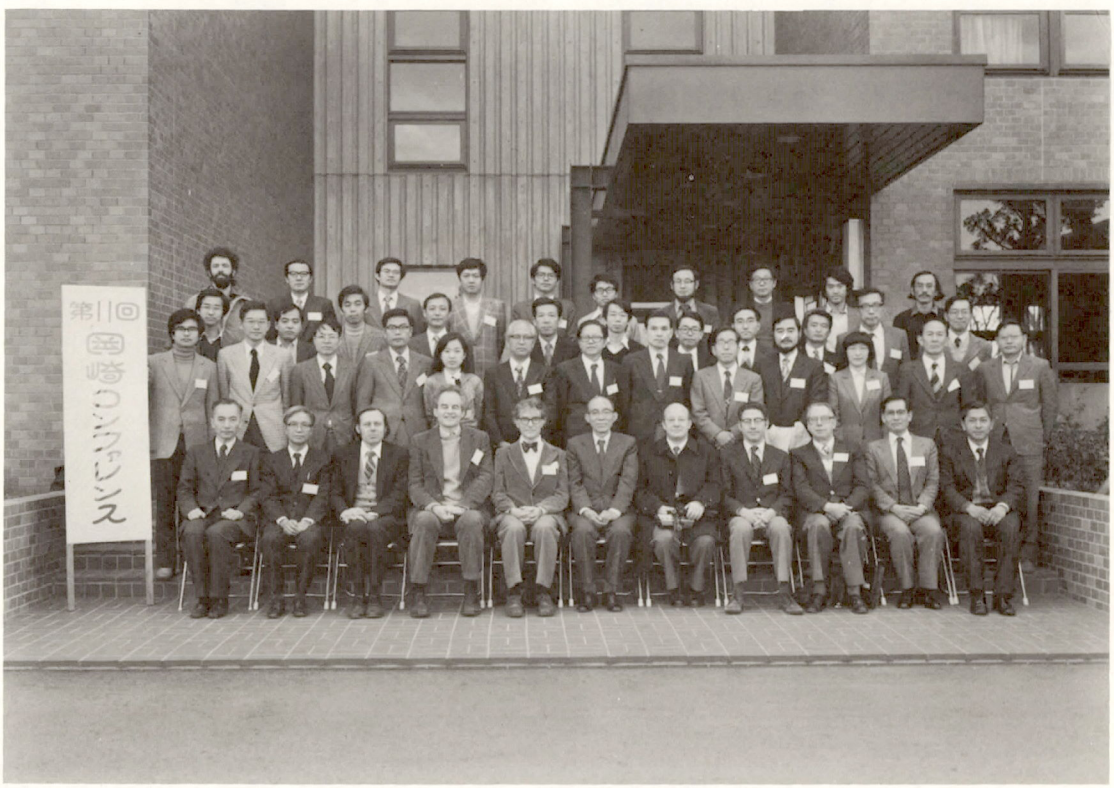

The Eleventh Okazaki Conference December 3–5, 1980

M. Mills from the United Kingdom, Professor Keiji Morokuma from IMS Fortunately, Dr. Jon T. Hougen of NBS was staying in IMS, and gave a lecture.

2) Vibrational Assignments.

The prediction of resonance frequencies and intensities of vibrational spectra is essential for the application of vibrational spectroscopy. This session represented one of the central ideas of this conference.

For these topics, we have invited Professor Giuseppe Zerbi from Italy, Professor Samuel Krimm from the United States, Professor Mitsuo Tatsumi, who was one of the organizers of this conference, also gave a paper on this subject.

3) Intermolecular Potential Functions.

Lectures were given on the difficulties in and importance of the study of intermolecular potential functions in condensed systems.

For these topics, Professor Michio Kobayashi of Osaka University, Dr. Yosuke Kataoka from Kyoto University were invited. Professor Tsunetake Fujiyama of IMS also made a presentation on this subject.

4) Highly Excited Vibrational States.

As a current topic, we intended to discuss the formation of local modes in highly excited vibrational states.

For this topic, we have invited Professor A. C. Albrecht from the United States and Professor Keietsu Tamagake from Okayama University.

Professor R. Norman Jones was invited to this conference as an after dinner speaker. He gave a talk on "Students Present and Spectroscopists Past".

The Twelfth Okazaki Conference

The Roles of Transition Metal Complexes in Chemical and Biochemical Conversions

(December 11—13, 1980)

Organizer: H. Takaya *(IMS)*
Invited Speakers: J. P. Collman *(Stanford Univ.)*, **R. Pettit** *(Univ. of Texas, Austin)*, **and J. K. Stille** *(Colorado State Univ.)*

Transition metal complexes play an extremely important role in chemical and biochemical

The Twelfth Okazaki Conference December 11–13, 1980

reactions. Especially it is one of the surprising characteristics of transition metals that they promote chemical reactions with very high selectivity under mild conditions. The purpose of the Twelfth Okazaki Conference was to understand the origin of these interesting and important characteristics of transition metals and to apply these results to the molecular design of new highly functional transition metal catalysts. Fifty-three scientists including three invited speakers from abroad participated in the Conference, and twenty-seven lectures were presented.

Since this conference covered a wide range of topics, it was devided into four sessions. In Session I (Transition Metal-Promoted Selective Organic Synthesis), Professor Stille made a special lecture on his recent results concerning with the mechanisms of reductive elimination from Group VIII transition metal alkyls, which is very important as the last step in many catalytic cycles. The Session II dealt with "Preparation, Properties, and Functions of Enzyme Model Compounds." Professor Collman in his special lecture entitled "Molecular Engineering" talked on the preparations and properties of a large number of binary, cyclophane, "face-to-face" porphyrins and their metal complexes. The Co(II) complexes are effective catalysts for the four-electron reduction of oxygen in aqueous medium at graphite electrode surfaces. This is a splended result of prudent design of molecules with desired functions. In Session III (New Energy Conversion Processes) Professor Pettit revealed his own work pertaining to the elucidation of the mechanism of the Fischer-Tropsch reaction, which is currently considered to be a promising candidate for the large scale conversion of coal to liquid hydrocarbons. On the last day in Session IV, our attention was focused on "Theoretical Aspects on the Stability and Reactivity of Metal Complexes.

JOINT STUDIES PROGRAMS

As one of the important functions of an inter-university research institution, IMS undertakes joint studies programs for which funds are available to cover research expenses as well as travel and living expenses of individuals. The proposals from domestic scientists are reviewed and controlled by the inter-university committee. The programs are carried out under one of four categories:

1) Joint Studies on special projects (a special project of significant relevance to the advancement of molecular science can be carried out by a team of several groups of scientists).
2) Research Symposia (on timely topics in collaboration with both outside and IMS scientists).
3) Cooperative Research (carried out in collaboration with both outside and IMS scientists).
4) Use of Facility (the Computer Center, Instrument Center and other research facilities at IMS are open to all researchers throughout the country).

In the fiscal year 1980, numbers of joint studies programs accepted amounted to 6, 11 and 170 for categories 1) ~ 3), respectively.

1) Joint Studies

Developments and Applications of New Spectroscopic Methods Using Tunable, Coherent, and High-Resolution Light Sources

Coordinators: **Eizi HIROTA** *(Department of Molecular Structure)*
Shuji SAITO *(Department of Molecular Structure)*

The emphasis has been mainly placed on development and application of the double-resonance technique. Prof. K. Takagi (*Toyama Univ.*) collaborated with S. Saito and T. Suzuki in extending MODR (microwave-optical double resonance) to the $\tilde{A}^1A''(020)$ of HNO. They observed four perturbed rotational transitions to clearly exhibit Zeeman effects. Dr. T. Amano (*Univ. of Tokyo*) was assisted by K. Kawaguchi et al. in continuing IODR (infrared-optical double resonance) on the NH_2 radical. They thus observed the $(0,9,0)2_{20} \rightarrow (0,8,0)3_{31}$ transition in the $\tilde{A}^2A_1$ state. Dr. M. Takami (*Inst. Phys. Chem. Res.*) has nearly completed observation of the CF_4 ν_3 band, by using microwave (or rf) infrared diode laser double resonance. Dr. N. Ohashi (*Kanazawa Univ.*), S. Saito, and T. Suzuki have succeeded in observing dye-laser excitation spectra of the CH_2 $\tilde{b}^1B_1 - \tilde{a}^1A_1$ transition, by photolyzing ketene with the Ar^+ laser 334 nm line. They observed 31 and 9 transitions, respectively, for the (0,14,0) − (0,0,0) and (0,13,0) − (0,0,0) bands. Prof. F. Shimizu (*Univ. of Tokyo*) has tested a resonance two-photon spectroscopic method on the Na $5s_{1/2} - 3p_{1/2} - 3s_{1/2}$ system, paying attention to laser-power dependence, frequency shifts, and other phenomena characteristic of the two-photon signal.

Intermolecular Interactions in the Two- and Three Dimensional Molecular Assemblies of Zwitter-ionic Surfactants

Coordinator: **Tsunetake FUJIYAMA** *(Department of Molecular Structure)*

Synthesis and Solid State Chemistry of Azaaromatic Solids

Coordinators: **Hiroo INOKUCHI** *(Department of Molecular Assemblies)*
Junji AOKI *(Toho University)*
Satoshi IWASHIMA *(Meisei University)*

When we introduce nitrogen atoms to a polycyclic aromatic hydrocarbon, its physico-chemical and also biological properties possess often very peculiar characters. In this joint research, we concentrate to prepare azabenzanthrone series and their condensed polycyclics. After careful preparations, we obtained 1-azabenzanthrone and 8-azabenzanthrone. The comparison of physico-

chemical properties between aza-aromatics and ordinary aromatics is in due course.

Development of Variable Temperature Molecular Beam Sources For Spectroscopic Studies of Gaseous Molecular Complexes

Coordinator: **Katsumi KIMURA** *(Department of Molecular Assemblies)*

In the last five years, great interest has been aroused in the spectroscopic studies of molecular complexes and jet-cooled molecules. Since molecular complexes and van der Waals molecules are efficiently formed and furthermore the temperature is known to be a very important factor for determining their concentrations, we decided to design and construct a variable temperature supersonic nozzle beam source. This low temperature nozzle beam source can be cooled down to the liquid nitrogen temperature by thermal conduction to the liq. N_2 reservoir. The desired temperature will be attained and controlled by resistively heating the beam source. The beam source assembly was designed in-house members. Its construction is under way after thorough discussions among the members of the present joint study during the meeting mentioned below.

Since an increasing number of invesigators have shown great interests in applications of molecular beam techniques and supersonic free expansion technique to various branches of physical chemistry, we held a meeting entitled "Molecular Beam Chemistry" on March 13 and 14, 1981. It was attended by 55 participants. The sessions were devoted to (1) the presentation of and discussions about the detailed design of the variable low temperature beam source, (2) a lecture on the aerodynamic point of view of the supersonic free expansion of atoms and molecules, and (3) its applications to various spectroscopies and reaction dynamics.

Ultraviolet Synchrotron Orbital Radiation (UVSOR)

Coordinator: **Katsumi KIMURA** *(Department of Molecular Assemblies)*

Ultraviolet synchrotron orbital radiation (UVSOR) facility has been proposed in the Institute for Molecular Science. In 1980, construction of optical instruments has been initiated. Construction of a 600 MeV electron storage ring with a 600 MeV injector synchrotron has started in 1981. We organized a working group for this UVSOR project by the following members : H. Inokuchi, K. Kimura, H. Watanabe, I. Koyano, K. Shobatake, and A. Uchida.

Under the present program, we had two UVSOR meetings, one of which is a small size meeting on UVSOR experiment systems (June 21, 1980), and the other is the second UVSOR Conference (December 8–9, 1980). The purpose of the second UVSOR Conference was to obtain critical comments and suggestions on the designs of our UVSOR experiment systems and the UVSOR machines from those who are interested in this field in Japan. The abstracts of these two meetings are published in UVSOR Pamphlets 5 and 6.

The UVSOR injector synchrotron has been designed by the following members : M. Watanabe (IMS), A. Uchida (IMS), O. Matsudo (IMS), K. Sakai (IMS), Dr. K. Takami (KURRI), Prof. T. Katayama (INS), Prof. K. Yoshida (INS), and M. Kihara (KEK, IMS). The detailed design of the UVSOR injector synchrotron is reported in UVSOR Pamphlet 7.

Accurate Determination of Electron-Density Distribution in Crystals and Developments of Techniques for Improving Accuracy

Coordinators: **Yoshihiko SAITO** *(Keio University)*
Tasuku ITO *(Department of Applied Molecular Science)*

A gas-stream cooling device for four-circle diffractometer newly designed by the present joint study has been installed at IMS. The device was further improved and at the steady state it is now possible to maintain the temperature range of ±1K at 95K.

Meetings were held twice at IMS in 1980–1981 and the recent results of accurate electron-density studies were discussed. The charge distribution in metallic chromium has been determined based on

reflection data measured up to $\sin\theta/\lambda = 1.72$ Å^{-1} with Ag Kα radiation using a spherical specimen. In the difference synthesis a positive peak of 1.4(1) e Å^{-3} was found in the direction toward the nearest neighbors at 0.25 Å from the Cr nucleus. This is presumably due to the asphericity arising from 3d electrons in t_{2g} orbitals. The result qualitatively agree with that calculated by APW method using orbital dependent pontentials. The electron-density distribution in crystals of $Mo_2(CH_3CO_2)_4$ has been determined by single-crystal diffractometry at 293K. The general features of the observed deformation density maps can be reasonably accounted for in terms of a picture of a quadruple Mo-Mo bond and also agree with the result of ab initio CI calculations for analogous $Mo_2(HCO_2)_4$. Other crystals studied by the present group are: KMF_3 [M = Mn, Co, Ni], K_2PtCl_4, U_3P_4 and clathrate compound, CH_3OH, $3C_6H_4(OH)_2$. This last study revealed that the data collection at liquid helium temperature is necessary to obtain sufficiently accurate data unaffected by thermal vibration.

2) Research Symposia

1. Inorganic Chemistry and Electronic Structure Theory
   (June 9th — 10th, 1980)
   Organizer: T. Yonezawa (IMS and Kyoto Univ.)
   No. of Participants: 37
2. Behaviour of Electrons in Biological Systems — around Chlorophyll
   (July 9th — 10th, 1980)
   Organizer: F. Hirota (Shizuoka Univ.)
   No. of Participants: 37
3. Photochemical Energy Conversion in Solutions, Including Dispersed Systems
   (August 12th — 13th)
   Organizer: K. Yoshihara (IMS)
   No. of Participants: 50
4. Development and Application of High-Sensitivity Microwave Spectrometer
   (August 23rd, 1980)
   Organizer: S. Saito (IMS)
   No. of Participants: 34
5. Dynamical Structures in Liquids and Solutions
   (September 22nd — 24th, 1980)
   Organizer: T. Yamamoto (Kyoto Univ.)
   No. of Participants: 47
6. Molecular Systems for Electronic Devices
   (November 26th — 29th, 1980)
   Organizer: H. Kuroda (Univ. of Tokyo)
   No. of Participants: 35
7. Survey and Progress of Theoretical Chemistry
   (December 1st — 3rd, 1980)
   Organizer: H. Nakatsuji (Kyoto Univ.)
   No. of Participants: 45
8. UVSOR Project — Design of Injector Syncrotron and Experiment Systems
   (December 8th — 9th, 1980)
   Organizer: K. Kimura (IMS)
   No. of Participants: 53
9. Elementary Process in Chemical Reactions
   (December 14th — 15th, 1980)
   Organizer: I. Kusunoki (Tohoku Univ.)
   No. of Participants: 40
10. Weak Molecular Interactions in Organic Molecules and Biological Systems
    (February 7th — 8th, 1981)
    Organizer: M. Hirota (Yokohama National Univ.)
    No. of Participants: 15
11. Recent Progress in the Theory of Electronically Excited Species
    (February 16th — 17th, 1981)
    Organizer: K. Morokuma (IMS)
    No. of Participants: 40

3) Cooperative Research

This is probably one of the most important programs IMS undertakes for conducting its own research as well as the research of the common interest to both outside and IMS scientists by using the facilities at IMS. During the first half of the fiscal year of 1980 ending on September 30, 90 outside scientists including 11 invited collaborated with IMS scientists; and during the second half of the year, 80 outside scientists including 7 invited worked in collaboration with IMS scientists. The names and the affilications of these collaborators are found in the Research Activities.

4) Use of Facility

The number of projects accepted for the Use of

Facility Program of the Computer Center during the fiscal year of 1980 amounted to 109 (255 users), and the computer time spent for these projects is 1,767 hours (39% of the total annual CPU time).

Two hundred and five projects were accepted for the Use of Facility Program of the Instrument Center during the fiscal year of 1980.

FOREIGN SCHOLARS

Visitors from abroad play an important role in research activities and are always welcomed at IMS. The following is the list of foreign scientists who visited IMS in the past year (Aug. 1980 - July 1981). The sign *1 indicates a visitor invited to attend an Okazaki Conference, *2 indicates a visitor on the Invited Foreign Scholars Program, and *3 a counsellor of IMS.

Prof. G. Poter*[3]	Royal Institution	(UK)	Aug. 1980
Prof. G. Allen	Science Research Council	(UK)	Aug. 1980
Dr. J. Melville	Science Research Council	(UK)	Aug. 1980
Dr. A. J. Cassidy	British Council	(UK)	Aug. 1980
Dr. D. Francis	Francis Lab.	(USA)	Aug. 1980
Prof. S. A. Soling	Michigan State Univ.	(USA)	Aug. 1980
Prof. R. D. McKelvey*[2]	Univ. of Wisconsin	(USA)	May – Aug. 1980
Prof. M. Silver	Univ. of North Carolina	(USA)	Aug. – Sept. 1980
Prof. D. S. Crumrine*[2]	Loyola Univ., Chicago	(USA)	Sept. – Dec. 1980
Prof. J. C. Dabrowiak	Syracuse Univ.	(USA)	Sept. 1980
Prof. G. Parry	Imperial College of Sci. & Tech.	(UK)	Sept. 1980
Prof. J. C. Marchon	Nuclear Research Center	(France)	Spet. 1980
Prof. A. R. H. Cole	Univ. of Western Australia	(Australia)	Oct. 1980
Dr. I. Shavitt*[2]	Battelle Memorial Institute	(USA)	Oct. – Nov. 1980
Prof. M. Calvin*[3]	Univ. of California, Berkeley	(USA)	Oct. 1980
Dr. B. Starck	Univ. of Ulm	(W. Germany)	Oct. 1980
Dr. D. R. Lide	NBS	(USA)	Oct. 1980
Prof. J-M. Lehn	Université Louis Pasteur	(France)	Oct. 1980
Prof. P. Lykos	Illinois Inst. of Tech.	(USA)	Oct. 1980
Prof. M. Mizushima	Univ. of Colorado	(USA)	Nov. 1980
Prof. W. A. Little	Stanford Univ.	(USA)	Nov. 1980
Prof. R. Wolfe	Stanford Unvi.	(USA)	Nov. 1980
Prof. R. Potember	Johns Hopkins Univ.	(USA)	Nov. 1980
Dr. R. Baughman	Allied Chemical Corp.	(USA)	Nov. 1980
Dr. A. Aviram	IBM	(USA)	Nov. 1980
Dr. B. Street	IBM	(USA)	Nov. 1980
Dr. J. T. Hougen*[2]	NBS	(USA)	Nov. 1980 – Arp. 1981
Dr. I. S. Chabay*[2]	NBS	(USA)	Nov. 1980 – June 1981
Dr. R. N. Jones*[1]	Royal Society of Canada	(Canada)	Dec. 1980
Prof. I. M. Milles*[1]	Univ. of Reading	(UK)	Dec. 1980
Prof. G. Zerbi*[1]	Univ. of Trieste	(Italy)	Dec. 1980
Prof. A. C. Albrecht*[1]	Cornell Univ.	(USA)	Dec. 1980
Prof. J. K. Stille*[1]	Colorado State Univ.	(USA)	Dec. 1980
Prof. J. P. Collman*[1]	Stanford Univ.	(USA)	Dec. 1980
Prof. R. Pettit*[1]	Univ. of Texas	(USA)	Dec. 1980
Prof. S. Krimm*[1]	Univ. of Michigan	(USA)	Dec. 1980
Prof. D. Phillips	Royal Institution	(UK)	Jan. 1981
Dr. K. H. Grellmann*[2]	Max-Planck-Institut, Göttingen	(W. Germany)	Jan. — Apr. 1981
Prof. S. D. Peyerimhoff*[2]	Univ. of Bonn	(W. Germany)	Feb. – Mar. 1981

Prof. M. Kryszewski	Center of Mol. & Macromol. Studies	(Poland)	Feb. 1981
Prof. H. Kim	Seoul National Univ.	(Korea)	Feb. 1981
Prof. T. Veszprémi	Tech. Univ. of Budapest	(Hungary)	Feb. — Mar. 1981
Prof. Z. Rappoport	Hebrew Univ.	(Israel)	Mar. 1981
Prof. Y. B. Kim	Univ. of Southern California	(USA)	Mar. 1981
Prof. J. C. Woo	Seoul National Univ.	(Korea)	Mar. 1981
Prof. M. I. Bán	JAIE Inst. of Phys. Chem.	(Hungary)	Mar. 1981
Dr. M. Archer	Cambridge Univ.	(UK)	Apr. 1981
Prof. R. D. Levine	Hebrew Univ.	(Israel)	Apr. 1981
Prof. F. Gutmann	Macquarie Univ.	(Australia)	Apr. 1981
Prof. M. Hanack	Univ. of Tübingen	(W. Germany)	Apr. 1981
Prof. D. Wöhrle	Univ. of Bremen	(W. Germany)	Apr. 1981
Prof. P. G. Gassman	Univ. of Minnesota	(USA)	Apr. 1981
Prof. W. R. Heineman	Univ. of Cincinnati	(USA)	May 1981
Prof. H. Hart	Michigan State Univ.	(USA)	May 1981
Prof. I. G. Csizmadia*[2]	Univ. of Toronto	(Canada)	May 1981
Mr. M. L. Steigerwald	California Inst. of Tech.	(USA)	May 1981
Prof. V. S. Srinivason	Bowling Green State Univ.	(USA)	June 1981
Prof. T. J. Barton	Iowa State Univ.	(USA)	June 1981
Dr. V. Saunders	Daresbury Lab.	(UK)	July 1981
Dr. I. Munro	Daresbury Lab.	(UK)	July 1981
Mr. G. Saxon	Daresbury Lab.	(UK)	July 1981
Dr. I. Hillier	Univ. of Manchester	(UK)	July 1981
Prof. R. Donovan	Univ. of Edinburgh	(UK)	July 1981
Prof. M. Wojeik	Univ.of Krakow	(Poland)	July 1981
Prof. B. R. Henry*[2]	Univ. of Manitoba	(Canada)	Apr. – July 1981
Prof. E. Lipczyńska-Kochany*[2]	Tech. Univ. of Warsaw	(Poland)	Apr. 1981 –

AWARD

Dr. Nobuaki Nakashima recieved a Chemical Society of Japan Award for Young Chemists in 1981 for his contribution to "Electronically excited states of charge-transfer complexes and benzene studied by nano- and picosecond spectroscopy".

Dr. Nakashima's Scientific Achievement:

Dr. Nakashima has made contributions in studies of charge-transfer complexes, energy transfer on surface, and of benzene.

1) He studied on dynamical behaviour of electronically excited state in s-tetracyanobenzene-toluene complex and exciplexes. The relaxation processes including the surrounding solvent molecules from the Franck-Condon state to the equilibrium state was elucidated by time-resolved fluorescence spectroscopy.

2) He applied the picosecond laser fluorometry to surface. He derived an formulation for two-dimentional energy transfer and analysed a very short and non-exponential fluorescence decay of a monolayer of rhodamine B on several organic crystals.

3) By nanosecond laser photolysis, he obtained for the first time the absorption spectrum from the first excited singlet state of benzene to the fourth π-electronic excited state (1^1E_{2g}) as well as the fifth π-electronic state (2^1E_{2g}). Non-radiative transition for the excitation at 248 nm was elucidated. Hot benzene and its relaxation to the thermal equilibrium state were observed spectroscopically. He found an interesting phenomenon: Mist formation through the nucleation of photoproducts under irradiation of a pulsed UV laser.

4) He developed picosecond laser photolysis and fluorometry with a ruby and a Nd:YAG laser systems. He found a new material (polyphospholic acid) for a picosecond continuum light as a monitor source of picosecond absorption spectroscopy.

LIST OF PUBLICATIONS

S. SAKAI and K. MOROKUMA, "Ab Initio Studies on the Electronic Structure of the FSO Radical", *Chem. Phys.* **52**, 33 (1980).

I. OHMINE and K. MOROKUMA, "Photoisomerization of Polyenes: Reaction Coordinate and Trajectory in Triplet Mechanism", *J. Chem. Phys.* **74**, 564 (1981).

K. KITAURA, S. OBARA and K. MOROKUMA, "Energy Gradient with the Effective Core Potential Approximation in the Ab Initio MO Method and its Application to the Structure of $Pt(H)_2(PH_3)_2$", *Chem. Phys. Lett.* **77**, 452 (1981).

S. NAKAGAWA, H. UMEYAMA, K. KITAURA and K. MOROKUMA, "A Molecular Orbital Study on Zinc-Water-Glu 270 System in Carboxypeptidase A", *Chem. Pharm. Bull. (Tokyo)*, **29**, 1 (1981).

Y. NISHIMURA, M. TSUBOI, S. KATO and K. MOROKUMA, "In-Plane Vibrational Modes in the Uracil Molecule from an Ab Initio MO Calculation", *J. Am. Chem. Soc.* **103**, 1354 (1981).

M. HANAMURA, S. NAGASE and K. MOROKUMA, "The Stability and Nature of an Ab Initio MO Study for 1,1-Dimethylsilaethylene", *Tetrahedron Lett.* **22**, 1813 (1981).

K. KITAURA, S. OBARA and K. MOROKUMA, "Transition State of Oxidative Addition Reaction: $Pt(PH_3)_2 + H_2 \rightarrow Pt(H)_2(PH_3)_2$", *J. Am. Chem. Soc.* **103**, 2891 (1981).

S. KATO and K. MOROKUMA, "A Theoretical Study of Unimolecular Reactions of Vinyl Fluoride. Potential Surface Characteristics and Their Mechanistic Implications", *J. Chem. Phys.* **74**, 6285 (1981).

Y. OSAMURA, Y. YAMABE, F. HIROTA, H. HOSOYA. S. IWATA, H. KASHIWAGI, K. MOROKUMA, M. TOGASHI, S. OBARA, K. TANAKA and K. OHNO, "Quantum Chemistry Literature Data Base", *J. Chem. Int. Comp. Sci.* **21**, 86 (1981).

S. KATO and K. MOROKUMA, "Photochemical Ring Opening Paths of Azirine — An Ab Initio GVB Energy Gradient Approach", *Chem. Lett.* 1021 (1981).

K. KITAURA, S. SAKAKI and K. MOROKUMA, "Bonding in $Ni(PH_3)_2(C_2H_4)$ and $Ni(PH_3)_2(C_2H_2)$. An Ab Initio SCF-MO Study", *Inorg. Chem.* **20**, 2292 (1981).

M. KUSUNOKI, K. KITAURA, K. MOROKUMA and C. NAGATA, "Molecular Orbital Study of Photosynthetic Water Decomposition: Roles of Manganese and Proton-Accepting Site", *FEBS Letters*, **117**, 179 (1980).

I. OHMINE and K. MOROKUMA, "Photoisomerization of Polyenes: Potential Energy Surfaces and Normal Mode Analysis", *J. Chem. Phys.* **73**, 1907 (1980).

K. MOROKUMA and G. WIPFF, "Theoretical Evidence for Intramolecular Hydrogen Bonding in 7-Norbornenol", *Chem. Phys. Lett.* **74**, 400 (1980).

Y. OSAMURA, S. YAMABE, F. HIROTA, H. HOSOYA, S. IWATA, H. KASHIWAGI, K. MOROKUMA, M. TOGASHI, S. OBARA, K. TANAKA and K. OHNO, "QCLDB—Quantum Chemistry Literature Data Base—A Trial", *Int. J. Quant. Chem.* **18**, 393 (1980).

G. WIPFF and K. MOROKUMA, "Nonplanarity of π Systems. An Ab Initio of Norbornene and Norbornadiene", *Tetrahedron Lett.* **21**, 4445 (1980).

S. KATO and K. MOROKUMA, "Potential Energy Characteristics and Energy Partitioning in Chemical Reactions: Ab Initio MO Study of Four-Centered Elimination Reaction $CH_3CH_2F \rightarrow CH_2=CH_2+HF$", *J. Chem. Phys.* **73**, 3900 (1980).

N. KOSUGI, H. KURODA and S. IWATA, "Double Breakdown of Koopman's Theorem and Strong Correlation Satellites in the He II Photoelectron Spectrum of O_3", *Chem. Phys.* **58**, 267 (1981).

K. MOROKUMA and K. KITAURA, "Variational Approach (SCF Ab Initio Calculations) to the Study of Molecular Interactions: the Origin of Molecular Interactions", in "Molecular Interactions", ed. H. Ratajczak and W. J. Orville-Thomas, *John Wiley*, p.21, 1980.

K. MOROKUMA and K. KITAURA, "Energy Decomposition Analysis of Molecular Interactions" in "Chemical Applications of Atomic and Molecular Electrostatic Potentials", ed. P. Politze and D. G. Truhlar, *Plenum*, New York (1981), p.215.

S. OHNISHI, M. TSUKADA and S. SUGANO, "The Electronic Structure Calculations of the Graphite Intercalation Compounds Based on the SCF-DV-Xα Cluster Model", *Physica* **B + C 105**, 179 (1981).

K. NAKAMURA, T. HOSHINO, M. TSUKADA, S. OHNISHI and S. SUGANO, "Self-Consistent DV-Xα Cluster Calculation of Electronic Structure of the Si(111) 7×7 Model Surface", *J. Phys. Soc. Jpn.* **49**, Suppl. A p.1051 (1980).

K. NAKAMURA, T. HOSHINO, M. TSUKADA, S. OHNISHI and S. SUGANO, "Electronic Structure of Buckled and Vacancy Models of Si(111) 7×7 Surface by DV-Xα Cluster Method", *J. Phys.* **C 14**, 2165 (1981).

T. HOSHINO and M. TSUKADA, "Electronic Structure of Chlorine Covered Si(111) 7 × 7 Surface by the Cluster Method", *Solid State Commun.* **38**, 231 (1981).

M. TSUKADA, E. MIYAZAKI and H. ADACHI, "Theory of Electronic Structure of the Polar ZnO Surface by the Cluster Models", *J. Phys. Soc. Jpn.* **50**, 3032 (1981).

C. SATOKO, "Direct Force Calculation in the Xα Method and Its Application to Chemisorption of an Oxygen Atom on the Al(111) Surface", *Chem. Phys. Lett.*, **83**, 111 (1981).

K. TAKAGI, S. SAITO, M. KAKIMOTO, and E. HIROTA, "Microwave Optical Double Resonance of HNO: Rotational Spectrum in $\tilde{A}^1A''(100)$", *J. Chem. Phys.*, **73**, 2570 (1980).

K. MATSUMURA, T. TANAKA, Y. ENDO, S. SAITO, and E. HIROTA, "Microwave Spectrum of Acetylene-d in Excited Vibrational States", *J. Phys. Chem.*, **84**, 1793 (1980).

M. TAKAMI, "Double Resonance and High Resolution Infrared Spectroscopy of the CF_4 ν_3 Fundamental. I. Infrared-Radiofrequency Double Resonance", *J. Chem. Phys.*, **73**, 2665 (1980).

Y. ENDO, K. YOSHIDA, S. SAITO, and E. HIROTA, "The Microwave Spectrum of Carbon Dioxide-^{18}O", *J. Chem. Phys.*, **73**, 3511 (1980).

J. T. HOUGEN, "Perturbations in the Vibration-Rotation-Torsion Energy Levels of an Ethane Molecule Exhibiting Internal Rotation Splittings", *J. Mol. Spectrosc.*, **82**, 92 (1980).

K. MATSUMURA, K. KAWAGUCHI, K. NAGAI, C. YAMADA, and E. HIROTA, "Infrared Diode Laser Spectroscopy of the NS Radical", *J. Mol. Spectrosc.*, **84**, 68 (1980).

K. NAGAI, K. KAWAGUCHI, C. YAMADA, K. HAYAKAWA, Y. TAKAGI, and E. HIROTA, "A High-Precision Wavelength Meter for Tunable Diode Laser", *J. Mol. Spectrosc.*, **84**, 197 (1980).

N. OHASHI, M. KAKIMOTO, S. SAITO, and E. HIROTA, "Doppler-Limited Dye Laser Excitation Spectroscopy of the DSO Radical", *J. Mol. Spectrosc.*, **84**, 204 (1980).

C. YAMADA, K. NAGAI, and E. HIROTA, "Diode Laser Spectroscopy of the CCl Radical", *J. Mol. Spectrosc.*, **85**, 416 (1981).

Y. ENDO, S. SAITO, and E. HIROTA, "Microwave Spectrum, Spin-Rotation and Hyperfine Interaction Constants, Dipole Moment, Molecular Structure, and Harmonic Force Constants of the FSO Radical", *J. Chem. Phys.*, **74**, 1568 (1981).

N. OHASHI, K. KAWAGUCHI, and E. HIROTA, "Diode Laser Spectroscopy of the ν_{11} Band of Ethylene-d_4", *J. Mol. Spectrosc.*, **85**, 427 (1981).

M. TAKAMI, "Double Resonance and High Resolution Infrared Spectroscopy of the CF_4 ν_3 Fundamental. II. Infrared-Microwave Double Resonance and Infrared Q-Branch Spectrum", *J. Chem. Phys.*, **74**, 4276 (1981).

K. KAWAGUCHI, C. YAMADA, Y. HAMADA, and E. HIROTA, "Infrared Diode Laser Spectroscopy of the CF Radical", *J. Mol. Spectrosc.*, **86**, 136 (1981).

M. TANAKA, K. NISHIKAWA, and T. FUJIYAMA, "X-Ray Diffraction Study of Liquid Methanol.", *Chem. Lett.*, 327 (1981).

N. ITO, K. SAITO, T. KATO, and T. FUJIYAMA, "Observation of Mutual Diffusion Coefficients

and Cooperative Motions in Binary Solutions of tert-Butyl Alcohol-Water and 2-Butoxy Ethanol-Water Systems." *Bull. Chem. Soc. Jpn.*, **54**, 991 (1981).

S. SOFUE, K. KAWAGUCHI, E. HIROTA, and T. FUJIYAMA, "Measurement and Analysis of the ν_4 Band of Fluoroform and Its Molecular Constants." *Bull. Chem. Soc. Jpn.*, **54**, 897 (1981).

T. KATO, M. YUDASAKA, and T. FUJIYAMA, "Brillouin Scattering Study of Clathrate Hydrate Formation in Acetone-Water Solution." *Bull. Chem. Soc. Jpn.*, **54**, 1632 (1981).

M. YUDASAKA, T. SUGAWARA, H. IWAMURA, and T. FUJIYAMA, "Chlorine-35 NMR Studies on Ion-Pairing of the Chloride Ion in Water and Aqueous Acetone." *Bull. Chem. Soc. Jpn.*, **54**, 1933 (1981).

N. ITO, M. YUDASAKA, and T. FUJIYAMA, "Light Scattering Study of the 12-Hydroxyoctadecanoic Acid and Benzene Mixture in the Gel State." *Bull. Chem. Soc. Jpn.*, **54**, 1939 (1981).

N. ITO, T. KATO, and T. FUJIYAMA, "Determination of Local Structure and Moving Unit Formed in Binary Solution of t-Butyl Alcohol and Water." *Bull. Chem. Soc. Jpn.*, **54**, 2573 (1981).

M. OKAZAKI, I. HARA, Y. K. TSUTSUI, and T. FUJIYAMA, "Spectroscopic Studies of Surfactant Solubility 3. Side-Chain Effects of Phosphatidyl Compounds in Chloroform Solutions." *Bull. Chem. Soc. Jpn.*, **54**, 2399 (1981).

S. SOFUE, K. KAWAGUCHI, E. HIROTA, and T. FUJIYAMA, "Absolute Intensity Measurement of ν_4 Band of Fluoroform by the Use of a Tunable Diode Laser Source." *Bull. Chem. Soc. Jpn.*, **54**, 2089 (1981).

N. NAKASHIMA, K. YOSHIHARA, and F. WILLIG, "Time-Resolved Measurements of Rhodamine B Monolayer on Surface of Organic Crystals", *J. Chem. Phys.*, **73**, 3553 (1980).

N. NAKASHIMA, H. INOUE, M. SUMITANI, and K. YOSHIHARA, "Laser Flash Photolysis of Benzene. II., Laser-Induced Cluster Formation in the Gas Phase", *J. Chem. Phys.*, **73**, 4693 (1980).

N. NAKASHIMA, H. INOUE, M. SUMITANI, and K. YOSHIHARA, "Laser Flash Photolysis of Benzene. III., $S_n \leftarrow S_1$ Absorption of Gaseous Benzene", *J. Chem. Phys.*, **73**, 5976 (1980).

H. NAKAMURA, J. TANAKA, N. NAKASHIMA, and K. YOSHIHARA, "Biphotonic Ionization of 8-Anilino-1-Naphthalenesulphonate in Polar Solvents", *Chem. Phys. Lett.*, **77**, 419 (1981).

H. SATO, M. KAWASAKI, K. KASATANI, Y. KUSUMOTO, N. NAKASHIMA, and K. YOSHIHARA, "Fluorescence Decay of the 3,3'-Diethylthiacarbocyanine Iodine — Sodium Lauryl Sulfate System: Deaggregation of the Dye and Dye — Detergent Aggregate Formation above and below the Critical Micelle Concentration", *Chem. Lett.*, 1529 (1980).

Y. KUSUMOTO, H. SATO, K. MAENO, S. YAHIRO, and N. NAKASHIMA, "Steady-State and Picosecond Studies of Energy Transfer between Dyes with Closely Located S_1 Levels. Phodamine-6G and 3,3'-Diethylthiacarbocyanine Iodide in Aceton Solution", *Bull. Chem. Soc. Jpn.*, **54**, 60 (1981).

M. MIGITA, T. OKADA, N. MATAGA, Y. SAKATA, S. MISUMI, N. NAKASHIMA, and K. YOSHIHARA, "Picosecond Laser Spectroscopy of Intramolecular Heteroexcimer Systems. Time-Resolved Fluorescence Studies of p-$(CH_3)_2NC_6H_4$-$(CH_2)_n$-(9-Anthryl), p-$(CH_3)_2NC_6H_4$-$(CH_2)_n$-(1-Pyrenyl) Systems and 9-9'-Bianthryl", *Bull. Chem. Soc. Jpn.*, **54**, 3304 (1981).

K. KAMOGAWA, A. NAMIKI, N. NAKASHIMA, K. YOSHIHARA, and I. IKEGAMI, "Picosecond Transient Behavior of the Reaction-Center Particles of Photosystem I Isolated from Spinach Chloroplasts. Energy Transfer and Eelectron Transfer at Single and Multiple Photon Excitation", *Photochem. Photobiol.*, **33**, 511 (1981).

M. ITOH, H. MIZUKOSHI, K. FUKE, S. MATSUKAWA, K. MAWATARI, Y. YONEYAMA, M. SUMITANI, and K. YOSHIHARA, "Tryptophan Fluorescence of Human Hemoglobin. I. Significant Change of Fluoresence Intensity and Lifetimes in the T — R Transition", *Biochem. Biophys. Res. Commun.*, **100**, 1259 (1981).

T. KAWAI and T. SAKATA, "Photocatalytic Hydrogen Production from Water by the Decomposition of Poly-vinylchloride, Protein, Algae, Dead Insects, and Excrement", *Chem. Lett.*, 81 (1981).

H. TRIBUTSCH, T. SAKATA and T. KAWAI, "Photoinduced Layer Phenomenon Caused by Iodine Formation in $MoSe_2$: Electrolyte (Iodide) Junctions", *Elecrochim. Acta*, **26**, 21 (1981).

T. SAKATA and T. KAWAI, "Heterogeneous Photocatalytic Production of Hydrogen and Methane from Ethanol and Water", *Chem. Phys. Lett.*, **80**, 341 (1981).

T. SAKATA and T. KAWAI, "Hydrogen Production from Biomass and Water by Photocatalytic Processes", *Nouv. J. Chim.*, **5**, 279 (1981).

T. SAKATA and T. KAWAI, "Photodecomposition of Water by Using Organic Compounds — Hydrogen Evolution by Powdered Semiconductor Photocatalysts", *J. Syn. Org. Chem. Jpn. (Yuki Gosei Kagaku)* (in Japanese), **39**, 589 (1981).

H. SHINOHARA, N. OKADA, N. MIZUTANI, K. KATO, and N. NISHI, "Pulsed Molecular Beam Apparatus for the Study of Molecular Photofragmentation Processes", *J. Vacuum Soc. Jpn.*, **24**, 196 (1981).

K. MATSUI, H. MORITA, N. NISHI, M. KINOSHITA, and S. NAGAKURA, "Study on the Triplet State of Tetramethyl-*p*-phenylenediamine by Microwave Induced Delayed Phosphorescence", *J. Chem. Phys.*, **73**, 5514 (1980).

I. HANAZAKI, K. KASATANI, and K. KUWATA, "Infrared Multiphoton Dissociation of Ammonia: Laser Energy and Pressure Dependence of the Emission from NH and NH_2", *Chem. Phys. Letters*, **75**, 123 (1980).

H. KATŌ, "Laser-induced Fluorescence of Cs_2 and Role of Kinetic Energy in the Franck-Condon Principle", *Int. J. Quant. Chem.*, **18**, 287 (1980).

H. KATŌ and C. NODA, "Laser-induced fluorescence of NaK and the Dissociated Atoms", *J. Chem. Phys.*, **73**, 4940 (1980).

K. NAKAGAWA, M. KOTANI, and H. TANAKA, "Detrapping of Charge Carriers by Singlet Excitons in Naphthalene Single Crystals", *Phys. Stat. Sol.* (b), **102**, 403 (1980).

Y. HIGUCHI, S. BANDO, M. KUSUNOKI, Y. MATSUURA, N. YASUOKA, M. KAKUDO, T. YAMANAKA, T. YAGI, and H. INOKUCHI, "The Structure of Cytochrome c_3 from *Desulfovibrio Vulgaris* Miyazaki at 2.5 Å Resolution", *J. Biochem.*, **89**, 1659 (1981).

N. SATO, K. SEKI, and H. INOKUCHI, "Ultraviolet Photoelectron Spectra of Tetrahalogeno-*p*-benzoquinones and Hexahalogenobenzenes in the Solid State", *J. Chem. Soc., Faraday Trans. 2*, **77**, 47 (1981).

K. NIKI, Y. TAKIZAWA, H. KUMAGAI, R. FUJIWARA, T. YAGI, and H. INOKUCHI, "Electrocatalytic Four-Electron Reduction of Oxygen at the Cytochrome c_3-Adsorbed Electrode", *Biochem. Biophys. Acta*, **636**, 136 (1981).

M. SANO, N. SATO, H. INOKUCHI, and S. TAMURA, "The Electrical Conductivity of Graphite Filaments and Their Alkali-Metal Intercalation Compounds", *Bull. Chem. Soc. Jpn.*, **54**, 2610 (1981).

M. SANO, T. ENOKI, N. SATO, and H. INOKUCHI, "Electrical Conductivity and Catalytic Activity of Alkali-Metal-Aromatics and -Graphite with Hydrogen", *Materials Science*, **7**, 347 (1981).

K. OHHASHI, S. SHIMOTORI, I. TSUJIKAWA, and H. INOKUCHI, "Electrical Resistance and Its Variation during Intercalation in the $FeCl_3$-Graphite System", *Synthetic Metals*, **3**, 289 (1981).

K. OHHASHI, I. TSUJIKAWA, and H. INOKUCHI, "Raman Scattering from Graphite Intercalated with $FeCl_{3-y}$", *Physica*, **105B**, 386 (1981).

G. SAITO and J. P. FERRARIS, "Requirements for an "Organic Metal"", *Bull. Chem. Soc. Jpn.*, **53**, 2141 (1980).

K. TANAKA, J. DURUP, T. KATO, and I. KOYANO, "Direct Determination of Individual Reaction Cross Sections for the Two Spin-Orbit States $Ar^+(^2P_{3/2}, {}^2P_{1/2})$", *J. Chem. Phys.*, **73**, 586 (1980).

K. TANAKA, J. DURUP, T. KATO, and I. KOYANO, "State Selected Ion-Molecule Reactions by a TESICO Technique. II. Separation of the Reactant Spin-Orbit States in the Reaction $Ar^+(^2P_{3/2}, {}^2P_{1/2}) + H_2(D_2) \rightarrow ArH^+(ArD^+) + H(D)$", *J. Chem. Phys.*, **74**, 5561 (1981).

K. TANAKA, T. KATO, and I. KOYANO, "State Selected Ion-Molecule Reactions by a TESICO Technique. III. $H_2^+(v) + Ar \rightarrow ArH^+ + H$, $Ar^+ + H_2$: Observation of Enhanced Charge-Transfer Cross Sections at Near-Resonance", *J. Chem. Phys.*, **75**, 4941 (1981).

Y. ACHIBA, T. YAMAZAKI, and K. KIMURA, "Re-Measurements of Partial Photoionization Cross-Section of CH_4, NH_3 and H_2O at 58.4 nm by He(I) Photoelectron Spectroscopy", *J. Electron Spectrosc. Relat. Phenom.*, **22**, 187 (1981).

Y. ACHIBA, T. YAMAZAKI, and K. KIMURA, "Vacuum UV Photoelectron Intensity of Gaseous Compounds. II. Experimental Processes of Determination of Differential and Partial Photoionization Cross Sections", *Bull. Chem. Soc. Jpn.*, **54**, 408 (1981).

T. SUGAWARA and H. IWAMURA, "Formation of *o*-(9-Fluorenyl)phenylnitrene in the Photoisomerization of 1-Azatriptycene", *J. Am. Chem. Soc.*, **102**, 7134 (1980).

M. IWAMURA, H. TUKADA, and H. IWAMURA, "Contrasting Photochemical Bridging Regioselectivity in Bridgehead Substituted 9,10-Etheno- *vs.* 9,10-[*o*-Benzeno]-9,10-dihydroanthracenes", *Tetrahedron Lett.*, **21**, 4865 (1980).

Y. KAWADA and H. IWAMURA, "Bis(4-chloro-1-triptycyl) Ether. Separation of a Pair of Phase Isomers of Labeled Bevel Gears", *J. Am. Chem. Soc.*, **103**, 958 (1981).

Y. KAWADA and H. IWAMURA, "Phase Isomerism in Gear-shaped Molecules", *Tetrahedron Lett.*, **22**, 1533 (1981).

Y. KAWADA and H. IWAMURA, "Carbonation of 1-Triptycyllithium Taking Place *via* an Electron Transfer-Recombination Mechanism", *J. Org. Chem.*, **46**, 3357 (1981).

G. A. RUSSELL, N. K. SULEMAN, H. IWAMURA, and O. W. WEBSTER, "Radical Anions of Triptycene Bis- and Tris(quinones)", *J. Am. Chem. Soc.*, **103**, 1560 (1981).

K. KOBAYASHI, T. SUGAWARA, and H. IWAMURA, "Diastereomeric Differentiation of Sulphone Oxygens by ^{17}O NMR Spectroscopy", *J. Chem. Soc., Chem. Commun.*, **1981**, 479.

W. NAKANISHI, T. JO, K. MIURA, Y. IKEDA, T. SUGAWARA, Y. KAWADA, and H. IWAMURA, "Thermal Decomposition of ^{17}O-Labeled *t*-Butyl *o*-Methylthio- and *o*-Phenylthioperoxybenzoates Studied by ^{17}O NMR. The Sulfuranyl Radical Structure of the *o*-Thiobenzoyloxy Radicals", *Chem. Lett.*, 387 (1981).

W. NAKANISHI, S. MATSUMOTO, Y. IKEDA, T. SUGAWARA, Y. KAWADA, and H. IWAMURA, "On the Structure of 2-Carboxyphenyl Methyl Selenoxide and Its Sodium Salt in Solution Studied by ^1H, ^{13}C and ^{77}Se NMR Spectroscopy", *Chem. Lett.*, 1353 (1981).

T. ITO, K. TORIUMI, F. B. UENO, and K. SAITO, "The Absolute Configuration of the $(-)_{589}$-Tris(acetylacetonato)germanium(IV) Ion", *Acta Crystallogr.*, **B36**, 2998 (1980).

T. ITO and K. TORIUMI, "The Structures of High- and Low-Spin Nickel Chloride Complexes Containing the Macrocyclic Ligand [7R(S),14S(R)]-5,5,7,12,12,14-Hexamethyl-1,4,8,11-tetraazacyclotetradecane", *Acta Crystallogr.*, **B37**, 88 (1981).

K. TORIUMI and T. ITO, "Structure of trans-Difluoro([7R(S),14S(R)]-5,5,7,12,12,14-hexamethyl-1,4,8,11-tetraazacyclotetradecane)nickel(II) Pentahydrate", *Acta Crystallogr.*, **B37**, 240 (1981).

S. ONAKA, Y. KONDO, K. TORIUMI, and T. ITO, "Synthesis and Molecular Structure of $TPPSn\text{-}Mn(CO)_4\text{-}Hg\text{-}Mn(CO)_5 \cdot 1/2CH_2Cl_2$: a Bent Sn-Mn-Hg-Mn Array Extended over a Porphyrin Ring", *Chem. Lett.*, **1980**, 1605.

K. KASHIWABARA, I. KINOSHITA, T. ITO, and J. FUJITA, "Absorption, Circular Dichroism, and Nuclear Magnetic Resonance Studies of Bis(acetylacetonato)cobalt(III) Complexes Containing 2-Aminoalkylphosphine Chelates with Phosphorus and Nitrogen Donor Atoms", *Bull. Chem. Soc. Jpn.*, **54**, 725 (1981).

T. ITO, Y. TSUTSUMI, Y. HIRATSUKA, K. MOCHIZUKI, and M. FUJIMOTO, "Dehydration Associated with Low-spin to High-spin Conversion of 5,5,7,12,12,14-Hexamethyl-1,4,8,11-tetraazacyclotetradecanenickel(II) Halide Dihydrate", *Bull. Chem. Soc. Jpn.*, **54**, 931 (1981).

T. ITO, K. TORIUMI, and H. ITO, "The Role Played by Water in Spin State Variations among Nickel (II) Halide Complexes Containing 7R(S),14S(R)-5,5,7,12,12,14-Hexamethyl-1,4,8,11-tetraazacyclotetradecane", *Bull. Chem. Soc. Jpn.*, **54**, 1096 (1981).

H. TOMIOKA, K. TAKAI, K. OSHIMA, H. NOZAKI, and K. TORIUMI, "Oxidation of Alcohols with Oxoperoxobis(n-phenylbenzohydroximato)molybdenum(IV)", *Tetrahedron Lett.*, **21**, 4843 (1980).

T. ITO, H. ITO, and K. TORIUMI, "The Structures of Both the Kinetic and the Thermodynamic Isomers of 1,4,8,11-Tetraazacyclotetradecanesilver(II) Perchlorate as Determined by X-ray Analyses", *Chem. Lett.*, **1981**, 1101.

M. SANO, Y. HATANO, H. KASHIWAGI, and H. YAMATERA, "An *Ab Initio* Calculation of the Electronic Structure of the $[Co(CN_6)]^{3-}$ Ion", *Bull. Chem. Soc. Jpn.*, **54**, 1523 (1981).

E. MIYOSHI, T. TAKADA, S. OBARA, H. KASHIWAGI, and K. OHNO, "Theoretical Study of Excitation Energies of Some CoF_6^{n-} Complexes", *Int. J. Quant. Chem.*, **19**, 451 (1981).

K. KIMURA, J. PETERSON, M. T. WILSON, D. J. COOKSON, and R. J. P. WILLIAMS, A Study of the Electron Transfer Properties of the Heme Undecapeptide from Cytochrome C by ^1H NMR Spectroscopy", *J. Inorg. Biochem.*, **15**, 11 (1981).

R. KUBOTA, H. KOBAYASHI, I. TSUJIKAWA, and T. ENOKI, "Electrical and Thermal Properties of the Partially Oxidized Salt of the Magnus Green Salt with the Formula $Pt_6(NH_3)_{10}Cl_{10}(HSO_4)_4$", *Inter. J. Quant. Chem.*, **18**, 1533 (1980).

B. NATSUME, N. NISHIKAWA, T. KANEDA, Y. SAKATA, S. MISUMI, T. ENOKI, and H. INOKUCHI, "Synthesis of 2,7-Bis(dimethylamino)pyrene and -tetrahydropyrene and Electrical Conductivities of Their CT Complexes", *Chem. Lett.*, **1981**, 601.

T. ENOKI and H. INOKUCHI, "Hydrogen in Aromatics 1. Electrical Conductivity and Electron Paramagnetic Resonance of Triphenylene-Potassium Complexes under Hydrogen Atmosphere", *J. Chem. Phys.*, **74**, 6440 (1981).

A. MIYASHITA, A. YASUDA, H. TAKAYA, K. TORIUMI, T. ITO, T. SOUCHI, and R. NOYORI, "Synthesis of 2,2'-Bis(diphenylphosphino)-1,1'-binaphthyl (BINAP), an Atropisomeric Chiral Bis-(triaryl)phosphine, and Its Use in the Rhodium(I)-Catalyzed Asymmetric Hydrogenation of α-(Acylamino)acrylic Acids", *J. Am. Chem. Soc.*, **102**, 7932 (1980).

A. MIYASHITA and R. H. GRUBBS, "Reactions of Nickel-Carbene Complexes Generated from Nickelacycle Complexes", *Tetrahedron Lett.*, **22**, 1255 (1981).

A. YASUDA, M. TAKAHASHI, and H. TAKAYA, "Stereoselective 1,4-Addition of Dialkylaluminum Benzenethiolate to Vinyl Oxiranes", *Tetrahedron Lett.*, **22**, 2413 (1981).

H. TAKAYA, T. SUZUKI, Y. KUMAGAI, M. YAMAKAWA, and R. NOYORI, "Nickel(0)-Catalyzed Reaction of Bicyclo[2.1.0]pentane and Electron-Deficient Olefins", *J. Org. Chem.*, **46**, 2846 (1981).

H. TAKAYA, T. SUZUKI, Y. KUMAGAI, M. HOSOYA, H. KAWAUCHI, and R. NOYORI, "Nickel(0)-Catalyzed Reactions of Bicyclo[1.1.0]butanes. Geminal Two-Bond Cleavage Reaction and the Stereospecific Olefin Trapping of the Carbenoid Intermediate", *J. Org. Chem.*, **46**, 2854 (1981).

A. MIYASHITA, M. TAKAHASHI, H. TAKAYA, "Reaction of Bicyclo[1.1.0]butanes with Pt(II) Complexes. Isolation and Characterization of New Platinacycle Compounds", *J. Am. Chem. Soc.*, **103**, 6257 (1981).

Y. TAKAGI, M. SUMITANI, and K. YOSHIHARA, "High-Speed Image Processor for Picosecond Time-Resolved Spectroscopy", *Rev. Sci. Instrum.*, **52**, 54 (1981).

Y. TAKAGI, Y. FUKUDA, K. YAMADA, and T. HASHI, "Optical Excitation of Zeeman Coherence in Ruby", *J. Phys. Soc. Jpn.*, **50**, 2672 (1981).

M. WATANABE, A. UCHIDA, O. MATSUDO, K. SAKAI, K. TAKAMI, T. KATAYAMA, K. YOSHIDA, and M. KIHARA, "Design of UVSOR Light Source at IMS", *IEEE Trans.* **NS-28**, 3175 (1981).

Review Articles and Textbooks

E. HIROTA, "Structural Studies of Transient Molecules by Laser Spectroscopy", in "Chemical and Biochemical Applications of Lasers", Vol. V, C. B. Moore Ed., *Academic Press*, pp.39–93 (1980).

E. HIROTA, "To What Extent Can Motions of Molecules Be Traced?", *Kagaku* (in Japanese), **36**, 3 (1981).

K. KAWAGUCHI, "Experience of Using Diode Lasers", *Bunko Kenkyu* (in Japanese), **29**, 404 (1980).

T. FUJIYAMA, T. KATO, and N. ITO, "Time-Correlation Spectroscopy." *Kagaku to Kogyo* (in Japanese), **34**, 346 (1981).

T. KATO and T. FUJIYAMA, "Molecular Association Viewed from Light Scattering Spectra." *Yukagaku* (in Japanese), **30**, 742 (1981).

N. NAKASHIMA, "Nanosecond Laser Photolysis of Benzene", *Rev. Laser Engineering* (in Japanese), **9**, 357 (1981).

K. YOSHIHARA, "Processes of Spinach Chloroplasts upon Picosecond Pulse Excitation", *Bioscience*, **31**, 601 (1981).

T. KAWAI and T. SAKATA, "Hydrogen Production by Using Photocatalyst — from Water, Sun and Organic Resources", *Gendai Kagaku* (in Japanese), 52 (1981).

T. SAKATA, "Photochemical Properties of Semiconductor Catalyst and Its Application to Solar Energy Conversion", in "Biological and Chemical Utilization of Solar Energy, III", K. Shibata, A. Ikegami, and A. Yamada Ed., Gakkaishi Kanko Center (1981), pp.24–32.

T. KAWAI, "Production of Hydrogen Fuel from Water and Organic Materials Using Semiconductor Photocatalyst", in "Biological and Chemical Utilization of Solar Energy, III", K. Shibata, A. Ikegami, and A. Yamada Ed., Gakkaishi Kanko Center (1981), pp.35–45.

M. KINOSHITA, N. IWASAKI, and N. NISHI, "Molecular Spectroscopy of the Triplet State through Optical Detection of Zero-Field Magnetic Resonance", *Appl. Spectrosc. Rev.*, **17**, 1 (1981).

H. HANAZAKI and K. YOSHIHARA, "Possibility of Control of Chemical Reaction with Laser and Its Future", *Kagaku Sosetsu* (in Japanese), **26**, 153 (1980).

I. HANAZAKI, "Determination of Absolute Configuration by Spectroscopic Methods", *Iwanami Gendai-Kagaku* (in Japanese), **13** (1980).

H. INOKUCHI, "Materials having Interesting Physico-Chemical Properties and General Principle to Find These Materials" (in Japanese) in "Material Chemistry", N. Ise, H. Inokuchi, and I. Tabushi Ed., *Iwanami*, pp.13–94 (1981).

H. INOKUCHI and T. YAGI, "Cytochrome c_3", *Kagaku* (in Japanese), **51**, 369 (1981).

G. SAITO and H. INOKUCHI, "Organic Conductors" in "Electroorganic Chemistry", *Kagaku-Zokan* (in Japanese), **86**, 45 (1980).

H. INOKUCHI and M. SANO, "Physical Chemistry of Graphite and Graphite Intercalation Compounds" in "Synthetic Metals", *Kagaku-Zokan* (in Japanese), **87**, 127 (1981).

K. KIMURA, "New Light-Synchrotron Orbital Radiation (SOR)", *Kagaku to Kogyo* (in Japanese), **34**, 360 (1981).

K. KIMURA, S. KATSUMATA, Y. ACHIBA, T. YAMAZAKI, and S. IWATA, "Handbook of HeI Photoelectron Spectra of Fundamental Organic Molecules", *Japan Scientific Societies Press and Halsted Press* (John Wiley & Son), 1981.

K. SHOBATAKE, "Molecular Beam Investigations of Chemical Reaction Processes", *Butsuri* (in Japanese), **36**, 105 (1981).

H. IWAMURA and W. NAKANISHI, "Recent Applications of ^{77}Se NMR Spectroscopy in

Organoselenium Chemistry", *J. Synth. Org. Chem.* (in Japanses), **39**, 795 (1981).
N. HARADA, "Absolute Stereochemistry of Organic Compounds as Determined by X-Ray and CD Methods — on the Reversal of Absolute Configuration of Clerodane Diterpenes", *Kagaku* (in Japanese), **35**, 856 (1980).
N. HARADA and K. NAKANISHI, "Circular Dichroic · Spectroscopy — Excition Coupling in Organic and Bioorganic Stereochemistry," University Science Books, California (1981).
R. NOYORI and H. TAKAYA, "Toward the Highly Selective Organic Synthesis. Transition Metal Catalyzed Asymmetric Reactions", *J. Syn. Org. Chem.* (in Japanese), **39**, 522—534 (1981).

Institute for Molecular Science, Myodaiji, Okazaki 444, Japan